New Receptivity Mechanisms of Supersonic Boundary Layers

a thesis presented for the degree of

Doctor of Philosophy of Imperial College London

and the

Diploma of Imperial College

by

Carlos González Hernández

Department of Mathematics

Imperial College London

180 Queen's Gate, London SW7 2BZ

September 2020

I certify that this thesis, and the research to which it refers, are the product of my own work, and that any ideas or quotations from the work of other people, published or otherwise, are fully acknowledged in accordance with the standard referencing practices of the discipline.

Signed: Carlos González Hernández

Copyright

The copyright of this thesis rests with the author. Unless otherwise indicated, its contents are licensed under a Creative Commons Attribution-Non Commercial 4.0 International Licence (CC BY-NC).

Under this licence, you may copy and redistribute the material in any medium or format. You may also create and distribute modified versions of the work. This is on the condition that: you credit the author and do not use it, or any derivative works, for a commercial purpose.

When reusing or sharing this work, ensure you make the licence terms clear to others by naming the licence and linking to the licence text. Where a work has been adapted, you should indicate that the work has been changed and describe those changes.

Please seek permission from the copyright holder for uses of this work that are not included in this licence or permitted under UK Copyright Law.

Abstract

In this thesis we investigate, using high-Reynolds-number asymptotic techniques, three problems related to the receptivity of supersonic boundary layers. The first problem concerns two new receptivity mechanism to impinging acoustic waves, whose phase velocity ($\mathcal{O}(R^{-1/8}U_\infty)$) is much slower than the free-stream velocity U_∞, where R is the Reynolds number based on L, the distance to the leading edge, and U_∞. A sound wave on this scale has the special property that it induces in the boundary layer a viscous response that is greater by a factor of $\mathcal{O}(R^{1/8})$ than the disturbance in the free-stream. The sound-sound, or sound-roughness, interactions generate a forcing in resonance with a neutral T-S wave. The triple-deck formalism is adopted to describe impingement and reflection of the acoustic waves, and ensuing receptivity, allowing the coupling coefficient to be calculated. The two receptivity processes are much more effective compared with those involving usual sound waves, with the coupling coefficient being greater by a factor of $\mathcal{O}(R^{1/4})$ and $\mathcal{O}(R^{1/8})$ in the S-S (sound-sound) and S-R (sound-roughness) interactions, respectively. A parametric study is conducted for representative T-S waves, to assess the influence of the streamwise and spanwise wavenumbers, and the phase speed of the sound wave.

The second problem deals with the connection of the inviscid and viscous branches of instability modes in supersonic boundary layers, following the previous investigation of Goldstein and Ricco (2018). The upper and lower branches of the neutral curve are connected, as indicated by finite-Reynolds-number calculations. A new intermediate regime, identified in a previous preliminary study (Yang, 2017), is discussed further in the present work. This regime is described by triple-deck theory, although its scaling is not standard. The instability is studied and the dispersion relation is calculated for different Mach numbers. It is shown that this regime was missed by the previous work of Goldstein and Ricco (2018).

The third problem concerns the study of a new mechanism for the generation of T-S waves, which involves an incident sound wave with its frequency and wavelength on the triple-deck scale and free-stream vortical disturbances with spanwise wavelength on the triple-deck scale too but long streamwise wavelength. The long-wavelength vortical disturbances with $\mathcal{O}(\varepsilon_v)$ intensity in the free-stream induce in the boundary layer much larger $\mathcal{O}(\varepsilon_v R^{3/8})$ streamwise velocity in response to them, which manifests as streaks. With the appropriate choice of the spanwise wavelength on the triple deck scale, the acoustic signature and streaks interact

in the main boundary layer as well as in the lower deck, to generate a forcing in resonance with a neutral T-S wave. The receptivity of this mechanism is found to be greater than those in Hernández and Wu (2019) and Wu (1999) by a factor of $\mathcal{O}(R^{1/8})$ and $\mathcal{O}(R^{3/8})$, respectively.

A la memoria de mi padre Miguel, para quien mi educación siempre fue su máxima prioridad.

Acknowledgments

I would like to express my gratitude to my supervisor Professor Xuesong Wu for his guidance and patience in the early stage of this work. I thank Dr. Shahid Mughal (Imperial) and Dr. Paul Hammerton (UEA) for accepting to be my examiners and for their useful corrections and suggestions which have greatly improved the quality of this manuscript. I would like to acknowledge the Department of Mathematics and EPSRC for the award of a Roth Doctoral Fellowship, which has enabled me to pursue a PhD thesis in the Department. I am grateful for the colleagues and friends at Imperial and for the scientific and non-technical discussions over these years, which have allowed me to grow both professionally and personally.

The decision to leave France for the UK was a tough one. Yet, my life would have been very different if I hadn't come to London. And it is always for the people. London is a curious amalgam of cultures, a collection of millions of personal stories linked to each other by space and time, but mostly by chance. In this way, I have been incredibly lucky to meet excellent people along the way and I would like to take this opportunity to send them a massive thank you for their friendship, for the many personal conversations and for the moments spent together.

Finally, I want to thank my family for their continuous and unconditional support over the years. My parents Miguel and Emilia Isabel have always placed my education high above all other matters, setting the hierarchy of priorities I had to follow right from the beginning. I would be nothing without it.

This thesis is dedicated to them.

List of figures

1.1 Neutral curve of a boundary layer, separating stable from unstable regions of spatial instability in the ω (forcing frequency) - Re (Reynolds number) parameter space. 18
1.2 Paths to transition to turbulence, from Morkovin et al. (1994). . . . 21

2.1 Sketch of the physical setting showing the impingment/penetration of two acoustic waves. 36
2.2 Neutral curve of the T-S wave in the ($\hat{\alpha}_{TS}$, $\hat{\beta}_{TS}$) plane for different Mach numbers. The dashed lines represent $\hat{\beta}_{TS} = \sqrt{M^2 - 1}\hat{\alpha}_{TS}$. . . 47
2.3 An ilustration showing the selection of the sound waves which satisfy the resonance conditions (2.27) for a given T-S wave (solid line, $M = 4.5$ case in figure 2.2). The dash-dotted line represents $\hat{\beta}_1 - \hat{\beta}_{TS} = -\sqrt{M^2 - 1}(\hat{\alpha}_1 - \hat{\alpha}_{TS})$. 48
2.4 Receptivity mechanism due to sound-sound interaction. 51
2.5 Sketch of the "difference-mode" interaction between a sound wave and a wavy wall (distributed roughness) in the supersonic regime, featuring Mach wave radiation. 55
2.6 $\mid \mathcal{R} \mid$ as a function of $\hat{\alpha}_1$ for $\hat{\beta}_1 = 0$, 0.1, 0.2, 0.5. The frequencies chosen are $\hat{\omega}_1 = 2\hat{\omega}_{TS}$ with $\hat{\omega}_{TS} = 0.28$ for $M = 1.2$, and $\hat{\omega}_{TS} = 0.13$ for $M = 4.5$. 60
2.7 Contour plot of $\mid \mathcal{R} \mid$ as a function of $\hat{\alpha}_1$ and $\hat{\beta}_1$ for $M = 1.2$ and $M = 4.5$. The frequency chosen is $\hat{\omega}_1 = 2\hat{\omega}_{TS}$ with $\hat{\omega}_{TS} = 0.28$. . . . 60
2.8 $\mid \mathcal{R} \mid$ as a function of $\hat{\alpha}_1$ for $\hat{\beta}_1 = 0$, 0.5, 1, 2. The frequency chosen is $\hat{\omega}_1 = 3$. 60
2.9 $\mid \mathcal{R} \mid$ as a function of $\hat{\omega}_1$ for $\hat{\beta}_1 = 0$, 0.05, 0.1 for the $M = 1.2$ case, and $\hat{\beta}_1 = 0$, 0.2, 0.5 for the $M = 4.5$ case. The streamwise wavenumber chosen is $\hat{\alpha}_1 = 0.2$. The asymptote (2.157) is plotted for $\hat{\beta}_1 = 0$ as the dashed lines. 61
2.10 $\mid \mathcal{R} \mid$ as a function of $\hat{\omega}_1$ for $\hat{\beta}_1 = 0$, 0.5, 1 in the M=1.2 case and $\hat{\beta}_1 = 0$, 1, 2 in the case M=4.5. The streamwise wavenumber chosen is $\hat{\alpha}_1 = 2$. The asymptote (2.157) is plotted for $\hat{\beta}_1 = 0$ as the dashed line on the right figure. 62
2.11 Contour plot of $\mid \mathcal{R} \mid$ as a function of $\hat{\alpha}_1$ and $\hat{\beta}_1$ for the $M = 1.2$ case (left) and $M = 4.5$ case (right). The frequency chosen is $\hat{\omega}_1 = 3$. 62
2.12 Contour plot of Λ_{SS} as a function of $\hat{\alpha}_1$ and $\hat{\beta}_1$. The neutral T-S mode excited has $\hat{\beta}_{TS} = 0.2$, for which $(\hat{\omega}_{TS}, \hat{\alpha}_{TS}) = (0.28, 0.13)$ at $M = 1.2$, and $(\hat{\omega}_{TS}, \hat{\alpha}_{TS}) = (0.13, 0.04)$ at $M = 4.5$. The sound-wave frequency chosen is $\hat{\omega}_1 = 2\hat{\omega}_{TS}$. 63

2.13 Λ_{SS} as a function of $\hat{c}_1$ for $\hat{\beta}_1 = 0$, 0.1, 0.2 and 0.3. The neutral T-S mode excited has $\hat{\beta}_{TS} = 0.2$, for which $(\hat{\omega}_{TS}, \hat{\alpha}_{TS}) = (0.28, 0.13)$ at $M = 1.2$, and $(\hat{\omega}_{TS}, \hat{\alpha}_{TS}) = (0.13, 0.04)$ at $M = 4.5$. The sound-wave frequencies chosen are $\hat{\omega}_1 = 2\hat{\omega}_{TS}$. 63
2.14 Contour plot of Λ_{SS} as a function of $\hat{\alpha}_1$ and $\hat{\beta}_1$. The neutral T-S mode excited has $\hat{\beta}_{TS} = 0.2$, for which $(\hat{\omega}_{TS}, \hat{\alpha}_{TS}) = (0.28, 0.13)$ at $M = 1.2$, and $(\hat{\omega}_{TS}, \hat{\alpha}_{TS}) = (0.13, 0.04)$ at $M = 4.5$. The frequency chosen is $\hat{\omega}_1 = 3$. 64
2.15 Λ_{SS} as a function of $\hat{c}_1$ for different values of $\hat{\beta}_1$. The neutral T-S mode excited has $\hat{\beta}_{TS} = 0.2$, for which $(\hat{\omega}_{TS}, \hat{\alpha}_{TS}) = (0.28, 0.13)$ at $M = 1.2$, and $(\hat{\omega}_{TS}, \hat{\alpha}_{TS}) = (0.13, 0.04)$ at $M = 4.5$. The sound-wave frequency chosen is $\hat{\omega}_1 = 3$. 65
2.16 Λ_{SS} as a function of $\hat{c}_1$ for $\hat{\alpha}_1 = 0.2$ (1st row), $\hat{\alpha}_1 = 1$ (2nd row) and different values of $\hat{\beta}_1$ at M=4.5. The neutral T-S modes excited have $\hat{\beta}_{TS} = 0.2$, for which $(\hat{\omega}_{TS}, \hat{\alpha}_{TS}) = (0.13, 0.04)$, and $\hat{\beta}_{TS} = 0.5$, for which $(\hat{\omega}_{TS}, \hat{\alpha}_{TS}) = (0.104, 0.029)$. The result for $\hat{\beta}_1 = 1$ and $\hat{\beta}_{TS} = 0.2$ is plotted to 1/8 of the original values. 65
2.17 Λ_{SR} as a function of $\hat{c}_1$ for $\hat{\beta}_1 = 0$, 0.2, 0.4 and 1 in the cases of S+R (first row) and S-R (second row) interactions for $\hat{\beta}_{TS} = 0.2$. The frequencies chosen are $\hat{\omega}_1 = \hat{\omega}_{TS}$ with $\hat{\omega}_{TS} = 0.28$ ($\hat{\alpha}_{TS} = 0.13$) for M=1.2 and $\hat{\omega}_{TS} = 0.13$ ($\hat{\alpha}_{TS} = 0.04$) for M=4.5. 66
2.18 Λ_{SR} as a function of $\hat{c}_1$ for $\hat{\beta}_1 = 0$, 0.2, 0.4 and 1 in the cases of S+R (first row) and S-R (second row) interactions for $\hat{\beta}_{TS} = 0.5$. The frequencies chosen are $\hat{\omega}_1 = \hat{\omega}_{TS}$ with $\hat{\omega}_{TS} = 0.1108$ ($\hat{\alpha}_{TS} = 0.032$) for M=1.2 and $\hat{\omega}_{TS} = 0.104$ ($\hat{\alpha}_{TS} = 0.029$) for M=4.5. 67

3.1 Triple-deck structure of the newly-identified regime 92
3.2 Real (a) and imaginary (b) parts of (3.180) for the case $M = 2$ and $\alpha_0 = 1$. The shaded region corresponds to positive values of the real part of RHS. The dashed line corresponds to the asymptote (3.187). 98
3.3 Real (a) and imaginary (b) parts of (3.180) for the case $M = 2$ and various α_0. 99
3.4 Growth rate $-\hat{\alpha}_{1i}$ as a function of $\hat{\omega}_0$, for $\hat{\alpha}_0 = 1$, $\hat{\beta}_1 = 0$ and $M = 2$ (left). Comparison for various Mach numbers (right). The shaded region represents the physically-realizable solutions ($a_r \geq 0$). When $a_i < 0$, a damped radiating mode appears while, when $a_i > 0$, a growing mode arises instead. 100

4.1 An illustration showing the selection of the acoustic and vortical waves which satisfy the resonance conditions (4.11) for a given T-S wave at $M = 4.5$. The shaded region in the centre (horizontal segment) represents the parameter space for the acoustic wave. . . . 131

4.2 Streamwise velocity profiles of streaks (main deck) at the position ($\tilde{x} = 1$) for $M = 4.5$ and various $\bar{k}_1$. The collapse of curves is plotted on the right, each calculated at $\tilde{x} = 1/\bar{k}_1$ (this is equivalent to plotting $\bar{u}$ at $\bar{x} = 1$) for various $\bar{k}_1$. 141
4.3 Velocity profiles of streaks $\bar{u}$ (left) and $\bar{w}$ (right) for $M = 3$, for validation against the solution of Ricco and Wu (2007), for $\bar{k}_1 = 1$. The numbers in the figure indicate the values of $\bar{x}$. 141
4.4 Streamwise velocity profiles of streaks ($\tilde{u}_0$) for various $\hat{\omega}_v$ (left) at the neutral position for $M = 1.2$. Profiles at various $\tilde{x}$ at $\hat{\omega}_v = \hat{\omega}_{TS}/10 = 0.029$ (right). The spanwise wavenumber has been chosen to be $\hat{\beta}_v = 0.2$. 142
4.5 Streamwise velocity profiles of streaks ($\tilde{u}_0$) for various $\hat{\omega}_v$ (left) at the neutral position for $M = 3$. Profiles at various $\tilde{x}$ at $\hat{\omega}_v = \hat{\omega}_{TS}/10 = 0.0211$ (right). The spanwise wavenumber has been chosen to be $\hat{\beta}_v = 0.2$. 142
4.6 Streamwise velocity profiles of streaks ($\tilde{u}_0$) for various $\hat{\omega}_v$ (left) at the neutral position for $M = 4.5$. Profiles at various $\tilde{x}$ at $\hat{\omega}_v = \hat{\omega}_{TS}/10 = 0.0176$ (right). The spanwise wavenumber has been chosen to be $\hat{\beta}_v = 0.2$. 143
4.7 Contour plot Λ_{SV} as a function of $\hat{\beta}_v$ and $\hat{\omega}_v \in [0, \hat{\omega}_{TS}/10]$ (sum-mode interaction) at Reynolds number 10^6 for Mach numbers $M = 1.2$ (top left), $M = 3$ (top right), $M = 4.5$ (bottom left), and $M = 6$ (bottom right). The neutral T-S mode excited has $\hat{\beta}_{TS} = 0.2$. . . . 144
4.8 Value of Λ_{SV} as a function of $\hat{\beta}_v$ (sum-mode interaction) at Reynolds number 10^6 for Mach numbers $M = 1.2$ (top left), $M = 3$ (top right), $M = 4.5$ (bottom left), and $M = 6$ (bottom right). Results for steady streak ($\bar{k}_1 = 0$). The neutral T-S mode excited has $\hat{\beta}_{TS} = 0.2$. 145
4.9 Value of Λ_{SV} as a function of $\hat{\omega}_v \in [0, \hat{\omega}_{TS}/10]$ (sum-mode interaction) at Reynolds number 10^6 for Mach numbers $M = 1.2$ (top left), $M = 3$ (top right), $M = 4.5$ (bottom left), and $M = 6$ (bottom right). The chosen spanwise wavenumbers are $\hat{\beta}_v = \hat{\beta}_{TS}$ and $\hat{\beta}_s = 0$. The neutral T-S mode excited has $\hat{\beta}_{TS} = 0.2$. 146
4.10 Contour plot of Λ_{SV} as a function of $\hat{\beta}_v$ and $\hat{\omega}_v \in [0, \hat{\omega}_{TS}/10]$ (sum-mode interaction) at Reynolds number 10^6 for Mach numbers $M = 1.2$ (top left), $M = 3$ (top right), $M = 4.5$ (bottom left), and $M = 6$ (bottom right). The neutral T-S mode excited has $\hat{\beta}_{TS} = 0.5$. . . . 147
4.11 Value of Λ_{SV} as a function of $\hat{\beta}_v$ (sum-mode interaction) at Reynolds number 10^6 for Mach numbers $M = 1.2$ (top left), $M = 3$ (top right), $M = 4.5$ (bottom left), and $M = 6$ (bottom right). Results for a steady streak ($\bar{k}_1 = 0$). The neutral T-S mode excited has $\hat{\beta}_{TS} = 0.5$. 148

B.1 Stencil used in the numerical scheme for the computation of the LUBL equations. 168

B.2 Profiles of the streamwise velocity $U_B = F'$ and temperature T of a compressible Blasius boundary layer, calculated numerically solving the compressible boundary layer equations for various Mach numbers. 169
B.3 Numerical solution of equations (I), (4.32)-(4.35). Velocity (left) and temperature (right) profiles for various Mach numbers. 170
B.4 Numerical solution of equations (II), (4.36)-(4.39). Velocity (left) and temperature (right) profiles for various Mach numbers. 170

List of tables

2.1 Typical values of the initial T-S mode amplitude u_{TS} and coupling coefficients, C_A and C_R (sum-mode interaction), at representative Reynolds numbers. The results labelled with 'isoth.' are for Sutherland's law and isothermal wall with $\tau_w = 3$. 69

4.1 Typical values of Λ_{SV} (sum-mode interaction) at Reynolds number 10^6 for two different Mach numbers ($M = 1.2$ and $M = 4.5$). "EXACT" means that the exact resonance condition (4.102) has been employed in contrast to the approximate condition (4.104). The parameters chosen for the evaluation of the profiles and coupling coefficients are $Pr = 0.7$, $\omega = 0.76$, $k_3 = 1$, $\hat{v}_\infty = 1$ and $\hat{w}_\infty = 1$. The boundary condition at the surface of the plate is adiabatic for the base flow. 149

Contents

1 Introduction **16**

2 Receptivity of supersonic boundary layers over smooth and wavy surfaces to impinging slow acoustic waves **27**

2.1 Introduction . . . 27
2.2 Formulation and scalings . . . 33
2.2.1 The base flow . . . 34
2.2.2 Equations for the perturbation . . . 35
2.2.3 Physical idea and resonant interaction . . . 36
2.2.4 Asymptotic scalings . . . 38
2.2.5 Upper deck . . . 39
2.2.6 Main deck . . . 42
2.2.7 Lower deck . . . 44
2.3 Receptivity: evolution from the forced response to eigenmode . . . 51
2.3.1 Matching between T-S wave solution and upstream forced response . . . 51
2.3.2 Coupling coefficients . . . 53
2.4 Receptivity to slow acoustic waves interacting with distributed roughness . . . 53
2.4.1 Physical idea and asymptotic scaling . . . 54
2.4.2 Upper deck . . . 55
2.4.3 Main deck . . . 56
2.4.4 Lower deck . . . 57
2.5 Parametric study and discussion . . . 59
2.5.1 Reflection coefficient . . . 59
2.5.2 Rescaled coupling coefficient for sound-sound interaction . . . 63
2.5.3 Rescaled coupling coefficient for sound-roughness interaction 66
2.5.4 Initial amplitude and coupling coefficient at typical Reynolds numbers . . . 68
2.6 Summary and conclusions . . . 69

3 Connection of the inviscid and viscous branches of instability modes in supersonic boundary layers **72**
3.1 Introduction . . . 72
3.2 Fedorov-Khokhlov theory . . . 74
3.2.1 Asymptotic structure of the disturbance field . . . 76
3.3 Wu/Yang intermediate regime: stability analysis . . . 78
3.3.1 The base flow . . . 79
3.3.2 Linearization . . . 79
3.3.3 Spatial instability . . . 81
3.3.4 Wavenumbers in both modes . . . 84
3.4 Scales of wavenumbers and frequency . . . 88
3.4.1 Upper deck . . . 89
3.4.2 New scaling: Wu/Yang regime . . . 90
3.4.3 Check for asymptotes . . . 100
3.4.4 Matching between Wu/Yang intermediate regime and Smith (1989) . . . 101
3.5 Relationship between G/R and W/Y regimes . . . 103
3.5.1 A $\rightarrow$ B . . . 104
3.5.2 B $\rightarrow$ A . . . 105
3.6 Calculation of growth rate in G/R regime . . . 106
3.6.1 Lower deck . . . 106
3.6.2 Main deck . . . 107
3.6.3 Upper deck . . . 107
3.7 Summary and conclusions . . . 109

4 Receptivity of a supersonic boundary layer to free-stream vortical and slow acoustic disturbances **110**
4.1 Introduction . . . 110
4.2 Formulation and scalings . . . 117
4.2.1 The base flow . . . 117
4.2.2 Physical idea and resonant interaction . . . 118
4.2.3 Asymptotic scalings . . . 119
4.2.4 Vortical wave . . . 120
4.2.5 Upper deck . . . 124
4.2.6 Main deck . . . 125
4.2.7 Lower deck . . . 130
4.3 Receptivity: evolution from the forced response to eigenmode . . . 139

4.3.1 Matching between T-S wave solution and upstream forced response . . . 139
4.3.2 Coupling coefficients . . . 139
4.4 Parametric study and discussion . . . 140
4.4.1 Neutral position . . . 140
4.4.2 Streak signature . . . 140
4.4.3 Coupling coefficient for sound-vortical interaction . . . 143
4.5 Summary and conclusions . . . 149

5 Summary and future work **151**
5.1 Summary and conclusions . . . 151
5.2 Future work . . . 152

References **163**

Appendix A Mean-flow distortion equations in the lower deck **164**

Appendix B Numerical solution and validation of numerical method **167**

1

Introduction

Laminar-turbulent transition of boundary layers is an extraordinarily complicated process, which is, at present not fully understood. In the supersonic regime, which is the focus of this thesis, boundary-layer transition plays a crucial role in the correct characterization of the flow and thermal fields around high-speed vehicles (Fedorov, 2011). As it will be depicted later, transition occurs via different routes depending on the level of external disturbances. The present thesis deals with three topics of interest in the field of instability and receptivity of supersonic boundary layers. We focus here on high Reynolds numbers so that the powerful asymptotic techniques available can be used.

Laminar to turbulent transition

Fluid flows can usually be identified as being either laminar or turbulent. A laminar flow is either steady or changing in time in a deterministic fashion, and exhibits an orderly spatial pattern characterised by regular streamlines. Turbulent flow on the other hand is 'rough': the flow changes randomly in both time and space. One of the early studies in the field of laminar-turbulent transition was by Osborne Reynolds (Reynolds, 1895). A dye was released along the centerline of the flow in a transparent pipe to study the flow structure. By observing the pattern of the resultant streakline, he determined that the flow states observed in the various experimental runs could be separated into laminar and turbulent, with a transitional regime between the two, through a single nondimensional parameter based

upon the velocity of the fluid $\mathcal{U}$, the diameter of the pipe $\mathcal{L}$, and the kinematic viscosity of the fluid ν. This parameter is now known as the Reynolds number

$$Re = \frac{\mathcal{U}\mathcal{L}}{\nu} \tag{1.1}$$

and represents the ratio of inertial forces to viscous forces within the flow. When the Reynolds number is small ($Re \ll 1$) viscous forces dominate, and inertial terms can be included as higher-order corrections to the flow. When the Reynolds number is large ($Re \gg 1$), viscous forces can be neglected everywhere except for a thin layer near the surface of the fluid boundary, where both forces are equally important (in steady boundary layers; otherwise viscous effects can be important elsewhere, e.g. in critical layers). Viscous forces adjust the flow in this thin boundary layer so that the fluid at the boundary does not move relative to it.

Either laminar or turbulent flow may be preferred depending on the situation. In general, a laminar flow produces less drag, but only does so while the boundary layer near the surface of the body remains attached. If separation of the boundary layer is triggered - by a sudden motion of the body itself, a deformation on its surface, or some other mechanism - then the total drag on the body can increase significantly, and for wings this can lead to aerodynamic stall. Turbulent flow on the other hand is generally less susceptible to separation because of its small-scale, chaotic internal motion, and so may be preferable to laminar flow. For flight, one of the main concerns during the design process is the fuel consumption of the aircraft. A turbulent boundary layer can produce as much as 10 times more drag compared to its laminar counterpart, and so it is highly desirable to design wings so that the boundary layers over them remain as laminar as possible (although this has unavoidable consequences over the control of the aircraft).

Shear flow instabilities

The instability of shear flows and the resulting transition from a laminar state to turbulence, despite being more than a century old, continue to be one of the most challenging problems in classical physics and applied mathematics. Shear flows are characterized by the fact that adjacent layers of fluid move parallel to each other with different speeds. Typical examples are boundary layers, mixing layers, wakes and jets. Their linear stability is studied by superposing a small perturbation onto the laminar base flow.

The classical inviscid and viscous linear stability theories for parallel incompress-

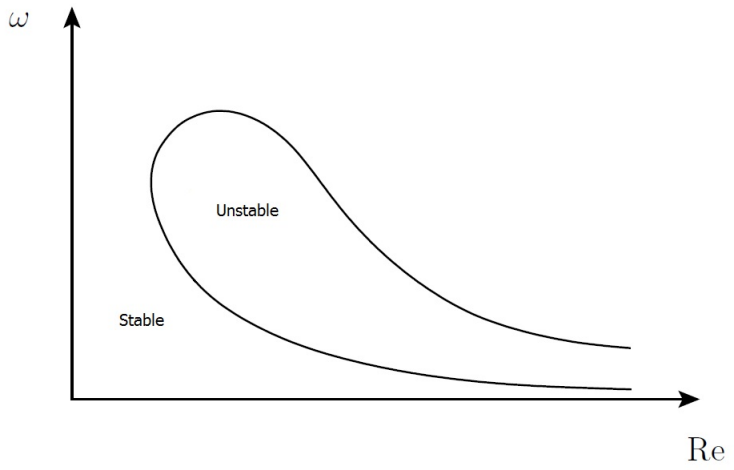


Figure 1.1: Neutral curve of a boundary layer, separating stable from unstable regions of spatial instability in the ω (forcing frequency) - Re (Reynolds number) parameter space.

ible fluid flows were formulated by Rayleigh (1879), and Orr (1907) and Sommerfeld (1908), respectively. The perturbations take the form of normal modes and the governing equations are called the Rayleigh and Orr–Sommerfeld (O–S) equations, respectively. For finite Reynolds numbers, the O–S equation can be used to compute the dispersion relation between the wavenumbers and frequencies of the modes, and predict the neutral curves (separatrix between stable and unstable regions in the parameter space) of various flows reasonably well when compared with experiments and direct numerical simulations of the Navier–Stokes equations.

Although the O–S equation is a useful tool for predicting flow stability, it has inconsistencies with regard to the assumptions made in its derivation. In the O–S theory the wavelength of the disturbance is assumed to be comparable to the boundary-layer thickness. This would mean that the viscous effect is of $\mathcal{O}(Re^{-1})$ magnitude and so the instability occurs due to retaining those small viscous terms. However, in the derivation of the O–S equation the nonparallel effects, which are of $\mathcal{O}(Re^{-1})$ magnitude too, were neglected. Therefore, mathematically the stability analysis of boundary layer flows requires the linearised N–S equations to be solved (Cowley and Wu, 1994). An asymptotic analysis had to be conducted in order to extract the relevant dominant physical effects. For example, Lin (1946) derived asymptotic expressions for the instability properties including the neutral curve at large Reynolds numbers for the Poiseuille and Blasius flow. For the latter, the analysis showed that viscosity was a leading order effect for the lower-branch instability while non-parallelism was a higher-order effect. Smith (1979b), over

30 years later, pointed out that the T–S wave scaling for the lower-branch, derived by Lin (1946), follows the triple-deck structure developed by Neiland (1969), Stewartson and Williams (1969), and Messiter (1970).

There are two types of stability analysis: temporal, for which the wavenumber is assumed to be real (and the frequency is complex), and spatial, for which the forcing frequency is assumed to be real (and the wavenumber is complex). Both stability analysis lead to the same neutral curve, which is sketched in figure 1.1. For boundary-layer flows, the neutral curve usually consists of a critical Reynolds number, a lower and an upper branch. The critical Reynolds number is the lowest Reynolds number below which the flow is stable for all frequencies/wavenumbers. The lower-branch is the border where the flow becomes linearly unstable, as the Reynolds number is increased. The upper-branch is the location where the flow becomes linearly stable again, as the Reynolds number is further increased.

Inviscid Instability

The O–S equation simplifies to the Rayleigh equation in the inviscid limit. Its eigensolutions, called the Rayleigh instability modes, may exist if the velocity profile has an inflection point. For a neutral mode, the Rayleigh equation becomes singular where the fluid flow velocity equals the phase speed of the mode. This location is called the critical level. The modes can be further categorised as regular (inflection point) or singular (noninflection point) modes. They are distinguished because for the former, the critical level is located at an inflection point and the eigensolution is regular to leading order in the vicinity of the critical level. The inviscid approximation becomes invalid as the critical level is approached and other effects such as viscosity, non-parallelism and nonlinearity have to be included to obtain regular solutions in this region (Lin, 1957).

The inflection-point theorem of Rayleigh (1879) states that unstable modes exist only for streamwise velocity profiles that have an inflection point. By this theorem, the plane Poiseuille flow and the Blasius boundary layer would be stable in the inviscid limit, because their streamwise velocity profiles are noninflectional. In this case viscosity is crucial for causing the overall instability of the flow.

Viscous Instability: Tollmien-Schlichting waves

In this thesis, we study the receptivity of T–S waves to different external disturbances. This section is dedicated to delve into the main features of this kind of

instability.

Tollmien-Schlichting (T-S) waves are generated by a two-dimensional shear instability that can occur in both two- and three-dimensional boundary layers. If first excited in the leading-edge flow, this instability initially takes the form of Lam-Rott eigensolutions (Lam and Rott, 1993). These decay and undergo wavelength shortening, and subsequently develop into T-S waves further downstream (Goldstein, 1983).

Unlike shear instabilities in flows with inflectional profiles, the T–S instability arises due to the destabilising role of viscosity. This may at first seem counterintuitive, as the diffusive nature of viscous effects would seem to smooth out any imbalance within the flow. Their existence in the plane Poiseuille flow was shown by Heisenberg (1924), and in the Blasius boundary layer was first shown by Tollmien (1929) and Schlichting (1933). The experimental verification was provided in the work by Schubauer and Skramstad (1947). The analysis by Lin (1946) showed that lower-branch modes have the characteristic wave number $\alpha = \mathcal{O}(R^{-1/4})$ rather than $\mathcal{O}(1)$, i.e., the characteristic wavelength is much longer than the local boundary layer thickness, the phase speed is $c = \mathcal{O}(R^{-1/4})$. With this asymptotic scaling, the instability is governed by the triple-deck structure (Smith, 1979a) consisting of the lower, main, and upper decks. The instability is a result of mutual interaction among the three layers.

Routes to Turbulence

Morkovin (Morkovin, 1969, Morkovin et al., 1994) described the different routes to laminar-turbulent transition, which apply in general to open high-Reynolds-number flows. There are several different ways a boundary layer can transition from laminar to turbulent, depending on the characteristic strength and spectral content of the external disturbances that are present in the environment, as sketched in figure 1.2.

If the disturbances are weak enough, they enter the boundary layer and affect transition via receptivity mechanisms, and the resulting flow can be thought of as the original boundary-layer solution superposed by a small perturbation. The size of the perturbation usually scales linearly with the external disturbance, so is also small, and thus nonlinear interactions can be neglected. As the perturbation develops through the growing boundary layer, it may enter a region where it is unstable, i.e. its amplitude increases in space as it propagates further down-

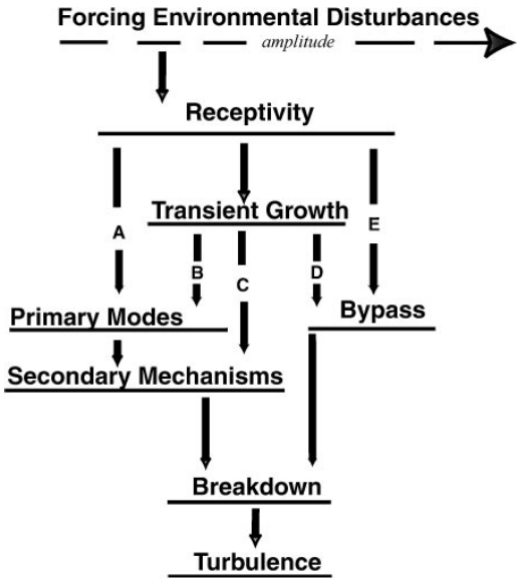


Figure 1.2: Paths to transition to turbulence, from Morkovin et al. (1994).

stream. If the perturbation grows to a large size within this region, nonlinear effects will become significant. In the nonlinear regime, the perturbation initially enters the weakly-nonlinear stage (Kachanov, 1994, Wu, 2019), where only certain interactions - such as those between specific eigenmodes - play an important role in the development of the flow. As the perturbation continues to amplify and becomes nonlinear, the full boundary-layer flow is altered by an $\mathcal{O}(1)$ amount and secondary instabilities can be triggered. These secondary instabilities often grow and break down rapidly, causing the flow to transition to a turbulent state. This is the sequence the boundary-layer flow follows if the initial disturbances are small enough.

If the disturbances are larger, the perturbed boundary layer may bypass both the receptivity and linear stages and begin directly at the nonlinear stage, or even immediately become turbulent. If this is the case, it is not useful to think of the resultant flow as a perturbation superposed onto the original flow, as they are of comparable size; instead the combined flow should be considered as a whole.

Receptivity

It has long been observed that transition depends strongly on external disturbances. These include fluctuations in the oncoming free-stream as well as surface deformations, roughness, suction/blowing, and surface temperature variations.

These disturbances excite instability modes inside the laminar boundary layer and set their initial amplitudes. Through these initial amplitudes, the external disturbances determine which instability will dominate in the subsequent flow. Receptivity theory investigates the interaction between the boundary layer and the surrounding perturbation field.

The problem of receptivity is mathematically different from that of stability: while the second looks for normal modes and leads to an eigenvalue problem, the first gives rise to an inhomogeneous boundary-value problem. Kovasznay (1953) showed that, at leading order, a general disturbance in a uniform compressible flow can be decomposed into three components: acoustic (pressure fluctuation), vorticity and entropy modes (these two are convected with the free-stream and have been used to model turbulence in many applications). None of these external disturbances can usually excite T-S waves alone, since its wavelength would differ from those of the latter if its frequency is chosen to be the same. The concept of scale-conversion mechanism, which allow long-wavelength free-stream fluctuations to generate small-wavelength instabilities within the boundary layer was first introduced by Goldstein (1983), Goldstein (1985) and Ruban (1984). The work by Goldstein (1983) showed that the rapidly-varying base flow near the leading edge of a flat plate is receptive to acoustic fluctuations in the free-stream, generating a perturbation within the boundary layer in the form of a Lam-Rott eigensolution (Lam and Rott, 1993) that subsequently undergoes wavelength-shortening and develops into a T-S wave further downstream. These eigensolutions undergo severe decay up to the lower-branch point. As a result, the T-S wave excited via this mechanism is relatively weak. Goldstein (1985) and Ruban (1984) both studied the generation of T-S waves by an acoustic wave interacting with the flow disturbance caused by small variations in surface geometry, such as roughness or changes in curvature. The flow disturbance and surface variation are assumed to have a frequency and length scales comparable with those of T-S waves. The interaction between these then generates an eigenmode by producing an unsteady forcing that is in resonance with it. Another receptivity mechanism that has been found to generate T-S waves is the interaction of free-stream vorticity with localised or distributed surface roughness (Duck et al., 1996, Wu, 2001a, Wu, 2001b), as well as the interaction between free-stream acoustic and vortical fluctuations, without the need for roughness (Wu, 1999). Duck et al. (1996) showed that the vortical disturbances do not directly enter the boundary layer, but interact with the roughness-induced signature at the outer edge of the boundary layer, producing a forcing in resonance with a T-S wave. Dietz (1999) performed an experimental study of the receptivity to vortical disturbances; these results were later used by

Wu (2001b), who extended the analysis of Duck et al. (1996) to second order and to vortical disturbances with an arbitrary transverse distribution; the latter made a quantitative comparison with experiment possible, finding a good agreement between the second-order theory and the measurements. More recently, De Tullio and Ruban (2015) performed direct numerical simulations (DNS) of the receptivity of subsonic compressible boundary layers to roughness-sound interaction. A comparison with the results of the asymptotic (triple-deck) theory showed that the latter hold down to moderate Reynolds numbers $R = \mathcal{O}(10^5)$, showing a good agreement for Mach number $M = 0.8$, and excellent agreement for $M = 0.2$.

Zhigulev and Fedorov (1987), Choudhari and Streett (1992) and Crouch (1992) formulated a finite-Reynolds-number approach to receptivity, which retained the essence of the Goldstein-Ruban theory, but used inhomogeneous O-S equations instead of the triple-deck equations to compute the mean-flow distortion as well as the resultant T-S waves. Even if this approach was accurate when compared to experiments, the O-S equations can only be applied to roughness with a sufficiently small height, since otherwise the mean-flow distortion would become nonlinear and the nonparallel effects would be the same order as the viscous effects (the former were neglected in this formulation). In that case, the triple-deck or interactive boundary-layer formalisms would need to be used instead (Bodonyi et al., 1989, Goldstein et al., 1987, Nayfeh and Ashour, 1994).

The receptivity to the interaction of sound waves or vortical disturbances with a distributed roughness was studied by Wu (2001a), who developed a (second-order) asymptotic theory based on the triple-deck formalism. They analysed the resonance region by accounting for the non-parallel-flow effect, which is essential for the calculation of the initial amplitude of the T-S waves. In fact, this had been missed by the previous studies by Crouch (1992, 1994), who used a finite-Reynolds-number approach.

Receptivity mechanisms can be very different in supersonic boundary layers, mainly because the majority of instability modes are inviscid (especially in hypersonic boundary layers). Mack (1984) and Ma and Zhong (2003) showed that supersonic boundary layers can support a plethora of viscous and inviscid instability modes. These were calculated by the numerical solution of O-S and Rayleigh equations, respectively. The high-Reynolds-number asymptotic description of these modes at large Mach number was studied by Smith (1989), Smith and Brown (1990) and Blackaby et al. (1993) among others, who reported a good agreement with the O-S solutions calculated by Mack (1984) and Ma and Zhong (2003). More recently, Liu et al. (2020) studied the receptivity of a supersonic boundary layer

to slow acoustic waves interacting with streamwise localised wall roughness, using triple-deck theory and DNS. Dong et al. (2020) investigated the inviscid first and second modes instead, also generated due to the scattering of free-stream sound by localised wall roughness, using DNS and an extension of finite-Reynolds-number theory to the supersonic regime.

Fedorov and Khokhlov (1991) and Fedorov (2003a) described theoretically the leading-edge receptivity mechanism operating in supersonic boundary layers, how the scattering and diffraction of acoustic waves in this region generate two branches of instability modes referred to as modes S (slow) and F (fast) (Fedorov, 2011), because their phase speeds approach in the upstream limit those of the fast and slow free-stream acoustic waves, respectively. Fedorov (2003b) analyzed the generation of second Mack modes due to acoustic waves interacting with localized and distributed surface roughness, while Fedorov (2013) investigated receptivity to small solid particles present in the free stream.

High-speed boundary layers often feature the presence of shocks. Qin and Wu (2016) studied the effect of an oblique shock on the receptivity of a hypersonic boundary layer over a wedge, at high-Reynolds numbers. When the shock angle with respect to the wedge wall is small, the instability is viscous and three-dimensional (Cowley and Wu, 1999). They showed that each of the three types of free-stream disturbances interacts with the shock to produce a slow acoustic wave downstream which can resonate with a T-S mode, without resorting to wall roughness.

Experimental studies of supersonic boundary-layer receptivity are extremely difficult, and only a few have been carried out (e.g. Kendall, 1975, Maslov et al., 2001, Semionov and Kosinov, 2008). This is the reason why direct numerical simulations are important for the study of receptivity. For example, Ma and Zhong (2003, 2005) and Balakumar (2003, 2005) performed DNS of the receptivity of the supersonic boundary layer over a flat plate. The leading edge and the shock are taken into account in their computations. The numerical results showed that in the presence of free-stream acoustical, vortical and entropy disturbances, the first and second modes are excited.

Present work

In Chapter 2, two new receptivity mechanisms to impinging acoustic waves operating in supersonic boundary layers are investigated. Unlike previous studies of acoustic receptivity, where the sound waves have phase speeds comparable with or

larger than the free-stream velocity U_∞, the acoustic waves here have much slower ($\mathcal{O}(R^{-1/8}U_\infty)$) phase velocity, and their characteristic wavelength and frequency are of $\mathcal{O}(R^{-3/8}L)$ and $\mathcal{O}(R^{1/4}U_\infty/L)$ respectively, compatible with the triple-deck structure, where L is the distance to the leading edge and R the Reynolds number based on L and U_∞. A significant feature of a sound wave on the triple-deck scale is that an $\mathcal{O}(\varepsilon_s)$ perturbation in the free stream generates much stronger ($\mathcal{O}(\varepsilon_s R^{1/8})$) velocity fluctuations in the boundary layer. Two receptivity mechanisms are considered. The first is new, involving the interaction of two such acoustic waves and operating in a boundary layer over a smooth wall. The second involves the interaction between an acoustic wave and the steady perturbation induced by a wavy wall. The sound-sound, or sound-roughness, interactions generate a forcing in resonance with a neutral Tollmien-Schlichting wave (first Mack modes in the supersonic regime). The latter is thus excited near the lower branch of the neutral curve, and subsequently undergoes exponential amplification. The excitation through sound-sound interaction may offer a possible explanation for the appearance of instability modes downstream of their neutral locations as was observed in a supersonic boundary layer over a smooth wall. The triple-deck formalism is adopted to describe impingement and reflection of the acoustic waves, and ensuing receptivity, allowing the coupling coefficient to be calculated. The two receptivity processes with the acoustic waves on the triple-deck scale are much more effective compared with those involving usual sound waves, with the coupling coefficient being greater by a factor of $\mathcal{O}(R^{1/4})$ and $\mathcal{O}(R^{1/8})$ in the sound-sound and sound-roughness interactions, respectively. A parametric study for both the reflection and coupling coefficients is conducted for representative T-S waves, to assess the influence of the streamwise and spanwise wavenumbers, and the phase speed (or frequency) of the acoustic wave.

In Chapter 3, the connection between the inviscid and viscous branches of instability modes in supersonic boundary layers is studied following the previous investigation of Goldstein and Ricco (2018). In the literature, a variety of instability modes have been identified, and they were found to originate from different mechanisms and exhibit distinct characteristics (Mack, 1984). Viscous modes owe their existence to the destabilizing role of viscosity, and have small phase speeds and large wavelengths, relative to the free-stream velocity U_∞ and the boundary-layer thickness δ^*, respectively (Smith, 1989). Inviscid modes are associated with the so-called generalised inflection point, but non-inflectional inviscid modes have also been found. The phase speeds and wavelengths of these modes are typically of $\mathcal{O}(U_\infty)$ and $\mathcal{O}(\delta^*)$ respectively. It is important to map out, in the relevant parameter space, the stable/unstable regions and the associated borders (i.e. neutral

curves) of all these modes. However, the information and picture remain incomplete. On the one hand, some neutral modes (i.e. modes with a zero growth rate) appear to be 'isolated' rather than on any of the neutral curves. On the other hand, viscous neutral modes form only a very small part of the lower branch of the neutral curve with the nature of the modes on the major portion remaining unknown. Furthermore, the upper and lower branches of the neutral curve are connected, as indicated by finite-Reynolds-number calculations. A new intermediate regime, identified in a previous preliminary study (Yang, 2017), is discussed further in the chapter. This regime is described by triple-deck theory, although its scaling is not standard. The instability is studied and the dispersion relation is calculated for different Mach numbers. It is shown that this regime was missed by the previous work of Goldstein and Ricco (2018).

In Chapter 4, a new mechanism for the generation of T-S waves is investigated, which operates in supersonic boundary layers over smooth surfaces and builds on the study in Chapter 2. The mechanism involves an incident sound wave with its frequency and wavelength on the triple-deck scale and free-stream vortical disturbances with spanwise wavelength on the triple-deck scale too but long streamwise wavelength comparable with L. The long-wavelength vortical disturbances with $\mathcal{O}(\varepsilon_v)$ intensity in the free-stream induce in the boundary layer much larger $\mathcal{O}(\varepsilon_v R^{3/8})$ streamwise velocity and temperature/density, which manifest as streaks. With the appropriate choice of the spanwise wavelength on the triple deck scale, the acoustic signature and streaks interact in the main boundary layer as well as in the lower deck, to generate a forcing that is in resonance with a neutral first Mack mode. The latter is thus excited near the lower branch of the neutral curve. At a high Reynolds number, the triple-deck formalism is adopted to describe the scale conversion process and make quantitative predictions of impingement and reflection of the acoustic wave and the streak's spanwise length scale. The receptivity of this mechanism is found to be greater than those in Hernández and Wu (2019) and Wu (1999) by a factor of $\mathcal{O}(R^{1/8})$ and $\mathcal{O}(R^{3/8})$, respectively.

The present PhD research therefore constitutes a theoretical study of several new receptivity mechanisms in supersonic boundary layers at high Reynolds numbers, building on the previous study by Wu (1999). The content of Chapter 2 has been published in the Journal of Fluid Mechanics, as Hernández and Wu (2019).

2

Receptivity of supersonic boundary layers over smooth and wavy surfaces to impinging slow acoustic waves

2.1 Introduction

Laminar-turbulent transition of boundary layers represents an extraordinarily complicated process, which is, at present, not fully understood. It has numerous technological applications, e.g. being important for the prediction and reduction of drag and noise. In the supersonic regime, boundary layer transition plays a crucial role in the correct characterization of the flow and thermal fields around high-speed vehicles (Fedorov, 2011). In the presence of low-level free-stream turbulence, transition occurs via the so-called the natural route, which involves a sequence of stages (Morkovin et al., 1994) starting with receptivity, followed by linear instability, nonlinear growth and breakdown to turbulence (Morkovin, 1969, Reshotko, 1976).

Boundary-layer receptivity refers to the process in which external perturbations (e.g. oncoming sound waves, free-stream turbulence and entropy, and localized or distributed roughness) excite instability modes. These intrinsic instabilities may amplify to attain amplitudes far above those of the external disturbances,

eventually leading the boundary layer to turbulence. Instability modes that may arise depend on the Mach number. In the subsonic regime, they are Tollmien-Schlichting (T-S) waves, which have a viscous origin. In the super- and hyper-sonic regimes, there exist multiple families of modes (Mack, 1984) including the so-called first Mack modes, which are continuation of T-S modes into the compressible regime, and the second Mack modes, which are essentially inviscid.

Mathematically, the problem of receptivity is different from that of stability. The latter seeks normal modes, which gives rise to an eigenvalue problem. In receptivity theory, because of external forcing, an inhomogeneous boundary-value problem arises. A general unsteady disturbance in a uniform compressible flow can, to leading order, be decomposed into three independent components: acoustic, vorticity and entropy modes (Kovasznay, 1953). The first is a pressure fluctuation, which propagates through the fluid with the speed of sound. The other two represent, respectively, vorticity and temperature perturbations being convected at the free-stream velocity, and they have been used to model free-stream turbulence in many applications. Usually, none of the external disturbances alone can excite T-S waves because its wavelength would differ from those of the latter if its frequency is chosen to be the same. A crucial task of receptivity study is to identify the scale conversion or matching mechanism, by which the length and time scales of external disturbances are adjusted to match those of the instability, or the external disturbances produce a forcing with the length and time scales matching with those of the instability. The main goal of studying receptivity is to determine the amplitudes of the generated instability waves and, linked to the former, to identify which types of external disturbances can trigger the instability more effectively.

Shapiro (1977) and Kachanov et al. (1979) were among the earliest to study experimentally the generation of T-S waves by free-stream acoustical and vortical disturbances, respectively. Although the leading edge region was found to be important for excitation, the precise mechanisms had remained unknown until several theoretical discoveries on boundary-layer receptivity were made in the 1980s; for a detailed review, see, for example, Goldstein and Hultgren (1989). The triple-deck theory, which is based on high-Reynolds-number asymptotic approximations, has played an important role; this is not surprising since this formalism simplifies the mathematical description of the instability and specifies precisely the time and length scales of the instability modes (Lin, 1945, Smith, 1979b), which is crucial for studying receptivity. Using this approach, Terent'ev (1981) first analysed the generation of T-S modes by a short vibrating section of a flat plate. The vibrating

section generates a T-S wave effectively when its frequency and length are comparable with the characteristic frequency and wavelength of the T-S wave. Goldstein (1983) showed that a long-wavelength sound wave interacts with the strongly non-parallel mean flow near the leading edge, first to excite an asymptotic eigensolution called Lam-Rott mode. As its wavelength shortens due to the increase of the boundary-layer thickness, the Lam-Rott eigensolution finally evolves into a lower-branch T-S mode. This solution however undergoes severe decay before reaching the neutral stability point, rendering the mechanism fairly weak. A more efficient mechanism was proposed independently by Ruban (1984) and Goldstein (1985), in which a weak sound wave interacts with a roughness-induced perturbation to excite a T-S wave downstream. They pointed out that for T-S waves to be generated by acoustic disturbances, a resonance condition must hold, which means that the frequency of the oncoming sound must be chosen to be that of the T-S waves. Since this choice would make the wavelength much larger than that of T-S waves, it is crucial to introduce a lengthscale comparable with the wavelength of the T-S waves. This is achieved by including a suitable wall roughness, which causes a stationary disturbance in the boundary layer; an acoustic wave interacts with it to produce an unsteady forcing, whose lenghtscale and frequency match those of the T-S waves. Ruban et al. (2016) extended this theory to transonic boundary layers. De Tullio and Ruban (2015) performed direct numerical simulations (DNS) of the receptivity of subsonic compressible boundary layers to roughness-sound interaction. A comparison with the results of the asymptotic (triple-deck) theory showed that the latter hold down to moderate Reynolds numbers $R = \mathcal{O}(10^5)$, showing a good agreement for Mach number $M = 0.8$, and excellent agreement for $M = 0.2$.

Duck et al. (1996) considered the receptivity to free-stream vortical disturbances interacting with a localised roughness element on a flat plate. They demonstrate that although this type of disturbance does not penetrate into the boundary layer, it can interact with the roughness-induced perturbation at the outer edge of the boundary layer, thereby producing a forcing to generate a T-S mode. Dietz (1999) conducted a detailed experimental study of the receptivity to vortical disturbances which were introduced in a controlled manner. A comprehensive set of data was acquired. Prompted by these data, Wu (2001b) extended the analysis of Duck et al. (1996) to second order and to vortical disturbances with an arbitrary transverse distribution; the latter made a quantitative comparison with experiment possible. A good agreement was found between the second-order theory and the measurements.

A finite-Reynolds-number approach to receptivity was formulated by Zhigulev and Fedorov (1987), Choudhari and Streett (1992) and Crouch (1992). This method retains the essence of the Goldstein-Ruban theory, but uses inhomogeneous O-S equations instead of the triple-deck equations to compute the mean-flow distortion as well as the resultant T-S waves. The accuracy of the predictions was confirmed by comparisons with experiments. Of course, this approach is applicable to roughness with a sufficiently small height. For roughness elements with large enough heights that the mean-flow distortion becomes nonlinear, the O-S equation fails to describe both the mean-flow distortion and the scattering. The triple-deck or interactive boundary-layer formalisms need to be used instead (Bodonyi et al., 1989, Goldstein et al., 1987, Nayfeh and Ashour, 1994).

Receptivity due to the interaction of sound waves or vortical disturbances with a distributed roughness has also been addressed in the literature. The interaction can produce an unsteady forcing that has the frequency and wavenumber of a neutral mode. A theoretical study was made by Crouch (1992, 1994), using a finite-Reynolds-number (O-S equation) approach. However, the analysis did not consider the resonance region in the vicinity of the neutral curve, where the forcing resonates with the neutral T-S mode. Wu (2001a) presented a (second-order) asymptotic theory based on the triple-deck formalism. By analysing the resonance region, which is of crucial importance for determining correctly the initial amplitude of the excited T-S wave, he showed that the distributed receptivity is much stronger than that for localised roughness, with the coupling coefficient being larger by a factor of $\mathcal{O}(R^{3/16})$. The resonance could only be correctly accommodated by accounting for the non-parallel-flow effect.

The receptivity mechanisms highlighted above have also been studied experimentally and by DNS. The reader is referred to King and Breuer (2002), Würz et al. (2003) and Saric et al. (2002) for details. In summary, in the subsonic regime, boundary-layer receptivity, especial to acoustical disturbances, is quite well understood and accurately predicted, except for the case of extremely strong sound waves, where nonlinear effects arise and require further investigation (Saric and White, 1998).

Receptivity of supersonic boundary layers is less well understood in comparison with their subsonic counterparts. Mack (1984) and Ma and Zhong (2003) documented in great detail various inviscid and viscous instability modes, which were identified primarily by extensive numerical computations solving the Rayleigh and O-S equations. Relevant high-Reynolds-number asymptotic descriptions were given by Smith (1989), Smith and Brown (1990) and Blackaby et al. (1993) among

others. Most receptivity mechanisms identified for subsonic boundary layers continue to operate, but with additional physical parameters (e.g. Mach number) and modes on different scalings, their effectiveness may differ significantly, and new mechanisms may be in action. Fedorov and Khokhlov (1991) and Fedorov (2003a) elucidated how the scattering and diffraction of acoustic waves in the leading-edge region generate the so-called slow and fast instability modes, which are the earliest form of instability. Fedorov (2003b) analyzed generation of second Mack modes due to acoustic waves interacting with localized and distributed surface roughness, whereas Fedorov (2013) investigated receptivity to small solid particles present in the free stream. Wu (1999) proposed a different mechanism, in which a sound wave and a vortical disturbance with suitable frequencies and wavenumbers interact to generate a forcing in resonance with, and hence generates, a neutral T-S mode. More recently, Qin and Wu (2016) studied the receptivity of a hypersonic boundary layer past a wedge, where the shock emanating from the apex makes a small angle with respect to the wedge surface, and thus changes the instability substantially (Blackaby et al., 1993). They showed that each of the three types of free-stream disturbances interacts with the shock to produce a slow acoustic wave downstream which can resonate with a T-S mode.

Experimental studies of supersonic boundary-layer receptivity are extremely difficult, and only a few have been carried out (e.g. Kendall, 1975, Maslov et al., 2001, Semionov and Kosinov, 2008). DNS therefore stand as a useful tool. Ma and Zhong (2003, 2005) and Balakumar (2003, 2005) performed DNS of the receptivity of the supersonic boundary layer over a flat plate. The leading edge and the shock were taken into account in their computations. The numerical results showed that in the presence of free-stream acoustical, vortical and entropy disturbances, the first and second modes are excited. Qualitatively similar findings have also been revealed for boundary layers over a parabola, blunt plates and cones; the reader is referred to Zhong and Wang (2012) for details. However, the precise excitation mechanisms and processes are yet to be fully clarified. It appeared that the free-stream disturbances interact first with the shock, generating acoustic waves downstream, which then excite slow and fast instability modes through the mechanism of Fedorov and Khokhlov (1991). The slow mode evolves into a first Mack mode. Further downstream, the first mode and the fast mode may be converted to a second mode at the so-called synchronization point (Fedorov and Khokhlov, 2001). This interpretation is applicable to instability modes with streamwise and spanwise wavenumbers, α and β, satisfying the restriction $\beta < \sqrt{M^2-1}\alpha$. For those with $\beta > \sqrt{M^2-1}\alpha$, the mechanism of sound-vorticity interaction (Wu, 1999) may be relevant. Recently, Goldstein and Ricco (2018) showed that the

direct excitation by vortical disturbances, as described by Ricco and Wu (2007), is likely to be operating.

In this chapter, we will investigate the excitation of lower-branch viscous first Mack modes by slow acoustic waves impinging on a supersonic boundary layer. Unlike previous studies of acoustic receptivity, where the phase speed of sound waves in the streamwise direction is of $\mathcal{O}(1)$ or much greater (in the incompressible limit), here we consider the sound waves which have much smaller, $\mathcal{O}(R^{-1/8})$, phase speeds, and their characteristic wavelength and frequency comply with the triple-deck structure. This particular scaling is significant because a perturbation of $\mathcal{O}(\varepsilon_s)$ in the free stream generates a signature of order $\mathcal{O}(\varepsilon_s R^{1/8})$ in the lower deck. The impingement and reflection of each sound wave is described by the triple-deck theory. A new receptivity mechanism is to be proposed, which involves the impingement of two acoustic waves on a supersonic boundary layer at certain angles, and the interaction between them generates a forcing in resonance with a neutral T-S mode. Unlike the mechanism in the Goldstein-Ruban theory, the scale conversion does not require any kind of wall roughness and therefore operates over smooth surfaces. This roughness-free receptivity is somewhat similar to the sound-vorticity mechanism of Wu (1999), but is much more effective. Additionally, we will also consider the receptivity due to the interaction of an acoustic wave with a wavy wall. The mechanism is in principle the same as for the subsonic regime, but is stronger by a factor of $\mathcal{O}(R^{1/8})$ now with the sound wave on the triple-deck scale.

The chapter is organized as follows. The problem is formulated in §2.2, where the equations for a supersonic boundary layer are presented and the physical idea of the present receptivity mechanism is explained using the dispersion relation for slow acoustic waves (§2.2.3). The asymptotic scalings for wavenumbers and frequencies are specified in §2.2.4. This is followed by the asymptotic expansions of the flow variables in the upper, main and lower decks (§2.2.5-§2.2.7). A neutral T-S eigenmode with a yet unknown amplitude function, has to be included at the right order in the expansions. The impingement and reflection of acoustic waves are analysed, and the interaction between the sound-wave-induced unsteady perturbation and the roughness-induced steady one is considered, leading to an evolution equation for the amplitude function. By matching the T-S wave solution to the upstream forced response, we are able to determine in §2.3 the meaningful amplitude thereby introducing an appropriate coupling coefficient, which measures the effectiveness of the receptivity mechanism. The interaction between a slow acoustic wave on the triple-deck scale and the perturbation caused by a wavy

wall is considered in §2.4. A parametric study is conducted in §2.5 to assess the influence of relevant parameters on the reflection and coupling coefficients. A summary and discussions are given in §2.6.

2.2 Formulation and scalings

We consider the two-dimensional compressible boundary layer over a semi-infinite flat plate. The oncoming flow is assumed to be uniform with a velocity U_∞, density ρ_∞, temperature T_∞ and sound speed a_∞. Superimposed on this background flow are three-dimensional small-amplitude disturbances of acoustic nature. We define the Reynolds number R and the Mach number M as

$$R = \rho_\infty U_\infty L/\mu_\infty, \quad M = U_\infty/a_\infty, \tag{2.1}$$

where μ_∞ is the free-stream dynamic viscosity and the reference length scale L is chosen to be the distance to the leading edge. In the present work, we will take R to be asymptotically large, $R \gg 1$, and focus on the supersonic regime, $M > 1$ with $M = \mathcal{O}(1)$.

We introduce a Cartesian coordinate system (x_1,x_2,x_3) with its origin at the leading edge of the plate, where x_1 and x_2 are along and normal to the surface, respectively, while x_3 is in the spanwise direction, all being non-dimensionalized by L. The time variable t is normalized by L/U_∞. The velocity $\mathbf{u} = (u, v, w)$, density ρ, temperature τ, pressure p, and the shear and bulk viscosities, μ and μ', are non-dimensionalized by U_∞, ρ_∞, T_∞, $\rho_\infty U_\infty^2$ and μ_∞ respectively. The fluid is taken to be a perfect gas with a constant ratio of specific heats, γ. The non-dimensional Navier-Stokes (N-S) equations then read,

$$\frac{\partial \rho}{\partial t} + \nabla \cdot (\rho \mathbf{u}) = 0, \tag{2.2}$$

$$\rho \frac{D\mathbf{u}}{Dt} = -\nabla p + \frac{1}{R}\nabla \cdot (2\mu \mathbf{e}) + \nabla((\mu' - \frac{2}{3}\mu)\nabla \cdot \mathbf{u}), \tag{2.3}$$

$$\rho \frac{D\tau}{Dt} = (\gamma - 1)M^2 \frac{Dp}{Dt} + \frac{1}{RPr}\nabla \cdot (\mu \nabla T) + \frac{(\gamma - 1)M^2}{R}\Phi, \tag{2.4}$$

$$\gamma M^2 p = \rho \tau, \tag{2.5}$$

where $\mathbf{e}$ and Φ stand for the strain rate tensor and the dissipation function, re-

spectively:

$$e_{ij} = \frac{1}{2}\left(\frac{\partial u_i}{\partial x_j} + \frac{\partial u_j}{\partial x_i}\right), \quad \Phi = 2\mu \mathbf{e} : \mathbf{e} + (\mu' - \frac{2}{3}\mu)(\nabla \cdot \mathbf{u})^2, \tag{2.6}$$

and Pr is the Prandtl number. Note that $\mu' = 0$ for a monoatomic gas. The viscosity μ may obey Chapman or Sutherland law. The operators such as ∇ are defined with respect to the Cartesian coordinates (x_1, x_2, x_3) defined above.

2.2.1 The base flow

In order to describe the boundary-layer flow, we introduce

$$(x, y, z) = (x_1, R^{1/2}x_2, x_3). \tag{2.7}$$

The base flow velocity is denoted by $(U_B, R^{-1/2}V_B, 0)$, the pressure by P_B, the density and temperature by R_B and T_B respectively. If, for simplicity, we assume that $Pr = 1$ and the wall is adiabatic, then $\partial T_B/\partial y = 0$ at $y = 0$ and the temperature profile $T_B(y)$ is related to $U_B(y)$ through $T_B = 1 + \frac{\gamma-1}{2}M^2(1 - U_B^2)$. Otherwise, the base flow is obtained by solving the similarity equations. Since $T_B \to 1$ and $R_B \to 1$ as $y \to \infty$ while P_B is independent of y, it follows that $P_B = 1/(\gamma M^2)$, and the state equation gives

$$R_B T_B = \gamma M^2 P_B. \tag{2.8}$$

For the case of a flat plate, there exists a compressible version of the Blasius similarity solution, and its streamwise velocity profile is given by (Stewartson, 1964)

$$U_B = F'(\eta) \quad \text{with} \quad \eta = \frac{1}{\sqrt{x}}\int_0^y R_B dy, \tag{2.9}$$

where η is the Dorodnitsyn-Howarth variable. The first-term expansion for the base flow as $y \to 0$ reads

$$U_B(y) \to \lambda C^{-1/2}\tau_w^{-1}y + \mathcal{O}(y^2), \tag{2.10}$$

where $\lambda = \lambda_0 x^{-1/2}$ is the local skin friction with $\lambda_0 = F''(0)$, τ_w is the temperature at the wall, and the constant $C = 1$ if the viscosity μ is the Chapman's viscosity law, but for the Sutherland's law, $C = \tau_w^{1/2}(1 + 110/T_\infty)/(\tau_w + 110/T_\infty)$. From

(2.8), $R_B = 1/T_B$ and so

$$R_B \to \tau_w^{-1} + \mathcal{O}(y^2) \quad \text{as} \quad y \to 0. \tag{2.11}$$

2.2.2 Equations for the perturbation

The total flow field consists of the steady compressible boundary-layer flow and a small-amplitude perturbation,

$$(u, v, w, p, \rho, \tau) = (U_B, R^{-1/2}V_B, 0, \frac{1}{\gamma M^2}, R_B, T_B) + (\tilde{u}, \tilde{v}, \tilde{w}, \tilde{p}, \tilde{\rho}, \tilde{\tau}). \tag{2.12}$$

After substituting (2.12) into (2.2)-(2.6), and using the second relation in (2.7), the governing equations for the perturbation read

$$\tilde{\rho}_t + U_B\tilde{\rho}_x + R_B\tilde{u}_x + \varepsilon^{-4}(R_B\tilde{v}_y + R_{B,y}\tilde{v}) + R_B\tilde{w}_z = N_c, \tag{2.13}$$

$$R_B(\tilde{u}_t + U_B\tilde{u}_x + \varepsilon^{-4}U_{B,y}\tilde{v}) = -\tilde{p}_x + (\mu_B\tilde{u}_y)_y + (U_{B,y}\tilde{\tau})_y + N_u, \tag{2.14}$$

$$R_B(\tilde{v}_t + U_B\tilde{v}_x) = -\varepsilon^{-4}\tilde{p}_y + 2(\mu_B\tilde{v}_y)_y + N_v, \tag{2.15}$$

$$R_B(\tilde{w}_t + U_B\tilde{w}_x) = -\tilde{p}_z + (\mu_B\tilde{w}_y)_y + (U_{B,y}\tilde{\tau})_y + N_w, \tag{2.16}$$

$$\begin{aligned} R_B(\tilde{\tau}_t + U_B\tilde{\tau}_x + \varepsilon^{-4}T_{B,y}\tilde{v}) =& (\gamma-1)M^2(\tilde{p}_t + U_B\tilde{p}_x) + (\mu_B\tilde{\tau}_y)_y + (T_{B,y}\tilde{\tau})_y \\ &+ 2(\gamma-1)M^2\mu_B U_{B,y}\tilde{u}_y + N_\tau, \end{aligned} \tag{2.17}$$

$$\gamma M^2\tilde{p} = T_B\tilde{\rho} + R_B\tilde{\tau} + \tilde{\rho}\tilde{\tau}, \tag{2.18}$$

where $\mu_B = \mu(T_B)$, and we have defined the small parameter $\varepsilon = R^{-1/8}$; the nonlinear terms are given by (Wu and Hogg, 2006)

$$N_c = -((\tilde{\rho}\tilde{u})_x + \varepsilon^{-4}(\tilde{\rho}\tilde{v})_y + (\tilde{\rho}\tilde{w})_z),$$

$$N_u = -R_B(\tilde{u}\tilde{u}_x + \varepsilon^{-4}\tilde{v}\tilde{u}_y + \tilde{w}\tilde{u}_z) + \tilde{\rho}\tilde{p}_x/R_B,$$

$$N_v = -R_B(\tilde{u}\tilde{v}_x + \varepsilon^{-4}\tilde{v}\tilde{v}_y + \tilde{w}\tilde{v}_z) + \varepsilon^{-4}\tilde{\rho}\tilde{p}_y/R_B,$$

$$N_w = -R_B(\tilde{u}\tilde{w}_x + \varepsilon^{-4}\tilde{v}\tilde{w}_y + \tilde{w}\tilde{w}_z) + \tilde{\rho}\tilde{p}_z/R_B,$$

$$N_\tau = -R_B(\tilde{u}\tilde{\tau}_x + \varepsilon^{-4}\tilde{v}\tilde{\tau}_y + \tilde{w}\tilde{\tau}_z) + (\gamma-1)M^2\left[(\tilde{u}\tilde{p}_x + \varepsilon^{-4}\tilde{v}\tilde{p}_y + \tilde{w}\tilde{p}_z) - \tilde{\rho}(\tilde{p}_t + U_B\tilde{p}_x)/R_B\right].$$

In (2.13)-(2.17), terms which are unimportant to the order of accuracy in the present work are ignored; these include the streamwise derivatives of the mean-flow quantities (e.g. $U_{B,x}$, $T_{B,x}$) representing the non-parallel-flow effect, the streamwise momentum and thermal diffusion, and all the terms in the dissipation function

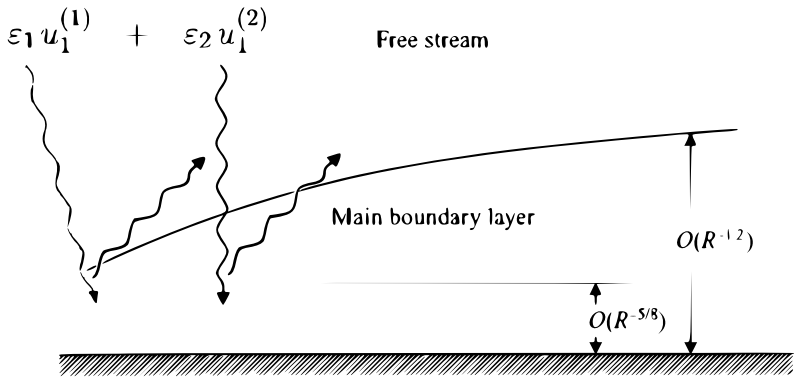


Figure 2.1: Sketch of the physical setting showing the impingment/penetration of two acoustic waves.

Φ, except the leading-order one (i.e. the second last term on the right-hand side of (2.17)).

It is convenient to combine equations (2.17) and (2.18) to give

$$\tilde{\rho}_t+U_B\tilde{\rho}_x+\varepsilon^{-4}R_{B,y}\tilde{v} = R_BM^2(\tilde{p}_t+U_B\tilde{p}_x)+T_B^2\tilde{\rho}_{yy}-2(\gamma-1)M^2U_{B,y}\tilde{u}_y+N_\rho, \quad (2.19)$$

with $N_\rho = -R_B(\partial_t + U_B\partial_x)(\tilde{\rho}\tilde{\tau}) - R_BN_\tau$.

2.2.3 Physical idea and resonant interaction

Suppose that two three-dimensional sound waves are present in the free stream (figure 2.1), and they are represented by

$$\varepsilon_1 e^{i(\alpha_1 x+\beta_1 z+\gamma_1 y-\omega_1 t)} \quad \text{and} \quad \varepsilon_2 e^{i(\alpha_2 x+\beta_2 z+\gamma_2 y-\omega_2 t)}. \quad (2.20)$$

From the dispersion relation obtained with the inviscid approximation, the phase speeds are

$$c = \frac{\omega}{\alpha} = 1 \pm \frac{\sqrt{\alpha^2+\beta^2+\gamma^2}}{\alpha M},$$

where $+/-$ stands for the fast/slow acoustic waves respectively, and α, β, γ and c refer to α_j, β_j, γ_j and c_j with $j = 1, 2$. The dispersion relation may be written as $M(\omega - \alpha) = \pm(\alpha^2+\beta^2+\gamma^2)^{1/2}$, or equivalently

$$(1-M^2)\left[\alpha - \frac{M^2\omega}{M^2-1}\right]^2 + \beta^2 + \gamma^2 = \frac{M^2\omega^2}{1-M^2}, \quad (2.21)$$

an equation representing a conic section for a given ω in the wavenumber space (α, β, γ): an ellipse if $M < 1$ and a hyperbola when $M > 1$. The hyperbola consists of the left and right branches, which lie in the regions $\alpha < M\omega/(M+1)$ and $\alpha > M\omega/(M-1)$ respectively. The interaction between the two waves in (2.20) generates two forms of forcing proportional to $e^{i\{(\alpha_1 \pm \alpha_2)x + (\beta_1 \pm \beta_2)z - (\omega_1 \pm \omega_2)t\}}$. The forcing from the sum/difference interactions, corresponding to the $+/-$ sign, would be in resonance with a neutral T-S mode $e^{i\{\alpha_{TS}x + \beta_{TS}z - \omega_{TS}t\}}$ if their wavenumbers and frequencies satisfy the relations

$$\alpha_1 \pm \alpha_2 = \alpha_{TS}, \quad \beta_1 \pm \beta_2 = \beta_{TS}, \quad \omega_1 \pm \omega_2 = \omega_{TS}, \tag{2.22}$$

which will be referred to as the resonance conditions. Our focus will be on first Mack modes, which have larger amplification rates than second Mack modes for $M < 4.5$, beyond which second modes become more unstable (Mack, 1984). In the lower-branch regime, first Mack modes have asymptotically small phase speeds, i.e. $\omega_{TS} \ll \alpha_{TS}$ (in fact, $\omega_{TS} = \mathcal{O}(R^{-1/8}\alpha_{TS})$, see below) at large R. Typical sound waves have $\mathcal{O}(1)$ phase speeds, $\omega_j = \mathcal{O}(\alpha_j)$ and so $\omega_1 + \omega_2 = \mathcal{O}(\alpha_1 + \alpha_2)$. The required resonance conditions for the sum interaction cannot possibly be met for first Mack modes. The resonance conditions for the difference interaction can be satisfied by a pair of sound waves with $\mathcal{O}(\alpha_1) = \mathcal{O}(\alpha_2) = \mathcal{O}(\alpha_{TS})$ but nearly the same frequencies, ω_1 and ω_2, suitably chosen such that $\omega_1 - \omega_2 = \omega_{TS} \ll \omega_1, \omega_2$. However, for sound waves with $c = \mathcal{O}(1)$, the induced signature in the boundary layer is of the same order of magnitude as in the free stream. They are less effective in generating first Mack modes that those with $c \ll 1$ or equivalently $\omega \ll \alpha$. It is however worth pointing out that the general mechanism of sound-sound interaction operates to excite second Mack modes as well; for example, the interaction of slow and fast sound waves does so, as was shown by DNS (Gao et al., 2015).

When $\omega \ll \alpha$, the dispersion relation (2.21) reduces to $\beta^2 + \gamma^2 = (M^2 - 1)\alpha^2$, which is possible only in the supersonic regime $M > 1$. It follows that the wavenumbers of the two interacting acoustic waves have to satisfy

$$|\beta_1| < \alpha_1\sqrt{M^2 - 1}, \quad |\beta_2| < \alpha_2\sqrt{M^2 - 1}. \tag{2.23}$$

The difference interaction between the two slow acoustic waves can excite a T-S mode if (2.22) with the $-$ sign hold. For a T-S wave, its wavenumbers must satisfy (Smith, 1989)

$$\beta_{TS} > \alpha_{TS}\sqrt{M^2 - 1}, \tag{2.24}$$

which requires that

$$\beta_1 - \beta_2 > (\alpha_1 - \alpha_2)\sqrt{M^2 - 1}. \tag{2.25}$$

We will show that for any $(\alpha_{TS}, \beta_{TS})$, it is always possible to find (α_1, β_1) and (α_2, β_2) to satisfy (2.22) and (2.25). In contrast, the forcing from the sum interaction cannot be in resonance since $\beta_1 + \beta_2 < (\alpha_1 + \alpha_2)\sqrt{M^2 - 1}$, and is therefore discarded.

In summary, we focus on the difference interaction between sound waves with phase speeds $c_j = \omega_j/\alpha_j \ll 1$. The ensuing receptivity mechanism is very strong, as will be shown later. A finite-Reynolds-number formulation for the receptivity is possible but is left to the future. Here we take a high-Reynolds-number approach, which has the advantage of being mathematically consistent, probing into the detailed excitation process and giving explicit analytical results.

2.2.4 Asymptotic scalings

The lower-branch first Mack modes in a supersonic boundary layer have the characteristic scalings $\omega_{TS} = R^{1/4}\hat{\omega}_{TS}$ and $(\alpha_{TS}, \beta_{TS}) = R^{3/8}(\hat{\alpha}_{TS}, \hat{\beta}_{TS})$ for the frequency and wavenumbers (Smith, 1989), the same as the T-S waves in the incompressible regime. In the present work, we assume that the two sound waves are both on the triple-deck scale, and thus their wavenumbers and frequencies are scaled as

$$(\alpha_j, \beta_j) = R^{3/8}C^{-3/8}\tau_w^{-3/2}(\hat{\alpha}_j, \hat{\beta}_j), \quad \omega_j = R^{2/8}C^{-1/4}\tau_w^{-1}\hat{\omega}_j, \quad (j = 1, 2). \tag{2.26}$$

Note that the phase speed $c_j = \mathcal{O}(R^{-1/8})$, which is what a 'slow acoustic wave' means precisely in the present work. In terms of the rescaled quantities $\hat{\alpha}_j$, $\hat{\beta}_j$ and $\hat{\omega}_j$, the resonance conditions (2.22) for the difference interaction are expressed as

$$\hat{\alpha}_1 - \hat{\alpha}_2 = \hat{\alpha}_{TS}, \quad \hat{\beta}_1 - \hat{\beta}_2 = \hat{\beta}_{TS}, \quad \hat{\omega}_1 - \hat{\omega}_2 = \hat{\omega}_{TS}. \tag{2.27}$$

In view of (2.26), we introduce the time, streamwise and spanwise variables

$$\bar{t} = R^{2/8}C^{-1/4}\tau_w^{-1}t, \quad \bar{x} = R^{3/8}C^{-3/8}\tau_w^{-3/2}x, \quad \bar{z} = R^{3/8}C^{-3/8}\tau_w^{-3/2}z. \tag{2.28}$$

The impingement of each sound wave is also described by the triple-deck theory, which allows us to calculate the reflection coefficient and the signature induced in the boundary layer.

Since the unsteady fluctuation driven by the acoustic pressure acquires $\mathcal{O}(\varepsilon_s R^{1/8})$

in the lower deck, the dominant interaction between the two impinging sound waves takes place there. As was first pointed out by Wu (1999) for the vortical-sound interaction, the forced response evolves into a T-S mode on approaching the neutral point, x_0, where the resonance conditions in (2.27) are met. In order to describe this change of the character, it is necessary to include the non-parallel-flow effect, which becomes important in an $\mathcal{O}(\bar{\varepsilon})$ neighbourhood of x_0, where $\bar{\varepsilon} = R^{-3/16}C^{3/16}\tau_w^{3/4}$ (Ruban, 1983, Hall and Smith, 1984). The evolution of the forced response to an eigenmode is described by the variable (Wu, 1999)

$$x_1 = (x - x_0)/\bar{\varepsilon}, \tag{2.29}$$

and the amplitude of the T-S wave will be a function of x_1. We may set $x_0 = 1$ by taking L to be the distance from the neutral point to the leading edge. The wall shear stress of the base flow, $\lambda = \lambda_0 x^{-1/2}$, is therefore expanded about $x_0 = 1$ as

$$\lambda = \lambda_0 + \bar{\varepsilon}\lambda_1 x_1 \quad \text{with} \quad \lambda_1 = -\lambda_0/2. \tag{2.30}$$

2.2.5 Upper deck

The transverse extent of the upper deck is $\mathcal{O}(R^{-3/8}L)$, and thus a wall-normal variable $\bar{y} = R^{-1/8}C^{-3/8}\tau_w^{-3/2}y$ is introduced. The mean flow is $(U_B, V_B, W_B, P_B, R_B, T_B) = (1, 0, 0, \frac{1}{\gamma M^2}, 1, 1)$, and the expansion for the perturbation takes the form

$$\tilde{\mathbf{u}} = \varepsilon_s \mathbf{u_1} + \varepsilon_s^2 \bar{\varepsilon}^{-1} R^{2/8}(\mathbf{u}_{TS}E_{TS} + \text{c.c.}) + \varepsilon_s^2 R^{2/8}\mathbf{u_2} + \cdots, \tag{2.31}$$

$$\tilde{p} = \varepsilon_s p_1 + \varepsilon_s^2 \bar{\varepsilon}^{-1} R^{2/8}(p_{TS}E_{TS} + \text{c.c.}) + \varepsilon_s^2 R^{2/8} p_2 + \cdots, \tag{2.32}$$

$$\tilde{\rho} = \varepsilon_s \rho_1 + \varepsilon_s^2 \bar{\varepsilon}^{-1} R^{2/8}(\rho_{TS}E_{TS} + \text{c.c.}) + \varepsilon_s^2 R^{2/8} \rho_2 + \cdots, \tag{2.33}$$

$$\tilde{\tau} = \varepsilon_s \tau_1 + \varepsilon_s^2 \bar{\varepsilon}^{-1} R^{2/8}(\tau_{TS}E_{TS} + \text{c.c.}) + \varepsilon_s^2 R^{2/8} \tau_2 + \cdots, \tag{2.34}$$

where

$$E_{TS} = \exp\left\{i(\hat{\alpha}_{TS}\bar{x} + \hat{\beta}_{TS}\bar{z} - \hat{\omega}_{TS}\bar{t})\right\},$$

and we remind the reader that $\varepsilon_1 = \varepsilon_2 = \varepsilon_s$ has been chosen without loss of generality. The $\mathcal{O}(\varepsilon_s)$ terms represent the impinging and reflected sound waves. The $\mathcal{O}(\varepsilon_s^2 R^{2/8})$ terms represent the upper-deck signature of the perturbation forced by the sound-sound interaction in the lower deck; these terms are greater than $\mathcal{O}(\varepsilon_s^2)$ terms which would be generated by the sound-sound interaction in the upper deck. Due to the resonant nature of the forcing, the T-S mode excited has a magnitude larger by a factor $\bar{\varepsilon}^{-1} = \mathcal{O}(R^{3/16})$. An additional condition must

be satisfied, $\varepsilon_s \ll R^{-7/16}$, so that the asymptotic expansions in (2.31)-(2.34) are ordered.

Leading order

Substitution of (2.31) – (2.34) along with the base flow and (2.28) into (2.13) – (2.18) yields, at $\mathcal{O}(\varepsilon_s)$, the linearized equations,

$$\frac{\partial \rho_1}{\partial \bar{x}} + \nabla \cdot \mathbf{u_1} = 0, \quad \frac{\partial \mathbf{u_1}}{\partial \bar{x}} = -\nabla p_1, \quad \frac{\partial \tau_1}{\partial \bar{x}} = (\gamma - 1) M^2 \frac{\partial p_1}{\partial \bar{x}}, \tag{2.35}$$

$$\gamma M^2 p_1 = \tau_1 + \rho_1. \tag{2.36}$$

Note that for perturbations with $\mathcal{O}(R^{2/8})$ frequency and $\mathcal{O}(R^{3/8})$ wavenumbers, their governing equations in the upper deck are quasi-steady. Equations (2.35) – (2.36) can be combined to obtain an equation for the pressure p_1,

$$M^2 \frac{\partial^2 p_1}{\partial \bar{x}^2} - \nabla^2 p_1 = 0, \tag{2.37}$$

where the operators ∇ and ∇^2 have been defined with respect to the upper-deck variables $\bar{x}$, $\bar{y}$ and $\bar{z}$.

The solution for $\mathbf{u_1}$, p_1, ρ_1 and τ_1 can be expressed as the sum of two acoustic modes,

$$\mathbf{u_1} = \mathbf{u_1^{(1)}} + \mathbf{u_1^{(2)}}, \quad p_1 = p_1^{(1)} + p_1^{(2)}, \quad \rho_1 = \rho_1^{(1)} + \rho_1^{(2)}, \quad \tau_1 = \tau_1^{(1)} + \tau_1^{(2)}, \tag{2.38}$$

where we assume the solution to be of the travelling-wave form, namely

$$(\mathbf{u_1^{(j)}}, p_1^{(j)}, \rho_1^{(j)}, \tau_1^{(j)}) = (\hat{\mathbf{u}}_\mathbf{1}^{(j)}, \hat{p}_1^{(j)}, \hat{\rho}_1^{(j)}, \hat{\tau}_1^{(j)}) E_j + \text{c.c} \quad \text{with} \quad E_j = e^{i(\hat{\alpha}_j \bar{x} + \hat{\beta}_j \bar{z} - \hat{\omega}_j \bar{t})}. \tag{2.39}$$

In order to allow for wave reflection, $\hat{p}_1^{(j)}$ will take the form

$$\hat{p}_1^{(j)} = p_a^{(j)} (e^{i\hat{\gamma}_j \bar{y}} + \mathcal{R}^{(j)} e^{-i\hat{\gamma}_j \bar{y}}), \tag{2.40}$$

where the first term represents the incident wave and the second the reflected wave, and $\mathcal{R}^{(j)}$ is the reflection coefficient to be found as part of the solution. In the following analysis, we will take $p_a^{(j)} = 1$ without losing generality. Substituting $p_1^{(j)}$ into (2.37) yields a relationship for the wavenumbers

$$(M^2 - 1)\hat{\alpha}_j^2 - \hat{\beta}_j^2 - \hat{\gamma}_j^2 = 0. \tag{2.41}$$

The matching condition with the main-deck solution reads

$$\frac{\partial p_1}{\partial \bar{y}} = -\frac{\partial v_1}{\partial \bar{x}} \quad \text{at} \quad \bar{y} = 0, \tag{2.42}$$

where v_1 will be given by the so-called outer limit of the main-deck solution.

T-S wave

Working with the $\mathcal{O}(\varepsilon_s^2 \bar{\varepsilon}^{-1} R^{2/8})$ terms in (2.31)-(2.34), we obtain the equations governing the T-S wave,

$$\frac{\partial^2 p_{TS}}{\partial \bar{y}^2} - \hat{\gamma}_{TS}^2 p_{TS} = 0, \quad i\hat{\alpha}_{TS} v_{TS} = -\frac{\partial p_{TS}}{\partial \bar{y}}, \tag{2.43}$$

where $\hat{\gamma}_{TS}^2 = (1 - M^2)\hat{\alpha}_{TS}^2 + \hat{\beta}_{TS}^2$. The solution is found as

$$p_{TS} = \hat{p}_{TS} A(x_1) e^{-\hat{\gamma}_{TS}\bar{y}}, \quad v_{TS} = -i\frac{\hat{\gamma}_{TS}}{\hat{\alpha}_{TS}} \hat{p}_{TS} A(x_1) e^{-\hat{\gamma}_{TS}\bar{y}}, \tag{2.44}$$

where $A(x_1)$ is the amplitude of the T-S wave. The main mathematical task is to derive the evolution equation for $A(x_1)$. This will done by analysing the solution at the next order, which represents the response to the sound-sound interaction. The reader may in the first reading skip the technical details, and turn directly to the key results of physical relevance, which include the reflection coefficient (2.82), the acoustic signature in the boundary layer, (2.85)-(2.86) and (2.87), the dispersion relation for the instability (2.93), and the final amplitude equation (2.108).

Response in the upper deck

At $\mathcal{O}(\varepsilon_s^2 R^{2/8})$, the equations are

$$\frac{\partial \rho_2}{\partial \bar{x}} + \nabla \cdot \mathbf{u_2} = -\left(\frac{\partial \rho_{TS}}{\partial x_1} + \frac{\partial u_{TS}}{\partial x_1}\right) E_{TS}, \tag{2.45}$$

$$\frac{\partial \mathbf{u_2}}{\partial \bar{x}} = -\nabla p_2 + \left(\frac{\partial \mathbf{u}_{TS}}{\partial x_1} - \frac{\partial p_{TS}}{\partial x_1}\mathbf{i}\right) E_{TS}, \tag{2.46}$$

$$\frac{\partial \tau_2}{\partial \bar{x}} = -\frac{\partial \tau_{TS}}{\partial x_1} E_{TS} + (\gamma - 1)M^2 \frac{\partial p_2}{\partial \bar{x}} + (\gamma - 1)M^2 \frac{\partial p_{TS}}{\partial x_1} E_{TS}, \tag{2.47}$$

$$\gamma M^2 p_2 = \tau_2 + \rho_2. \tag{2.48}$$

Elimination of $\mathbf{u}_2$, τ_2 and ρ_2 among (2.45) – (2.48) gives the equation for p_2,

$$M^2\frac{\partial^2 p_2}{\partial \bar{x}^2} - \nabla^2 p_2 = 2i(1-M^2)\hat{\alpha}_{TS}A'(x_1)\hat{p}_{TS}e^{-\hat{\gamma}_{TS}\bar{y}}E_{TS}. \tag{2.49}$$

The solution for p_2 takes the form $p_2 = (\hat{P}_2(\bar{y})E_{TS} + \text{c.c.})$, where

$$\hat{P}_2 = \left\{\hat{p}_2 + \frac{i\hat{\alpha}_{TS}}{\hat{\gamma}_{TS}}(1-M^2)A'\bar{y}\right\}e^{-\hat{\gamma}_{TS}\bar{y}}. \tag{2.50}$$

with $\hat{p}_2$ being an arbitrary function of x_1. The vertical velocity v_2 can readily be obtained from the vertical momentum equation in (2.46) after substituting p_2, but it suffices to note that as $\bar{y} \to 0$,

$$p_2 \to \hat{p}_2 E_{TS}, \tag{2.51}$$

$$v_2 \to \left(-\frac{(1-M^2)}{\hat{\gamma}_{TS}}A'\hat{p}_{TS} + \frac{\hat{\gamma}_{TS}}{i\hat{\alpha}_{TS}}\hat{p}_2 + \frac{\hat{\gamma}_{TS}}{\hat{\alpha}_{TS}^2}A'\hat{p}_{TS}\right)E_{TS}. \tag{2.52}$$

2.2.6 Main deck

The transverse variable is now $\tilde{y} = C^{-1/2}\tau_w^{-1}y = \mathcal{O}(1)$ and the expansion for the perturbation takes the form

$$\tilde{u} = C^{1/8}\tau_w^{1/2}\left[\varepsilon_s R^{1/8}(\hat{u}_1^{(1)}E_1 + \hat{u}_1^{(2)}E_2) + \varepsilon_s^2\bar{\varepsilon}^{-1}R^{3/8}\tilde{u}_{TS} + \varepsilon_s^2 R^{3/8}\hat{u}_2 E_{TS} + \cdots\right], \tag{2.53}$$

$$\tilde{v} = C^{1/4}\left[\varepsilon_s(\hat{v}_1^{(1)}E_1 + \hat{v}_1^{(2)}E_2) + \varepsilon_s^2\bar{\varepsilon}^{-1}R^{2/8}\tilde{v}_{TS} + \varepsilon_s^2 R^{2/8}\hat{v}_2 E_{TS} + \cdots\right], \tag{2.54}$$

$$\tilde{w} = C^{1/4}\tau_w\left[\varepsilon_s(\hat{w}_1^{(1)}E_1 + \hat{w}_1^{(2)}E_2) + \varepsilon_s^2\bar{\varepsilon}^{-1}R^{2/8}\tilde{w}_{TS} + \varepsilon_s^2 R^{2/8}\hat{w}_2 E_{TS} + \cdots\right], \tag{2.55}$$

$$\tilde{p} = C^{1/4}\left[\varepsilon_s(\hat{p}_1^{(1)}E_1 + \hat{p}_1^{(2)}E_2) + \varepsilon_s^2\bar{\varepsilon}^{-1}R^{2/8}\tilde{p}_{TS} + \varepsilon_s^2 R^{2/8}\hat{p}_2 E_{TS} + \cdots\right], \tag{2.56}$$

$$\tilde{\rho} = C^{1/8}\tau_w^{1/2}\left[\varepsilon_s R^{1/8}(\hat{R}_1^{(1)}E_1 + \hat{R}_1^{(2)}E_2) + \varepsilon_s^2\bar{\varepsilon}^{-1}R^{3/8}\tilde{R}_{TS} + \varepsilon_s^2 R^{3/8}\hat{R}_2 E_{TS} + \cdots\right], \tag{2.57}$$

$$\tilde{\tau} = C^{1/8}\tau_w^{1/2}\left[\varepsilon_s R^{1/8}(\hat{\tau}_1^{(1)}E_1 + \hat{\tau}_1^{(2)}E_2) + \varepsilon_s^2\bar{\varepsilon}^{-1}R^{3/8}\tilde{\tau}_{TS} + \varepsilon_s^2 R^{3/8}\hat{\tau}_2 E_{TS} + \cdots\right]. \tag{2.58}$$

Leading order

Inserting (2.53) – (2.58) into (2.13) – (2.18), we obtain at leading order $\mathcal{O}(\varepsilon_s R^{1/8})$ the equations,

$$\left.\begin{aligned} &i\hat{\alpha}_1 U_B \hat{R}_1 + i\hat{\alpha}_1 R_B \hat{u}_1 + R'_B \hat{v}_1 + R_B \tfrac{\partial \hat{v}_1}{\partial \tilde{y}} = 0, \\ &i\hat{\alpha}_1 U_B \hat{u}_1 + U'_B \hat{v}_1 = 0, \quad i\hat{\alpha}_1 R_B U_B \hat{w}_1 = -i\hat{\beta}_1 \hat{p}_1, \quad i\hat{\alpha}_1 U_B \hat{R}_1 + R'_B \hat{v}_1 = 0, \end{aligned}\right\} \tag{2.59}$$

whose solution is

$$\left.\begin{aligned} &\hat{u}_1 = \hat{A}_1 U'_B, \quad \hat{v}_1 = -i\hat{\alpha}\hat{A}_1 U_B, \quad \hat{w}_1 = -(\hat{\beta}_1/\hat{\alpha}_1)\hat{p}_1/(R_B U_B), \\ &\hat{R}_1 = \hat{A}_1 R'_B, \quad \hat{\tau}_1 = -\hat{A}_1 R'_B/R_B^2, \end{aligned}\right\} \tag{2.60}$$

where we have used the state equation to obtain τ_1. The matching condition (2.42) gives

$$i\hat{\gamma}_1(1 - \mathcal{R}^{(1)}) = -\hat{\alpha}_1^2 \hat{A}_1, \tag{2.61}$$

where $\mathcal{R}^{(1)}$ is the reflection coefficient which will be later defined in (2.82). The streamwise and normal velocities of the T-S wave,

$$\tilde{u}_{TS} = BU'_B(\tilde{y})E_{TS} + \text{c.c.}, \quad \tilde{v}_{TS} = -\frac{\partial}{\partial \bar{x}}(BU_B(\tilde{y})E_{TS} + \text{c.c.}), \tag{2.62}$$

where $\frac{\partial}{\partial \bar{x}} \to \frac{\partial}{\partial \bar{x}} + \bar{\varepsilon}\frac{\partial}{\partial x_1}$. The displacement function B must be expanded as (Wu, 1999)

$$B = A(x_1)B_1 + \bar{\varepsilon}B_2(x_1), \tag{2.63}$$

so that the matching with the upper-deck solution can be carried out. The inner and outer limits of the main-deck solution (2.62) are then

$$\tilde{u}_{TS} \to \left[\lambda_0 AB_1 + \bar{\varepsilon}(\lambda_1 x_1 AB_1 + \lambda_0 B_2)\right] E_{TS} + \text{c.c.} \quad \text{as} \quad \tilde{y} \to 0, \tag{2.64}$$

$$\tilde{v}_{TS} \to -\left[i\hat{\alpha}_{TS} AB_1 + \bar{\varepsilon}(A'B_1 + i\hat{\alpha}_{TS} B_2)\right] E_{TS} + \text{c.c.} \quad \text{as} \quad \tilde{y} \to \infty. \tag{2.65}$$

Noting that $\tilde{p}_{TS} = \hat{P}_{TS}E_{TS}$, and matching the upper-deck solutions (2.44) and (2.52) with the leading-order and second terms of the main-deck solution (2.65) respectively, we have,

$$\hat{\gamma}_{TS}\hat{P}_{TS} = \hat{\alpha}_{TS}^2 B_1, \tag{2.66}$$

$$\hat{\alpha}_{TS}^2 B_2 - 2i\hat{\alpha}_{TS} A'(x_1)B_1 = \hat{\gamma}_{TS}\hat{P}_2 - i\frac{\hat{\alpha}_{TS}}{\hat{\gamma}_{TS}}(1 - M^2)A'(x_1)\hat{P}_{TS}. \tag{2.67}$$

2.2.7 Lower deck

The wall-normal variable is $Y = R^{1/8}C^{-5/8}\tau_w^{-3/2}y$. The base flow is approximated as

$$U_B(Y) = R^{-1/8}C^{1/8}\tau_w^{1/2}(\lambda_0 + \bar{\varepsilon}\lambda_1 x_1)Y + \cdots . \tag{2.68}$$

The expansion takes the form

$$\tilde{u} = C^{1/8}\tau_w^{1/2}\left[\varepsilon_s R^{1/8}(\hat{U}_1^{(1)}E_1 + \hat{U}_1^{(2)}E_2) + \varepsilon_s^2 R^{3/8}(\bar{\varepsilon}^{-1}A(x_1)\hat{U}_{TS} + \hat{U}_2)E_{TS} + \cdots\right], \tag{2.69}$$

$$\tilde{v} = C^{3/8}\tau_w^{1/2}\left[\varepsilon_s R^{-1/8}(\hat{V}_1^{(1)}E_1 + \hat{V}_1^{(2)}E_2) + \varepsilon_s^2 R^{1/8}(\bar{\varepsilon}^{-1}A(x_1)\hat{V}_{TS} + \hat{V}_2)E_{TS} + \cdots\right], \tag{2.70}$$

$$\tilde{w} = C^{1/8}\tau_w^{1/2}\left[\varepsilon_s R^{1/8}(\hat{W}_1^{(1)}E_1 + \hat{W}_1^{(2)}E_2) + \varepsilon_s^2 R^{3/8}(\bar{\varepsilon}^{-1}A(x_1)\hat{W}_{TS} + \hat{W}_2)E_{TS} + \cdots\right], \tag{2.71}$$

$$\tilde{p} = C^{1/4}\left[\varepsilon_s(\hat{P}_1^{(1)}E_1 + \hat{P}_1^{(2)}E_2) + \varepsilon_s^2 R^{2/8}(\bar{\varepsilon}^{-1}A(x_1)\hat{P}_{TS} + \hat{P}_2)E_{TS} + \cdots\right]. \tag{2.72}$$

The temperature and density disturbances are not considered since it is well known that in the lower deck they do not enter the continuity and momentum equations at leading order. The solution for each term in the expansion (2.69)-(2.72) is now considered.

Signature of sound waves

The leading-order terms in (2.69)-(2.72) represent the unsteady fluctuation driven by the sound waves. It is important to note that the streamwise and spanwise velocities are of $\mathcal{O}(\varepsilon_s R^{1/8})$, larger than those in the free stream by a factor of $R^{1/8}$. This makes sound waves on the triple-deck scale ($c \ll 1$) a more effective receptivity agent than usual acoustic waves. A similar feature arises for gravity waves on the triple-deck scale (Wu and Zhang, 2008). The velocities $\hat{U}_1$, $\hat{V}_1$ and $\hat{W}_1$ would be governed by the fully nonlinear triple-deck equations if $\varepsilon_s = \mathcal{O}(R^{-2/8})$. In the present study, we assume that $\varepsilon_s \ll R^{-2/8}$ so that the linear triple-deck equations suffice. Since the solutions for the two acoustic waves are entirely analogous, only the first one needs to be considered. The linearised equations are

$$\left.\begin{aligned} &i\hat{\alpha}_1\hat{U}_1 + \hat{V}_{1,Y} + i\hat{\beta}_1\hat{W}_1 = 0, \\ &i(\hat{\alpha}_1\lambda_0 Y - \hat{\omega}_1)\hat{U}_1 + \lambda_0\hat{V}_1 = -i\hat{\alpha}_1\hat{P}_1 + \hat{U}_{1,YY}, \\ &i(\hat{\alpha}_1\lambda_0 Y - \hat{\omega}_1)\hat{W}_1 = -i\hat{\beta}_1\hat{P}_1 + \hat{W}_{1,YY}, \end{aligned}\right\} \tag{2.73}$$

with the no-slip condition at the wall,

$$\hat{U}_1 = \hat{V}_1 = \hat{W}_1 = 0 \quad \text{at} \quad Y = 0, \tag{2.74}$$

and the matching condition with the main-deck solution (2.60),

$$\hat{U}_1 \to \lambda_0 \hat{A}_1, \quad \hat{W}_1 \to 0 \quad \text{as} \quad Y \to \infty. \tag{2.75}$$

Eliminating $\hat{P}_1$ from (2.73), we arrive at

$$\left\{ \frac{\partial^2}{\partial Y^2} - i(\hat{\alpha}_1 \lambda_0 Y - \hat{\omega}_1) \right\} \hat{V}_{1,YY} = 0. \tag{2.76}$$

After the change of variable

$$\eta = (i\hat{\alpha}_1 \lambda_0)^{1/3} Y + \eta_0 \quad \text{with} \quad \eta_0 = -i\hat{\omega}_1 / (i\hat{\alpha}_1 \lambda_0)^{2/3}, \tag{2.77}$$

we can write (2.76) into the standard Airy equation for $\hat{V}_{1,YY}$, and the solution for $\hat{V}_{1,Y}$ is

$$\hat{V}_{1,Y} = q_1 \int_{\eta_0}^{\eta} Ai(\eta') d\eta', \tag{2.78}$$

where q_1 is a constant. Now, the matching condition (2.75) implies that $\hat{V}_{1,Y} \to -i\hat{\alpha}_1 \lambda_0 \hat{A}_1$ as $Y \to \infty$, which gives

$$q_1 \int_{\eta_0}^{\infty} Ai(\eta) d\eta = -i\hat{\alpha}_1 \lambda_0 \hat{A}_1. \tag{2.79}$$

The boundary condition (2.74) implies that $\hat{V}_{1,YYY} = (\hat{\alpha}_1^2 + \hat{\beta}_1^2)\hat{P}_1$ at $Y = 0$, use of which on (2.78) leads to

$$(i\hat{\alpha}_1 \lambda_0)^{2/3} Ai'(\eta_0) q_1 = (\hat{\alpha}_1^2 + \hat{\beta}_1^2)\hat{P}_1. \tag{2.80}$$

Since the pressure is transmitted from the upper deck down to the lower deck without variation, from (2.40) it follows that $\hat{P}_1 = \hat{p}_1(0)$, i.e.

$$\hat{P}_1 = 1 + \mathcal{R}^{(1)}. \tag{2.81}$$

From (2.61) and (2.79)-(2.81), we obtain the reflection coefficient,

$$\mathcal{R}^{(1)} = -(\hat{\alpha}_1(\hat{\alpha}_1^2 + \hat{\beta}_1^2) \int_{\eta_0}^{\infty} Ai(\eta) d\eta + \hat{\gamma}_1 \lambda_0 Ai'(\eta_0)(i\hat{\alpha}_1 \lambda_0)^{2/3}) / \Delta_1, \tag{2.82}$$

and the constants q_1 and $\hat{P}_1$,

$$q_1 = -2\hat{\gamma}_1\lambda_0(\hat{\alpha}_1^2+\hat{\beta}_1^2)/\Delta_1, \quad \hat{P}_1 = -2\hat{\gamma}_1\lambda_0 Ai'(\eta_0)(i\hat{\alpha}_1\lambda_0)^{2/3}/\Delta_1, \tag{2.83}$$

where

$$\Delta_1 = \hat{\alpha}_1(\hat{\alpha}_1^2+\hat{\beta}_1^2)\int_{\eta_0}^{\infty} Ai(\eta)d\eta - \hat{\gamma}_1\lambda_0 Ai'(\eta_0)(i\hat{\alpha}_1\lambda_0)^{2/3}. \tag{2.84}$$

The solution for $\hat{V}_1$ and $\hat{W}_1$ is found as

$$\hat{V}_1 = \frac{(\hat{\alpha}_1^2+\hat{\beta}_1^2)\hat{P}_1}{Ai'(\eta_0)(i\hat{\alpha}_1\lambda_0)}\left(\eta\int_{\eta_0}^{\eta} Ai(\eta)d\eta - Ai'(\eta) + Ai'(\eta_0)\right), \tag{2.85}$$

$$\hat{W}_1 = \frac{i\hat{\beta}_1\pi}{(i\hat{\alpha}_1\lambda_0)^{2/3}}\hat{P}_1\Big(d_0 Ai(\eta) - Gi(\eta)\Big), \tag{2.86}$$

where $d_0 = Bi(\eta_0)\int_{\eta_0}^{\infty} Ai(\eta)d\eta/Ai(\eta_0)$, and $Gi(\eta)$ denotes Scorer's function

$$Gi(\eta) = Ai(\eta)\int_{\eta_0}^{\eta} Bi(\eta)d\eta - Bi(\eta)\int_{\infty}^{\eta} Ai(\eta)d\eta.$$

From the continuity equation (2.73) follows the solution for $\hat{U}_1$,

$$\hat{U}_1 = \frac{i}{\hat{\alpha}_1}\frac{(\hat{\alpha}_1^2+\hat{\beta}_1^2)\hat{P}_1}{Ai'(\eta_0)(i\hat{\alpha}_1\lambda_0)^{2/3}}\int_{\eta_0}^{\eta} Ai(\eta)d\eta + \frac{i\hat{\beta}_1^2\pi}{\hat{\alpha}_1(i\hat{\alpha}_1\lambda_0)^{2/3}}\hat{P}_1\Big(d_0 Ai(\eta) - Gi(\eta)\Big), \tag{2.87}$$

which is in contrast to the Stokes solution driven by sound waves with $\mathcal{O}(1)$ phase speeds (cf. Ruban, 1984, Goldstein, 1985), which includes a term with $e^{i^{3/2}\hat{\omega}_0^{1/2}Y}$.

The solution for the other sound wave is the same as (2.85)-(2.87), provided that the corresponding wavenumbers ($\hat{\alpha}_1$, $\hat{\beta}_1$) and frequency $\hat{\omega}_1$ are replaced by ($\hat{\alpha}_2$, $\hat{\beta}_2$) and $\hat{\omega}_2$, respectively.

T-S waves

The T-S wave satisfies the equations (2.73), provided that $\hat{\alpha}_1$, $\hat{\beta}_1$ and $\hat{\omega}_1$ are replaced by $\hat{\alpha}_{TS}$, $\hat{\beta}_{TS}$ and $\hat{\omega}_{TS}$, respectively. As expected, $\hat{V}_{TS,YY}$ is governed by the equation (cf. (2.76)),

$$\left\{\frac{\partial^2}{\partial Y^2} - i(\hat{\alpha}_{TS}\lambda_0 Y - \hat{\omega}_{TS})\right\}\hat{V}_{TS,YY} = 0, \tag{2.88}$$

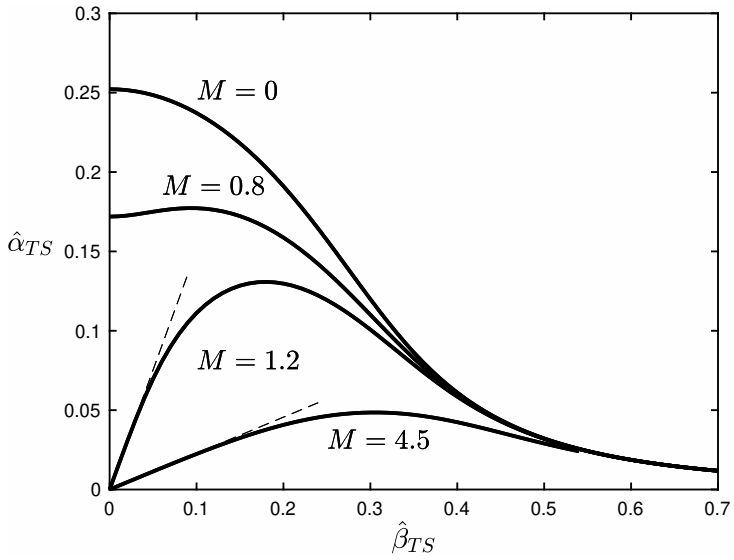


Figure 2.2: Neutral curve of the T-S wave in the ($\hat{\alpha}_{TS}$, $\hat{\beta}_{TS}$) plane for different Mach numbers. The dashed lines represent $\hat{\beta}_{TS} = \sqrt{M^2 - 1}\hat{\alpha}_{TS}$.

and its solution is therefore

$$\hat{V}_{TS,Y} = q_{TS} \int_{\tilde{\eta}_0}^{\tilde{\eta}} Ai(\eta')d\eta', \tag{2.89}$$

where $q_{TS} = 1$ is taken for normalization and the variable

$$\tilde{\eta} = (i\hat{\alpha}_{TS}\lambda_0)^{1/3}Y + \tilde{\eta}_0 \quad \text{with} \quad \tilde{\eta}_0 = -i\hat{\omega}_{TS}(i\hat{\alpha}_{TS}\lambda_0)^{-2/3}. \tag{2.90}$$

The matching and boundary conditions become $\hat{V}_{TS,Y} \to -i\hat{\alpha}_{TS}\lambda_0 B_1$ as $\tilde{\eta} \to \infty$, and $\hat{V}_{TS,YYY}(0) = (\hat{\alpha}_{TS}^2 + \hat{\beta}_{TS}^2)\hat{P}_{TS}$, which give, respectively,

$$\int_{\tilde{\eta}_0}^{\infty} Ai(\eta)d\eta = -i\hat{\alpha}_{TS}\lambda_0 B_1, \tag{2.91}$$

and

$$(i\hat{\alpha}_{TS}\lambda_0)^{2/3}Ai'(\tilde{\eta}_0) = (\hat{\alpha}_{TS}^2 + \hat{\beta}_{TS}^2)\hat{P}_{TS}. \tag{2.92}$$

From (2.91), (2.92) and (2.66) follows the dispersion relation (Smith, 1989)

$$\Delta(\lambda_0) \equiv i\hat{\alpha}_{TS}(\hat{\alpha}_{TS}^2 + \hat{\beta}_{TS}^2) \int_{\tilde{\eta}_0}^{\infty} Ai(\eta)d\eta - \lambda_0\hat{\gamma}_{TS}(i\hat{\alpha}_{TS}\lambda_0)^{2/3}Ai'(\tilde{\eta}_0) = 0. \tag{2.93}$$

The neutral wavenumber and frequency can be determined by

$$\hat{\alpha}_{TS} = \lambda_0^{5/4}\alpha_N, \quad \hat{\beta}_{TS} = \lambda_0^{5/4}\beta_N, \quad \hat{\omega}_{TS} = \lambda_0^{3/2}\omega_N, \tag{2.94}$$

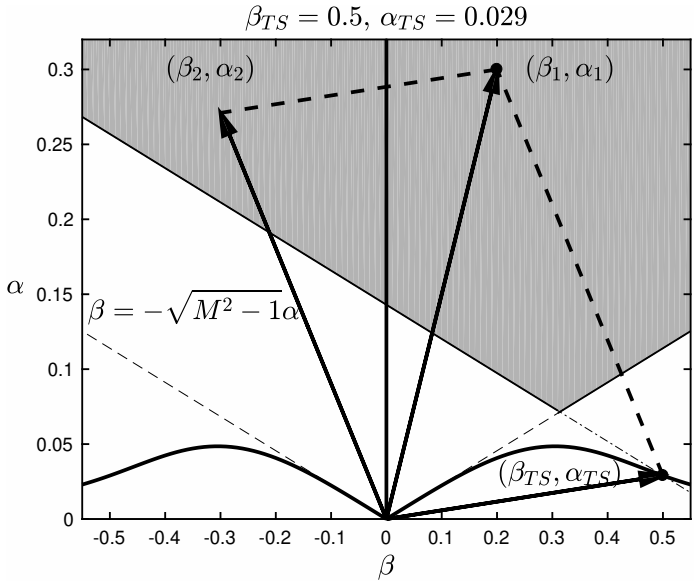


Figure 2.3: An ilustration showing the selection of the sound waves which satisfy the resonance conditions (2.27) for a given T-S wave (solid line, $M = 4.5$ case in figure 2.2). The dash-dotted line represents $\hat{\beta}_1 - \hat{\beta}_{TS} = -\sqrt{M^2-1}(\hat{\alpha}_1 - \hat{\alpha}_{TS})$.

with α_N, β_N and ω_N given by (Smith, 1989)

$$\alpha_N^{1/3}(\alpha_N^2 + \beta_N^2) = d_1\left[(1-M^2)\alpha_N^2 + \beta_N^2\right]^{1/2}, \quad \omega_N = d_2\alpha_N^{2/3}, \tag{2.95}$$

where $d_1 \approx 1.001$ and $d_2 \approx 2.299$. The relations (2.94)-(2.95) mean that for each $\hat{\beta}_{TS}$, $\hat{\alpha}_{TS} = \hat{\alpha}_{TS}(\hat{\beta}_{TS})$ and $\hat{\omega}_{TS} = \hat{\omega}_{TS}(\hat{\beta}_{TS})$ are found with $\hat{\beta}_{TS} > \sqrt{M^2-1}\hat{\alpha}_{TS}$. The neutral curves for four different subsonic and supersonic Mach numbers are plotted in figure 2.2. The neutral curve can be extended to $\hat{\beta}_{TS} < 0$ by symmetry.

A T-S mode can be excited by different combinations of two slow sound waves. A procedure for the choice of the sound waves is ilustrated in figure 2.3 and described below.

1. Choice of sound wave 1 ($\hat{\alpha}_1$, $\hat{\beta}_1$, $\hat{\omega}_1$). Its frequency can be arbitrary, but its wavenumbers must satisfy $\mid \hat{\beta}_1 \mid < \sqrt{M^2-1}\hat{\alpha}_1$.

2. Choice of sound wave 2 ($\hat{\alpha}_2$, $\hat{\beta}_2$, $\hat{\omega}_2$). Its wavenumbers and frequency are determined from the resonance conditions (2.27). The wavenumbers must be in the region $\mid \hat{\beta}_2 \mid < \sqrt{M^2-1}\hat{\alpha}_2$ too, this is, on recalling (2.27),

$$\hat{\beta}_1 - \hat{\beta}_{TS} > -\sqrt{M^2-1}(\hat{\alpha}_1 - \hat{\alpha}_{TS}), \tag{2.96}$$

which together with $\hat{\beta}_1 < \sqrt{M^2-1}\hat{\alpha}_1$ (see (2.23)) represents the shaded region in

figure 2.3. For any ($\hat{\alpha}_1$, $\hat{\beta}_1$) in that region, it is always possible to find another sound wave to satisfy the resonance conditions, thereby exciting the T-S wave.

Forced response

At next order, the equations in the lower deck read

$$\left.\begin{aligned} &i\hat{\alpha}_{TS}\hat{U}_2 + \hat{V}_{2,Y} + i\hat{\beta}_{TS}\hat{W}_2 = -A'(x_1)\hat{u}_{TS}, \\ &i(\hat{\alpha}_{TS}\lambda_0 Y - \hat{\omega}_{TS})\hat{U}_2 + \lambda_0\hat{V}_2 = -i\hat{\alpha}_{TS}\hat{P}_2 + \hat{U}_{2,YY} - \lambda_1 x_1\hat{v}_{TS} \\ &\qquad\qquad -\Lambda(x_1)Y\hat{u}_{TS} - A'(x_1)\hat{p}_{TS} - N_1, \\ &i(\hat{\alpha}_{TS}\lambda_0 Y - \hat{\omega}_{TS})\hat{W}_2 = -i\hat{\beta}_{TS}\hat{P}_2 + \hat{W}_{2,YY} - \Lambda(x_1)Y\hat{w}_{TS} - N_3, \end{aligned}\right\} \tag{2.97}$$

where Λ is defined by

$$\Lambda(x_1) = \lambda_0 A'(x_1) + i\hat{\alpha}_{TS}\lambda_1 x_1 A, \tag{2.98}$$

and the inhomogeneous terms N_1 and N_3 are given by

$$\left.\begin{aligned} N_1 &= i(\hat{\alpha}_1 - \hat{\alpha}_2)\hat{U}_1^{(1)}\hat{U}_1^{(2)*} + i\hat{\beta}_1\hat{W}_1^{(2)*}\hat{U}_1^{(1)} - i\hat{\beta}_2\hat{W}_1^{(1)}\hat{U}_1^{(2)*} + \hat{V}_1^{(1)}\hat{U}_{1Y}^{(2)*} + \hat{V}_1^{(2)*}\hat{U}_{1Y}^{(1)}, \\ N_3 &= i\hat{\alpha}_1\hat{W}_1^{(1)}\hat{U}_1^{(2)*} - i\hat{\alpha}_2\hat{W}_1^{(2)*}\hat{U}_1^{(1)} + i(\hat{\beta}_1 - \hat{\beta}_2)\hat{W}_1^{(1)}\hat{W}_1^{(2)*} + \hat{V}_1^{(1)}\hat{W}_{1Y}^{(2)*} + \hat{V}_1^{(2)*}\hat{W}_{1Y}^{(1)}. \end{aligned}\right\} \tag{2.99}$$

After rearranging (2.97) as we did before with (2.73), an inhomogeneous Airy equation for $\hat{V}_{2,YY}$ can be obtained,

$$\left\{\frac{\partial^2}{\partial Y^2} - i(\hat{\alpha}_{TS}\lambda_0 Y - \hat{\omega}_{TS})\right\}\hat{V}_{2,YY} = \Lambda Y\hat{V}_{TS,YY} - i(\hat{\alpha}_{TS}N_1 + \hat{\beta}_{TS}N_3)_Y. \tag{2.100}$$

The solution can be expressed as (cf. Wu, 2001a)

$$\begin{aligned} \hat{V}_{2,Y} = \frac{1}{3}(i\hat{\alpha}_{TS}\lambda_0)^{-1}\Lambda(x_1)\left\{(\tilde{\eta} - 3\tilde{\eta}_0)Ai(\tilde{\eta}) + 2\tilde{\eta}_0 Ai(\tilde{\eta}_0)\right\} \\ + \int_{\tilde{\eta}_0}^{\tilde{\eta}} \tilde{M}(\eta', \tilde{\eta}_0)d\eta' + q_2\int_{\tilde{\eta}_0}^{\tilde{\eta}} Ai(\eta')d\eta', \end{aligned} \tag{2.101}$$

where q_2 is a function of x_1, and $\tilde{M}$ is given by

$$\tilde{M}(\tilde{\eta}, \tilde{\eta}_0) = \pi\left\{Bi(\tilde{\eta})\int_{\infty}^{\tilde{\eta}} Ai(\eta')H(Y')d\eta' - Ai(\tilde{\eta})\int_{\tilde{\eta}_0}^{\tilde{\eta}} Bi(\eta')H(Y')d\eta'\right\}, \tag{2.102}$$

with $H = -(\hat{\alpha}_{TS}\lambda_0)^{-1}\left[\hat{\alpha}_{TS}N_1 + \hat{\beta}_{TS}N_3\right]_Y$, and Bi being the Airy function.

At this order, the matching condition with the main-deck solution (2.64) reads

$$\hat{V}_{2,Y} \to -i\hat{\alpha}_{TS}\lambda_0 B_2 - (i\hat{\alpha}_{TS}\lambda_1 x_1 A + \lambda_0 A'(x_1))B_1 \quad \text{as} \quad Y \to \infty, \tag{2.103}$$

and thus

$$\begin{aligned} -i\hat{\alpha}_{TS}\lambda_0 B_2 - (i\hat{\alpha}_{TS}\lambda_1 x_1 A + \lambda_0 A'(x_1))B_1 = \frac{2}{3}(i\hat{\alpha}_{TS}\lambda_0)^{-1}\Lambda\tilde{\eta}_0 Ai(\tilde{\eta}_0) \\ + \int_{\tilde{\eta}_0}^{\infty} \tilde{M}(\eta', \tilde{\eta}_0)d\eta' + q_2 \int_{\tilde{\eta}_0}^{\infty} Ai(\eta')d\eta'. \end{aligned} \tag{2.104}$$

The no-slip condition is

$$\hat{V}_{2,YYY} = (\hat{\alpha}_{TS}^2 + \hat{\beta}_{TS}^2)\hat{P}_2 - 2i\hat{\alpha}_{TS}A'(x_1)\hat{P}_{TS} \quad \text{at} \quad Y = 0, \tag{2.105}$$

leading to

$$\begin{aligned} \frac{2}{3}(i\hat{\alpha}_{TS}\lambda_0)^{-1/3}\Lambda\left\{Ai'(\tilde{\eta}_0) - \tilde{\eta}_0 Ai''(\tilde{\eta}_0)\right\} + (i\hat{\alpha}_{TS}\lambda_0)^{2/3}\left\{\pi Bi'(\tilde{\eta}_0)\int_{\infty}^{\tilde{\eta}_0} Ai(\eta')H(Y')d\eta'\right\} \\ + (i\hat{\alpha}_{TS}\lambda_0)^{2/3}q_2 Ai'(\tilde{\eta}_0) = (\hat{\alpha}_{TS}^2 + \hat{\beta}_{TS}^2)\hat{P}_2 - 2i\hat{\alpha}_{TS}A'(x_1)\hat{P}_{TS}. \end{aligned} \tag{2.106}$$

With B_1 and $\hat{P}_{TS}$ being determined from (2.91) and (2.92), the relations (2.104), (2.67) and (2.106) form a system of 3 equations for 4 unknowns: q_2, P_2, B_2 and $A(x_1)$. The elimination of P_2 and B_2 yields

$$aA' + b(i\hat{\alpha}_{TS}\lambda_1 x_1/\lambda_0)A + (\hat{\alpha}_{TS}^2 + \hat{\beta}_{TS}^2)^{-1}\Delta(\lambda_0)q_2 = \mathcal{F}, \tag{2.107}$$

where

$$\begin{aligned} a =& \frac{2}{3}\tilde{\eta}_0 Ai(\tilde{\eta}_0) + \left(\frac{\hat{\beta}_{TS}^2}{\hat{\gamma}_{TS}^2} + \frac{2\hat{\alpha}_{TS}^2}{\hat{\alpha}_{TS}^2 + \hat{\beta}_{TS}^2}\right)\int_{\tilde{\eta}_0}^{\infty} Ai(\eta')d\eta' \\ &+ \frac{2}{3}\frac{\hat{\gamma}_{TS}(i\hat{\alpha}_{TS}\lambda_0)^{5/3}}{\hat{\alpha}_{TS}^2(\hat{\alpha}_{TS}^2 + \hat{\beta}_{TS}^2)}\left\{Ai'(\tilde{\eta}_0) - \tilde{\eta}_0 Ai''(\tilde{\eta}_0)\right\}, \\ b =& \frac{2}{3}\tilde{\eta}_0 Ai(\tilde{\eta}_0) - \int_{\tilde{\eta}_0}^{\infty} Ai(\eta')d\eta' + \frac{2}{3}\frac{\hat{\gamma}_{TS}(i\hat{\alpha}_{TS}\lambda_0)^{5/3}}{\hat{\alpha}_{TS}^2(\hat{\alpha}_{TS}^2 + \hat{\beta}_{TS}^2)}\left\{Ai'(\tilde{\eta}_0) - \tilde{\eta}_0 Ai''(\tilde{\eta}_0)\right\}, \\ \mathcal{F} =& \chi\int_{\infty}^{\tilde{\eta}_0} Ai(\eta')H(Y')d\eta' - i\hat{\alpha}_{TS}\int_{\tilde{\eta}_0}^{\infty}\tilde{M}(\eta', \tilde{\eta}_0)d\eta', \\ \chi =& \pi\lambda_0\hat{\gamma}_{TS}(i\hat{\alpha}_{TS}\lambda_0)^{2/3}Bi'(\tilde{\eta}_0)/(\hat{\alpha}_{TS}^2 + \hat{\beta}_{TS}^2). \end{aligned}$$

Since $\Delta(\lambda_0) = 0$, we arrive at the evolution equation for $A(x_1)$,

$$A'(x_1) = \sigma x_1 A + N, \tag{2.108}$$

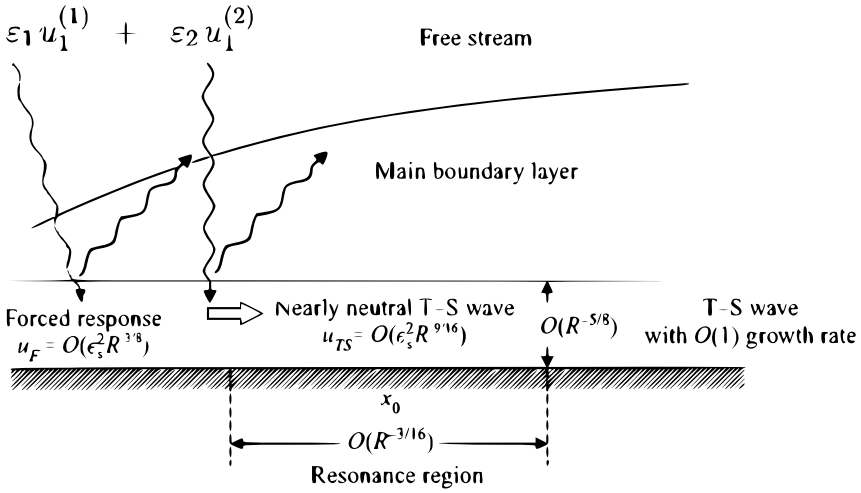


Figure 2.4: Receptivity mechanism due to sound-sound interaction.

where

$$\sigma = -i\hat{\alpha}_{TS}\lambda_1 b/(\lambda_0 a), \quad N = \mathcal{F}/a. \tag{2.109}$$

2.3 Receptivity: evolution from the forced response to eigenmode

2.3.1 Matching between T-S wave solution and upstream forced response

The amplitude equation (2.108) describes the evolution of the forced response upstream to the T-S wave (figure 2.4). On assuming that the amplitude of the T-S wave vanishes, i.e. $A(x_1) \to 0$ as $x_1 \to -\infty$, the equation (2.108) has the solution (Wu, 1999)

$$A(x_1) = Ne^{\sigma x_1^2/2} \int_{-\infty}^{x_1} e^{-\sigma\xi^2/2} d\xi. \tag{2.110}$$

It can be shown that as $x_1 \to -\infty$,

$$A(x_1) \to \frac{N}{\sigma(-x_1)} + \mathcal{O}(x_1^{-3}). \tag{2.111}$$

To demonstrate the matching with the upstream response, we note that at an upstream position x (figure 2.4), q_2 represents the amplitude of the forced response

(2.107), A_F,

$$A_F \equiv q_2 = \frac{\hat{\alpha}_{TS}^2 + \hat{\beta}_{TS}^2}{\Delta(\lambda)}\mathcal{F},$$

By performing a Taylor expansion of $\Delta(\lambda)$ about λ_0,

$$\Delta(\lambda) = \Delta(\lambda_0) + \left.\frac{\partial \Delta}{\partial \lambda}\right|_{\lambda_0}(\lambda - \lambda_0) + \cdots = -\frac{\hat{\alpha}_{TS}(\hat{\alpha}_{TS}^2 + \hat{\beta}_{TS}^2)\lambda_0 b}{i\lambda_0^2}(\lambda - \lambda_0) + \cdots, \tag{2.112}$$

the behaviour of A_F as $x \to x_0$ is obtained,

$$A_F \to \frac{\lambda_0 \mathcal{F}}{i\hat{\alpha}_{TS} b(\lambda - \lambda_0)}. \tag{2.113}$$

Substitution of (2.30) and (2.109) into (2.113) shows that

$$A_F \to R^{3/16}\frac{N}{\sigma(-x_1)}, \tag{2.114}$$

which confirms that

$$R^{3/16}A(x_1) \to A_F \quad \text{as} \quad x_1 \to -\infty. \tag{2.115}$$

In the downstream limit $x_1 \to +\infty$, it can be shown that

$$A(x_1) \to A_\infty e^{\sigma x_1^2/2}, \tag{2.116}$$

with

$$A_\infty = N\int_{-\infty}^{+\infty} e^{-\sigma\xi^2/2}d\xi = N\sqrt{\frac{2\pi}{\sigma}}. \tag{2.117}$$

Further downstream where $x_1 = \mathcal{O}(R^{3/16})$, the T-S wave eventually acquires an $\mathcal{O}(1)$ growth rate (figure 2.4), and evolves exponentially over the fast streamwise scale $\bar{x}$. The amplitude takes the form (Wu, 1999, Wu, 2001a)

$$Ae^{i\hat{\alpha}_{TS}\bar{x}} = A_\infty \exp\left\{iR^{3/8}\int_{x_0}^{x}\hat{\alpha}_{TS}(x)dx\right\}, \tag{2.118}$$

which shows that the downstream development is equivalent to a free modal evolution with A_∞ being the initial amplitude.

2.3.2 Coupling coefficients

A convenient representation of the magnitude of the T-S wave is the maximum value of its streamwise velocity, which can be directly measured in experiments, e.g. King and Breuer (2002). Solving the spanwise momentum equation, we obtain the spanwise velocity

$$\hat{W}_{TS} = \frac{i\hat{\beta}_{TS} Ai'(\tilde{\eta}_0)}{\hat{\alpha}_{TS}^2 + \hat{\beta}_{TS}^2} L(\tilde{\eta}), \tag{2.119}$$

where $L(\tilde{\eta})$ is the solution to the equation $L'' - \tilde{\eta}L = 1$ satisfying the boundary conditions $L(\tilde{\eta}_0) = 0$ and $L(\infty) = 0$. From the continuity equation, (2.89) and (2.69), it follows that the streamwise velocity at the neutral point is given by

$$u_{TS} = \varepsilon_s^2 \bar{\varepsilon}^{-1} R^{3/8} C^{1/8} \tau_w^{1/2} \hat{\alpha}_{TS}^{-1} A_\infty U_m, \tag{2.120}$$

where

$$U_m = \max_{\tilde{\eta}} \left| \int_{\tilde{\eta}_0}^{\tilde{\eta}} Ai(\eta')d\eta' - \frac{\beta_N^2}{\alpha_N^2 + \beta_N^2} Ai'(\tilde{\eta}_0) L(\tilde{\eta}) \right|. \tag{2.121}$$

The coupling coefficient for the sound-sound interaction can be defined as

$$C_A \equiv u_{TS}/\varepsilon_s = \varepsilon_s R^{9/16} C^{-1/16} \tau_w^{-1/4} \hat{\alpha}_{TS}^{-1} A_\infty U_m \equiv \varepsilon_s R^{9/16} \Lambda_{SS}. \tag{2.122}$$

Clearly, Λ_{SS} is the rescaled coupling coefficient, and depends on the parameters such as $\hat{\omega}_1$, $\hat{c}_1$, etc.

2.4 Receptivity to slow acoustic waves interacting with distributed roughness

In this section, we consider the generation of T-S waves due to a sound wave interacting with distributed roughness. This receptivity mechanism has been studied previously for incompressible boundary layers (e.g. Choudhari, 1993, Wu, 2001a) and compressible boundary layers (Fedorov, 2003b). The frequency of the sound wave is taken to be $\mathcal{O}(R^{2/8})$, comparable with that of the T-S wave. Earlier studies assumed that its phase speed was of $\mathcal{O}(1)$ so that the wavenumber is $\mathcal{O}(R^{2/8})$; in the incompressible limit, the phase speed and wavenumber are infinite and zero, respectively. In this chapter, the sound wave is taken to have a much smaller speed $c = \mathcal{O}(R^{-1/8})$ so that its wavenumber is $\mathcal{O}(R^{3/8})$. Although the frequency and wavenumbers of such sound waves are comparable with those of T-S waves, the former does not excite the latter directly because they have different dispersion

relations. A scale tuning mechanism is still required in order to satisfy the required resonance conditions. This can be provided by suitable distributed surface roughness. Sound waves on the triple-deck scale will lead to stronger receptivity.

2.4.1 Physical idea and asymptotic scaling

Suppose that a three-dimensional sound wave, $\varepsilon_s \left\{ e^{i(\hat{\alpha}_s \bar{x} + \hat{\beta}_s \bar{z} + \hat{\gamma}_s \bar{y} - \hat{\omega}_s \bar{t})} + \text{c.c.} \right\}$, impinges on the boundary layer and, that a distributed roughness is present (figure 2.5), represented by a wavy wall, whose position is given by

$$Y = h\hat{F}_w \left\{ e^{i(\hat{\alpha}_w \bar{x} + \hat{\beta}_w \bar{z} + \hat{\gamma}_w \bar{y})} + \text{c.c.} \right\}, \tag{2.123}$$

where $h \ll 1$ is a measure of the roughness height, which is related to the physical height h^* by the equation

$$h = R^{5/8} C^{-5/8} \tau_w^{-3/2} h^* / L. \tag{2.124}$$

In (2.123), $\hat{F}_w$ is of $\mathcal{O}(1)$ and can be set to unity, but is retained for book-keeping purpose. With the same scaling (2.26) for the wavenumbers as in the previous problem, the resonance conditions for the present mechanism are:

$$\hat{\alpha}_s - \hat{\alpha}_w = \hat{\alpha}_{TS}, \quad \hat{\beta}_s - \hat{\beta}_w = \hat{\beta}_{TS}, \quad \hat{\omega}_s = \hat{\omega}_{TS}, \tag{2.125}$$

which ensure that the difference mode produced through the interaction excites the T-S mode. It is interesting to note that in this case, the sum mode may excite T-S modes as well because one of the interacting elements, the roughness, is not subject to the restriction $\hat{\beta}_w < \sqrt{M^2 - 1}\hat{\alpha}_w$. The corresponding resonance conditions to meet would be

$$\hat{\alpha}_s + \hat{\alpha}_w = \hat{\alpha}_{TS}, \quad \hat{\beta}_s + \hat{\beta}_w = \hat{\beta}_{TS}, \quad \hat{\omega}_s = \hat{\omega}_{TS}. \tag{2.126}$$

For the present mechanism, the solutions for the sound wave and the T-S eigenmode are the same as in the sound-sound interaction. We will thus consider only the solution for the roughness-induced mean-flow distortion and its interaction with the sound wave.

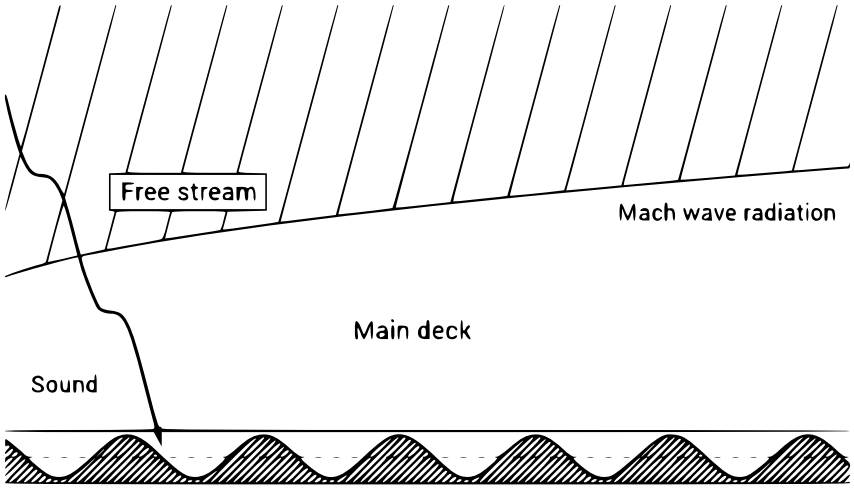


Figure 2.5: Sketch of the "difference-mode" interaction between a sound wave and a wavy wall (distributed roughness) in the supersonic regime, featuring Mach wave radiation.

2.4.2 Upper deck

As in the previous problem, the wall-normal variable is $\bar{y} = R^{-1/8}C^{-3/8}\tau_w^{-3/2}y$, but the expansions become

$$\tilde{\mathbf{u}} = \varepsilon_s \mathbf{u_s} + hR^{-2/8}\mathbf{u_M} + \varepsilon_s h\bar{\varepsilon}^{-1}(\mathbf{u}_{TS}E_{TS} + \text{c.c.}) + \varepsilon_s h\mathbf{u_2} + \cdots , \tag{2.127}$$

$$\tilde{p} = \varepsilon_s p_s + hR^{-2/8}p_M + \varepsilon_s h\bar{\varepsilon}^{-1}(p_{TS}E_{TS} + \text{c.c.}) + \varepsilon_s h p_2 + \cdots , \tag{2.128}$$

$$\tilde{\rho} = \varepsilon_s R_s + hR^{-2/8}R_M + \varepsilon_s h\bar{\varepsilon}^{-1}(R_{TS}E_{TS} + \text{c.c.}) + \varepsilon_s h R_2 + \cdots , \tag{2.129}$$

$$\tilde{\tau} = \varepsilon_s \tau_s + hR^{-2/8}\tau_M + \varepsilon_s h\bar{\varepsilon}^{-1}(\tau_{TS}E_{TS} + \text{c.c.}) + \varepsilon_s h\tau_2 + \cdots . \tag{2.130}$$

Substitution of (2.127) − (2.130) into (2.2) − (2.6) yields, at order $\mathcal{O}(\varepsilon_s)$ the same linearized equations for the sound wave as in the previous problem, and at $\mathcal{O}(hR^{-2/8})$, the equations for the roughness-induced mean-flow distortion. The solution for the latter is now considered. The general expression for the pressure is

$$p_M = P_M\left(r^+ e^{i\hat{\gamma}_w\bar{y}} + r^- e^{-i\hat{\gamma}_w\bar{y}}\right)E_w \quad \text{with} \quad E_w = e^{i(\hat{\alpha}_w\bar{x}+\hat{\beta}_w\bar{z})}, \tag{2.131}$$

where $\hat{\gamma}_w = \sqrt{(M^2-1)\hat{\alpha}_w^2 - \hat{\beta}_w^2}$, and $r^\pm$ are constants. Two cases have to be distinguished, depending on whether $\sqrt{M^2-1}\hat{\alpha}_w - \hat{\beta}_w$ is positive or negative. For the former case, two families of straight lines,

$$\hat{\alpha}_w\bar{x} \pm \sqrt{(M^2-1)\hat{\alpha}_w^2 - \hat{\beta}_w^2}\bar{y} = \text{constant}, \tag{2.132}$$

represent the fronts of the so-called *Mach waves*. We need to make use of the principle of causality, or equivalently, the requirement that the vertical group velocity is positive, $\frac{\partial\hat{\omega}_w}{\partial\hat{\gamma}_w} > 0$, in order to choose the correct branch for the outgoing wave. By using the dispersion relation $-M^2(\hat{\alpha}_w - \hat{\omega}_w)^2 + \hat{\alpha}_w^2 + \hat{\beta}_w^2 + \hat{\gamma}_w^2 = 0$ and differentiating with respect to $\hat{\gamma}_w$, it follows that

$$\frac{\partial\hat{\omega}_w}{\partial\hat{\gamma}_w} = -\left.\frac{\hat{\gamma}_w}{M^2(\hat{\alpha}_w - \hat{\omega}_w)}\right|_{\hat{\omega}_w\to 0} > 0, \tag{2.133}$$

which is possible only if $\hat{\gamma}_w < 0$. Thus, the outgoing wave is $e^{-i\hat{\gamma}_w\bar{y}}$ and the correct branch is $e^{-i\sqrt{(M^2-1)\hat{\alpha}_w^2-\hat{\beta}_w^2}\bar{y}}$ (see figure 2.5); we set $r^+ = 0$ and $r^- = 1$ in (2.131) on the understanding that r^- can be absorbed into P_M. On the other hand, if $\hat{\beta}_w > \sqrt{M^2-1}\hat{\alpha}_w$, the other branch $e^{i\sqrt{(M^2-1)\hat{\alpha}_w^2-\hat{\beta}_w^2}\bar{y}}$, with $r^+ = 1$ and $r^- = 0$, needs to be chosen to ensure that $p_M \sim e^{-\nu\bar{y}}$ with $\nu = \sqrt{\hat{\beta}_w^2 - (M^2-1)\hat{\alpha}_w^2}$ being a real number. In this case, the roughness-induced perturbation is trapped within the boundary layer.

At next orders, equations similar to those for the sound-sound interaction hold: $\mathcal{O}(\varepsilon_s h R^{3/16})$ for the T-S wave and $\mathcal{O}(\varepsilon_s h)$ for the response. It turns out that, in order for the sum mode to generate a T-S wave, the wavenumbers must satisfy $\hat{\beta}_w > \sqrt{M^2-1}\hat{\alpha}_w$, while for the difference mode to generate a T-S wave $\hat{\beta}_w < \sqrt{M^2-1}\hat{\alpha}_w$ instead.

2.4.3 Main deck

The transverse variable is $\tilde{y} = C^{-1/2}\tau_w^{-1}y = \mathcal{O}(1)$, and the expansions take the form

$$\tilde{u} = C^{1/8}\tau_w^{1/2}\left[\varepsilon_s R^{1/8}\hat{u}_s + hR^{-1/8}\hat{u}_M E_w + \varepsilon_s h\bar{\varepsilon}^{-1}R^{1/8}\tilde{u}_{TS} + \varepsilon_s hR^{1/8}\hat{u}_2 E_{TS} + \cdots\right], \tag{2.134}$$

$$\tilde{v} = C^{1/4}\left[\varepsilon_s\hat{v}_s + hR^{-2/8}\hat{v}_M E_w + \varepsilon_s^2\bar{\varepsilon}^{-1}\tilde{v}_{TS} + \varepsilon_s h\hat{v}_2 E_{TS} + \cdots\right], \tag{2.135}$$

$$\tilde{w} = C^{1/4}\tau_w\left[\varepsilon_s\hat{w}_s + hR^{-2/8}\hat{w}_M E_w + \varepsilon_s h\bar{\varepsilon}^{-1}\tilde{w}_{TS} + \varepsilon_s h\hat{w}_2 E_{TS} + \cdots\right], \tag{2.136}$$

$$\tilde{p} = C^{1/4}\left[\varepsilon_s\hat{p}_s + hR^{-2/8}\hat{p}_M E_w + \varepsilon_s h\bar{\varepsilon}^{-1}\tilde{p}_{TS} + \varepsilon_s h\hat{p}_2 E_{TS} + \cdots\right], \tag{2.137}$$

$$\tilde{\rho} = C^{1/8}\tau_w^{1/2}\left[\varepsilon_s R^{1/8}\hat{R}_s + hR^{-1/8}\hat{R}_M E_w + \varepsilon_s h\bar{\varepsilon}^{-1}R^{1/8}\tilde{R}_{TS} + \varepsilon_s hR^{1/8}\hat{R}_2 E_{TS} + \cdots\right], \tag{2.138}$$

$$\tilde{\tau} = C^{1/8}\tau_w^{1/2}\left[\varepsilon_s R^{1/8}\hat{\tau}_s + h\hat{\tau}_M E_w + \varepsilon_s h\bar{\varepsilon}^{-1}R^{2/8}\tilde{\tau}_{TS} + \varepsilon_s hR^{2/8}\hat{\tau}_2 E_{TS} + \cdots\right]. \tag{2.139}$$

The solution for the mean-flow distortion is (Smith et al., 1977)

$$\hat{u}_M = \hat{A}_M U_B', \quad \hat{v}_M = -i\alpha_w \hat{A}_M U_B, \tag{2.140}$$

where $\hat{A}_M$ is a constant.

2.4.4 Lower deck

The expansions take the form

$$\tilde{u} = C^{1/8}\tau_w^{1/2}\left[\varepsilon_s R^{1/8}\hat{U}_s + hR^{-1/8}\hat{U}_M E_w + \varepsilon_s h R^{1/8}(\bar{\varepsilon}^{-1}A(x_1)\hat{U}_{TS} + \hat{U}_2)E_{TS} + \cdots\right], \tag{2.141}$$

$$\tilde{v} = C^{3/8}\tau_w^{1/2}\left[\varepsilon_s R^{-1/8}\hat{V}_s + hR^{-3/8}\hat{V}_M E_w + \varepsilon_s h R^{-1/8}(\bar{\varepsilon}^{-1}A(x_1)\hat{V}_{TS} + \hat{V}_2)E_{TS} + \cdots\right], \tag{2.142}$$

$$\tilde{w} = C^{1/8}\tau_w^{1/2}\left[\varepsilon_s R^{1/8}\hat{W}_s + hR^{-1/8}\hat{W}_M E_w + \varepsilon_s h R^{1/8}(\bar{\varepsilon}^{-1}A(x_1)\hat{W}_{TS} + \hat{W}_2)E_{TS} + \cdots\right], \tag{2.143}$$

$$\tilde{p} = C^{1/4}\left[\varepsilon_s \hat{P}_s + hR^{-1/4}\hat{P}_M E_w + \varepsilon_s h(\bar{\varepsilon}^{-1}A(x_1)\hat{P}_{TS} + \hat{P}_2)E_{TS} + \cdots\right]. \tag{2.144}$$

The expansions for the density and temperature are omitted again since they play no role at leading order. The solution for the roughness-induced mean-flow distortion is given in Appendix A.

Forced response

We now consider the forced response, which satisfies the same equations (2.97) for the interaction between two slow sound waves, except that the inhomogeneous terms N_1 and N_3 now read

$$\left.\begin{aligned} N_1 &= i(\hat{\alpha}_s - \hat{\alpha}_w)\hat{U}_s\hat{U}_M^* + i\hat{\beta}_s\hat{W}_M^*\hat{U}_s - i\hat{\beta}_w\hat{W}_s\hat{U}_M^* + \hat{V}_s\hat{U}_{MY}^* + \hat{V}_M^*\hat{U}_{sY}, \\ N_3 &= i\hat{\alpha}_s\hat{W}_s\hat{U}_M^* - i\hat{\alpha}_w\hat{W}_M^*\hat{U}_s + i(\hat{\beta}_s - \hat{\beta}_w)\hat{W}_s\hat{W}_M^* + \hat{V}_s\hat{W}_{MY}^* + \hat{V}_M^*\hat{W}_{sY}, \end{aligned}\right\} \tag{2.145}$$

for the excitation by the difference mode. The forcing terms for the sum mode are

$$\left.\begin{aligned} N_1 &= i(\hat{\alpha}_s + \hat{\alpha}_w)\hat{U}_s\hat{U}_M + i\hat{\beta}_s\hat{W}_M\hat{U}_s + i\hat{\beta}_w\hat{W}_s\hat{U}_M + \hat{V}_s\hat{U}_{MY} + \hat{V}_M\hat{U}_{sY}, \\ N_3 &= i\hat{\alpha}_s\hat{W}_s\hat{U}_M + i\hat{\alpha}_w\hat{W}_M\hat{U}_s + i(\hat{\beta}_s + \hat{\beta}_w)\hat{W}_s\hat{W}_M + \hat{V}_s\hat{W}_{MY} + \hat{V}_M\hat{W}_{sY}. \end{aligned}\right\} \tag{2.146}$$

Note that the transverse velocity $\hat{V}_s$ of the acoustic-induced fluctuation contributes to the forcing for a sound wave on the triple-deck scale.

The boundary conditions for the forced response, for both difference- and sum-

mode cases, read

$$\hat{U}_2(0) = -(i\hat{\alpha}_s\lambda_0)^{1/3}\hat{U}_s'(\eta_0)\hat{F}_w, \quad \hat{V}_2(0) = 0, \quad \hat{W}_2(0) = -(i\hat{\alpha}_s\lambda_0)^{1/3}\hat{W}_s'(\eta_0)\hat{F}_w, \tag{2.147}$$

which implies that $\hat{V}_{2,Y}(0) = i(i\hat{\alpha}_s\lambda_0)^{1/3}\left\{\hat{\alpha}_{TS}\hat{U}_s'(\eta_0) + \hat{\beta}_{TS}\hat{W}_s'(\eta_0)\right\}\hat{F}_w$, with the expressions for $\hat{U}_s'(\eta_0)$ and $\hat{W}_s'(\eta_0)$ being deduced from (2.87) and (2.86), respectively, as

$$\hat{U}_s'(\eta_0) = \frac{i\hat{P}_s}{\hat{\alpha}_s(i\hat{\alpha}_s\lambda_0)^{2/3}}\left[\frac{(\hat{\alpha}_s^2+\hat{\beta}_s^2)Ai(\eta_0)}{Ai'(\eta_0)} - \hat{\beta}_s^2\int_{\eta_0}^{\infty} Ai(\tilde{\eta})d\tilde{\eta}\right], \tag{2.148}$$

$$\hat{W}_s'(\eta_0) = -\hat{\beta}_s\hat{P}_s\int_{\eta_0}^{\infty} Ai(\tilde{\eta})d\tilde{\eta}. \tag{2.149}$$

Rearranging the forced-response equations in the same way as we did for (2.97), it can be shown that the no-slip condition (2.147) implies that

$$\begin{aligned}\hat{V}_{2,YYY} = {} & (\hat{\alpha}_{TS}^2+\hat{\beta}_{TS}^2)\hat{P}_2 - 2i\hat{\alpha}_{TS}A'(x_1)\hat{P}_{TS} \\ & + \hat{\omega}_{TS}(i\hat{\alpha}_s\lambda_0)^{1/3}\left\{\hat{\alpha}_{TS}\hat{U}_s'(\eta_0) + \hat{\beta}_{TS}\hat{W}_s'(\eta_0)\right\}\hat{F}_w \quad \text{at} \quad Y=0. \end{aligned} \tag{2.150}$$

An inhomogeneous Airy equation (2.100) for $\hat{V}_{2,YY}$ is obtained and solved to give

$$\begin{aligned}\hat{V}_{2,Y} = {} & \frac{1}{3}(i\hat{\alpha}_{TS}\lambda_0)^{-1}\Lambda(x_1)\left\{(\tilde{\eta}-3\tilde{\eta}_0)Ai(\tilde{\eta}) + 2\tilde{\eta}_0 Ai(\tilde{\eta}_0)\right\} + \int_{\tilde{\eta}_0}^{\tilde{\eta}}\tilde{M}(\eta',\tilde{\eta}_0)d\eta' \\ & + q_2\int_{\tilde{\eta}_0}^{\tilde{\eta}} Ai(\eta')d\eta' + i(i\hat{\alpha}_s\lambda_0)^{1/3}\left\{\hat{\alpha}_{TS}\hat{U}_s'(\eta_0) + \hat{\beta}_{TS}\hat{W}_s'(\eta_0)\right\}\hat{F}_w, \end{aligned} \tag{2.151}$$

where q_2 is a function of x_1, and $\tilde{M}$ has the same expression as (2.102) but with H being replaced by the forcing (2.145) or (2.146) pertaining to the present problem.

The matching condition with the main-deck solution (2.64) gives (2.103), but with the solution (2.151) it leads to

$$\begin{aligned}-i\hat{\alpha}_{TS}\lambda_0\hat{B}_2 - (i\hat{\alpha}_{TS}\lambda_1 x_1\hat{A} + \lambda_0 A'(x_1))B_1 = {} & \frac{2}{3}(i\hat{\alpha}_{TS}\lambda_0)^{-1}\Lambda\tilde{\eta}_0 Ai(\tilde{\eta}_0) + \int_{\tilde{\eta}_0}^{\infty}\tilde{M}(\eta',\tilde{\eta}_0)d\eta' \\ & + i(i\hat{\alpha}_s\lambda_0)^{1/3}\left\{\hat{\alpha}_{TS}\hat{U}_s'(\eta_0) + \hat{\beta}_{TS}\hat{W}_s'(\eta_0)\right\}\hat{F}_w + q_2\int_{\tilde{\eta}_0}^{\infty} Ai(\eta')d\eta'. \end{aligned} \tag{2.152}$$

Use of (2.151) in (2.150) gives

$$\frac{2}{3}(i\hat{\alpha}_{TS}\lambda_0)^{-1/3}\Lambda\left\{Ai'(\tilde{\eta}_0)-\tilde{\eta}_0 Ai''(\tilde{\eta}_0)\right\}+(i\hat{\alpha}_{TS}\lambda_0)^{2/3}\left\{\pi Bi'(\tilde{\eta}_0)\int_\infty^{\tilde{\eta}_0}Ai(\eta')H(Y')d\eta'\right\}$$
$$+(i\hat{\alpha}_{TS}\lambda_0)^{2/3}q_2Ai'(\tilde{\eta}_0)=(\hat{\alpha}_{TS}^2+\hat{\beta}_{TS}^2)\hat{P}_2-2i\hat{\alpha}_{TS}A'(x_1)\hat{P}_{TS}$$
$$+\hat{\omega}_{TS}(i\hat{\alpha}_s\lambda_0)^{1/3}\left\{\hat{\alpha}_{TS}\hat{U}_s'(\eta_0)+\hat{\beta}_{TS}\hat{W}_s'(\eta_0)\right\}\hat{F}_w. \quad (2.153)$$

The relation (2.67), which follows from the matching between the upper-deck solution and the second term of the main-deck solution, remains valid. From (2.67) and (2.152)-(2.153), we obtain the same amplitude equation as (2.108) but N is now given by

$$N=\frac{1}{a}\left\{\mathcal{F}_R-\frac{\hat{\omega}_{TS}\lambda_0\hat{\gamma}_{TS}(i\hat{\alpha}_s\lambda_0)^{1/3}}{\hat{\alpha}_{TS}^2+\hat{\beta}_{TS}^2}\left(1+\frac{r_A}{\tilde{\eta}_0}\right)\hat{F}_w\left(\hat{\alpha}_{TS}\hat{U}_s'(\eta_0)+\hat{\beta}_{TS}\hat{W}_s'(\eta_0)\right)\right\}, \quad (2.154)$$

where $\mathcal{F}_R$ is the same as $\mathcal{F}$, provided that H is replaced by the one pertaining to the sound-roughness interaction, and $r_A=Ai'(\tilde{\eta}_0)/\int_{\tilde{\eta}_0}^\infty Ai(\eta')d\eta'$.

In the present case of a slow sound wave interacting with a wavy wall, the excited T-S mode has a streamwise velocity $u_{TS}=\varepsilon_s h\bar{\varepsilon}^{-1}R^{1/8}C^{1/8}\tau_w^{1/2}\hat{\alpha}_{TS}^{-1}A_\infty U_m$, as (2.141) indicates, and the coupling coefficient is defined as

$$C_R=u_{TS}/\varepsilon_s=hR^{5/16}C^{-1/16}\tau_w^{-1/4}\hat{\alpha}_{TS}^{-1}A_\infty U_m\equiv hR^{5/16}\Lambda_{SR}, \quad (2.155)$$

which may, after using (2.124), be written as

$$C_R=\frac{h^*}{L}R^{15/16}C^{-11/16}\tau_w^{-7/4}\hat{\alpha}_{TS}^{-1}A_\infty U_m. \quad (2.156)$$

2.5 Parametric study and discussion

The analysis until now has provided the expressions for the two quantities of interest, the coupling coefficient, Λ_{SS} or Λ_{SR}, and the reflection coefficient $\mathcal{R}$. Using Matlab, we will now evaluate them for typical values of the relevant parametres.

2.5.1 Reflection coefficient

The reflection coefficient $\mathcal{R}$ depends on the frequency $\hat{\omega}_1$ and wavenumbers $\hat{\alpha}_1$ and $\hat{\beta}_1$. We first consider $\hat{\omega}_1$ whose size is comparable with $\hat{\omega}_{TS}$. Figure 2.6 shows how

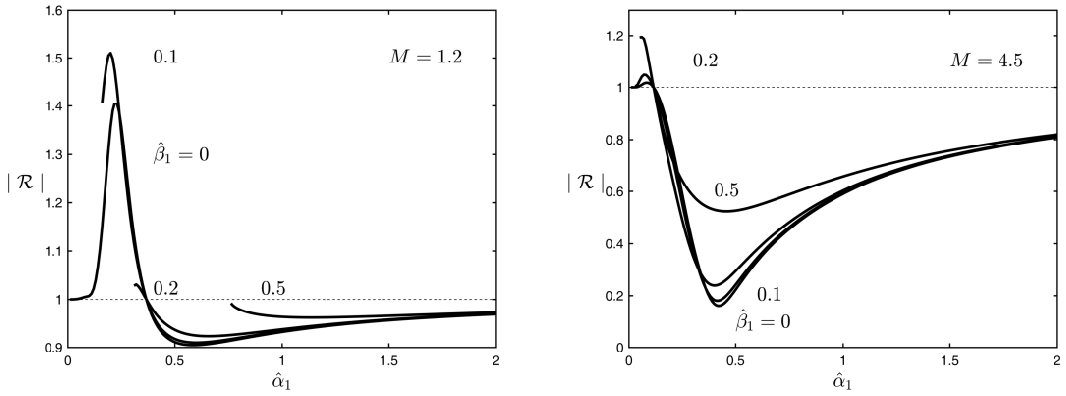


Figure 2.6: $|\mathcal{R}|$ as a function of $\hat{\alpha}_1$ for $\hat{\beta}_1 = 0,\ 0.1,\ 0.2,\ 0.5$. The frequencies chosen are $\hat{\omega}_1 = 2\hat{\omega}_{TS}$ with $\hat{\omega}_{TS} = 0.28$ for $M = 1.2$, and $\hat{\omega}_{TS} = 0.13$ for $M = 4.5$.

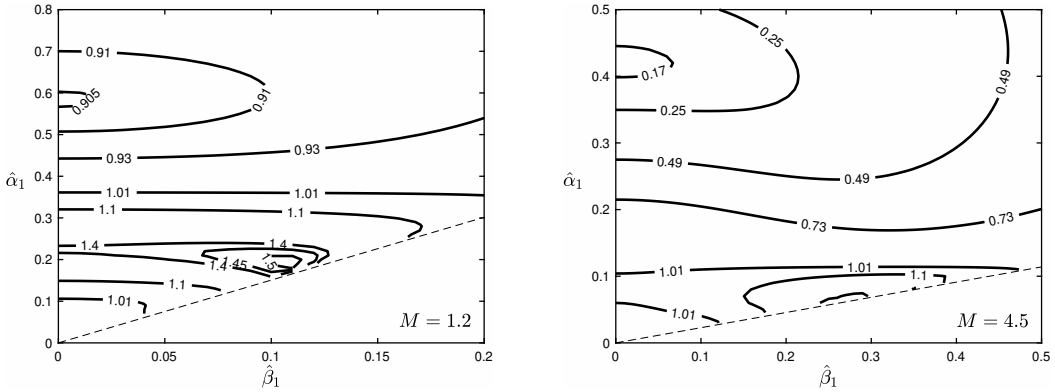


Figure 2.7: Contour plot of $|\mathcal{R}|$ as a function of $\hat{\alpha}_1$ and $\hat{\beta}_1$ for $M = 1.2$ and $M = 4.5$. The frequency chosen is $\hat{\omega}_1 = 2\hat{\omega}_{TS}$ with $\hat{\omega}_{TS} = 0.28$.

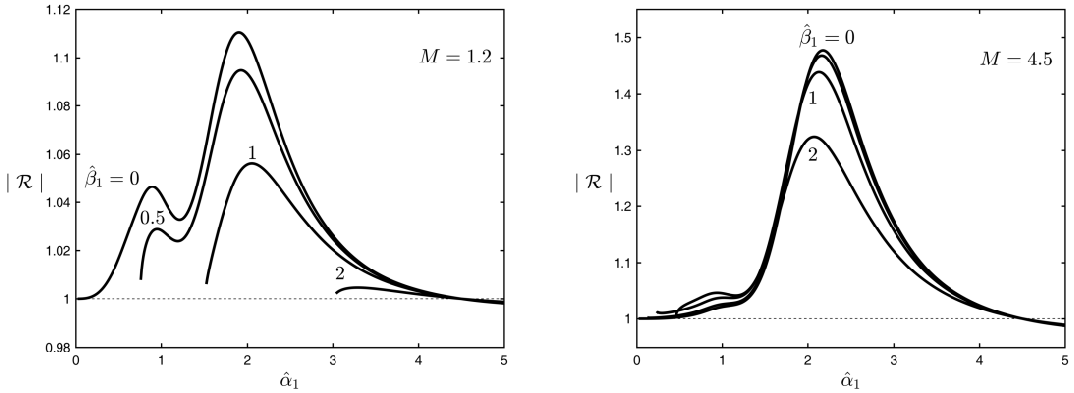


Figure 2.8: $|\mathcal{R}|$ as a function of $\hat{\alpha}_1$ for $\hat{\beta}_1 = 0,\ 0.5,\ 1,\ 2$. The frequency chosen is $\hat{\omega}_1 = 3$.

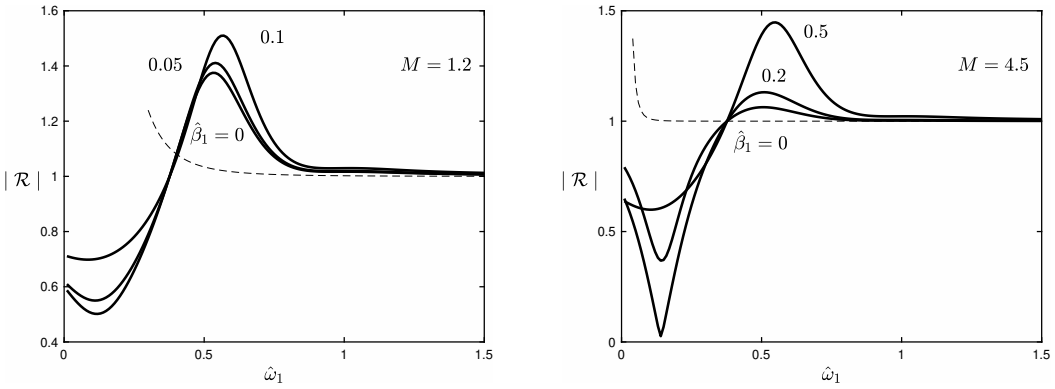


Figure 2.9: $|\mathcal{R}|$ as a function of $\hat{\omega}_1$ for $\hat{\beta}_1 = 0$, 0.05, 0.1 for the $M = 1.2$ case, and $\hat{\beta}_1 = 0$, 0.2, 0.5 for the $M = 4.5$ case. The streamwise wavenumber chosen is $\hat{\alpha}_1 = 0.2$. The asymptote (2.157) is plotted for $\hat{\beta}_1 = 0$ as the dashed lines.

$|\mathcal{R}|$ varies with $\hat{\alpha}_1$ and $\hat{\beta}_1$ at two Mach numbers $M = 1.2$ and $M = 4.5$. In each case, for relatively small $\hat{\beta}_1$, there exists a small interval of $\hat{\alpha}_1$, for which $|\mathcal{R}| > 1$, i.e. over-reflection takes place (the amplitude of the reflected acoustic waves is greater than that of the impinging waves). When $\hat{\beta}_1$ exceeds a critical value, $|\mathcal{R}| < 1$ for all $\hat{\alpha}_1$. In order to give an overview of the reflection property, figure 2.7 shows contours of $|\mathcal{R}|$ as a function of the streamwise and spanwise wavenumbers. Note that $\hat{\alpha}_1 > \hat{\beta}_1/\sqrt{M^2 - 1}$ for a sound wave to exist in the supersonic regime. In the $M = 1.2$ case, $|\mathcal{R}|$ is nearly unity in the majority of the parameter plane, except in a small region surrounding the maximum at $(\hat{\alpha}_1, \hat{\beta}_1) \simeq (0.2, 0.1)$, where $|\mathcal{R}|$ is significantly greater than 1, indicating over-reflection. In the $M = 4.5$ case, $|\mathcal{R}|$ varies in a greater region, and $|\mathcal{R}| < 1$ in the majority of the parameter space, that is, the boundary layer is absorbing. Moderate over-reflection occurs for a small region of the parameter space near the maximum $(\hat{\alpha}_1, \hat{\beta}_1) \simeq (0.07, 0.28)$.

We now consider another typical case, namely, $\hat{\omega}_1$ and $\hat{\omega}_2$ are appreciably greater than $\hat{\omega}_{TS}$, but still of order one. An $\hat{\omega}_1 = \mathcal{O}(1)$ means that for $c_1 = \mathcal{O}(1)$, $\hat{\alpha}_1$ must also be of $\mathcal{O}(1)$. Figure 2.8 shows the variation of $|\mathcal{R}|$ with $\hat{\alpha}_1$ for a range of $\hat{\beta}_1$. A mild over-reflection occurs for small $\hat{\alpha}_1$ in the $M = 1.2$ case. Over-reflection is more pronounced for the $M = 4.5$ case.

In figures 2.9 and 2.10, $|\mathcal{R}|$ is plotted against $\hat{\omega}_1$ for different spanwise wavenumbers, each with a fixed $\hat{\alpha}_1$. For low frequencies, under-reflection takes place, while for moderate frequencies, over-reflection is observed. $|\mathcal{R}|$ exhibits a peak at $\hat{\omega}_1 \sim \mathcal{O}(\hat{\alpha}_1)$, after which $|\mathcal{R}|$ decays monotonically and approaches unity as $\hat{\omega}_1 \to \infty$. This behaviour can be demonstrated analytically by noting that $\int_{\eta_0}^{\infty} Ai(\eta')d\eta'/Ai'(\eta_0) \sim -\eta_0^{-1}(1 - \eta_0^{-3/2} + \cdots)$ for $\eta_0 = -i\hat{\omega}_1/(i\hat{\alpha}_1\lambda_0)^{2/3} \gg 1$. It

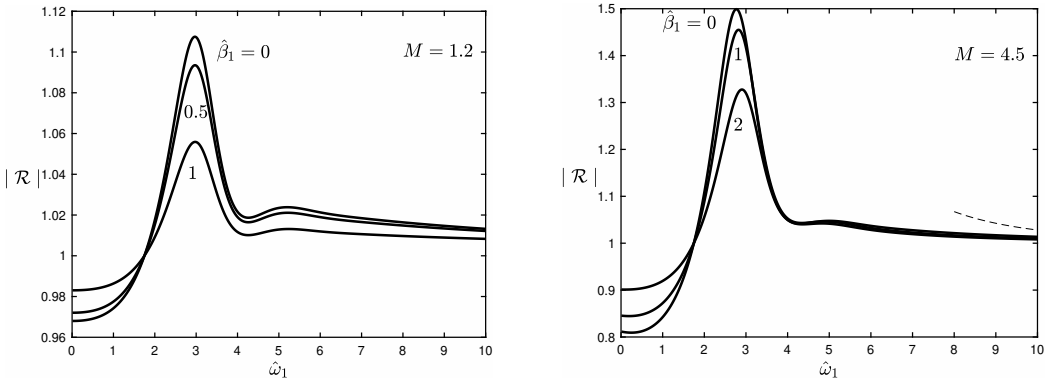


Figure 2.10: $|\mathcal{R}|$ as a function of $\hat{\omega}_1$ for $\hat{\beta}_1 = 0$, 0.5, 1 in the M=1.2 case and $\hat{\beta}_1 = 0$, 1, 2 in the case M=4.5. The streamwise wavenumber chosen is $\hat{\alpha}_1 = 2$. The asymptote (2.157) is plotted for $\hat{\beta}_1 = 0$ as the dashed line on the right figure.

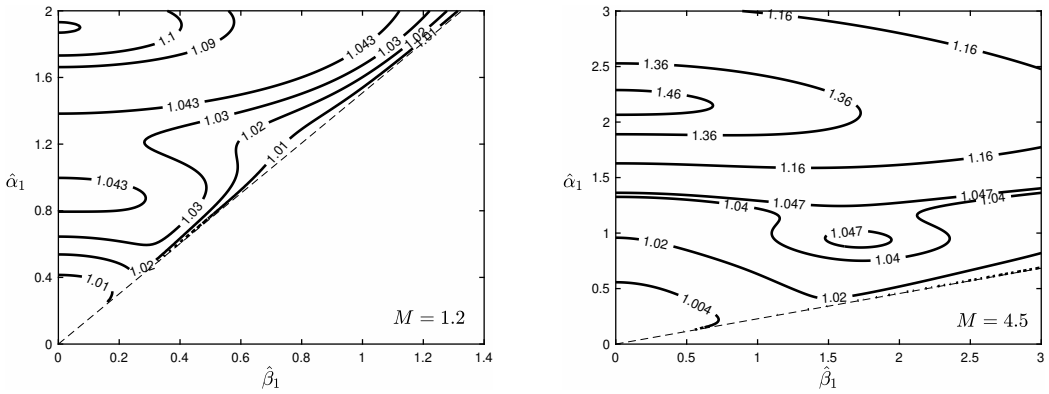


Figure 2.11: Contour plot of $|\mathcal{R}|$ as a function of $\hat{\alpha}_1$ and $\hat{\beta}_1$ for the $M = 1.2$ case (left) and $M = 4.5$ case (right). The frequency chosen is $\hat{\omega}_1 = 3$.

follows from (2.82) that as $\hat{\omega}_1 \to \infty$,

$$\mathcal{R} = 1 - \frac{2i\hat{\alpha}_1(\hat{\alpha}_1^2 + \hat{\beta}_1^2)}{\hat{\gamma}_1\lambda_0}\hat{\omega}_1^{-1} - \frac{2\hat{\alpha}_1^2(\hat{\alpha}_1^2 + \hat{\beta}_1^2)^2}{\hat{\gamma}_1^2\lambda_0^2}\hat{\omega}_1^{-2} + \cdots . \tag{2.157}$$

Figure 2.11 shows contour plots of $|\mathcal{R}|$ as a function of $\hat{\alpha}_1$ and $\hat{\beta}_1$ for the two different Mach numbers considered already. This time, the frequency chosen is $\hat{\omega}_1 = 3$. Two local maxima for $|\mathcal{R}|$ are found in the $M = 1.2$ case, at $(\hat{\alpha}_1, \hat{\beta}_1) \simeq (0.9, 0)$ and $(\hat{\alpha}_1, \hat{\beta}_1) \simeq (1.9, 0)$. In the M=4.5 case, a strong over-reflection occurs near $(\hat{\alpha}_1, \hat{\beta}_1) \simeq (2.2, 0)$, and very moderate over-reflection takes place at a much higher spanwise wavenumber $\hat{\beta}_1 \simeq 1.7$ and $\hat{\alpha}_1 \simeq 1$.

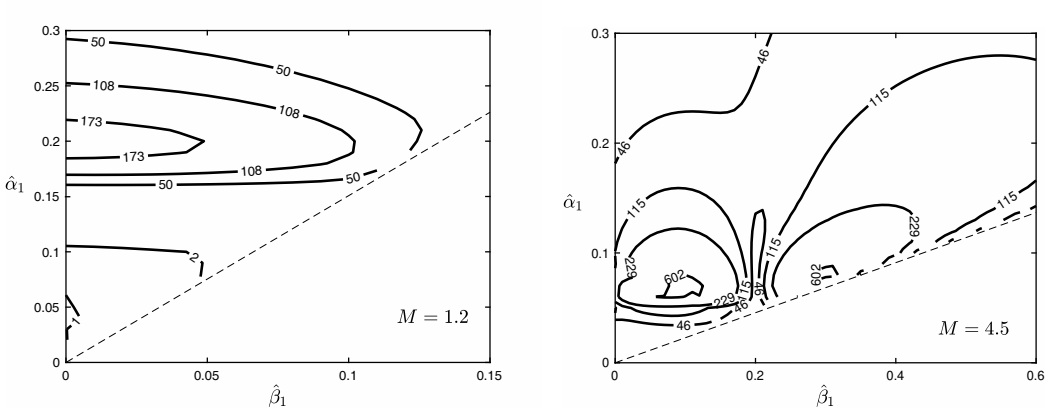


Figure 2.12: Contour plot of Λ_{SS} as a function of $\hat{\alpha}_1$ and $\hat{\beta}_1$. The neutral T-S mode excited has $\hat{\beta}_{TS} = 0.2$, for which $(\hat{\omega}_{TS}, \hat{\alpha}_{TS}) = (0.28, 0.13)$ at $M = 1.2$, and $(\hat{\omega}_{TS}, \hat{\alpha}_{TS}) = (0.13, 0.04)$ at $M = 4.5$. The sound-wave frequency chosen is $\hat{\omega}_1 = 2\hat{\omega}_{TS}$.

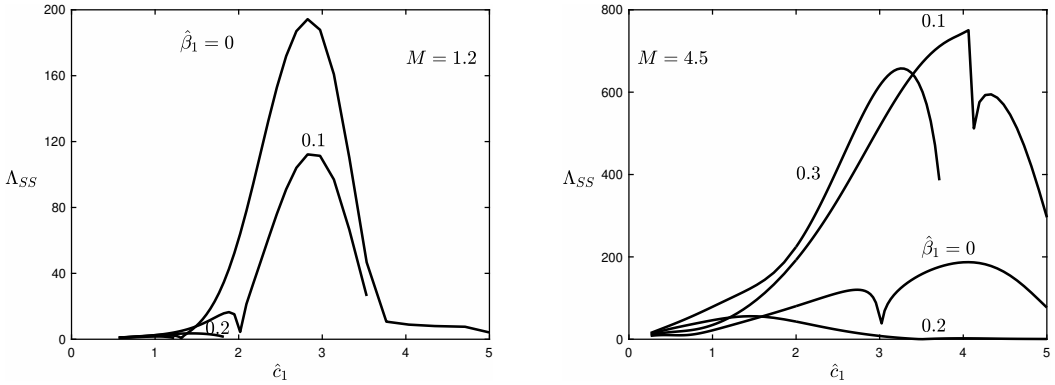


Figure 2.13: Λ_{SS} as a function of $\hat{c}_1$ for $\hat{\beta}_1 = 0$, 0.1, 0.2 and 0.3. The neutral T-S mode excited has $\hat{\beta}_{TS} = 0.2$, for which $(\hat{\omega}_{TS}, \hat{\alpha}_{TS}) = (0.28, 0.13)$ at $M = 1.2$, and $(\hat{\omega}_{TS}, \hat{\alpha}_{TS}) = (0.13, 0.04)$ at $M = 4.5$. The sound-wave frequencies chosen are $\hat{\omega}_1 = 2\hat{\omega}_{TS}$.

2.5.2 Rescaled coupling coefficient for sound-sound interaction

The main quantity of interest, the coupling coefficient, is now investigated for different conditions. Figure 2.12 shows contour plots of the rescaled coupling coefficients Λ_{SS} as a function of $\hat{\alpha}_1$ and $\hat{\beta}_1$ for $M = 1.2$ and $M = 4.5$ respectively. For the $M = 1.2$ case, a maximum $\Lambda_{SS} \approx 200$ appears near $(\hat{\alpha}_1, \hat{\beta}_1) = (0.2, 0)$. For the $M = 4.5$ case, two maxima occur, both with $\Lambda_{SS} \approx 600$. Note that in all these cases, the coupling coefficient peaks are found in the regions of $\hat{\alpha}_1 \sim \mathcal{O}(\hat{\omega}_1)$, i.e. $\hat{c}_1 = \mathcal{O}(1)$.

Figure 2.13 shows the coupling coefficient against the phase speed of the sound wave, for four different spanwise wavenumbers. In the $M = 1.2$ case, the maximum coupling coefficient is attained at $\hat{\beta}_1 = 0$. In the $M = 4.5$ case, $\hat{\beta}_1 = 0.1$ appears

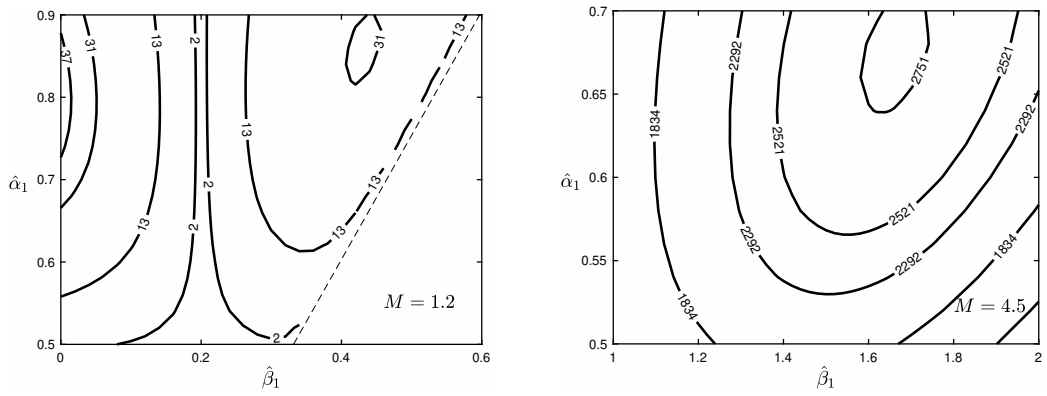


Figure 2.14: Contour plot of Λ_{SS} as a function of $\hat{\alpha}_1$ and $\hat{\beta}_1$. The neutral T-S mode excited has $\hat{\beta}_{TS} = 0.2$, for which $(\hat{\omega}_{TS}, \hat{\alpha}_{TS}) = (0.28, 0.13)$ at $M = 1.2$, and $(\hat{\omega}_{TS}, \hat{\alpha}_{TS}) = (0.13, 0.04)$ at $M = 4.5$. The frequency chosen is $\hat{\omega}_1 = 3$.

as the spanwise wavenumber that maximizes Λ_{SS}. In both cases, Λ_{SS} concentrates around $\hat{c}_1 = \mathcal{O}(1)$, and diminishes rapidly as $\hat{c}_1$ increases, indicating that the slow acoustic waves on the triple-deck scale are most effective in generating T-S modes.

We now consider the cases where the frequencies of the two sound waves, $\hat{\omega}_1$ and $\hat{\omega}_2$, are both much greater than $\hat{\omega}_{TS}$, but $\hat{\omega}_1 - \hat{\omega}_2 = \hat{\omega}_{TS}$. Figure 2.14 (left) shows the contours of Λ_{SS} for $M = 1.2$. Two maxima were observed: one at $(\hat{\alpha}_1, \hat{\beta}_1) = (0.86, 0.42)$, and the other at $(\hat{\alpha}_1, \hat{\beta}_1) = (0.8, 0)$. The maxima are both about $\Lambda_{SS} \approx 40$. Figure 2.14 (right) displays the contours of Λ_{SS} for the $M = 4.5$ case. The coupling coefficient is much larger with a maximum $\Lambda_{SS} \approx 3000$ at $(\hat{\alpha}_1, \hat{\beta}_1) = (0.67, 1.65)$. A comparison of the results in figures 2.12a and 2.14b suggests that at lower Mach numbers, acoustic waves with $\hat{\omega}_1 = \mathcal{O}(\hat{\omega}_{TS})$ are more effective, whereas at high Mach numbers, the boundary layer is more receptive to acoustic with relatively high frequencies.

Figure 2.15 shows Λ_{SS} against $\hat{c}_1$ for the two Mach numbers considered. Λ_{SS} attains its largest values for $\hat{c}_1 = \mathcal{O}(1)$, and its size decreases as $\hat{c}_1$ increases for all spanwise wavenumbers.

A further parametric study of Λ_{SS} as a function of $\hat{c}_1$ has been carried out for two different neutral T-S modes, $\hat{\beta}_{TS} = 0.2$ and $\hat{\beta}_{TS} = 0.5$, which are in the increasing and decreasing portions of the neutral curve (figure 2.2) respectively at the Mach number $M = 4.5$. The results are displayed in figure 2.16 (for $\hat{\alpha}_1 = 0.2$ and $\hat{\alpha}_1 = 1$). Λ_{SS} reaches $\mathcal{O}(10^2)$ and $\mathcal{O}(10^4)$ magnitude for moderate values of $\hat{c}_1$ in the $\hat{\beta}_{TS} = 0.2$ and $\hat{\beta}_{TS} = 0.5$ cases respectively. As $\hat{c}_1$ is increased further, Λ_{SS} decreases, indicating the significance of the slow acoustic waves on the triple-deck scaling, as expected on the theoretical basis.

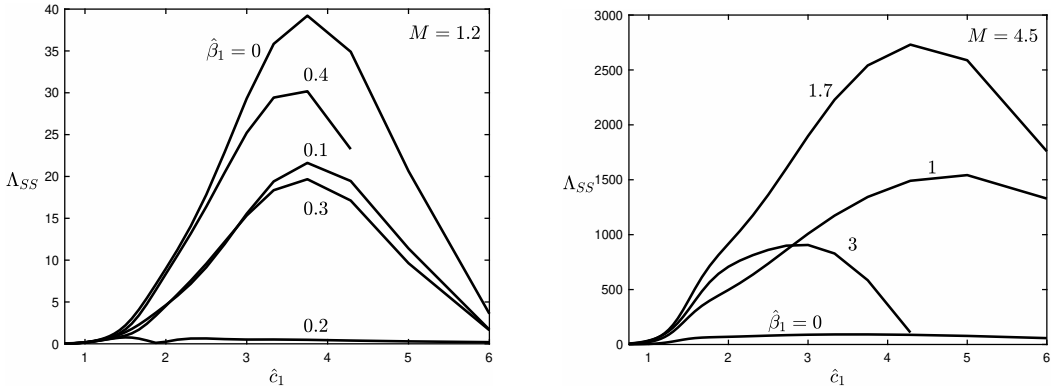


Figure 2.15: Λ_{SS} as a function of $\hat{c}_1$ for different values of $\hat{\beta}_1$. The neutral T-S mode excited has $\hat{\beta}_{TS} = 0.2$, for which $(\hat{\omega}_{TS}, \hat{\alpha}_{TS}) = (0.28, 0.13)$ at $M = 1.2$, and $(\hat{\omega}_{TS}, \hat{\alpha}_{TS}) = (0.13, 0.04)$ at $M = 4.5$. The sound-wave frequency chosen is $\hat{\omega}_1 = 3$.

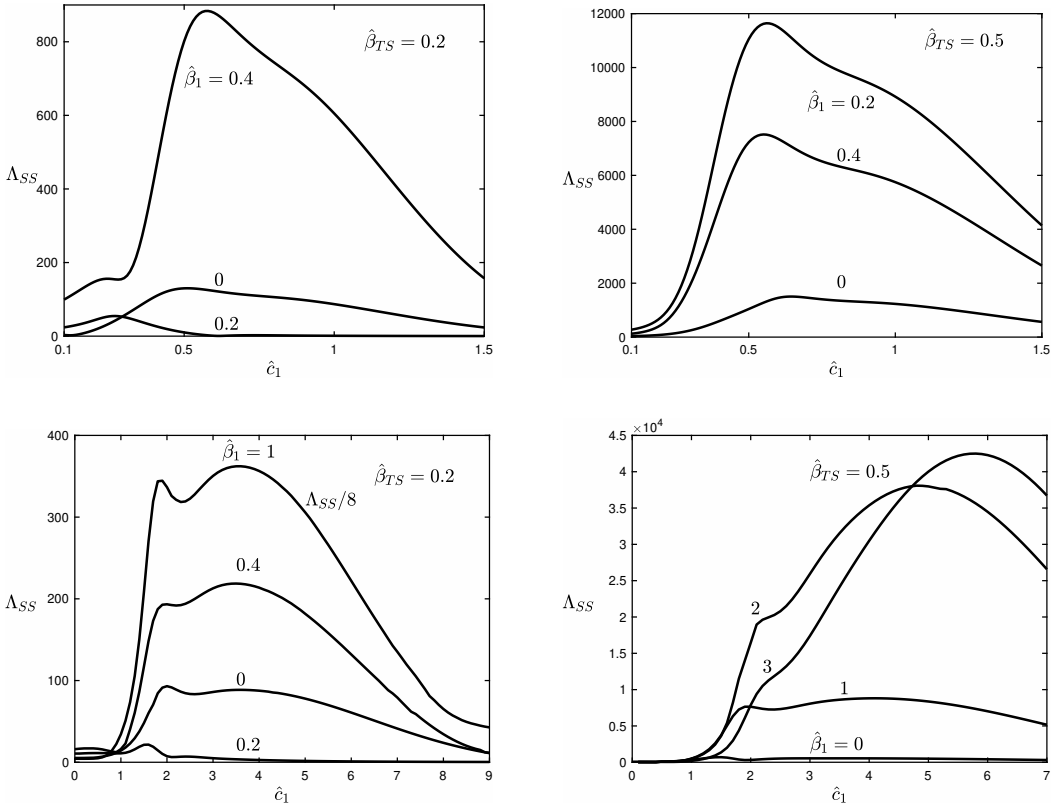


Figure 2.16: Λ_{SS} as a function of $\hat{c}_1$ for $\hat{\alpha}_1 = 0.2$ (1st row), $\hat{\alpha}_1 = 1$ (2nd row) and different values of $\hat{\beta}_1$ at M=4.5. The neutral T-S modes excited have $\hat{\beta}_{TS} = 0.2$, for which $(\hat{\omega}_{TS}, \hat{\alpha}_{TS}) = (0.13, 0.04)$, and $\hat{\beta}_{TS} = 0.5$, for which $(\hat{\omega}_{TS}, \hat{\alpha}_{TS}) = (0.104, 0.029)$. The result for $\hat{\beta}_1 = 1$ and $\hat{\beta}_{TS} = 0.2$ is plotted to $1/8$ of the original values.

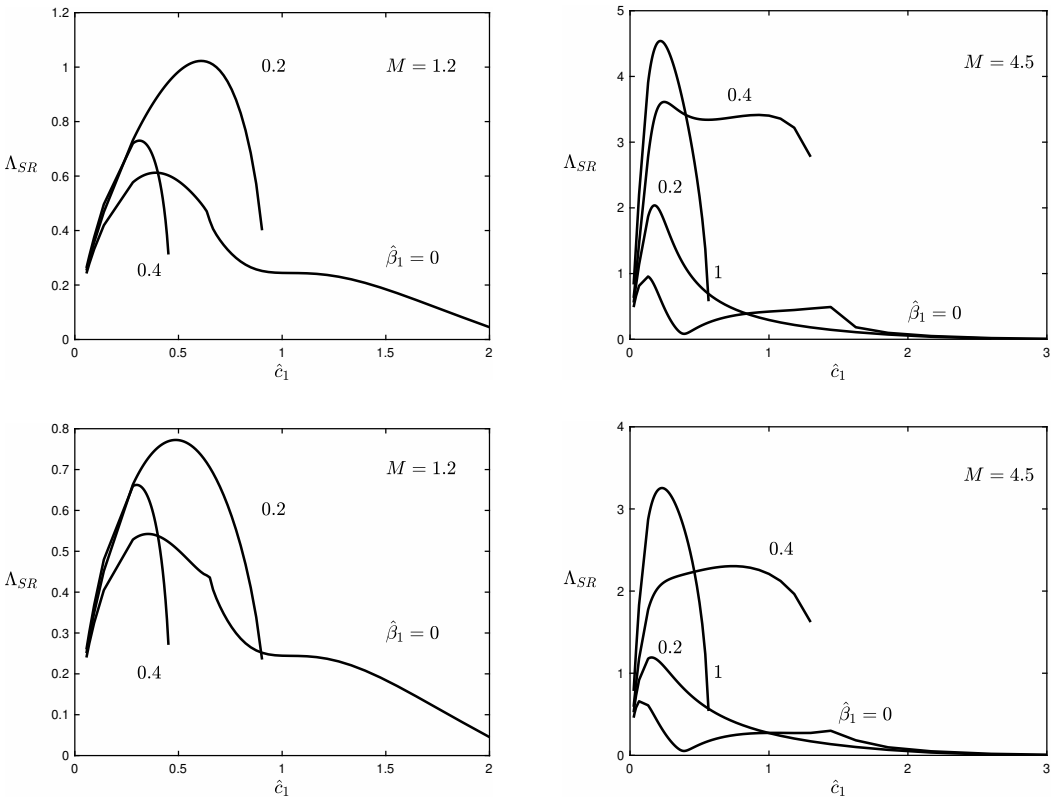


Figure 2.17: Λ_{SR} as a function of $\hat{c}_1$ for $\hat{\beta}_1 = 0$, 0.2, 0.4 and 1 in the cases of S+R (first row) and S-R (second row) interactions for $\hat{\beta}_{TS} = 0.2$. The frequencies chosen are $\hat{\omega}_1 = \hat{\omega}_{TS}$ with $\hat{\omega}_{TS} = 0.28$ ($\hat{\alpha}_{TS} = 0.13$) for M=1.2 and $\hat{\omega}_{TS} = 0.13$ ($\hat{\alpha}_{TS} = 0.04$) for M=4.5.

2.5.3 Rescaled coupling coefficient for sound-roughness interaction

Results for the receptivity due to sound-roughness interactions are now presented. The rescaled coupling coefficient Λ_{SR} against $\hat{c}_1$ is shown in figure 2.17 for $\hat{\beta}_{TS} = 0.2$ at two different Mach numbers. The excitation through the difference and sum modes is referred to as S-R and S+R, respectively. One notes that Λ_{SR} acquires $\mathcal{O}(1)$ values, and the results for S+R and S-R interactions are very similar. Receptivity is considerably stronger for $M = 4.5$ than for $M = 1.2$. Figure 2.18 shows Λ_{SR} for the T-S mode with $\hat{\beta}_{TS} = 0.5$. The trend is similar to the case of $\hat{\beta}_{TS} = 0.2$. However, the coupling coefficients are about twice and five times of those for $\hat{\beta}_{TS} = 0.2$ at $M = 1.2$ and 4.5, respectively.

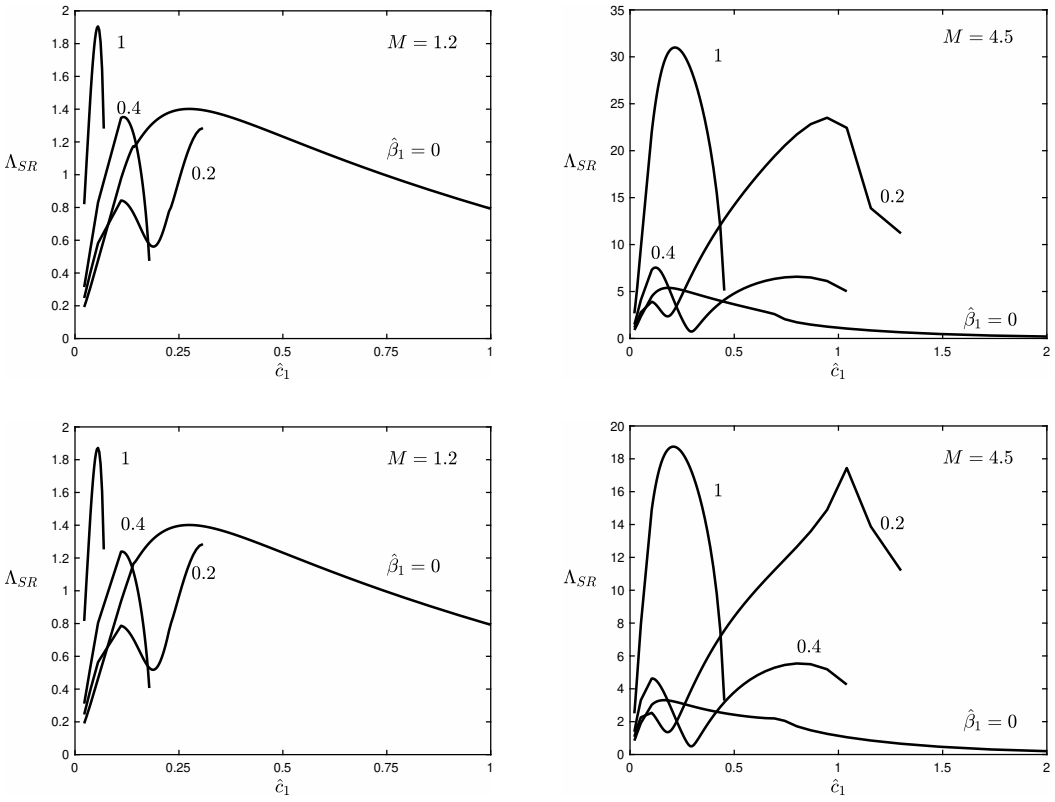


Figure 2.18: Λ_{SR} as a function of $\hat{c}_1$ for $\hat{\beta}_1 = 0,\ 0.2,\ 0.4$ and 1 in the cases of S+R (first row) and S-R (second row) interactions for $\hat{\beta}_{TS} = 0.5$. The frequencies chosen are $\hat{\omega}_1 = \hat{\omega}_{TS}$ with $\hat{\omega}_{TS} = 0.1108$ ($\hat{\alpha}_{TS} = 0.032$) for M=1.2 and $\hat{\omega}_{TS} = 0.104$ ($\hat{\alpha}_{TS} = 0.029$) for M=4.5.

2.5.4 Initial amplitude and coupling coefficient at typical Reynolds numbers

The results displayed in §2.5.2 and §2.5.3 for the rescaled coupling coefficients Λ_{SS} and Λ_{SR} (as well as the frequencies, wavenumbers and phase speeds) are independent of the Reynolds number R. The corresponding coupling coefficients, C_A and C_R, and the initial magnitude of u_{TS} are calculated for representative values of R, $\hat{\alpha}_1$, $\hat{\beta}_1$ and $\hat{\omega}_1$, the wavenumbers and frequency of the sound wave involved in the generation of the T-S mode. The normalised roughness amplitude h is related to the physical height h^* through the relation (2.124). The sound-wave amplitude ε_s, the roughness height h^* and the value of L are taken to be those of King and Breuer (2002): $\varepsilon_s = 10^{-5}$, $h^* = 20 \times 10^{-6}$ m and $L = 0.5$ m. For the three Mach numbers considered, the Reynolds number is chosen to be $R = 10^6$ for $M = 1.2$, $2 \cdot 10^6$ for $M = 3$ and $R = 4 \cdot 10^6$ for $M = 4.5$, typical values encountered in aeronautical applications. As is shown in Table 4.1, for sound-sound interaction the coupling coefficient $C_A = \mathcal{O}(1)$ at $M = 1.2$, and at $M = 3$ and 4.5, C_A is of $\mathcal{O}(1)$ for low-frequency sound but of $\mathcal{O}(10)$ for high-frequency sound. The coupling coefficient for the sound-roughness interaction, C_R, is of $\mathcal{O}(10)$ at $M = 1.2$ and 3, and increases to $\mathcal{O}(10^2)$ at 4.5 with an isothermal wall. This means that the amplitude of the generated T-S modes could vary from several up to nearly 100 times that of the impinging sound waves. Calculations have been carried out using Sutherland's law and isothermal wall condition with ($T_\infty = 300K$) and $\tau_w = 3$, for the cases of $M = 3$ and 4.5, where the local wall shear $\lambda_0 = 0.40037$ and 0.406 respectively. For the moderate Mach numbers considered, the results are not significantly different from those for the Chapman's law and adiabatic walls. It is worth noting that the level of acoustic waves in supersonic wind tunnel experiments is likely to be much higher than $\varepsilon_s = 10^{-5}$ used here. If ε_s raises to 10^{-4}, the initial amplitude and coupling coefficient would be 100 and 10 times as large respectively for the sound-sound interaction. For the sound-roughness interaction, equation (2.156) indicates a strong dependence on the wall temperature, $C_R \sim \tau_w^{-7/4}$. For an insulated wall at large Mach numbers, $\tau_w \sim \mathcal{O}(0.2M^2)$, but for a severely cooled wall, $\tau_w \sim \mathcal{O}(1)$ and so the receptivity would be much stronger, which could substantially reduce, or even offset, the benefit of wall cooling for stabilizing the first Mack (T-S) modes.

M	$\hat{\beta}_{TS}$	$\hat{\alpha}_{TS}$	$\hat{\omega}_{TS}$	$\hat{\alpha}_1$	$\hat{\beta}_1$	$\hat{\omega}_1$	Λ_{SS}	R	c_{TS}	c_1	u_{TS}	C_A
1.2	0.2	0.130	0.283	0.3	0.05	0.57	28.97	10^6	0.44	0.38	6.87×10^{-6}	0.687
1.2	0.3	0.101	0.239	1.2	0.7	3	42.71	10^6	0.478	0.505	1.01×10^{-5}	1.013
3	0.2	0.06	0.169	0.2	0.05	0.33	92.24	$2 \cdot 10^6$	0.769	0.460	3.23×10^{-5}	3.23
3	0.2	0.06	0.169	2	1.7	3	160.18	$2 \cdot 10^6$	0.769	0.409	5.61×10^{-5}	5.61
3 (isoth.)	0.2	0.065	0.201	0.2	0.05	0.33	36.52	$2 \cdot 10^6$	0.841	0.446	1.28×10^{-5}	1.28
3 (isoth.)	0.2	0.065	0.201	2	1.7	3	68.57	$2 \cdot 10^6$	0.841	0.405	2.40×10^{-5}	2.40
4.5	0.2	0.041	0.131	0.2	0.05	0.31	59.92	$4 \cdot 10^6$	1.077	0.438	3.10×10^{-5}	3.10
4.5	0.2	0.041	0.131	2	1.7	3	403.7	$4 \cdot 10^6$	1.077	0.504	3.50×10^{-4}	34.96
4.5 (isoth.)	0.2	0.043	0.155	0.2	0.05	0.31	43.35	$4 \cdot 10^6$	0.892	0.384	2.24×10^{-5}	2.24
4.5 (isoth.)	0.2	0.043	0.155	2	1.7	3	196.95	$4 \cdot 10^6$	0.892	0.372	1.02×10^{-4}	10.19

M	$\hat{\beta}_{TS}$	$\hat{\alpha}_{TS}$	$\hat{\omega}_{TS}$	$\hat{\alpha}_1$	$\hat{\beta}_1$	$\hat{\omega}_1$	Λ_{SR}	R	c_{TS}	c_1	u_{TS}	C_R
1.2	0.2	0.130	0.283	0.5	0.2	0.283	1.01	10^6	0.44	0.114	1.17×10^{-4}	11.66
3	0.2	0.06	0.169	0.5	1	0.169	1.83	$2 \cdot 10^6$	0.769	0.092	1.26×10^{-4}	12.60
3 (isoth.)	0.2	0.065	0.201	0.5	1	0.201	2.23	$2 \cdot 10^6$	0.841	0.109	1.73×10^{-4}	17.27
4.5	0.2	0.041	0.131	0.5	1	0.131	4.55	$4 \cdot 10^6$	1.077	0.088	2.48×10^{-4}	24.81
4.5 (isoth.)	0.2	0.043	0.155	0.5	1	0.155	4.20	$4 \cdot 10^6$	0.892	0.077	6.23×10^{-4}	62.34

Table 2.1: Typical values of the initial T-S mode amplitude u_{TS} and coupling coefficients, C_A and C_R (sum-mode interaction), at representative Reynolds numbers. The results labelled with 'isoth.' are for Sutherland's law and isothermal wall with $\tau_w = 3$.

2.6 Summary and conclusions

In this chapter, the response and receptivity of supersonic boundary layers over smooth and wavy walls to impinging slow acoustic waves were investigated theoretically in the limit of asymptotically large Reynolds numbers. Two receptivity scenarios were considered. The first one involves the interaction of two slow acoustic waves, and is a new mechanism that operates in boundary layers over a smooth wall. The second one involves the interaction between a sound wave and the stationary perturbation induced by a wavy wall. In both cases, it was demonstrated that with suitable frequencies and wavenumbers of the sound waves and roughness elements, the Tollmien-Schlichting (first Mack) instability modes are excited near the lower branch of the neutral curve. The expressions for the coupling coefficient for the sound-sound and sound-roughness cases were derived, and a parametric study as a function of the oncoming perturbations was carried out for two representative Mach numbers.

The present high-Reynolds-number analysis elucidates the scale matching or resonance mechanisms, which are at the core of receptivity. It led us to identify the most relevant scaling, and obtain a relatively simple and explicit expression for the coupling coefficient in each of the two mechanisms. A significant aspect

of the present mechanisms is that the characteristic frequency and wavelength of the sound waves are on the triple-deck scale, and so their phase speed is small, being of $\mathcal{O}(R^{-1/8})$. The impingement and reflection of such a slow sound wave become interactive, and are described by the triple-deck theory. The most important consequence of this choice of scaling is that $\mathcal{O}(\varepsilon_s)$ fluctuations in the free stream generate much larger, $\mathcal{O}(\varepsilon_s R^{1/8})$, velocity signature in the lower deck, i.e. the boundary layer acts as an amplifier. This is in contrast to the usual scaling of the phase speed being $\mathcal{O}(1)$ or larger, for which such an amplification effect is absent: an $\mathcal{O}(\varepsilon_s)$ free-stream perturbation generates a response of the same order of magnitude. For the sound waves on the triple-deck scale, the receptivity is therefore much more efficient. For the sound-sound interaction, the initial amplitude, which is due to the dominant interaction in the lower deck, is of $\mathcal{O}(\varepsilon_s^2 R^{9/16})$, greater than that for the usual scaling by a factor of $\mathcal{O}(R^{1/4})$. In the case of sound-roughness interaction, the initial amplitude of the T-S wave excited is of $\mathcal{O}(\varepsilon_s h R^{5/16})$, greater than the standard result (cf. Wu, 2001a) by a factor of $\mathcal{O}(R^{1/8})$.

It is our hope that the present theoretical work, which characterises and emphasizes the special role of slow acoustic waves in the receptivity of supersonic boundary layers, would stimulate related experimental studies. It is almost certain that the receptivity mechanisms investigated operate in wind tunnel experiments because the sound waves emitted by the walls are pretty strong (Laufer, 1961, Kendall, 1975, Schneider, 2001). Kendall (1975) observed that instability waves arise downstream of their neutral points in a supersonic boundary layer over a smooth wall. Later, Kendall (1987) suggested that the excitation might be attributed to the Mach waves, which were radiated by the turbulent boundary layers over the tunnel walls and propagate at speeds less than the free-stream velocity. In order to support this idea, he generated pressure fluctuations using a rotor device in the free stream. Instability modes were indeed detected, but the excitation was due to the fact that the pressure waves generated were highly localized in the streamwise direction. However, a single (more-or-less) sinusoidal pressure wave such as Mach waves alone cannot trigger instability modes. Our work shows that the interaction of *two* suitable sound waves can. This may offer a possible explanation for the original finding of Kendall (1975), where T-S waves were triggered by acoustic waves in a boundary layer over a flat plate without relying on any surface roughness, but a firm conclusion requires further investigations. Our theory shows that an instability mode can be excited by a continuum of pairs of sound waves. Given that noise in wind tunnels is broadband and random in its nature, a statistical approach is necessary to account for all possible acoustic components contributing to the excitation of a mode. Further theoretical

developments in this direction would enable us to characterise the effect of tunnel noise and calibrate the laboratory transition data so that they could be used to the flight condition.

Supersonic boundary-layer transition indeed occurs at large Reynolds numbers, but receptivity may take place at moderate Reynolds numbers of $\mathcal{O}(10^5)$ or somewhat higher, depending on the disturbances frequency. It is thus necessary to comment on the accuracy of the high-Reynolds-number asymptotic approach as applied to such values of R. For first Mack modes, the wavenumbers/phase speeds predicted by triple-deck theory are found to be about 40% smaller/greater than those given by finite-Reynolds-number calculations for R of $\mathcal{O}(10^5)$. A similar level of error might be expected in the receptivity result. While 40% inaccuracy in the wavenumber and phase speed is rather substantial, the asymptotic prediction with the same level of error for the coupling coefficient still provides the correct order-of-magnitude. Past studies suggest that with the consistent treatments of forcing and instability in triple deck theory the error in receptivity actually tends to be smaller. For example, comparisons with experiments (Wu 2001a, b) indicate that the theory, especially with the extension to second-order accuracy, predicts fairly accurately receptivity in the incompressible regime. Recent DNS studies (Mengaldo et al., 2015, De Tullio and Ruban, 2015) showed that the same is true for subsonic boundary layers. Nevertheless, further work is still needed in order to validate the present theoretical results for supersonic boundary layers. With the key mechanisms being understood, it is possible to reformulate a receptivity theory on a finite-Reynolds-number basis in the same spirit as in Choudhari and Streett (1992) and Crouch (1992), or in Zhigulev and Fedorov (1987) and Fedorov (2003b). In this undertaking, it is important to take into account the streamwise variation of the base flow in order to describe properly the resonant nature of the interactions between the distributed perturbations (driven by impinging acoustic waves and surface roughness). As an alternative, or in addition, to the finite-Reynolds-number approach, DNS may be performed.

3

Connection of the inviscid and viscous branches of instability modes in supersonic boundary layers

3.1 Introduction

The instability of supersonic boundary layers was reviewed by Mack (1984), in which the origin of the different modes arising is investigated. Smith (1989) studied viscous modes, which have a small phase speed (slow modes, $c = \mathcal{O}(R^{-1/8})$) and large wavelengths, compared to the free-stream velocity U_∞ and the boundary-layer thickness δ^*, respectively. In particular, he found that $\beta > \sqrt{M^2 - 1}\alpha$, where α and β are the streamwise and spanwise wavenumbers, respectively. He also showed that these viscous instabilities can have obliqueness angles θ greater than the critical angle θ_c, where $\theta = \tan^{-1}(\beta/\alpha)$ and $\theta_c \equiv \cos^{-1} 1/M$, and that they have the same triple-deck structure as their subsonic counterpart T-S waves near the lower branch of the neutral curve. Fedorov and Khokhlov (1991), studied, on the other hand, the inviscid modes, which have phase speeds and wavelengths of $\mathcal{O}(U_\infty)$ and $\mathcal{O}(\delta^*)$, respectively. For this type of modes, $\beta < \sqrt{M^2 - 1}\alpha$. Besides instability, Fedorov (2003a) and Fedorov (2011) dealt with the leading-edge receptivity of supersonic boundary layers to acoustic waves.

Fedorov and Khokhlov (1991) and Fedorov (2003a) investigated the generation of inviscid instabilities in a supersonic boundary layer over a flat plate, by fast and slow acoustic disturbances. In particular, Fedorov (2003a) considered the case where the deviation $\Delta\theta \equiv \theta_c - \theta$ of the obliqueness angle from its critical value is $\Delta\theta = \mathcal{O}(1)$, and showed that slow acoustic modes propagating downstream with $\Delta\theta > 0$ generate unsteady disturbances in the boundary layer that match onto the inviscid first Mack mode. This mode arises at $x = \mathcal{O}(\varepsilon^{-6})$, where x has been nondimensionalized with the frequency of the acoustic disturbances ω^* and the free-stream velocity U^*_∞, and $\varepsilon \equiv F^{1/6}$ is the small parameter for the asymptotic expansion, where F is the frequency parameter defined by $F = \nu^*_\infty \omega^* / U^{*2}_\infty$. However, Goldstein and Ricco (2018) showed that this region is too far downstream to be of practical interest for actual flight conditions.

Goldstein and Ricco (2018) found that the slow mode generated by the Fedorov / Khokhlov (F/K hereinafter) mechanism exists for obliqueness angles with $\Delta\theta < 0$, but the streamwise wavenumber then becomes negative, meaning that the acoustic disturbances propagate upstream and cannot produce first Mack mode instabilities propagating downstream. They found a different situation for the triple-deck instabilities: while their deviation angle $\Delta\theta$ is also negative, their streamwise wavenumber is positive and the solution can match the downstream propagating first Mack mode. Goldstein and Ricco (2018) also extended the analysis of F/K to small values of $\Delta\theta$ in the case in which the deviation of the obliqueness angle from its critical value is $\Delta\theta = \varepsilon^{2/3}$, where $\theta = \tan^{-1}(\beta/\alpha)$. In that case, the time dependent term must balance the convective term in the wall layer equations, so $x = (\Delta\theta)^{5/2}\tilde{\tilde{x}}_2\varepsilon^{-3}$ in the diffraction region, where $\tilde{\tilde{x}}_2$ is the rescaled streamwise coordinate in the diffraction region (Goldstein and Ricco, 2018); therefore the regime they found is located at $x = \mathcal{O}(\varepsilon^{-4/3})$.

The work by Yang (2017) studied the appearance of a new regime (apparently missed by previous investigations, including Goldstein and Ricco, 2018) with a (non-standard) triple-deck structure, using a different normalisation compared to F/K and Goldstein and Ricco (2018). The goal of the present study is to clarify the connection between the inviscid and viscous branches and to find out what happens when $\beta \to \sqrt{M^2 - 1}\alpha$, or equivalently, $\theta \to \theta_c$. For this, the first step is to clarify the discrepancy between the regimes observed in the work by Yang (2017),

$$\alpha_L \sim R^{1/3}, \quad \beta_L \sim R^{1/3}, \quad \omega_L \sim R^{2/9} \quad \text{and} \quad c_L \sim R^{-1/9}, \tag{3.1}$$

where R is the local Reynolds number based on the distance to the leading edge;

and in Goldstein and Ricco (2018),

$$\alpha \sim \varepsilon^{-2}, \quad \beta \sim \varepsilon^{-2}, \quad \omega \sim \varepsilon^{-4/3} \quad \text{and} \quad c \sim \varepsilon^{2/3}, \tag{3.2}$$

where α, β, ω and c have been non-dimensionalized with $L^* \equiv U^*_\infty/\omega^*$. These two studies use a framework in which the normalisation employed is different in each case ("global" in Goldstein and Ricco, 2018 and "local" in Yang, 2017). Goldstein and Ricco (2018) were interested in the case $\Delta\theta = \varepsilon^{2/3}$, which corresponds to the location $x = \mathcal{O}(\varepsilon^{-4/3})$, where the small parameter of the expansions is ε and the dimensional length scale is $L^*_{GR} = U^*_\infty/\omega^*$. Yang (2017) used a local normalization instead, with L^*_{WY} being the distance from the leading edge to the neutral point. A scheme for the conversion between the two frameworks is therefore introduced, leading to the conclusion that the regime studied in Yang (2017) has not been considered in the analysis by Goldstein and Ricco (2018). Finally, the matching of the intermediate regime found in Yang (2017) to Fedorov's regime (Fedorov, 2003a) when $\hat{\omega}_0 \to \infty$ and to Smith (1989) when $\beta \to \sqrt{M^2 - 1}\alpha$ is considered.

3.2 Fedorov-Khokhlov theory

Fedorov and Khokhlov (1991) and Fedorov (2003a) considered the supersonic flow of an ideal gas over a semi-infinite flat plate. The oncoming flow is assumed to be uniform with a velocity U^*_∞, density ρ^*_∞, temperature T^*_∞ and sound speed a^*_∞. Superimposed on this background flow are three-dimensional small-amplitude disturbances of acoustic nature with angular frequency ω^*. The Reynolds number R and the Mach number M are defined as

$$R = \rho^*_\infty U^*_\infty L^*/\mu^*_\infty, \quad M = U^*_\infty/a^*_\infty, \tag{3.3}$$

where μ^*_∞ is the free-stream dynamic viscosity and the reference length scale L^* is chosen to be the distance to the leading edge. In this theory, R will be taken to be asymptotically large, $R \gg 1$, and the focus is on the supersonic regime, $M > 1$ with $M = \mathcal{O}(1)$.

A Cartesian coordinate system (x,y,z) is introduced, with its origin at the leading edge of the plate, where x and y are along and normal to the surface, respectively, while z is in the spanwise direction, all being non-dimensionalized by $L^* = U^*_\infty/\omega^*$. The time variable t is normalized by ω^*. The velocity $\mathbf{u} = (u, v, w)$, density ρ, temperature τ, pressure p, and the shear and bulk viscosities, μ and μ', are non-dimensionalized by U^*_∞, ρ^*_∞, T^*_∞, $\rho^*_\infty U^{*2}_\infty$ and μ^*_∞ respectively. The fluid is taken

to be a perfect gas with a constant ratio of specific heats, κ.

The non-dimensional frequency parameter $F = \nu_\infty^* \omega^* / U_\infty^{*2}$ is assumed to be small. It is also assumed that the disturbance amplitude is small enough for the linear theory to be applicable. As indicated earlier, the Reynolds number is assumed to be large, so the asymptotic theory is used to explain how the imposed harmonic distortion (acoustic wave) generates oblique instabilities further downstream in the viscous boundary layer that forms on the surface of the plate. The distortion is inviscid at lowest approximation and can be decomposed (Kovasznay, 1953) into acoustic, vortical and entropic modes. Here, only the acoustic mode is considered, which is governed by the linearized equations,

$$\left(\frac{\partial}{\partial t} + \frac{\partial}{\partial x}\right) \rho_a + \nabla \cdot \mathbf{u_a} = 0, \quad \left(\frac{\partial}{\partial t} + \frac{\partial}{\partial x}\right) \mathbf{u_a} = -\nabla p_a, \tag{3.4}$$

$$\left(\frac{\partial}{\partial t} + \frac{\partial}{\partial x}\right) \tau_a = (\kappa - 1) M^2 \left(\frac{\partial}{\partial t} + \frac{\partial}{\partial x}\right) p_a, \quad \kappa M^2 p_a = \tau_a + \rho_a. \tag{3.5}$$

Equations $(3.4) - (3.5)$ can be combined to obtain an equation for the pressure p_a,

$$M^2 \left(\frac{\partial}{\partial t} + \frac{\partial}{\partial x}\right)^2 p_a - \nabla^2 p_a = 0, \tag{3.6}$$

whose solution is given by

$$(u_a, v_a, w_a, p_a, \rho_a, \tau_a) = \hat{\delta} p_\infty \left(\frac{\alpha}{1-\alpha}, \frac{\gamma}{1-\alpha}, \frac{\beta}{1-\alpha}, 1, M^2, (\kappa-1)M^2\right) \times \exp\left[i(\alpha x + \gamma y + \beta z - t)\right], \tag{3.7}$$

where

$$\gamma = \sqrt{(M^2-1)(\alpha-\alpha_1)(\alpha-\alpha_2)}, \quad \alpha_{1,2} = \frac{M^2 \pm \sqrt{M^2 + \beta^2(M^2-1)}}{M^2-1}. \tag{3.8}$$

The incidence angle of the acoustic disturbance is chosen to be zero $\theta_y = tan^{-1}(\gamma/\alpha) = 0$ (i.e. $\gamma = 0$) to avoid large scattered fields and so that diffraction is the only dominant mechanism. The wavenumbers $\alpha_{1,2}$ and the correspondent phase speeds $c_{1,2} = 1/\alpha_{1,2}$ can be written in terms of the sweep angle θ as

$$\alpha_{1,2} = \frac{M\cos\theta}{M\cos\theta \mp 1}, \quad c_{1,2} = 1 \mp \frac{1}{M\cos\theta}, \quad \theta = \tan^{-1}\left(\frac{\beta}{\alpha}\right). \tag{3.9}$$

Equation (3.9) shows that the slow mode wavenumber becomes infinite when $\theta =$

θ_c.

3.2.1 Asymptotic structure of the disturbance field

Here we reproduce the analysis carried out by F/K and Goldstein and Ricco (2018). The small parameter for the asymptotic expansion is

$$\varepsilon \equiv F^{1/6}, \tag{3.10}$$

where, as indicated earlier,

$$F \equiv \frac{\nu_\infty^* \omega^*}{U_\infty^{*2}} \tag{3.11}$$

is the frequency parameter.

Fedorov and Khokhlov (1991) showed that diffraction of the slow acoustic wave by the non-parallel boundary layer flow can produce a first Mack (inviscid) mode instability in the downstream region where $x = \mathcal{O}(\varepsilon^{-6})$ when its obliqueness angle is lower than the critical angle

$$\cos\theta_c \equiv \frac{1}{M}, \tag{3.12}$$

and the deviation $\Delta\theta \equiv \theta_c - \theta$ is $\mathcal{O}(1)$. Equation (3.9) shows that the slow mode wavenumber becomes infinite when the obliqueness angle equals the critical angle (3.12). The acoustic disturbances will only have large spanwise wavenumbers when their obliqueness angle θ are close to the critical angle θ_c, i.e. when $\Delta\theta \ll 1$. By performing a Taylor expansion for the small parameter $\Delta\theta$,

$$\cos(\theta_c - \Delta\theta) = \cos\theta_c + \Delta\theta \sin\theta_c + \mathcal{O}((\Delta\theta)^2), \tag{3.13}$$

$$\tan(\theta_c - \Delta\theta) = \tan\theta_c - \frac{\Delta\theta}{\cos^2\theta_c} + \mathcal{O}((\Delta\theta)^2), \tag{3.14}$$

And for the spanwise and streamwise wavenumbers, respectively,

$$\beta = \beta_0 + \frac{\beta_1}{\Delta\theta}, \tag{3.15}$$

$$\alpha = \alpha_0 + \frac{\alpha_1}{\Delta\theta}, \tag{3.16}$$

where, by using (3.9), it follows that

$$\alpha_0 = \frac{1}{\sin^2\theta_c}, \quad \alpha_1 = \frac{1}{\tan\theta_c}, \quad \beta_0 = 0, \quad \beta_1 = 1. \tag{3.17}$$

The F/K diffraction region (boundary layer thickness is $\mathcal{O}(\varepsilon)$) equations do not provide an appropriate asymptotic balance when $\Delta\theta \ll 1$ and new equations have to be derived to extend the analysis to the small-$\Delta\theta$ regime.

The expansion takes the following form in the diffraction layer (Fedorov and Khokhlov, 1991, Fedorov, 2003a)

$$(u, v, w, \tau, p) = (1, 0, 0, 1, 1) + \hat{\delta}(u_2(x_2, y_2), \varepsilon^{3/2} v_2(x_2, y_2), w_2(x_2, y_2), \tau_2(x_2, y_2), p_2(x_2, y_2)) \times \exp\left\{ i \left[\left(\alpha_0 + \frac{\alpha_1}{\Delta\theta} \right) x + \frac{\beta_1}{\Delta\theta} z - t \right] \right\}, \quad (3.18)$$

where

$$x_2 = x\varepsilon^3 = \mathcal{O}(1), \quad y_2 = y\varepsilon^{3/2} = \mathcal{O}(1). \quad (3.19)$$

The equation for the pressure fluctuation can be found substituting (3.18) into the N-S equations (Fedorov and Khokhlov, 1991, Fedorov, 2003a),

$$\frac{\partial^2 p_2}{\partial y_2^2} = 2i[M^2(\alpha - 1) - \alpha] \frac{\partial p_2}{\partial x_2}, \quad (3.20)$$

subject to the boundary conditions

$$p_2(x_2, \infty) = p_2(0, y_2) = 1, \quad (3.21)$$

$$\frac{\partial p_2}{\partial y_2} = -i(\alpha - 1) v_2(x_2, 0). \quad (3.22)$$

The matching conditions are

$$v_2(y_2 \to 0) = v_1(y_1 \to \infty), \quad p_2(x_2, y_2 \to 0) = p_1(x_2). \quad (3.23)$$

The solution $v_1(x_2, \infty)$ is related to p_1 by

$$v_1(x_2, \infty) = \frac{i\alpha k}{\cos^2\theta} \sqrt{x_2} p_1(x_2), \quad (3.24)$$

where k is a constant. When the obliqueness angle is close to the critical angle, (3.20) and (3.21)-(3.22) become

$$\frac{\partial^2 p_2}{\partial y_2^2} = 2i\alpha(M^2 - 1) \frac{\partial p_2}{\partial x_2}, \quad (3.25)$$

subject to the boundary conditions

$$p_2(x_2, \infty) = p_2(0, y_2) = 1, \quad (3.26)$$

$$\frac{\partial p_2}{\partial y_2} = -i\alpha v_2(x_2, 0). \tag{3.27}$$

The solution to the problem (3.26)-(3.27) can be found in Fedorov and Khokhlov (1991).

3.3 Wu/Yang intermediate regime: stability analysis

We begin our analysis by the study of the instability in the W/Y framework. As will be shown later, the instability found here admits a triple-deck structure. We consider the two-dimensional compressible boundary layer over a semi-infinite flat plate. The oncoming flow is assumed to be uniform with a velocity U^*_∞, density ρ^*_∞, temperature T^*_∞ and sound speed a^*_∞. Superimposed on this background flow are three-dimensional small-amplitude disturbances of acoustic nature. We define the Reynolds number R_δ and the Mach number M as

$$R_\delta = \rho^*_\infty U^*_\infty \delta^* / \mu^*_\infty, \quad M = U^*_\infty / a^*_\infty, \tag{3.28}$$

where μ^*_∞ is the free-stream dynamic viscosity and δ^* is the boundary layer thickness. In the present paper, we will take R_δ to be asymptotically large, $R_\delta \gg 1$, and focus on the supersonic regime, $M > 1$ with $M = \mathcal{O}(1)$.

We introduce a Cartesian coordinate system (x_1,x_2,x_3) with its origin at the leading edge of the plate, where x_1 and x_2 are along and normal to the surface, respectively, while x_3 is in the spanwise direction, all being non-dimensionalized by δ^*. The time variable t is normalized by δ^*/U^*_∞. The velocity $\mathbf{u} = (u, v, w)$, density ρ, temperature τ, pressure p, and the shear and bulk viscosities, μ and μ', are non-dimensionalized by U^*_∞, ρ^*_∞, T^*_∞, $\rho^*_\infty, U^{*2}_\infty$ and μ^*_∞ respectively. The fluid is taken to be a perfect gas with a constant ratio of specific heats, γ. The non-dimensional Navier-Stokes (N-S) equations then read,

$$\frac{\partial \rho}{\partial t} + \nabla \cdot (\rho \mathbf{u}) = 0, \tag{3.29}$$

$$\rho \frac{D\mathbf{u}}{Dt} = -\nabla p + \frac{1}{R_\delta} \nabla \cdot (2\mu \mathbf{e}) + \nabla((\mu' - \frac{2}{3}\mu)\nabla \cdot \mathbf{u}), \tag{3.30}$$

$$\rho \frac{D\tau}{Dt} = (\gamma - 1)M^2 \frac{Dp}{Dt} + \frac{1}{R_\delta Pr} \nabla \cdot (\mu \nabla T) + \frac{(\gamma - 1)M^2}{R_\delta} \Phi, \tag{3.31}$$

$$\gamma M^2 p = \rho \tau, \tag{3.32}$$

where $\mathbf{e}$ and Φ stand for the strain rate tensor and the dissipation function, re-

spectively:

$$e_{ij} = \frac{1}{2}\left(\frac{\partial u_i}{\partial x_j} + \frac{\partial u_j}{\partial x_i}\right), \quad \Phi = 2\mu \mathbf{e} : \mathbf{e} + (\mu' - \frac{2}{3}\mu)(\nabla \cdot \mathbf{u})^2, \tag{3.33}$$

and Pr is the Prandtl number. Note that $\mu' = 0$ for a monoatomic gas. The viscosity μ may obey the Chapman or Sutherland law. The operators such as ∇ are defined with respect to the Cartesian coordinates (x_1, x_2, x_3) defined above.

3.3.1 The base flow

In order to describe the boundary-layer flow, we introduce

$$(x, y, z) = (x_1, R_\delta x_2, x_3). \tag{3.34}$$

The base flow can be written as

$$(U_B, R_\delta^{-1} V_B, 0, P_B, R_B, T_B), \tag{3.35}$$

as in chapter 2.

3.3.2 Linearization

The total flow field consists of the steady compressible boundary-layer flow and a perturbation

$$(u, v, w, p, \rho, \tau) = \left(U_B, R_\delta^{-1} V_B, 0, \frac{1}{\gamma M^2}, R_B, T_B\right) + h(\tilde{u}, \tilde{v}, \tilde{w}, \tilde{p}, \tilde{\rho}, \tilde{\tau}), \tag{3.36}$$

with $U_B(y, \bar{x})$, $R_B(y, \bar{x}) = 1/T_B$, where $\bar{x} = x/R_\delta$ is the slow streamwise variable and $h \ll 1$. After substituting (3.36) into (3.29)-(3.33), the linearized equations for the perturbation read

$$\left(\frac{\partial}{\partial t} + U_B \frac{\partial}{\partial x}\right)\tilde{\rho} + R_B\left(\frac{\partial \tilde{u}}{\partial x} + \frac{\partial \tilde{v}}{\partial y} + \frac{\partial \tilde{w}}{\partial z}\right) + R_B' \tilde{v} = 0, \tag{3.37}$$

$$R_B\left(\frac{\partial}{\partial t} + U_B \frac{\partial}{\partial x}\right)\tilde{u} + R_B U_B' \tilde{v} = -\frac{\partial \tilde{p}}{\partial x}, \tag{3.38}$$

$$R_B\left(\frac{\partial}{\partial t} + U_B \frac{\partial}{\partial x}\right)\tilde{v} = -\frac{\partial \tilde{p}}{\partial y}, \tag{3.39}$$

$$R_B\left(\frac{\partial}{\partial t}+U_B\frac{\partial}{\partial x}\right)\tilde{w}=-\frac{\partial\tilde{p}}{\partial z}, \tag{3.40}$$

$$R_B\left(\frac{\partial}{\partial t}+U_B\frac{\partial}{\partial x}\right)\tilde{\tau}+\frac{T_B'}{T_B}\tilde{v}=(\gamma-1)M^2\left(\frac{\partial}{\partial t}+U_B\frac{\partial}{\partial x}\right)\tilde{p}, \tag{3.41}$$

$$\gamma M^2\tilde{p}=R_B\tilde{\tau}+T_B\tilde{\rho}, \tag{3.42}$$

where the prime represents a derivative with respect to y. By seeking normal modes of the form

$$(\tilde{u},\tilde{v},\tilde{w},\tilde{p},\tilde{\rho},\tilde{\tau})=(\hat{u},\hat{v},\hat{w},\hat{p},\hat{\rho},\hat{\tau})e^{i(\alpha x+\beta z-\omega t)}+\text{c.c.}, \tag{3.43}$$

we arrive at the equations

$$i\left(\alpha U_B-\omega\right)\hat{\rho}+R_B\left(i\alpha\hat{u}+\hat{v}'+i\beta\hat{w}\right)+R_B'\hat{v}=0, \tag{3.44}$$

$$R_Bi\left(\alpha U_B-\omega\right)\hat{u}+R_BU_B'\hat{v}=-i\alpha\hat{p}, \tag{3.45}$$

$$R_Bi\left(\alpha U_B-\omega\right)\hat{v}=-\hat{p}', \tag{3.46}$$

$$R_Bi\left(\alpha U_B-\omega\right)\hat{w}=-i\beta\hat{p}, \tag{3.47}$$

$$R_Bi\left(\alpha U_B-\omega\right)\hat{\tau}+\frac{T_B'}{T_B}\hat{v}=(\gamma-1)M^2i\left(\alpha U_B-\omega\right)\hat{p}, \tag{3.48}$$

$$\gamma M^2\hat{p}=R_B\hat{\tau}+T_B\hat{\rho}. \tag{3.49}$$

By rearranging (3.44)-(3.49), we obtain an equation for the pressure:

$$\hat{p}''+\left(\frac{T_B'}{T_B}-\frac{2U_B}{U_B-c}\right)\hat{p}'-\left[(\alpha^2+\beta^2)-\frac{M^2\alpha^2(U_B-c)^2}{T_B}\right]\hat{p}=0, \tag{3.50}$$

with the boundary conditions

$$\hat{p}\to 0\quad\text{as}\quad y\to\infty, \tag{3.51}$$

$$\frac{\partial\hat{p}}{\partial y}=0\quad\text{at}\quad y=0. \tag{3.52}$$

where (3.52) is deduced from (3.39) when $y=0$ ($\hat{v}=0$). The base flow satisfies

$$T_B\to 1,\quad T_B'\to 0,\quad U_B\to 1,\quad U_B'\to 0\quad\text{as}\quad y\to\infty. \tag{3.53}$$

With (3.53), the equation (3.50) can be written as

$$\hat{p}''-\left[(\alpha^2+\beta^2)-M^2\alpha^2(1-c)^2\right]\hat{p}=0. \tag{3.54}$$

To solve the equation (3.54), let $\hat{p} = Ce^{\gamma y}$, with C an arbitrary constant. It follows that

$$\gamma^2 - \left[(\alpha^2 + \beta^2) - M^2\alpha^2(1-c)^2\right] = 0, \tag{3.55}$$

which can be written as

$$\gamma = \pm\sqrt{(\alpha^2 + \beta^2) - M^2\alpha^2(1-c)^2}. \tag{3.56}$$

Thus, $\hat{p}$ has the form

$$\hat{p} = C_1 e^{\gamma y} + C_2 e^{-\gamma y}. \tag{3.57}$$

For $\hat{p}$ to decay as $y \to \infty$, we take $C_1 = 0$ and therefore,

$$\hat{p} = C_2 e^{-\gamma y}. \tag{3.58}$$

3.3.3 Spatial instability

The spatial stability can be studied by choosing the frequency and spanwise wavenumber to be real numbers i.e. $\omega, \beta \in \mathbb{R}$, so that the streamwise wavenumber is complex ($\alpha \in \mathbb{C}$). In order to have instability, γ has to be small (small angle of incidence in the x-y plane, therefore the vertical wavenumber is also small). By choosing $\gamma = 0$, we obtain

$$c = 1 \pm \frac{\sqrt{\alpha^2 + \beta^2}}{\alpha M} \equiv c_a. \tag{3.59}$$

There exist two modes: a fast mode, whose phase speed is

$$c_a = 1 + \frac{\sqrt{\alpha^2 + \beta^2}}{\alpha M}, \tag{3.60}$$

and a slow mode with phase speed

$$c_a = 1 - \frac{\sqrt{\alpha^2 + \beta^2}}{\alpha M}. \tag{3.61}$$

The expression for c can be extended, when $\omega \to 0$, as

$$c = 1 \pm \frac{\sqrt{\alpha^2 + \beta^2}}{\alpha M} + \omega^2 c_1, \tag{3.62}$$

where $\omega^2 c_1$ is a small correction term. Similarly for α,

$$\alpha = \frac{\omega}{c} = \frac{\omega}{c_a} + \omega^3 \alpha_1 = \frac{\omega}{c_a}\left(\frac{1}{1+\omega^2 c_a^{-1} c_1}\right) \sim \frac{\omega}{c_a}\left(1 - \omega^2 c_a^{-1} c_1\right) = \frac{\omega}{c_a} - \omega^3 c_a^{-2} c_1. \tag{3.63}$$

Identifying the coefficients with the following expansions

$$\alpha = \alpha_0 \omega + \omega^3 \alpha_1, \tag{3.64}$$

$$\beta = \beta_0 \omega, \tag{3.65}$$

therefore $\alpha_0 = c_a^{-1}$ and $\alpha_1 = -c_a^{-2} c_1$, with $(\alpha_0, \beta_0) \sim \mathcal{O}(1)$. Now we calculate the order of magnitude of γ by substituting the expressions for α, β and c in,

$$\gamma = \sqrt{\alpha^2 + \beta^2 - M^2(\alpha - \omega)^2} = \sqrt{(1-M^2)\alpha^2 + \beta^2 + 2M^2\alpha\omega - M^2\omega^2} \tag{3.66}$$

$$= \sqrt{(1-M^2)(\alpha_0^2\omega^2 + \omega^6\alpha_1^2 + 2\omega^4\alpha_0\alpha_1) + \beta^2 + 2M^2\alpha_0\omega^2 + 2M^2\alpha_1\omega^4 - M^2\omega^2}. \tag{3.67}$$

As mentioned earlier, in order to have instability γ has to be small. By setting $\gamma = \mathcal{O}(\omega)$ in (3.66)

$$(1-M^2)\alpha_0^2 + 2M^2\alpha_0 + \beta_0^2 - M^2 = 0. \tag{3.68}$$

In fact, (3.68) is equivalent to (3.62). Let us have a closer look at this. Equation (3.68) can be rearranged as

$$\alpha_0^2 + \beta_0^2 - M^2(1-\alpha_0)^2 = 0, \tag{3.69}$$

On the other hand, for the slow mode we have

$$c_a = 1 - \frac{\sqrt{\alpha_0^2 + \beta_0^2}}{\alpha_0 M} \equiv \frac{1}{\alpha_0}. \tag{3.70}$$

Therefore,

$$\alpha_0 = 1 - \frac{\sqrt{\alpha_0^2 + \beta_0^2}}{M}. \tag{3.71}$$

In effect, α_0 plays the role of c_a at leading order, by comparison of (3.71) to (3.59).

If two-dimensional modes are considered ($\beta_0 = 0$), then

$$\alpha_0 = \left(\frac{M}{1+M}, -\frac{M}{1-M}\right). \tag{3.72}$$

Now, by setting $\gamma \ll \mathcal{O}(\omega)$ in (3.66), we have

$$(1-M^2)2\alpha_0\alpha_1 + 2M^2\alpha_1 = 0 \rightarrow \alpha_0 = -\frac{M^2}{1-M^2}. \tag{3.73}$$

Therefore,

$$\gamma = \sqrt{(1-M^2)(2\omega^4\alpha_0\alpha_1) + 2M^2\omega^4\alpha_1} = \omega^2\sqrt{2\alpha_1}\sqrt{(1-M^2)\alpha_0 + M^2}. \tag{3.74}$$

The aim now is to obtain an equation for α_1 by matching solutions between the main and upper decks.

Main deck

From the y-momentum equation (3.46) we have, as $y \rightarrow \infty$,

$$\hat{v} = -\frac{\hat{p}'}{i(\alpha-\omega)} \sim \frac{\omega^2}{\omega} = \omega. \tag{3.75}$$

The order of the rest of variables can be found by balancing terms; we rescale as follows

$$(\hat{u}, \hat{v}, \hat{w}, \hat{\tau}, \hat{p}, \hat{\rho}) = (\hat{u}_1, \omega\hat{v}_1, \hat{w}_1, \hat{\tau}_1, \hat{p}_1, \hat{\rho}_1), \tag{3.76}$$

therefore,

$$\frac{\partial \hat{p}_1}{\partial y} = 0. \tag{3.77}$$

Rearranging the equations (3.44)-(3.49),

$$\left[\frac{\hat{v}_1}{i\alpha_0(U_B - c_a)}\right]' = \hat{p}_1\left[\frac{(\alpha_0^2+\beta_0^2)T_B}{\alpha_0^2(U_B-c_a)^2} - M^2\right], \tag{3.78}$$

and integrating with respect to y

$$\frac{\hat{v}_1}{i\alpha_0(U_B - c_a)} = \hat{p}_1\int_0^y \left[\frac{(\alpha_0^2+\beta_0^2)T_B}{\alpha_0^2(U_B-c_a)^2} - M^2\right] dy. \tag{3.79}$$

In order to match with the upper deck, we take $y \rightarrow \infty$, $U_B \rightarrow 1$,

$$\hat{v}_1 = i\alpha_0(1-c_a)\hat{p}_1\int_0^\infty \left[\frac{(\alpha_0^2+\beta_0^2)T_B}{\alpha_0^2(U_B-c_a)^2} - M^2\right] dy \equiv \hat{v}_\infty. \tag{3.80}$$

Upper deck

Using $\gamma = \mathcal{O}(\omega^2)$, we rescale y such that

$$\hat{y} = \omega^2 y \Rightarrow \hat{p}_1 \sim C_2 e^{-\hat{\gamma}\hat{y}}, \tag{3.81}$$

where $\hat{\gamma} = \sqrt{2\alpha_1}\sqrt{(1-M^2)\alpha_0 + M^2}$. The y-momentum equation is

$$i\alpha_0(1-c_a)\bar{v}_1 = -\frac{\partial \hat{p}_1}{\partial \hat{y}}. \tag{3.82}$$

Matching with main deck: $\overline{v}_1 \to v_\infty$ as $\hat{y} \to 0$,

$$\sqrt{2\alpha_1}\sqrt{(1-M^2)\alpha_0 + M^2} = -\alpha_0^2(1-c_a)^2 k \Rightarrow \alpha_1 = \frac{\alpha_0^4(1-c_a)^4 k^2}{2[(1-M^2)\alpha_0 + M^2]}, \tag{3.83}$$

where

$$k = \int_0^\infty \left[\frac{(\alpha_0^2 + \beta_0^2)T_B}{\alpha_0^2(U_B - c_a)^2} - M^2\right] dy. \tag{3.84}$$

Equation (3.83) can be compared to the growth rate λ (2.9) in Fedorov (2003a) notation:

$$\lambda = -\frac{(\alpha_{1,2}-1)^2 k}{\sqrt{2\pi i[M^2(\alpha_{1,2}-1) - \alpha_{1,2}]}}, \tag{3.85}$$

where $\alpha_{1,2}$ (Fedorov notation) plays the role of α_0 (present notation). By manipulating the expression (3.85), we find that

$$\lambda^2 = i\frac{\alpha_1}{\pi}. \tag{3.86}$$

The exponential is

$$i\int_{x_2} \alpha_1 x_2 dx_2 = i\alpha_1 x_2^2/2 = \pi\lambda^2 x_2^2/2 \tag{3.87}$$

as in (2.11) (Fedorov, 2003a). It has been made clear that both notations can be related to each other.

3.3.4 Wavenumbers in both modes

In order to obtain an expression for α, the value of k (3.84) for $0 < U_B < 1$ has to be computed first. We are interested here in the slow mode, studied in Smith (1989) and Fedorov and Khokhlov (1991), however the fast mode will be considered too as some parts of the k integral for the slow mode have a resemblance to the fast one.

Fast mode

The phase speed of the fast mode is (3.59)

$$c_a = 1 + \frac{\sqrt{\alpha^2 + \beta^2}}{\alpha M}, \tag{3.88}$$

and

$$U_B - c_a \neq 0. \tag{3.89}$$

The base flow $T_B \to 1$ and $U_B \to 1$ as $y \to \infty$, which implies

$$(U_B - c_a)^2 \to \left(1 - 1 - \frac{\sqrt{\alpha^2 + \beta^2)}}{\alpha M}\right)^2 = \frac{\alpha^2 + \beta^2}{\alpha^2 M^2}. \tag{3.90}$$

Thus,

$$\frac{T_B}{(U_B - c_a)^2} \to \frac{\alpha^2 M^2}{\alpha^2 + \beta^2}. \tag{3.91}$$

And since, for small ω we have

$$\frac{\sqrt{\alpha^2 + \beta^2}}{\alpha M} \sim \frac{\sqrt{\alpha_0^2 + \beta_0^2}}{\alpha_0 M} \sim \mathcal{O}(1), \tag{3.92}$$

the integrand in (3.84) is

$$\frac{(\alpha_0^2 + \beta_0^2)T_B}{\alpha_0^2(U_B - c_a)^2} - M^2 = \frac{(\alpha_0^2 + \beta_0^2)}{\alpha_0^2}\frac{\alpha_0^2 M^2}{(\alpha_0^2 + \beta_0^2)} - M^2 \to 0. \tag{3.93}$$

Therefore, the integrand is convergent and a real constant. The expression of α for the fast mode is obtained using (3.83)

$$\alpha = \frac{\omega}{c_a} + \omega^3 \frac{\alpha_0^4(1 - c_a)^4 k^2}{2[(1 - M^2)\alpha_0 + M^2]}. \tag{3.94}$$

Slow mode

The phase speed of the slow mode is (3.59)

$$c_a = 1 - \frac{\sqrt{\alpha^2 + \beta^2}}{\alpha M} < 1. \tag{3.95}$$

For this mode, there exists a critical layer, say at y_c, where

$$U_B(y_c) = c_a. \tag{3.96}$$

Since

$$U_B(y_c) - c_a \to 0, \quad \text{thus} \quad \frac{1}{(U_B - c_a)^2} \to \infty. \tag{3.97}$$

We perform a Taylor expansion of the base flow about the critical level by assuming that $y - y_c = \delta^* \ll 1$,

$$\begin{aligned} U_B(y_c) - c_a &= U_B(y_c) + U_B'(y_c)(y - y_c) + \frac{1}{2}U_B''(y_c)(y - y_c)^2 - c_a \\ &= U_B'(y_c)(y - y_c)\left[1 + \frac{1}{2}\frac{U_B''(y_c)}{U_B'(y_c)}(y - y_c)\right], \end{aligned} \tag{3.98}$$

and

$$T_B(y_c) = T_B(y_c) + T_B'(y_c)(y - y_c). \tag{3.99}$$

The integral k (3.84) has to be split into three integrals

$$\begin{aligned} k = &\int_0^{y_c-\delta^*} \left[\frac{(\alpha_0^2 + \beta_0^2)T_B}{\alpha_0^2(U_B - c_a)^2} - M^2\right] dy + \int_{y_c+\delta^*}^{\infty} \left[\frac{(\alpha_0^2 + \beta_0^2)T_B}{\alpha_0^2(U_B - c_a)^2} - M^2\right] dy \\ &+ \int_{y_c-\delta^*}^{y_c+\delta^*} \left[\frac{\alpha_0^2 + \beta_0^2}{\alpha_0^2} \frac{T_B(y_c)\left[1 + \frac{T_B'(y_c)}{T_B(y_c)}(y - y_c)\right]}{U_B'^2(y_c)(y - y_c)^2\left[1 + \frac{1}{2}\frac{U_B''(y_c)}{U_B'(y_c)}(y - y_c)\right]^2} - M^2\right] dy. \end{aligned} \tag{3.100}$$

The first and second terms of k can be computed in an analogous way to the fast mode (both terms are convergent and real constants). For the third term, we need to approximate the integrand,

$$\begin{aligned} \left[1 + \frac{1}{2}\frac{U_B''(y_c)}{U_B'(y_c)}(y - y_c)\right]^2 &= 1 + \frac{1}{2}\frac{U_B''(y_c)}{U_B'(y_c)}(y - y_c) + \frac{1}{4}\frac{U_B''^2(y_c)}{U_B'^2(y_c)}(y - y_c)^2 \\ &\approx 1 + \frac{1}{2}\frac{U_B''(y_c)}{U_B'(y_c)}(y - y_c), \end{aligned} \tag{3.101}$$

and since $y - y_c = \delta^* \ll 1$, we have

$$\frac{1}{1 + \frac{1}{2}\frac{U_B''(y_c)}{U_B'(y_c)}(y - y_c)} \approx 1 - \frac{1}{4}\frac{U_B''(y_c)}{U_B'(y_c)}(y - y_c). \tag{3.102}$$

The third term k_3 can now be calculated

$$k_3 = \int_{y_c-\delta^*}^{y_c+\delta^*} \left[\frac{\alpha_0^2+\beta_0^2}{\alpha_0^2} \frac{T_B(y_c)}{U_B'^2(y_c)} \frac{1+\frac{T_B'(y_c)}{T_B(y_c)}(y-y_c)}{(y-y_c)^2} \left(1 - \frac{U_B''(y_c)}{U_B'(y_c)}(y-y_c)\right) - M^2 \right] dy$$
$$= \frac{\alpha_0^2+\beta_0^2}{\alpha_0^2} \frac{T_B(y_c)}{U_B'^2(y_c)} \left[-\frac{2}{\delta^*} + \left(\frac{T_B'(y_c)}{T_B(y_c)} - \frac{U_B''(y_c)}{U_B'(y_c)} \right) (ln(\delta^*) - ln(-\delta^*)) \right] - 2M^2\delta^*. \tag{3.103}$$

and the integral is

$$k_3 = \frac{\alpha_0^2+\beta_0^2}{\alpha_0^2} \frac{T_B(y_c)}{U_B'^2(y_c)} \left[-\frac{2}{\delta^*} + i\pi \left(\frac{T_B'(y_c)}{T_B(y_c)} - \frac{U_B''(y_c)}{U_B'(y_c)} \right) \right] - 2M^2\delta^*, \tag{3.104}$$

where the phase jump is π (viscous critical layer analysis in Lin, 1957). Substitution of (3.104) into (3.100) gives

$$k = \int_0^{y_c-\delta^*} \left[\frac{(\alpha_0^2+\beta_0^2)T_B}{\alpha_0^2(U_B-c_a)^2} - M^2 \right] dy + \int_{y_c+\delta^*}^{\infty} \left[\frac{(\alpha_0^2+\beta_0^2)T_B}{\alpha_0^2(U_B-c_a)^2} - M^2 \right] dy$$
$$- \left(\frac{2}{\delta^*} \frac{\alpha_0^2+\beta_0^2}{\alpha_0^2} \frac{T_B(y_c)}{U_B'^2(y_c)} + 2M^2\delta^* \right) - \frac{\alpha_0^2+\beta_0^2}{\alpha_0^2} \frac{T_B(y_c)}{U_B'^2(y_c)} \left(\frac{T_B'(y_c)}{T_B(y_c)} - \frac{U_B''(y_c)}{U_B'(y_c)} \right) i\pi, \tag{3.105}$$

which is a complex number. As $\delta^* \to 0$, $\frac{2}{\delta^*} \to \infty$, $2M^2\delta^* \to 0$, therefore, the sum of the first three terms in (3.105) is a constant B and the integral is

$$k = B - \frac{\alpha_0^2+\beta_0^2}{\alpha_0^2} \frac{T_B(y_c)}{U_B'^2(y_c)} \left(\frac{T_B'(y_c)}{T_B(y_c)} - \frac{U_B''(y_c)}{U_B'(y_c)} \right) i\pi, \tag{3.106}$$

By substitution of (3.106) in (3.83), we obtain an expression for α

$$\alpha = \frac{\omega}{c_a} + \omega^3 \frac{(\alpha_0^2+\beta_0^2)^2}{2M^4[(1-M^2)\alpha_0+M^2]} \left[B^2 - \frac{(\alpha_0^2+\beta_0^2)^2}{\alpha_0^4} \frac{T_B(y_c)^2}{U_B(y_c)'^4} \left(\frac{T_B(y_c)'}{T_B(y_c)} - \frac{U_B(y_c)''}{U_B(y_c)'} \right)^2 \pi^2 \right.$$
$$\left. -2B \frac{(\alpha_0^2+\beta_0^2)}{\alpha_0^2} \frac{T_B(y_c)}{U_B(y_c)'^2} \left(\frac{T_B(y_c)'}{T_B(y_c)} - \frac{U_B(y_c)''}{U_B(y_c)'} \right) i\pi \right], \tag{3.107}$$

where B is a constant given by

$$B = \int_0^{y_c-\delta^*} \left[\frac{(\alpha_0^2+\beta_0^2)T_B}{\alpha_0^2(U_B-c_a)^2} - M^2 \right] dy + \int_{y_c+\delta^*}^{\infty} \left[\frac{(\alpha_0^2+\beta_0^2)T_B}{\alpha_0^2(U_B-c_a)^2} - M^2 \right] dy$$
$$- \frac{2}{\delta^*} \frac{\alpha_0^2+\beta_0^2}{\alpha_0^2} \frac{T_B(y_c)}{U_B(y_c)'^2} \quad \text{as} \quad \delta^* \to 0. \tag{3.108}$$

The expression for α is the main result of Fedorov's theory. The limit $y_c \to 0$, $c_a \to 0$ is of especial relevance as it will be used later on to match the intermediate

regime when $\hat{\omega}_0 \to \infty$ (outer limit upstream). When $y_c \to 0$, $c_a \to 0$, the critical layer approaches with the Stokes layer and

$$\begin{aligned} U_B(y_c) &= c_a \to 0, \\ U_B(y_c)' &\to \lambda_0 C^{-1/2} \tau_w^{-1}, \\ U_B(y_c)'' &\to 0, \\ T_B(y_c)' &\to 0. \end{aligned} \tag{3.109}$$

The order of magnitude of B can be estimated as

$$\begin{aligned} B &\sim \int_0^\infty \left[\frac{(\alpha_0^2+\beta_0^2)T_B}{\alpha_0^2 (U_B - c_a)^2} - M^2 \right] dy \sim \frac{(\alpha_0^2+\beta_0^2)\tau_w}{\alpha_0^2} \int_0^\infty \frac{dy}{(\lambda_0 C^{-1/2}\tau_w^{-1} y - c_a)^2} \\ &= -\frac{(\alpha_0^2+\beta_0^2)\tau_w}{\alpha_0^2 \lambda_0 C^{-1/2} \tau_w^{-1} c_a} = -\frac{(\alpha_0^2+\beta_0^2)\tau_w^2}{\alpha_0 \lambda_0 C^{-1/2}}. \end{aligned} \tag{3.110}$$

When $c_a \to 0$, an additional constraint needs to be satisfied; by (3.71),

$$\alpha_0 \gg 1, \beta_0 \gg 1. \tag{3.111}$$

The order of magnitude of α_1 is therefore estimated as

$$\begin{aligned} \alpha_1 &\sim \frac{(\alpha_0^2+\beta_0^2)^2}{2M^4[(1-M^2)\alpha_0 + M^2]} B^2 \sim \frac{(\alpha_0^2+\beta_0^2)^2}{2M^4[(1-M^2)\alpha_0 + M^2]} \left(\frac{(\alpha_0^2+\beta_0^2)\tau_w}{\alpha_0 \lambda_0 C^{-1/2} \tau_w^{-1}} \right)^2 \\ &\frac{(\alpha_0^2+\beta_0^2)^4 \tau_w^2}{2M^4 \lambda_0^2 C^{-1} \tau_w^{-2} \alpha_0^2 [(1-M^2)\alpha_0 + M^2]} = \frac{\alpha_0^8 M^8 \tau_w^2}{2M^4 \lambda_0^2 C^{-1} \tau_w^{-2} \alpha_0^2 [(1-M^2)\alpha_0 + M^2]} \\ &= \frac{\alpha_0^6 M^4 \tau_w^2}{2\lambda_0^2 C^{-1} \tau_w^{-2} [(1-M^2)\alpha_0 + M^2]} = \frac{\alpha_0^6 M^4 \tau_w^2}{2\lambda_0^2 C^{-1} \tau_w^{-2} (1-M^2)\alpha_0 [1 + \frac{M^2}{(1-M^2)\alpha_0}]} \\ &\sim \frac{\alpha_0^6 M^4 \tau_w^2}{2\lambda_0^2 C^{-1} \tau_w^{-2} (1-M^2)\alpha_0} \left[1 - \frac{M^2}{(1-M^2)\alpha_0} \right] \sim -\frac{\alpha_0^5 M^4 C \tau_w^4}{2\lambda_0^2 (M^2-1)}. \end{aligned} \tag{3.112}$$

This limit is of especial relevance as it will be used later on to match the intermediate regime when $\hat{\omega}_0 \to \infty$.

3.4 Scales of wavenumbers and frequency

We will now study the slow mode ($c \to 0$) in the intermediate regime defined by the extremes of the problems considered by Fedorov and Khokhlov (1991) and Smith (1989), this is, when $\beta \to \sqrt{M^2-1}\alpha$. At the critical level y_c, we have $U_B(y_c) = c \to 0$, as $y_c \to 0$.

We express β by making use of a small correction term

$$\beta = \sqrt{M^2 - 1}\alpha + \omega^\sigma \beta_1 \alpha \tag{3.113}$$

for $0 < \sigma < 1$ and $\omega \to 0$. We introduce a triple-deck framework in order to compute σ.

3.4.1 Upper deck

We compute the order of the rescaled vertical wavenumber $\hat{\gamma} = \gamma\omega^{-2}$ taking into account that the phase speed of the slow mode is

$$c_a \to 0 \Rightarrow c \to c_1. \tag{3.114}$$

Therefore, from (3.56) we have

$$\begin{aligned}
\hat{\gamma} &= \sqrt{\alpha^2\left[1 - M^2(1-c)^2\right] + \beta^2} \\
&= \alpha M \sqrt{\frac{\alpha^2 + \beta^2}{\alpha^2 M^2} - (1 - c_1)^2} \\
&= \alpha M \sqrt{\frac{\alpha^2 + \beta^2}{\alpha^2 M^2} - 1 + 2c_1 - c_1^2} \\
&\sim \alpha M \sqrt{2c_1} \\
&\sim \omega^{1-\sigma}\omega^{\frac{\sigma}{2}} \\
&\sim \omega^{1-\frac{\sigma}{2}}.
\end{aligned} \tag{3.115}$$

From the y-momemtum equation,

$$\frac{\partial \hat{v}}{\partial t} + \frac{\partial \hat{v}}{\partial x} = -\frac{\partial \hat{p}}{\partial y}, \tag{3.116}$$

where

$$-\frac{\partial \hat{p}}{\partial y} = \hat{\gamma}\hat{p}, \tag{3.117}$$

$$\frac{\partial \hat{v}}{\partial t} + \frac{\partial \hat{v}}{\partial x} = i(\alpha - \omega)\hat{v} \sim \mathcal{O}(\alpha\hat{v}), \tag{3.118}$$

since $\omega \ll \alpha$ and $\hat{v} = \mathcal{O}(\alpha)$; therefore

$$\hat{p} = \frac{\omega^{2-2\sigma}}{\omega^{1-\frac{\sigma}{2}}} = \omega^{1-\frac{3}{2}\sigma}. \tag{3.119}$$

This result is important since the order of $\hat{p}$ is the same across all three decks. Now, in the lower deck

$$U_B \sim \lambda y \sim c. \tag{3.120}$$

From the x-momentum equation

$$\frac{\partial \hat{u}}{\partial t} + U_B \frac{\partial \hat{u}}{\partial x} = -\frac{\partial \hat{p}}{\partial x} + \frac{1}{R_\delta}\frac{\partial^2 \hat{u}}{\partial y^2}, \tag{3.121}$$

we compute the order of all terms

$$\frac{\partial \hat{u}}{\partial t} \sim \omega, \tag{3.122}$$

$$U_B \frac{\partial \hat{u}}{\partial x} \sim \omega^\sigma \omega^{1-\sigma} = \omega, \tag{3.123}$$

$$\frac{\partial \hat{p}}{\partial x} \sim \omega^{1-\sigma}\omega^{1-\frac{3}{2}\sigma} = \omega^{2-\frac{5}{2}\sigma}, \tag{3.124}$$

$$\frac{1}{R_\delta}\frac{\partial^2 \hat{u}}{\partial y^2} \sim \frac{1}{R_\delta}\frac{1}{(\omega^\sigma)^2}. \tag{3.125}$$

The value for σ can be computed by balancing the first and third terms as (Yang, 2017)

$$\omega^{2-\frac{5}{2}\sigma} \sim \omega \Rightarrow \sigma = \frac{5}{2}. \tag{3.126}$$

Furthermore, the relationship between R_δ and ω is (Yang, 2017)

$$\frac{1}{R_\delta}\frac{1}{(\omega^\sigma)^2} = \omega \Rightarrow \omega = R_\delta^{-5/9}, \tag{3.127}$$

$$\alpha = \omega^{1-\sigma} = \omega^{3/5} = R_\delta^{-1/3}, \tag{3.128}$$

$$c = \omega^{2/5} = R_\delta^{-2/9}. \tag{3.129}$$

3.4.2 New scaling: Wu/Yang regime

The scaling for the wavenumbers and frequency provided in Yang's work (3.11a-d in Yang, 2017) is

$$\begin{aligned} \alpha_\delta &= R_\delta^{-1/3}\hat{\alpha}_0, \\ \beta_\delta &= R_\delta^{-1/3}\hat{\beta}_0, \\ \omega_\delta &= R_\delta^{-5/9}\hat{\omega}_0, \\ c_\delta &= R_\delta^{-2/9}\hat{c}_0, \end{aligned} \tag{3.130}$$

where $(\alpha, \beta, \omega, c)_\delta = (\alpha^*, \beta^*, \omega^*, c^*)\delta$ represent the non-dimensionalized quantities with the boundary-layer thickness δ (which have been used until here and which will be denoted with the subscript $(.)_\delta$ from now onwards to make difference with $(.)_L$ and $(\alpha^*, \beta^*, \omega^*, c^*)$ the dimensional quantities. R_δ is the Reynolds number based on δ. Note that the hat $\hat{}$ has been dropped in the former sections. The relationship between the non-dimensionalization by L and δ is

$$(\alpha, \beta, \omega, c)_\delta \equiv (\alpha^*, \beta^*, \omega^*, c^*)\delta = (\alpha^*, \beta^*, \omega^*, c^*)L\frac{\delta}{L} = R^{-1/2}(\alpha, \beta, \omega, c)_L, \quad (3.131)$$

where R is the Reynolds number based on L. The relationship between R and R_δ is $R_\delta = R^{1/2}$. The scaling (3.130) can now be written using R (Smith, 1989) as

$$\begin{aligned} \alpha_L &= R^{1/3}C^{-3/8}\tau_w^{-3/2}\hat{\alpha}_0, \\ \beta_L &= R^{1/3}C^{-3/8}\tau_w^{-3/2}\hat{\beta}_0, \\ \omega_L &= R^{2/9}C^{-2/8}\tau_w^{-1}\hat{\omega}_0, \\ c_L &= R^{-1/9}C^{1/8}\tau_w^{1/2}\hat{c}_0. \end{aligned} \quad (3.132)$$

where the scalings with C and τ_w have also been included. The expressions (3.132) can be expanded as

$$\begin{aligned} \alpha_L &= R^{1/3}C^{-3/8}\tau_w^{-3/2}\left[\hat{\alpha}_0 + R^{-1/9}\hat{\alpha}_1\right], \\ \beta_L &= R^{1/3}C^{-3/8}\tau_w^{-3/2}\left[\hat{\beta}_0 + R^{-1/9}\hat{\beta}_1\right], \\ \omega_L &= R^{2/9}C^{-2/8}\tau_w^{-1}\left[\hat{\omega}_0 + R^{-1/9}\hat{\omega}_1\right], \\ c_L &= R^{-1/9}C^{1/8}\tau_w^{1/2}\left[\hat{c}_0 + R^{-1/9}\hat{c}_1\right], \end{aligned} \quad (3.133)$$

where the next-order corrections are $c_L = \mathcal{O}(R^{-1/9})$. It is now straightforward to calculate the thickness of the lower (y_{ld}) and upper decks (y_{ud})

$$\begin{aligned} y_{ld} &= R_\delta^{2/9}y_{md} = R^{1/9}y_{md}, \\ y_{ud} &= R_\delta^{-4/9}y_{md} = R^{-2/9}y_{md}. \end{aligned} \quad (3.134)$$

Thus, including C and τ_w as in (3.132), we have

$$\begin{aligned} y_{ud} &= R^{5/18}C^{-3/8}\tau_w^{-3/2}y, \\ y_{md} &= R^{1/2}C^{-1/2}\tau_w^{-1}y, \\ y_{ld} &= R^{11/18}C^{-5/8}\tau_w^{-3/2}y. \end{aligned} \quad (3.135)$$

The scaling for the spatial and temporal variables is

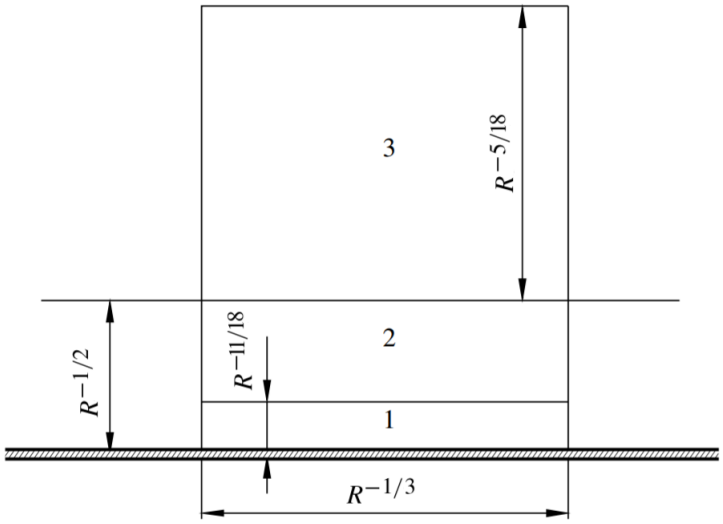


Figure 3.1: Triple-deck structure of the newly-identified regime

$$\begin{aligned} X &= R^{1/3}C^{-3/8}\tau_w^{-3/2}x, \\ Z &= R^{1/3}C^{-3/8}\tau_w^{-3/2}z, \\ T &= R^{2/9}C^{-2/8}\tau_w^{-1}t, \end{aligned} \tag{3.136}$$

where X, Z, T are of order $\mathcal{O}(1)$.

Upper deck

The wall-normal variable is now $\bar{y} = R^{5/18}C^{-5/18}\tau_w^{-3/2}y$, with $\bar{y} = \mathcal{O}(1)$. The expansion for the perturbation takes the form

$$\begin{aligned} u &= C^{2/8}[R^{-2/9}\bar{u}_0(X,\bar{y},Z,T) + R^{-1/3}\bar{u}_1(X,\bar{y},Z,T) + \cdots], \\ v &= C^{2/8}[R^{-5/18}\bar{v}_0(X,\bar{y},Z,T) + R^{-7/18}\bar{v}_1(X,\bar{y},Z,T) + \cdots], \\ w &= C^{2/8}[R^{-2/9}\bar{w}_0(X,\bar{y},Z,T) + R^{-1/3}\bar{w}_1(X,\bar{y},Z,T) + \cdots], \\ p &= C^{2/8}[R^{-2/9}\bar{p}_0(X,\bar{y},Z,T) + R^{-1/3}\bar{p}_1(X,\bar{y},Z,T) + \cdots], \\ \rho &= C^{2/8}[R^{-2/9}\bar{\rho}_0(X,\bar{y},Z,T) + R^{-1/3}\bar{\rho}_1(X,\bar{y},Z,T) + \cdots], \\ \tau &= C^{2/8}[R^{-2/9}\bar{\tau}_0(X,\bar{y},Z,T) + R^{-1/3}\bar{\tau}_1(X,\bar{y},Z,T) + \cdots]. \end{aligned} \tag{3.137}$$

The resulting equations are

$$\begin{aligned}
\bar{\rho}_{0X} + \bar{u}_{0X} + \bar{w}_{0Z} &= 0, \\
\bar{u}_{0X} &= -\bar{p}_{0X}, \\
\bar{w}_{0X} &= -\bar{p}_{0Z}, \\
\bar{\tau}_{0X} &= (\kappa - 1)M^2 \bar{p}_{0X}, \\
\kappa M^2 \bar{p}_0 &= \bar{\rho}_0 + \bar{\tau}_0,
\end{aligned} \tag{3.138}$$

where κ is the ratio of specific heats. At next order, the governing equations read

$$\bar{\rho}_{0T} + \bar{\rho}_{1X} + \bar{u}_{1X} + \bar{v}_{0\bar{y}} + \bar{w}_{1Z} = 0, \tag{3.139}$$

$$\bar{u}_{0T} + \bar{u}_{1X} = -\bar{p}_{1X}, \tag{3.140}$$

$$\bar{w}_{0T} + \bar{w}_{1X} = -\bar{p}_{1Z}, \tag{3.141}$$

$$\bar{\tau}_{0T} + \bar{\tau}_{1X} = (\kappa - 1)M^2(\bar{p}_{0T} + \bar{p}_{1X}), \tag{3.142}$$

$$\kappa M^2 \bar{p}_1 = \bar{\rho}_1 + \bar{\tau}_1. \tag{3.143}$$

With a relatively small disturbance of order h and a normal mode decomposition, so that

$$(u, v, w, p, \rho, \tau) = h(\tilde{u}, \tilde{v}, \tilde{w}, \tilde{p}, \tilde{\rho}, \tilde{\tau})e^{i(\alpha X + \beta Z - \omega T)} + \text{c.c.}, \tag{3.144}$$

the governing equations (3.139)-(3.143) with (3.133) reduce to

$$i\hat{\alpha}_0\tilde{\rho}_1 + i\hat{\alpha}_0\tilde{u}_1 + i\hat{\beta}_0\tilde{w}_1 = -v_{0\bar{y}} + i\hat{\omega}_0\tilde{\rho}_0 - i\hat{\alpha}_1(\tilde{\rho}_0 + u_0) - i\hat{\beta}_1\tilde{w}_0, \tag{3.145}$$

$$i\hat{\alpha}_0\tilde{u}_1 = -i\hat{\alpha}_0\tilde{p}_1 - i\hat{\alpha}_1\tilde{p}_0 + i\hat{\omega}_0\tilde{u}_0 - i\hat{\alpha}_1\tilde{u}_0, \tag{3.146}$$

$$i\hat{\alpha}_0\tilde{w}_1 = -i\hat{\beta}_0\tilde{p}_1 - i\hat{\beta}_1\tilde{p}_0 + i\hat{\omega}_0\tilde{w}_0 - i\hat{\alpha}_1\tilde{w}_0, \tag{3.147}$$

$$i\hat{\alpha}_0\tilde{\tau}_1 = (\kappa - 1)M^2(-i\hat{\omega}_0\tilde{p}_0 + i\hat{\alpha}_0\tilde{p}_1 + i\hat{\alpha}_1\tilde{p}_0) + i\hat{\omega}_0\tilde{\tau}_0 - i\hat{\alpha}_1\tilde{\tau}_0, \tag{3.148}$$

$$\kappa M^2\tilde{p}_1 = \tilde{\rho}_1 + \tilde{\tau}_1. \tag{3.149}$$

Introducing the state equation (3.149) into the energy equation (3.148),

$$i\hat{\alpha}_0\kappa M^2\tilde{p}_1 - i\hat{\alpha}_0\tilde{\rho}_1 = (\kappa-1)M^2(-i\hat{\omega}_0\tilde{p}_0 + i\hat{\alpha}_0\tilde{p}_1 + i\hat{\alpha}_1\tilde{p}_0) + i\hat{\omega}_0(\kappa-1)M^2\tilde{p}_0 - i\hat{\alpha}_1(\kappa-1)M^2\tilde{p}_0. \tag{3.150}$$

We introduce now the x- and z-momentum equations (3.146) and (3.147) into the continuity equation (3.145), together with the y-momentum equation at leading

order $\tilde{v}_0 = -\tilde{p}_{0\bar{y}}/(i\hat{\alpha}_0)$,

$$i\hat{\alpha}_0\tilde{\rho}_1 - i\hat{\alpha}_0\tilde{p}_1 - i\hat{\alpha}_1\tilde{p}_0 - i\hat{\omega}_0\tilde{p}_0 + i\hat{\alpha}_1\tilde{p}_0 + \frac{\hat{\beta}_0}{\hat{\alpha}_0}\left(-i\hat{\beta}_0\tilde{p}_1 - i\hat{\beta}_1\tilde{p}_0 - \frac{i\hat{\omega}_0\hat{\beta}_0\tilde{p}_0}{\hat{\alpha}_0} + \frac{i\hat{\alpha}_1\hat{\beta}_0\tilde{p}_0}{\hat{\alpha}_0}\right) = \frac{\tilde{p}_{0\bar{y}\bar{y}}}{i\hat{\alpha}_0} + i\hat{\omega}_0 M^2\tilde{p}_0 - i\hat{\alpha}_1(M^2-1)\tilde{p}_0 + \frac{i\hat{\beta}_1\hat{\beta}_0\tilde{p}_0}{\hat{\alpha}_0}. \quad (3.151)$$

Simplifying this equation further,

$$-i\hat{\alpha}_0\tilde{\rho}_1 = -i\hat{\alpha}_0\left(1 + \frac{\hat{\beta}_0^2}{\hat{\alpha}_0^2}\right)\tilde{p}_1 - i\hat{\omega}_0\tilde{p}_0 - \frac{2i\hat{\beta}_0\hat{\beta}_1}{\hat{\alpha}_0}\tilde{p}_0 - \frac{i\hat{\omega}_0\hat{\beta}_0^2}{\hat{\alpha}_0^2}\tilde{p}_0 + \frac{i\hat{\alpha}_1\hat{\beta}_0^2}{\hat{\alpha}_0^2}\tilde{p}_0 - \frac{\tilde{p}_{0\bar{y}\bar{y}}}{i\hat{\alpha}_0} - i\hat{\omega}_0 M^2\tilde{p}_0 + i\hat{\alpha}_1(M^2-1)\tilde{p}_0, \quad (3.152)$$

Introducing (3.152) into (3.150), we obtain

$$\begin{aligned} &i\hat{\alpha}_0\kappa M^2\tilde{p}_1 - i\hat{\alpha}_0 M^2\tilde{p}_1 - i\hat{\omega}_0(M^2+1)\tilde{p}_0 - \frac{2i\hat{\beta}_0\hat{\beta}_1}{\hat{\alpha}_0}\tilde{p}_0 - \frac{i\hat{\omega}_0\hat{\beta}_0^2}{\hat{\alpha}_0^2}\tilde{p}_0 + \frac{i\hat{\alpha}_1\hat{\beta}_0^2}{\hat{\alpha}_0^2}\tilde{p}_0 - \frac{\tilde{p}_{0\bar{y}\bar{y}}}{i\hat{\alpha}_0} + i\hat{\alpha}_1(M^2-1)\tilde{p}_0 \\ &= -i\hat{\omega}_0(\kappa-1)M^2\tilde{p}_0 + i\hat{\alpha}_0(\kappa-1)M^2\tilde{p}_1 + i\hat{\alpha}_1(\kappa-1)M^2\tilde{p}_0 + i\hat{\omega}_0(\kappa-1)M^2\tilde{p}_0 - i\hat{\alpha}_1(\kappa-1)M^2\tilde{p}_0, \end{aligned} \quad (3.153)$$

and, finally, an equation for $\tilde{p}_0$

$$\tilde{p}_{0\bar{y}\bar{y}} + \left(-\hat{\omega}_0\hat{\alpha}_0(M^2+1) - 2\hat{\beta}_0\hat{\beta}_1 - \frac{\hat{\omega}_0\hat{\beta}_0^2}{\hat{\alpha}_0} + \frac{\hat{\alpha}_1\hat{\beta}_0^2}{\hat{\alpha}_0} + \hat{\alpha}_0\hat{\alpha}_1(M^2-1)\right)\tilde{p}_0 = 0. \quad (3.154)$$

On eliminating $\hat{\beta}_0$ by making use of

$$\hat{\beta}_0^2 = (M^2-1)\hat{\alpha}_0^2, \quad (3.155)$$

we obtain

$$\tilde{p}_{0\bar{y}\bar{y}} - 2\hat{\alpha}_0\left(M^2\hat{\omega}_0 + \sqrt{M^2-1}\hat{\beta}_1 + (1-M^2)\hat{\alpha}_1\right)\tilde{p}_0 = 0. \quad (3.156)$$

Writing $\tilde{p}_0 = e^{-\lambda\bar{y}}$, we obtain λ as

$$\lambda = \pm\sqrt{2\hat{\alpha}_0[M^2\hat{\omega}_0 + \sqrt{M^2-1}\hat{\beta}_1 + (1-M^2)\hat{\alpha}_1]}. \quad (3.157)$$

The matching condition with the main deck reads

$$p_0 = P_1 \quad \text{and} \quad \frac{\partial p_0}{\partial\bar{y}} = A_{XX} \quad \text{as} \quad \bar{y} \to 0, \quad (3.158)$$

which gives

$$\sqrt{2\hat{\alpha}_0[M^2\hat{\omega}_0+\sqrt{M^2-1}\hat{\beta}_1+(1-M^2)\hat{\alpha}_1]}\tilde{P}_1=\hat{\alpha}_0^2\tilde{A}. \tag{3.159}$$

Main deck

The wall-normal variable is $\tilde{y}=R^{1/2}C^{-1/2}\tau_w^{-1}y$, with $\tilde{y}=\mathcal{O}(1)$. The expansion for the perturbation takes the form

$$\begin{aligned}
u&=R^{-1/9}C^{1/8}\tau_w^{1/2}u_1(X,\tilde{y},Z,T),\\
v&=R^{-5/18}C^{2/8}v_1(X,\tilde{y},Z,T),\\
w&=R^{-2/9}C^{2/8}\tau_w w_1(X,\tilde{y},Z,T),\\
p&=R^{-2/9}C^{2/8}p_1(X,\tilde{y},Z,T),\\
\rho&=R^{-1/9}C^{1/8}\tau_w^{1/2}\rho_1(X,\tilde{y},Z,T),\\
\tau&=R^{-1/9}C^{1/8}\tau_w^{1/2}\tau_1(X,\tilde{y},Z,T).
\end{aligned} \tag{3.160}$$

Inserting (3.160) in the N-S equations, we obtain the equations

$$\begin{aligned}
\rho_{1X}U_B+R_Bu_{1X}+R_{B\tilde{y}}v_1+R_Bv_{1\tilde{y}}&=0,\\
U_Bu_{1X}+v_1U_{B\tilde{y}}&=0,\\
p_{1\tilde{y}}&=0,\\
R_BU_Bw_{1X}&=-p_{1Z},\\
U_B\tau_{1X}+v_1T_{B\tilde{y}}&=0,\\
R_B\tau_1+\rho_1T_B&=0.
\end{aligned} \tag{3.161}$$

With a relatively small disturbance of order h and a normal mode decomposition, so that

$$(u_1,v_1,w_1,p_1,\rho_1,\tau_1)=h(\hat{u}_1,\hat{v}_1,\hat{w}_1,\hat{p}_1,\hat{\rho}_1,\hat{\tau}_1)e^{i(\alpha X+\beta Z-\omega T)}+\text{c.c.}, \tag{3.162}$$

where $h \ll 1$. We obtain

$$\begin{aligned} i\hat{\alpha}_0\hat{\rho}_1 U_B + i\hat{\alpha}_0 R_B\hat{u}_1 + R_{B\tilde{y}}\hat{v}_1 + R_B\hat{v}_{1\tilde{y}} = 0,\\ i\hat{\alpha}_0 U_B\hat{u}_1 + \hat{v}_1 U_{B\tilde{y}} = 0,\\ \hat{p}_{1\tilde{y}} = 0,\\ i\hat{\alpha}_0 R_B U_B\hat{w}_1 = -i\hat{\beta}_0\hat{p}_1,\\ i\hat{\alpha}_0 U_B\hat{\tau}_1 + \hat{v}_1 T_{B\tilde{y}} = 0,\\ R_B\hat{\tau}_1 + \hat{\rho}_1 T_B = 0. \end{aligned} \tag{3.163}$$

Manipulating the equations (3.163), we obtain a simplified version

$$\begin{aligned} i\hat{\alpha}_0\hat{u}_1 + \hat{v}_{1\tilde{y}} = 0,\\ i\hat{\alpha}_0 U_B\hat{u}_1 + \hat{v}_1 U_{B\tilde{y}} = 0,\\ \hat{p}_{1\tilde{y}} = 0,\\ \frac{\hat{\alpha}_0}{\hat{\beta}_0}\frac{U_B}{T_B}\hat{w}_1 = -\hat{p}_1, \end{aligned} \tag{3.164}$$

whose solution is given by

$$\begin{aligned} \hat{u}_1 = A(X,Z,T)U_{B\tilde{y}},\\ \hat{v}_1 = -A_X(X,Z,T)U_B,\\ \hat{w}_1 = -\frac{\hat{\beta}_0}{\hat{\alpha}_0}\frac{T_B}{U_B}\hat{p}_1(X,Z,T),\\ \hat{p}_1 = \hat{p}_1(X,Z,T), \end{aligned} \tag{3.165}$$

where A is the displacement function.

Lower deck

The wall-normal variable is now $Y = R^{11/18}C^{-5/8}\tau_w^{-3/2}y$, with $Y = \mathcal{O}(1)$. The expansion for the perturbation takes the form

$$\begin{aligned} u = R^{-1/9}C^{1/8}\tau_w^{1/2}U_1(X,Y,Z,T),\\ v = R^{-7/18}C^{3/8}\tau_w^{1/2}V_1(X,Y,Z,T),\\ w = R^{-1/9}C^{1/8}\tau_w^{1/2}W_1(X,Y,Z,T),\\ p = R^{-2/9}C^{2/8}P_1(X,Y,Z,T). \end{aligned} \tag{3.166}$$

The resulting equations are

$$\begin{aligned} U_{1X} + V_{1Y} + W_{1Z} &= 0, \\ U_{1T} + U_1 U_{1X} + V_1 U_{1Y} + W_1 U_{1Z} &= -P_{1X} + U_{1YY}, \\ P_{1Y} &= 0, \\ W_{1T} + U_1 W_{1X} + V_1 W_{1Y} + W_1 W_{1Z} &= -P_{1Z} + W_{1YY}, \end{aligned} \tag{3.167}$$

with the no-slip condition at the bottom

$$U_1 = V_1 = W_1 = 0 \quad \text{at} \quad Y = 0, \tag{3.168}$$

and the matching condition with the main-deck solution (3.165)

$$U_1 \to \lambda_0 (Y + A), \quad W_1 \to 0 \quad \text{as} \quad Y \to \infty. \tag{3.169}$$

As is well known, the temperature or density disturbances do not enter the continuity and momentum equations at leading order.

The solution for Tollmien-Schlichting waves is

$$(U_1, V_1, W_1, P_1, A) = (\lambda_0 Y, 0, 0, 0, 0) + h(\hat{U}_1, \hat{V}_1, \hat{W}_1, \hat{P}_1, \hat{A}) e^{i(\alpha X + \beta Z - \omega T)} + \text{c.c.} \tag{3.170}$$

where $h \ll 1$. The linearized equations read

$$\begin{aligned} i\hat{\alpha}_0 \hat{U}_1 + \hat{V}_{1Y} + i\hat{\beta}_0 \hat{W}_1 &= 0, \\ -i\hat{\omega}_0 \hat{U}_1 + i\hat{\alpha}_0 \lambda_0 Y \hat{U}_1 + \lambda_0 \hat{V}_1 &= -i\hat{\alpha}_0 \hat{P}_1 + \hat{U}_{1YY} \\ \hat{P}_{1Y} &= 0, \\ -i\hat{\omega}_0 \hat{W}_1 + i\hat{\alpha}_0 \lambda_0 Y \hat{W}_1 &= -\hat{\beta}_0 \hat{P}_1 + \hat{W}_{1YY}, \end{aligned} \tag{3.171}$$

with the no-slip condition at the bottom

$$\hat{U}_1 = \hat{V}_1 = \hat{W}_1 = 0 \quad \text{at} \quad Y = 0, \tag{3.172}$$

and the matching condition with the main-deck solution (3.165)

$$\hat{U}_1 \to \lambda_0 \hat{A}, \quad \hat{W}_1 \to 0 \quad \text{as} \quad Y \to \infty. \tag{3.173}$$

Eliminating $\hat{P}_1$ from (3.171), we arrive at

$$\left\{ \frac{\partial^2}{\partial Y^2} - i(\hat{\alpha}_0 \lambda_0 Y - \hat{\omega}_0) \right\} \hat{V}_{1,YY} = 0. \tag{3.174}$$

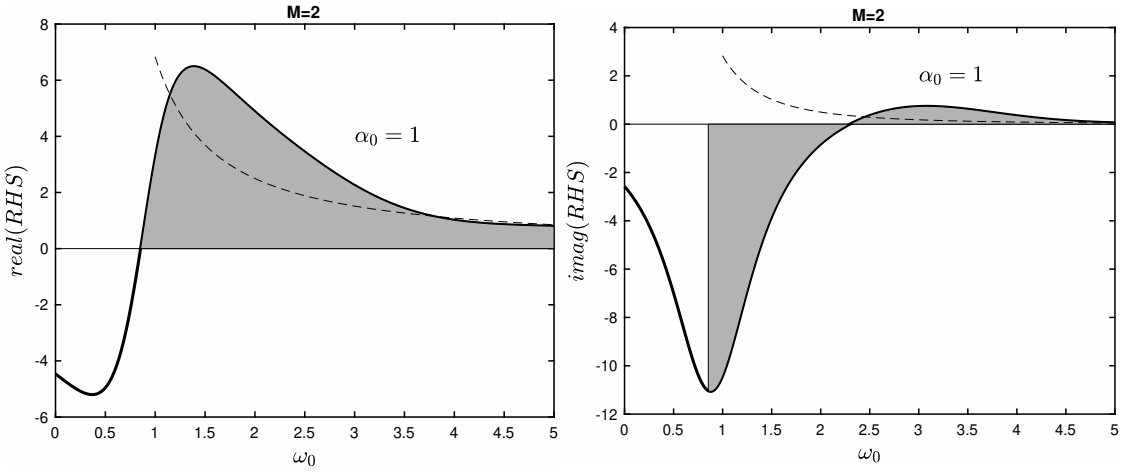


Figure 3.2: Real (a) and imaginary (b) parts of (3.180) for the case $M = 2$ and $\alpha_0 = 1$. The shaded region corresponds to positive values of the real part of RHS. The dashed line corresponds to the asymptote (3.187).

After the change of variables

$$\eta = (i\hat{\alpha}_0\lambda_0)^{1/3}Y + \eta_0, \quad \text{with} \quad \eta_0 = -\frac{i\hat{\omega}_0}{(i\hat{\alpha}_0\lambda_0)^{2/3}} \tag{3.175}$$

we can write (3.174) into the standard Airy equation for $\hat{V}_{1YY}$ and its solution is therefore

$$\hat{V}_{1Y} = C\int_0^Y Ai(y')dy'. \tag{3.176}$$

From the application of the boundary condition $\hat{V}_1(Y = 0) = 0$ we have

$$\hat{V}_{1YYY}(0) = (\hat{\alpha}_0^2 + \hat{\beta}_0^2)\tilde{P}_1 \quad \text{at} \quad Y = 0, \tag{3.177}$$

leading to

$$C(i\hat{\alpha}_0\lambda_0)^{2/3}Ai'(\eta_0) = (\hat{\alpha}_0^2 + \hat{\beta}_0^2)\tilde{P}_1. \tag{3.178}$$

From the matching condition with the lower deck $\hat{V}_{1Y} \to -i\hat{\alpha}_0\lambda_0\tilde{A}$ as $Y \to \infty$,

$$C\int_{\eta_0}^{\infty} Ai(\eta')d\eta' = -i\hat{\alpha}_0\lambda_0\tilde{A}. \tag{3.179}$$

Combining (3.178), (3.179) and (3.159),

$$\sqrt{2\hat{\alpha}_0[M^2\hat{\omega}_0 + \sqrt{M^2-1}\hat{\beta}_1 + (1-M^2)\hat{\alpha}_1]} = \frac{iM^2\hat{\alpha}_0^3\int_{\eta_0}^{\infty} Ai(\eta')d\eta'}{\lambda_0(i\hat{\alpha}_0\lambda_0)^{2/3}Ai'(\eta_0)} \equiv \text{RHS}. \tag{3.180}$$

The real and imaginary parts of RHS are plotted versus $\hat{\omega}_0$ for $\alpha_0 = 1$ on figure

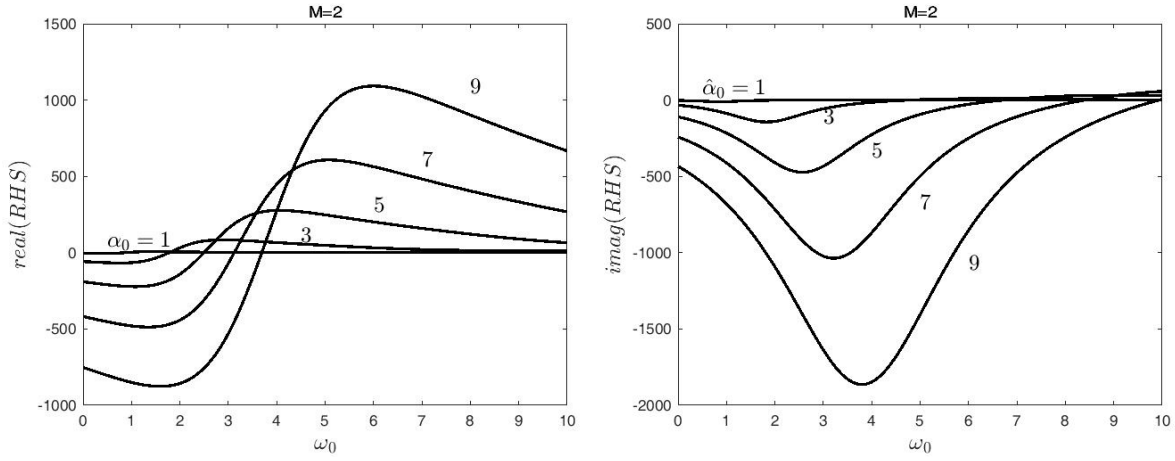


Figure 3.3: Real (a) and imaginary (b) parts of (3.180) for the case $M = 2$ and various α_0.

3.2 and for various values of α_0 on figure 3.3. An additional constraint has to be satisfied - the real part of RHS needs to be positive for λ to be positive and therefore the pressure $\tilde{p}_0$ in (3.156) decay. The expression for $\hat{\alpha}_1$ is

$$\hat{\alpha}_1(\hat{\alpha}_0, \hat{\omega}_0, \hat{\beta}_1, M) = \frac{1}{2\hat{\alpha}_0(M^2-1)}\left[\frac{M^2\hat{\alpha}_0^3 \int_{\eta_0}^{\infty} Ai(\eta')d\eta'}{(i\hat{\alpha}_0\lambda_0)^{2/3}Ai'(\eta_0)}\right]^2 + \frac{M^2}{M^2-1}\hat{\omega}_0 + \frac{\hat{\beta}_1}{\sqrt{M^2-1}}. \tag{3.181}$$

RHS (3.180) is a complex number, i.e. RHS $= a_r + ia_i$. Therefore, the growth rate can be calculated as

$$-\hat{\alpha}_{1i} = \frac{a_r a_i}{\hat{\alpha}_0(M^2-1)}. \tag{3.182}$$

The choice $a_r < 0$ does not represent a physical solution because the eigenfunction would not decay in the far field. $a_r = 0$ represents a radiating neutral mode ($a_i \neq 0$) and happens at $\omega_0 = 0.85$. Now, for $a_r > 0$ we have the following cases depending on a_i:

1. $a_i = 0$ implies that $-\hat{\alpha}_{1i} = 0$. This means that the neutral mode is non-radiating (trapped). This happens for $\omega_0 \approx 2.3$ (figure 3.2).

2. When $a_i \neq 0$, we have to make use of the principle of causality, or equivalently, that the vertical group velocity is positive, $\frac{\partial\hat{\omega}_0}{\partial\lambda} > 0$, in order to choose the correct branch for the outgoing wave. From (3.157),

$$\frac{\partial\hat{\omega}_0}{\partial\lambda} = \frac{\lambda}{\hat{\alpha}_0 M^2} > 0 \quad \text{if} \quad \lambda > 0. \tag{3.183}$$

Therefore, if $a_i > 0$, the outgoing wave is $e^{\lambda y} = e^{ia_i y}$, while if $a_i < 0$, the

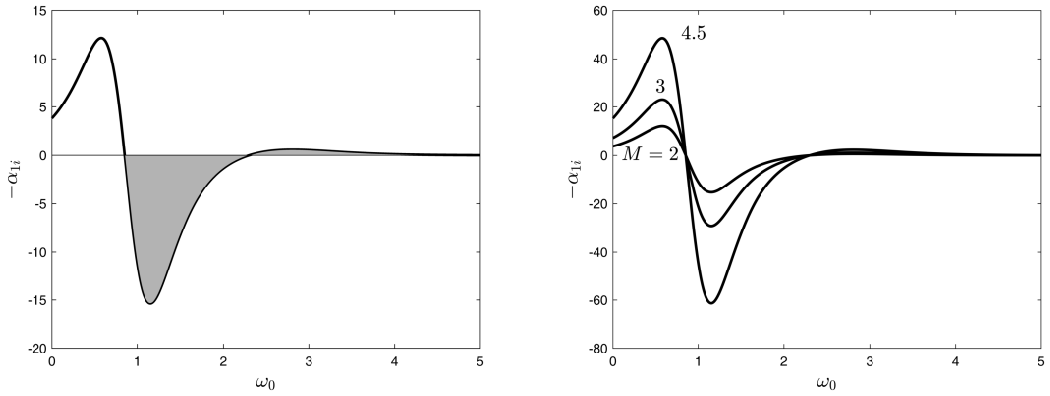


Figure 3.4: Growth rate $-\hat{\alpha}_{1i}$ as a function of $\hat{\omega}_0$, for $\hat{\alpha}_0 = 1$, $\hat{\beta}_1 = 0$ and $M = 2$ (left). Comparison for various Mach numbers (right). The shaded region represents the physically-realizable solutions ($a_r \geq 0$). When $a_i < 0$, a damped radiating mode appears while, when $a_i > 0$, a growing mode arises instead.

correct branch is $e^{-\lambda y} = e^{-ia_i y}$. Both cases are radiating modes.

The growth rate $-\hat{\alpha}_{1i}$ is plotted as a function of $\hat{\omega}_0$ for $\hat{\alpha}_0 = 1$, $\hat{\beta}_1 = 0$ and $M = 2$ (left) in figure (3.4), and for various Mach numbers (right).

3.4.3 Check for asymptotes

When $\hat{\omega}_0 = 0$, we have

$$Ai'(0) = -\frac{1}{3^{1/3}\Lambda(1/3)} = -0.25881, \quad \int_0^\infty Ai(\eta')d\eta' = 1/3. \tag{3.184}$$

Therefore,

$$\text{RHS}(M = 2, \hat{\alpha}_0 = 1) = -4.4614 - 2.5758i, \tag{3.185}$$

which agrees with figures (3.2) and (3.4) for $\hat{\alpha}_0 = 1$ and $\hat{\omega}_0 = 0$. When $\hat{\omega}_0 \to \infty$ ($\eta_0 \to \infty$), we have

$$\frac{\int_{\eta_0}^\infty Ai(\eta')d\eta'}{Ai'(\eta_0)} \sim -\frac{1}{\eta_0}(1 - {\eta_0}^{-3/2}), \tag{3.186}$$

where η_0 is given by (3.175). Thus,

$$\text{RHS} \to M^2\hat{\alpha}_0^3\hat{\omega}_0^{-1} - M^2\hat{\alpha}_0^4 i^{5/2}\hat{\omega}_0^{-5/2} + \cdots \quad \text{as} \quad \hat{\omega}_0 \to \infty. \tag{3.187}$$

$\hat{\alpha}_1$ as $\hat{\omega}_0 \to \infty$ can be obtained as

$$\left[\frac{M^2\hat{\alpha}_0^3}{\lambda_0(i\hat{\alpha}_0\lambda_0)^{2/3}}(-\eta_0^{-1}+\eta_0^{-5/2})\right]^2 \sim -\frac{M^4\hat{\alpha}_0^6}{\lambda_0^2}\hat{\omega}_0^{-2}+\cdots \tag{3.188}$$

at leading order. Therefore, $\hat{\alpha}_1$ goes as

$$\hat{\alpha}_1 \to -\frac{M^4\hat{\alpha}_0^5}{2\lambda_0^2(M^2-1)}\hat{\omega}_0^{-2}+\frac{M^2}{M^2-1}\hat{\omega}_0+\frac{\hat{\beta}_1}{\sqrt{M^2-1}}+\cdots \quad \text{as} \quad \hat{\omega}_0 \to \infty. \tag{3.189}$$

By introducing (3.130) (including the scalings for C and τ_w) into (3.64), we obtain

$$\alpha = \alpha_0 C^{-2/8}\tau_w^{-1}R_\delta^{-5/9}\hat{\omega}_0+\alpha_1 R_\delta^{-5/3}C^{-6/8}\tau_w^{-3}\hat{\omega}_0^3+\cdots \tag{3.190}$$

By matching (3.133) with (3.190), we have

$$C^{-3/8}\tau_w^{-3/2}R_\delta^{-1/3}\hat{\alpha}_0 = \alpha_0 C^{-2/8}\tau_w^{-1}R_\delta^{-5/9}\hat{\omega}_0, \tag{3.191}$$

$$C^{-3/8}\tau_w^{-3/2}R_\delta^{-5/9}\hat{\alpha}_1 = \alpha_1 R_\delta^{-5/3}C^{-6/8}\tau_w^{-3}\hat{\omega}_0^3. \tag{3.192}$$

Therefore,

$$\hat{\alpha}_0 = R_\delta^{-2/9}C^{1/8}\tau_w^{1/2}\alpha_0\hat{\omega}_0, \tag{3.193}$$

$$\hat{\alpha}_1 = R_\delta^{-10/9}C^{-3/8}\tau_w^{-3/2}\alpha_1\hat{\omega}_0^3. \tag{3.194}$$

Introducing (3.193)-(3.194) in (3.189) we obtain, at leading order

$$\alpha_1 = -\frac{M^4 C\tau_w^4\alpha_0^5}{2\lambda_0^2(M^2-1)} \quad \text{as} \quad \hat{\omega}_0 \to \infty \tag{3.195}$$

which agrees with (3.112).

3.4.4 Matching between Wu/Yang intermediate regime and Smith (1989)

The Wu/Yang intermediate regime, characterized by the scalings (3.133) needs to be matched to Smith (1989), by finding the power σ of R which is used to expand $\hat{\alpha}_0$. The relationship between wavenumbers and frequency between Wu/Yang intermediate regime and Smith (1989) is

$$R^{1/3}C^{-3/8}\tau_w^{-3/2}\hat{\alpha}_0 = R^{3/8}C^{-3/8}\tau_w^{-3/2}\hat{\alpha}_{TS}, \tag{3.196}$$

$$R^{1/3}C^{-3/8}\tau_w^{-3/2}\hat{\beta}_0 = R^{3/8}C^{-3/8}\tau_w^{-3/2}\hat{\beta}_{TS}, \tag{3.197}$$

$$R^{2/9}C^{-2/8}\tau_w^{-1}\hat{\omega}_0 = R^{2/8}C^{-2/8}\tau_w^{-1}\hat{\omega}_{TS}. \tag{3.198}$$

Therefore,

$$\hat{\alpha}_{TS} = R^{-1/24}\hat{\alpha}_0, \tag{3.199}$$

$$\hat{\beta}_{TS} = R^{-1/24}\hat{\beta}_0, \tag{3.200}$$

$$\hat{\omega}_{TS} = R^{-1/36}\hat{\omega}_0. \tag{3.201}$$

We now check that $\eta_{0,WY}$ is $\mathcal{O}(1)$

$$\eta_{0,TS} = -\frac{i\hat{\omega}_{TS}}{(i\hat{\alpha}_{TS}\lambda_0)^{2/3}} = -\frac{R^{-1/36}i\hat{\omega}_0}{R^{-1/36}(i\hat{\alpha}_0\lambda_0)^{2/3}} = \eta_{0,WY}. \tag{3.202}$$

Smith (1989)'s equation for the neutral curve is

$$i\hat{\alpha}_{TS}(\hat{\alpha}_{TS}^2 + \hat{\beta}_{TS}^2)\int_{\eta_0}^{\infty} Ai(\eta')d\eta' - \lambda_0\hat{\gamma}_{TS}(i\hat{\alpha}_{TS}\lambda_0)^{2/3}Ai'(\eta_0) = 0, \tag{3.203}$$

which, in W/Y variables (3.199)-(3.201) leads to

$$i\hat{\alpha}_0(\hat{\alpha}_0^2 + \hat{\beta}_0^2)\int_{\eta_0}^{\infty} Ai(\eta')d\eta' - R^{1/18}\lambda_0\hat{\gamma}_0(i\hat{\alpha}_0\lambda_0)^{2/3}Ai'(\eta_0) = 0. \tag{3.204}$$

Now, by expanding $\hat{\alpha}_0$ with a small term of the form

$$\hat{\alpha}_0 \to \frac{\hat{\beta}_0}{\sqrt{M^2-1}} + R^{\sigma}\hat{\alpha}_1, \tag{3.205}$$

it follows that

$$\begin{aligned} &i\left[\hat{\alpha}_0^3 M^2 + \cdots\right]\int_{\eta_0}^{\infty} Ai(\eta')d\eta' \\ &- R^{1/18}\sqrt{(1-M^2)\hat{\alpha}_0^2 + \hat{\beta}_0^2 + R^{\sigma}(1-M^2)2\hat{\alpha}_0\hat{\alpha}_1}(i\hat{\alpha}_0\lambda_0)^{2/3}Ai'(\eta_0) = 0, \end{aligned} \tag{3.206}$$

where $(1-M^2)\hat{\alpha}_0^2 + \hat{\beta}_0^2 = 0$. Balancing, at leading order,

$$0 = \frac{1}{18} + \frac{\sigma}{2}. \tag{3.207}$$

Therefore,

$$\sigma = -\frac{1}{9}. \tag{3.208}$$

We obtain

$$\hat{\alpha}_1 = \frac{1}{2\hat{\alpha}_0(M^2-1)}\left[\frac{M^2\hat{\alpha}_0^3\int_{\eta_0}^{\infty} Ai(\eta')d\eta'}{(i\hat{\alpha}_0\lambda_0)^{2/3}Ai'(\eta_0)}\right]^2. \tag{3.209}$$

According to (3.199)-(3.201), we check the order of magnitude of the terms in (3.181)

$$\frac{1}{2\hat{\alpha}_0(M^2-1)}\left[\frac{M^2\hat{\alpha}_0^3\int_{\eta_0}^{\infty}Ai(\eta')d\eta'}{(i\hat{\alpha}_0\lambda_0)^{2/3}Ai'(\eta_0)}\right]^2=\mathcal{O}(\hat{\alpha}_0^{11/3})=\mathcal{O}(R^{11/72}), \tag{3.210}$$

$$\frac{M^2}{M^2-1}\hat{\omega}_0=\mathcal{O}(R^{1/36}). \tag{3.211}$$

Therefore,

$$\frac{1}{2\hat{\alpha}_0(M^2-1)}\left[\frac{M^2\hat{\alpha}_0^3\int_{\eta_0}^{\infty}Ai(\eta')d\eta'}{(i\hat{\alpha}_0\lambda_0)^{2/3}Ai'(\eta_0)}\right]^2\gg\frac{M^2}{M^2-1}\hat{\omega}_0. \tag{3.212}$$

The expression (3.209) coincides with (3.181), except for the second term, which is found to be negligible (3.212) and the third term, which has been set to zero ($\hat{\beta}_1=0$). Therefore, the Wu/Yang intermediate regime and Smith (1989) have been matched.

3.5 Relationship between G/R and W/Y regimes

The G/R and W/Y approaches use a different normalization ("global" in the G/R case and "local" in the W/Y case). Goldstein and Ricco (2018) were interested in the case $\Delta\theta=\varepsilon^{1-r}=\varepsilon^{2/3}$ for $r=\frac{1}{3}$, where ε is given by (3.10). From (4.36) (Goldstein and Ricco, 2018), in the diffraction region $x=(\Delta\theta)^{5/2}\tilde{\tilde{x}}_2\varepsilon^{-3}$, which, for the situation under consideration $\Delta\theta=\varepsilon^{2/3}$, gives $x=\mathcal{O}(\varepsilon^{-4/3})$.

We denote as "A" the G/R regime, in which the small parameter of the expansions is ε and the dimensional length scale is $L^*_{GR}=U^*_\infty/\omega^*$. "B" denotes the W/Y regime, in which the scalings are expressed using the Reynolds number $R=U^*_\infty L^*_{WY}/\nu^*_\infty$ and the length scale is L^*_{WY}. The aim is to be able to express the G/R regime using the normalisation employed in W/Y, and to express the W/Y regime using the normalisation in G/R. In other words, the goal of this section is to find out whether the regimes (5.1) (Goldstein and Ricco, 2018) and (3.130) are the same or not, by being able to convert from A to B and viceversa.

3.5.1 A → B

The length scale in the A framework is chosen to be $L^*_{GR} = U^*_\infty/\omega^*$. The wavenumbers and frequencies in physical units are given by

$$\alpha^* = \frac{\kappa\omega^*}{U^*_\infty\varepsilon}, \quad \beta^* = \frac{\bar{\beta}\omega^*}{U^*_\infty\varepsilon}, \quad \omega^* = \frac{U^*_\infty}{L^*_{GR}}, \quad c^* = \frac{U^*_\infty\varepsilon}{\kappa}, \tag{3.213}$$

where κ, $\bar{\beta}$ are non-dimensional wavenumbers defined in Goldstein and Ricco (2018). By starting from the same physical parameters (3.213), the aim is to find the relationship between the two normalizations, in particular, we aim to describe the direction A → B. The normalization in the B framework is described as

$$\alpha = x^*\alpha^*, \quad \beta = x^*\beta^*, \quad \omega = (x^*/U^*_\infty)\omega^*, \quad c = c^*/U^*_\infty, \tag{3.214}$$

where x^* can be calculated at the location of interest $x = \mathcal{O}(\varepsilon^{-4/3})$ issued from (4.36) in Goldstein and Ricco (2018) and the fact that $\Delta\theta = \varepsilon^{2/3}$, as

$$x^* = xL^*_{GR} = \varepsilon^{-4/3}L^*_{GR} = F^{-2/9}\frac{U^*_\infty}{\omega^*} = \frac{U^{*13/9}_\infty}{\omega^{*11/9}\nu^{*2/9}_\infty}. \tag{3.215}$$

By combining (3.213), (3.214) and using (3.215), relationships for the ratios α/κ, $\beta/\bar{\beta}$ and $\omega/1$ can be obtained

$$\frac{\alpha}{\kappa} = \varepsilon^{-7/3}, \quad \frac{\beta}{\bar{\beta}} = \varepsilon^{-7/3}, \quad \frac{\omega}{1} = \varepsilon^{-4/3}, \tag{3.216}$$

where the frequency ω has been taken to be unity in Goldstein and Ricco (2018) and we preserve their notation here. At first order, $\kappa = \kappa_0$ (5.4 Goldstein and Ricco, 2018). From (5.23a-c) Goldstein and Ricco (2018), $\bar{\bar{\beta}}$, $\bar{\kappa}_0$ and $\hat{x}_1$ are defined as follows

$$\bar{\bar{\beta}} = \bar{\beta}/\varepsilon^{1/3}, \quad \bar{\kappa}_0 = \kappa_0/\varepsilon^{1/3}, \quad \hat{x}_1 = x_1\varepsilon^{4/3}, \tag{3.217}$$

where these rescaled variables are $\mathcal{O}(1)$. Therefore, $\bar{\kappa}_0 = \mathcal{O}(1)$, $\bar{\bar{\beta}} = \mathcal{O}(1)$, so $\kappa_0 \sim \bar{\beta} = \mathcal{O}(\varepsilon^{1/3})$:

$$\alpha \sim \varepsilon^{-2}, \quad \beta \sim \varepsilon^{-2}, \quad \omega \sim \varepsilon^{-4/3} \quad \text{and} \quad c \sim \varepsilon^{2/3}. \tag{3.218}$$

We proceed now to calculate the Reynolds number at the considered location

$$R_x = \frac{U^*_\infty x^*}{\nu^*_\infty} = \left(\frac{U^{*2}_\infty}{\omega^*\nu^*_\infty}\right)^{11/9} = F^{-11/9} = \varepsilon^{-22/3}. \tag{3.219}$$

This calculation is of crucial importance as we are expressing the Reynolds number (in which the W/Y's scaling is written) at the desired location ($x = \mathcal{O}(\varepsilon^{-4/3})$) as a function of ε (or F), which is the key parameter in the G/R framework. Now, (3.218) is fully expressed in the W/Y framework

$$\alpha \sim R^{3/11}, \quad \beta \sim R^{3/11}, \quad \omega \sim R^{2/11} \quad \text{and} \quad c \sim R^{-1/11}. \tag{3.220}$$

We have thus been able to express the G/R regime of Goldstein and Ricco (2018) in the W/Y framework, using R, the local Reynolds number.

3.5.2 B $\rightarrow$ A

In the W/Y framework, the wavenumber, frequency and phase speed scale with the "local" Reynolds number as follow

$$\alpha = R^{1/3}\left[\hat{\alpha}_0 + R^{-1/9}\hat{\alpha}_1\right], \tag{3.221}$$

$$\omega = R^{2/9}\left[\hat{\omega}_0 + R^{-1/9}\hat{\omega}_1\right], \tag{3.222}$$

$$c = R^{-1/9}\left[\hat{c}_0 + R^{-1/9}\hat{c}_1\right]. \tag{3.223}$$

Using (3.222), the location x^* at which this regime operates can be found as a function of U^*_∞, ω^* and ν^*_∞

$$\frac{\omega^* x^*}{U^*_\infty} = R^{2/9} = \left(\frac{U^*_\infty x^*}{\nu^*_\infty}\right)^{2/9} \rightarrow x^* = \frac{U^{*4/7}_\infty}{\nu^{*2/7}_\infty \omega^{*2/7}} \frac{U^*_\infty}{\omega^*} = F^{-2/7} L^*_{GR} = \varepsilon^{-12/7} L^*_{GR}. \tag{3.224}$$

This location just calculated (B) has to be nondimensionalized using the length scale from the G/R framework (A) as follows (B $\rightarrow$ A)

$$x = \frac{x^*}{L^*_{GR}} = \varepsilon^{-12/7}. \tag{3.225}$$

As in A $\rightarrow$ B, the local Reynolds number can be calculated as

$$R_x = \frac{U^*_\infty x^*}{\nu^*_\infty} = F^{-1}\varepsilon^{-12/7} = \varepsilon^{-54/7}. \tag{3.226}$$

The relationship between the two normalizations for the streamwise wavenumber is worked out using (3.213) and (3.224)

$$\alpha = x^*\alpha^* = \frac{\varepsilon^{-12/7} U^*_\infty}{\omega^*} \frac{\kappa \omega^*}{U^*_\infty \varepsilon} = \varepsilon^{-19/7}\kappa, \tag{3.227}$$

for the frequency we have

$$\omega = \frac{x^*}{U_\infty^*}\omega^* = \varepsilon^{-12/7} \tag{3.228}$$

and the phase speed is obtained using (3.213) and (3.214)

$$c = \varepsilon\frac{1}{\kappa}, \tag{3.229}$$

Now, if we substitute (3.227)-(3.229) in (3.221)-(3.223) we obtain the following in the G/R framework

$$\kappa = \varepsilon^{1/7}\left[\hat{\alpha}_0 + \varepsilon^{12/7}\hat{\alpha}_1\right], \tag{3.230}$$

$$1 = 1 \cdot \left[\hat{\omega}_0 + \varepsilon^{18/7}\hat{\omega}_1\right], \tag{3.231}$$

$$c = \varepsilon^{6/7}\left[\hat{c}_0 + \varepsilon^{6/7}\hat{c}_1\right]. \tag{3.232}$$

Therefore, we have been able to express the scalings of the W/Y regime (3.221)-(3.223) in the G/R framework, using the small parameter ε.

3.6 Calculation of growth rate in G/R regime

The streamwise wavenumber of the G/R regime is, at leading order (3.220)

$$\alpha \sim R^{3/11}. \tag{3.233}$$

We are interested in calculating the next-order term, α_1, i.e.,

$$\alpha = R^{3/11}\left[\hat{\alpha}_0 + R^\sigma\hat{\alpha}_1\right], \tag{3.234}$$

where σ is unknown, in the W/Y framework using the "local" Reynolds number R.

3.6.1 Lower deck

In the lower deck we have

$$y \sim (\alpha R^{3/2})^{-1/3}, \tag{3.235}$$

where y and α are nondimensionalized with L. In fact, for Smith (1989) we have $\alpha \sim R^{3/8}$, thus by (3.235) we obtain $y \sim R^{-5/8}$. For G/R regime we have (3.233),

therefore by (3.235) we obtain

$$y \sim R^{-13/22}. \tag{3.236}$$

If $u = \mathcal{O}(\varepsilon)$ (a small parameter different from the one defined in (3.10)), then by continuity we have

$$R^{3/11}\varepsilon \sim R^{13/22}v \rightarrow v \sim \varepsilon R^{-7/22}. \tag{3.237}$$

The unsteady term, the convective term, the diffusion term and the streamwise gradient of the pressure balance, therefore

$$\varepsilon R^{2/11} \sim pR^{3/11} \rightarrow p \sim \varepsilon R^{-1/11}. \tag{3.238}$$

3.6.2 Main deck

By continuity we have for v,

$$R^{3/11}\varepsilon \sim R^{1/2}v \rightarrow v \sim \varepsilon R^{-5/22}. \tag{3.239}$$

The pressure p has the same order of magnitude in every deck,

$$p \sim \varepsilon R^{-1/11}. \tag{3.240}$$

3.6.3 Upper deck

The matching condition with the main deck reads (Smith, 1989)

$$\frac{\partial p}{\partial \bar{y}} = -\frac{\partial v}{\partial \bar{x}}. \tag{3.241}$$

By using (3.239), (3.240) in (3.241) we obtain the vertical size of the upper deck

$$\bar{y} \sim R^{-3/22}. \tag{3.242}$$

The streamwise velocity, u, (at leading order) has the same order of magnitude as p (as well as ρ)

$$u \sim \varepsilon R^{-1/11}. \tag{3.243}$$

The four terms on the RHS of equation (3.146) balance and their orders of magnitude are

$$\alpha_0 p_1 = \mathcal{O}(R^{3/11}p_1), \tag{3.244}$$

$$\alpha_1 p_0 = \mathcal{O}(\alpha_1 \varepsilon R^{-1/11}), \tag{3.245}$$

$$\omega_0 u_0 = \mathcal{O}(R^{2/11} \varepsilon R^{-1/11}), \tag{3.246}$$

$$\alpha_1 u_0 = \mathcal{O}(\alpha_1 \varepsilon R^{-1/11}). \tag{3.247}$$

From (3.245) and (3.246),

$$\alpha_1 \varepsilon R^{-1/11} \sim \varepsilon R^{1/11} \to \alpha_1 \sim R^{2/11}, \tag{3.248}$$

and thus the correction with respect to the leading-order term for the streamwise wavenumber is $R^{-1/11}$. Therefore,

$$\alpha = R^{3/11} \left[\hat{\alpha}_0 + R^{-1/11} \hat{\alpha}_1 \right], \tag{3.249}$$

$$\omega = R^{2/11} \left[\hat{\omega}_0 + R^{-1/11} \hat{\omega}_1 \right], \tag{3.250}$$

$$c = R^{-1/11} \left[\hat{c}_0 + R^{-1/11} \hat{c}_1 \right]. \tag{3.251}$$

The upper deck width is determined by the vertical wavenumber γ, where

$$\gamma^2 = M^2(\alpha - \omega)^2 - \alpha^2 - \beta^2 \tag{3.252}$$

is the dispersion relation satisfied by the wavenumbers and frequency in the upper deck. The upper deck width is then $\mathcal{O}(\gamma^{-1})$. Since $\alpha, \beta = \mathcal{O}(R^{3/11})$ and $\omega = \mathcal{O}(R^{2/11})$ from (3.249) and (3.251), respectively, and in order for γ to be $\mathcal{O}(R^{3/22})$ (3.242), the streamwise wavenumber must be expanded as

$$\alpha = R^{3/11} \left[\hat{\alpha}_0 + R^{-1/11} \hat{\alpha}_1 + R^{-2/11} \hat{\alpha}_2 + R^{-3/11} \hat{\alpha}_3 \right] \tag{3.253}$$

for fixed $\beta = R^{3/11} \hat{\beta}_0$ and $\omega = R^{2/11} \hat{\omega}_0$. Substituting (3.253) into (3.252) and equating the terms at different orders, we obtain

$$\hat{\alpha}_0 = \frac{\hat{\beta}_0}{\sqrt{M^2 - 1}}, \tag{3.254}$$

$$\hat{\alpha}_1 = \frac{M^2 \hat{\omega}_0}{M^2 - 1}, \tag{3.255}$$

$$\hat{\alpha}_2 = \frac{M^2 \hat{\omega}_0^2}{2\hat{\alpha}_0 (M^2 - 1)^2}, \tag{3.256}$$

with

$$\gamma = R^{3/22} \left[(M^2 - 1)(2\hat{\alpha}_0 \hat{\alpha}_3) \right]^{1/2}. \tag{3.257}$$

It can be observed (3.257) that γ is independent on $\hat{\alpha}_1$ and $\hat{\alpha}_2$, which are real. Therefore, the growth rate corresponds to the fourth term in the expansion $\hat{\alpha}_3$, which is $\mathcal{O}(1)$.

3.7 Summary and conclusions

In this Chapter, an attempt to connect the inviscid (studied by Fedorov, 2003a and Fedorov, 2011) and viscous (studied by Smith, 1989) branches of the neutral curve of a supersonic boundary layer in the large-Reynolds-number asymptotic limit was undertaken following the recent work by Goldstein and Ricco (2018). The goal of the present study was to clarify the connection between the two branches and to find out what happened when $\beta \to \sqrt{M^2-1}\alpha$. First, the theories of Fedorov/Khokhlov and Smith were introduced, followed by the investigation of the discrepancy between the regimes observed in the work by Yang (2017) and by Goldstein and Ricco (2018). Since these two independent studies used a framework in which the normalisation employed was different in each case ("global" in Goldstein and Ricco, 2018 and "local" in Yang, 2017), a conversion between the two normalisations was done, leading to the conclusion that the regime studied in Yang (2017) had not been considered in the analysis by Goldstein and Ricco (2018), since the conversion between normalisations led to different scalings for the two regimes. Finally, the matching of the intermediate regime found in Yang (2017) to Fedorov's regime (Fedorov, 2003a) was carried out when $\hat{\omega}_0 \to \infty$ and to Smith (1989) when $\beta \to \sqrt{M^2-1}\alpha$.

Finite-Reynolds-number calculations suggesting that the upper and lower branches of the neutral curve are connected have therefore been confirmed mathematically in the large-Reynolds-number asymptotic limit. The receptivity to sound-sound and sound-roughness (as in chapter 2) of the instability studied by Yang (2017) and further discussed in this work, could be investigated in the future. Another natural follow-up of the present work is extending the framework provided by Fedorov (2003a) to account for shock waves (Qin and Wu, 2016), which can be of interest for very-high-speed flows (hypersonic regime, $M > 4.5$).

4

Receptivity of a supersonic boundary layer to free-stream vortical and slow acoustic disturbances

4.1 Introduction

Laminar-turbulent transition in a boundary layer is known to be crucially affected by free-stream disturbances. These disturbances generally consist of acoustic, vortical and entropy modes (Kovasznay, 1953), but they are often referred to as free-stream turbulence (FST) and are characterized by a turbulence level Tu, the RMS value of the velocity fluctuations, and turbulence length scales. The observation that the transition Reynolds number strongly depends on Tu was first made by Dryden (1955). At a very low turbulence level, transition is initiated by the growth of T-S waves, which can be excited by receptivity processes, such as the leading-edge adjustment mechanism (Goldstein, 1983) or the interaction of the free-stream disturbances with local and distributed surface inhomogeneities or with a local separation of the mean boundary layer (Goldstein, 1985, Goldstein and Hultgren, 1989). At a moderate level of FST, discernible instability waves may still be observed but their wavelength, frequency and growth rate are substantially altered. When a relatively high level of FST is present, transition takes the so-

called bypass route (Morkovin, 1984), without apparently involving T-S waves.

Dryden (1936) and Taylor (1939) performed the first experimental studies of transition under the influence of high FST at low speeds. They observed that the response of the boundary layer to FST was characterized by spanwise alternating low- and high-speed regions, which were elongated in the streamwise direction. They suggested that the development of this kind of "breathing modes" could be a precursor of transition. However, the interest to boundary layers perturbed by very low Tu was soon shifted by the experiments of Schubauer and Skramstad (1947) (which verified the linear stability theory of Tollmien, 1929 and Schlichting, 1933). Later, the work of Klebanoff (1971) revived the interest in this topic and stimulated much further work e.g. Arnal and Juillen (1978), Kendall (1985), Kendall (1990), Kendall (1991), Westin et al. (1994), and Matsubara and Alfredsson (2001) and Fransson et al. (2005b) performed measurements of the fluctuations within the boundary layer induced by FST of relatively high level.

All the above studies confirmed that fluctuations in the core of the boundary layer consist of predominantly low-frequency components and that the streamwise velocity has a much larger magnitude than both the normal and spanwise velocities. Perturbations of this form thus manifest themselves as streamwise-elongated streaks, referred to nowadays as "Klebanoff modes". The role of streaks in transition still remains a topic of debate. It has been suggested that streaks, once exceeding a certain threshold amplitude, may cause a new form of instability leading to transition. Matsubara and Alfredsson (2001) provided some supporting evidence in their experiments, which indicate that the streaks undergo oscillatory meandering motion before the eventual breakdown to turbulence. Wu and Choudhari (2003) investigated the stability of unsteady streaks with a spanwise length scale much larger than the local boundary-layer thickness so that the boundary-layer equations could be used to compute the signature of the streaks. It was shown that streaks of this kind may cause inviscid instability when their amplitude exceeds a critical value, but is still small enough for the linearized equations to provide a valid approximation.

Bypass transition induced by free-stream turbulence has also been studied by direct numerical simulations (DNS). For example, FST has been modelled by the continuous spectra of the Orr-Sommerfeld and Squire operators in Jacobs and Durbin (2001) and Zaki and Durbin (2005). They found that streaks remain stable until they lift towards the outer edge of the boundary layer to form backward jets. In that case, breakdown to turbulent spots may occur only when the new base flow is perturbed by a high-frequency disturbance (Zaki and Durbin, 2005). A similar

DNS carried out by Brandt et al. (2004) found that, at the same level of intensity, FST with a larger integral length scale causes transition to happen earlier than with a smaller scale.

The role of streaks on boundary-layer instability is however not fully understood. On one hand, Kendall (1990), Kendall (1991), Kendall (1998) found that in the presence of moderate FST (Tu less than 1%), TS-like waves tend to have higher growth rates than when FST is absent. On the other hand, Kachanov and Tararykin (1987), Bakchinov et al. (1995), Fransson et al. (2005a) observed that artificially generated steady streaks of amplitude below the threshold amplitude for inviscid instability apparently stabilize viscous T-S waves. Cossu and Brandt (2002) corroborated this stabilizing effect by a stability analysis of the streaks modelled by the optimal perturbations. Fasel (2002) studied the interaction of a forced two-dimensional T-S wave with the streaks that are generated by an artificial body force. He found that the growth rate of the planar T-S waves was reduced, but the interaction also generated oblique waves which underwent very rapid amplification to overtake the planar waves.

There may be a number of possible reasons for the disagreement on the role of streaks on stability. The DNS result of Fasel (2002) showed that streaks stabilize some T-S waves but may destabilize other waves, like oblique waves with spanwise wavelength twice that of the streaks because these waves may be in parametric subharmonic resonance with the streaks. The second reason may be in the mathematical modelling of streaks: Andersson et al. (2001) modelled the streaks in an ad hoc manner without considering what kind of external perturbations might excite them. Klebanoff modes are however not strictly steady (unlike in Andersson et al., 2001), and this inherent unsteadiness may be crucial for instability, as showed by Wu and Choudhari (2003). However, the treatment in the DNS by Fasel (2002) is not entirely satisfactory because the perturbations prescribed at the inlet of the computational domain, i.e. the continuous spectra of O-S and Squire equations, do not necessarily represent the actual disturbances that have penetrated into the boundary layer upstream since the non-parallel effect, which plays a crucial role for the entrainment of the most relevant long-wavelength free-stream disturbances, is neglected (Wu et al., 2011, Wu and Dong, 2016a, Wu and Dong, 2016b, Xu et al., 2017, Xu et al., 2020).

The fact that the relevant perturbations for streak formation are of low frequency and long wavelength means that the streamwise viscous diffusion terms can be neglected. The viscous diffusion and the pressure gradient in the spanwise direction are retained in order to describe the typical streaks with spanwise length scale com-

parable with the boundary layer thickness (Leib et al., 1999, Ricco et al., 2011). The Navier-Stokes equations then simplify to the so-called boundary-region equations (Kemp, 1951). These equations are elliptic in the spanwise direction, but parabolic in the streamwise direction. This property means that the equations can be marched downstream. The initial condition is provided by asymptotic matching with the small-distance limit of the boundary-layer solution. The external disturbances in the free-stream are not entirely independent of the boundary layer - they are simultaneously influenced by the viscous displacement. This approach is based on the linearized-unsteady boundary-region (LUBR) equations and Leib et al. (1999) used it to calculate the signature of the streaks induced by FST of a given spectrum. They showed that the boundary layer acts as a filter, letting low-frequency fluctuations into the boundary later and amplify downstream, while blocking high-frequency components. Their predictions agree quantitatively well with the measurements.

Unlike the incompressible counterpart, bypass transition in compressible boundary layers remains largely unexplored. A fair number of experiments have been performed primarily to establish the gross correlation between the transition Reynolds number and FST. Dryden (1955) and Schneider (2001) showed that the transition position shifts significantly depending on the FST level and Pate (1971) on surface roughness. However, the physics underpinning such correlations are largely unstudied. Laufer (1961) observed that stronger vortical disturbances cause transition to occur earlier for Mach numbers $M < 2.5$. For $M > 2.5$, the transition location is hardly affected by the amplitude of vortical disturbances. A possible reason for this is that the composition of FST varies with the Mach number. For $M > 2.5$, acoustic disturbances become dominant because the unsteady fluctuations in the turbulent boundary layers on the tunnel walls radiate considerable amount of sound (Laufer, 1961) to influence transition of the boundary layer of the test model. In general, such facility-produced acoustic noise result in the transition Reynolds number measured in laboratory experiments being significantly lower than that in flight conditions (Schneider, 2001). Therefore, a systematical correction of laboratory data has to be carried out in order to extrapolate to flight conditions.

Kendall (1975) studied experimentally supersonic boundary-layer transition to high-level FST. He found that fluctuations over a wide frequency range undergo substantial growth within the boundary layer. Sufficiently downstream, a spectral peak emerges, which corresponds to the Mack first mode in the low-Mach-number supersonic range ($M < 4.5$) (Mack, 1984). For higher Mach numbers, a secondary,

less pronounced peak representing Mack's second mode was observed. The results supports the idea that some kind of receptivity mechanism operates to generate instability waves in an otherwise flat plate. On the other hand, the broadband amplification cannot be explained by linear instability theory. Mack (1975) proposed a forcing theory to calculate the boundary-layer response to oncoming sound waves. Kendall (1975) found that the prediction of this theory was in agreement with the measurements in some (but not all) of the cases investigated. He also pointed out that at low speeds, tunnel sound may not be the only disturbance - vortical disturbances cannot be excluded. Graziosi and Brown (2002) studied the transition process in a Mach-3 boundary layer. They found that the dominant boundary-layer fluctuations were of low frequency with the energy being concentrated at the frequencies below the Mack first mode instability range. The onset of high-frequency disturbances was preceded by spikes in the time traces. The interval between two successive spikes scaled with the time scale of the low-frequency fluctuations, leading them to speculate that these acoustically forced disturbances may play an active role in the eventual breakdown into small-scale motions.

Although acoustic disturbances are the main concern in most experimental studies, this does not imply that vortical disturbances are not relevant, in fact, their influence is quite significant in the low supersonic speed range ($M < 2.5$) (Laufer, 1961, Kendall, 1975). In flight conditions, acoustic disturbances are usually less intense, and so vortical fluctuations are likely to be the primary external disturbances affecting the transition location. Free-stream disturbances may interact with the boundary layer when other types of external disturbances, such as surface roughness and wall transpiration, are also at play. A DNS study on the receptivity of a supersonic boundary layer to free-stream acoustic and vortical perturbations in the presence of surface step excrescences was performed by Sescu et al. (2016). The boundary layer was also perturbed by two-dimensional wall transpiration imposed upstream of the step. The results confirmed that two-dimensional roughness elements act to stabilize high-speed boundary layers, thus delaying the onset of transition.

From Kovasznay (1953), vortical disturbances are not associated with any pressure gradient, and thus do not penetrate into the boundary layer in the sense that their signature is exponentially small there as was shown mathematically by Gulyaev et al. (1989). This, together with the fact that the local mean-flow distortion produced by a roughness concentrates in the region near the wall, one might conclude that vortical disturbances are unable to excite T-S waves. Duck et al. (1996) found such conclusion to be wrong, observing that the roughness-induced

mean flow outside the boundary layer, though of relatively small magnitude, does not vanish completely, so it can interact with the vortical disturbance to generate T-S waves. The coupling coefficient for this receptivity mechanism was found to be a factor of $R^{-1/8}$ smaller than in the corresponding acoustic case.

Ricco and Wu (2007) calculated the fluctuations induced by free-stream vortical disturbances in a laminar boundary layer, extending the work of Leib et al. (1999) to the compressible regime, with a focus on components with long streamwise wavelength. The boundary-layer response is governed by the linearized unsteady boundary-region equations in the typical streamwise region where the local boundary-layer thickness is comparable with the spanwise length scale of the disturbances. They found that low-frequency vortical disturbances penetrate into the boundary layer to form slowly modulating streamwise-elongated velocity streaks. In the compressible regime, vortical disturbances are found to induce substantial temperature fluctuations so that 'thermal streaks' also form. Their calculations indicate that for a vortical disturbance with a relatively large spanwise length scale, the induced boundary-layer fluctuation ultimately evolves into an amplifying wave. This is due to a receptivity mechanism, in which a vortical disturbance first excites a decaying quasi-three-dimensional Lam–Rott eigensolution. The latter then undergoes wavelength shortening to generate a spanwise pressure gradient, which eventually converts the Lam–Rott mode into an exponentially growing mode. The latter is recognized to be a highly oblique Tollmien–Schlichting wave.

Marensi (2016) subsequently studied the nonlinear response of a compressible boundary layer to low-frequency unsteady free-stream vortical fluctuations of the convected-gust type, which induce strong streamwise-elongated components of the boundary-layer disturbances (Klebanoff modes). The amplitude of the disturbances is intense enough (amplitude of the induced streaks comparable with the mean flow) for nonlinear interactions to occur within the boundary layer. Their generation and nonlinear evolution is described by the mathematical framework of the nonlinear unsteady compressible boundary-region equations (NUBRE). The previous works by Ricco and Wu (2007) and Ricco et al. (2011) were extended to take into account both compressibility and nonlinear effects.

Two important studies precede the present work. Wu (1999) studied the generation of T-S waves by the interaction of acoustic and vortical waves of suitable frequencies and wavenumbers so as to achieve scale conversion. Unlike the mechanism in the Goldstein-Ruban theory (Ruban, 1984, Goldstein, 1985), the conversion of the external scales does not require any form of non-homogeneity on the wall or in the mean flow. In the case considered by Wu (1999), the dominant interac-

tion takes place in the upper deck. Hernández and Wu (2019) considered slow ($c_s = \mathcal{O}(R^{-1/8})$) acoustic waves penetrating the boundary layer and interacting in the lower deck, leading to a much stronger receptivity than that of Wu (1999). The same holds for the interaction between a slow acoustic wave and the mean-flow distortion caused by a distributed roughness, also considered in Hernández and Wu (2019). More recently, Liu et al. (2020) studied the receptivity of a supersonic boundary layer to slow acoustic waves (in the sense of Hernández and Wu (2019)) interacting with streamwise isolated wall roughness, and Dong et al. (2020) extended the analysis to inviscid modes.

In the present work, we shall propose a new and extremely efficient receptivity mechanism for the generation of T-S waves (first Mack modes in the supersonic regime), which operates in supersonic boundary layers over smooth surfaces and builds on the two studies mentioned above. The mechanism involves an incident sound wave with its frequency and wavelength on the triple-deck scale and free-stream vortical disturbances with spanwise wavelength on the triple-deck scale too but long streamwise wavelength comparable with L, the distance to the leading edge. Such a sound wave has the special feature that its streamwise velocity and temperature/density fluctuations in the boundary layer acquire an amplitude of $\mathcal{O}(\varepsilon_s R^{1/8})$, much stronger than the $\mathcal{O}(\varepsilon_s)$ fluctuation in the free-stream. The long-wavelength vortical disturbances with $\mathcal{O}(\varepsilon_v)$ intensity in the free-stream induce in the boundary layer much larger $\mathcal{O}(\varepsilon_v R^{3/8})$ streamwise velocity and temperature/density, which manifest as streaks. With the appropriate choice of the spanwise wavelength on the triple deck scale, the acoustic signature and streaks interact in the main boundary layer as well as in the lower deck, to generate a forcing that is in resonance with a neutral first Mack mode. The latter is thus excited near the lower branch of the neutral curve, and subsequently undergoes exponential amplification. At a high Reynolds number, the triple-deck formalism is adopted to describe the scale conversion process and make quantitative predictions of impingement and reflection of the acoustic wave and the streak's spanwise length scale. The receptivity of this mechanism is found to be greater than those in Chapter 2 and Wu (1999) by a factor of $\mathcal{O}(R^{1/8})$ and $\mathcal{O}(R^{3/8})$, respectively.

4.2 Formulation and scalings

We consider the two-dimensional compressible boundary layer over a semi-infinite flat plate. The oncoming flow is assumed to be uniform with a velocity U_∞, density ρ_∞, temperature T_∞ and sound speed a_∞. Superimposed on this background flow are three-dimensional small-amplitude disturbances of acoustic and vortical nature. The acoustic waves are essentially pressure fluctuations while the vortical waves are of convected gust type, i.e. they are passively advected by the mean flow. For convenience, we define the Reynolds number R_L based on the distance of the neutral position to the leading edge L and the Mach number M as

$$R_L = \rho_\infty U_\infty L/\mu_\infty, \quad M = U_\infty/a_\infty, \tag{4.1}$$

where μ_∞ is the free-stream dynamic viscosity and the reference length scale Λ is chosen to be the spanwise wavelength of the vortical disturbance. In the work, we will take R_L to be asymptotically large, $R_L \gg 1$, and focus on the supersonic regime, $M > 1$ with $M = \mathcal{O}(1)$.

We introduce a Cartesian coordinate system (x_1,x_2,x_3), where x_1 and x_2 are along and normal to the surface, respectively, while x_3 is in the spanwise direction, all being non-dimensionalized by L. The time variable t is normalized by L/U_∞. The velocity $\mathbf{u} = (u, v, w)$, density ρ, temperature τ, pressure p, and the shear and bulk viscosities, μ and μ', are non-dimensionalized by U_∞, ρ_∞, T_∞, $\rho_\infty U_\infty^2$ and μ_∞ respectively. The fluid is taken to be a perfect gas with a constant ratio of specific heats, γ. The non-dimensional Navier-Stokes (N-S) equations are given by (2.2)-(2.6) in chapter 2.

It is important to note that we have employed the distance to the leading edge L to non-dimensionalize equations (2.2)-(2.6); but we remind the reader that these equations also describe vortical waves, for which the spanwise wavelength Λ is more suitable as a reference scale. In the following section, the precise relation between the streamwise and spanwise length scales $\Lambda/L = \mathcal{O}(R_L^{-3/8})$ will be derived, so the conversion between non-dimensionalizations will be established.

4.2.1 The base flow

The base flow is given in section 2.2.1 of chapter 2. In this work, the variation of the viscosity with the temperature is assumed to obey the power law $\mu = T^\omega$, with $\omega = 0.76$.

4.2.2 Physical idea and resonant interaction

Let us first explain the basic idea of our receptivity mechanism in general terms before presenting it in the mathematical framework of triple-deck theory. Suppose that a three-dimensional sound wave, $\varepsilon_s \left\{ e^{i(\alpha_s x+\gamma_s y+\beta_s z-\omega_s t)} + \text{c.c.} \right\}$ and a convective gust $\varepsilon_v \left\{ e^{i(k_1 x+k_2 y+k_3 z-\omega_v t)} + \text{c.c.} \right\}$ impinge on the boundary layer developing over a flat plate (note that the wavenumbers and coordinate variables for the convective gust are non-dimensionalized by Λ, in contrast to the reference length scale used for the sound wave, L; the relation between the two will be derived later). We focus on quasi-steady ($k_1 = \omega_v \ll \omega_s$) long-wavelength ($k_1 \ll \alpha_s$) vortical disturbances or "streaks". From the dispersion relation obtained with the inviscid approximation, the phase speeds are

$$c_s = \frac{\omega_s}{\alpha_s} = 1 \pm \frac{\sqrt{\alpha_s^2 + \beta_s^2 + \gamma_s^2}}{\alpha_s M} \quad \text{and} \quad c_v = 1, \tag{4.2}$$

where the plus and minus signs stand for the fast/slow acoustic waves respectively. The interaction between the two waves as defined earlier generates two forms of forcing proportional to $e^{i\{(\alpha_s \pm k_1)x+(\beta_s \pm k_3)z-(\omega_s \pm \omega_v)t\}}$. Hereinafter we will consider the forcing from the difference interaction, corresponding to the minus sign, which would be in resonance with a neutral T-S mode $e^{i\{\alpha_{TS}x+\beta_{TS}z-\omega_{TS}t\}}$ if their wavenumbers and frequencies satisfy the relations

$$\alpha_s = \alpha_{TS}, \quad \beta_s - k_3 = \beta_{TS}, \quad \omega_s = \omega_{TS}, \tag{4.3}$$

which will be referred to as the resonance conditions. The difference interaction considered here may be linked to Wu (1999) in the limiting case. Our focus will be on first Mack modes, which have a larger amplification rate than second Mack modes for $M < 4.5$, beyond which second modes become more unstable (Mack, 1984). In the lower-branch regime, first Mack modes have asymptotically small speeds, i.e. $\omega_{TS} \ll \alpha_{TS}$ (in fact, $\omega_{TS} = \mathcal{O}(R_L^{-1/8}\alpha_{TS})$, see below) at large R_L. Typical sound waves have $\mathcal{O}(1)$ phase speeds, $\omega_s = \mathcal{O}(\alpha_s)$ and vortical waves exactly satisfy $\omega_v = k_1$. However, for sound waves with $c_s = \mathcal{O}(1)$, the induced signature in the boundary layer is of the same order of magnitude as in the free stream. They are less effective in generating first Mack modes than those with $c_s \ll 1$ or equivalently $\omega_s \ll \alpha_s$.

When $\omega_s \ll \alpha_s$, the dispersion relation (4.2) reduces to $\beta_s^2+\gamma_s^2 = (M^2-1)\alpha_s^2$, which is possible only in the supersonic regime $M > 1$. It follows that the wavenumbers

of the acoustic wave have to satisfy

$$|\beta_s| < \sqrt{M^2 - 1}\alpha_s \tag{4.4}$$

For a T-S wave, its wavenumbers must satisfy (Smith, 1989)

$$\beta_{TS} > \sqrt{M^2 - 1}\alpha_{TS} \tag{4.5}$$

In summary, we focus on the difference interaction between a sound wave and a vortical wave with phase speeds $c_s = \omega_s/\alpha_s \ll 1$ and $c_v = 1$, respectively. The resulting mechanism is very strong, as will be shown later.

4.2.3 Asymptotic scalings

The lower-branch first Mack modes in a supersonic boundary layer have the characteristic scalings $\omega_{TS} = R_L^{2/8}\hat{\omega}_{TS}$ and $(\alpha_{TS}, \beta_{TS}) = R_L^{3/8}(\hat{\alpha}_{TS}, \hat{\beta}_{TS})$ for the frequency and wavenumbers (Smith, 1989), the same as the T-S waves in the incompressible regime. In the present work, we assume the acoustic wave's streamwise and spanwise wavenumbers, frequency and the streak's spanwise wavenumber to be on the triple-deck scale:

$$\alpha_s = R_L^{3/8}C^{-3/8}\tau_w^{-3/2}\hat{\alpha}_s, \quad \beta_s = R_L^{3/8}C^{-3/8}\tau_w^{-3/2}\hat{\beta}_s, \quad \omega_s = R_L^{2/8}C^{-1/4}\tau_w^{-1}\hat{\omega}_s, \tag{4.6}$$

Note that the phase speed $c_s = \mathcal{O}(R_L^{-1/8})$, which is what a 'slow acoustic wave' means precisely in the present work, following Hernández and Wu (2019). The precise relations between Λ and L, and between R_Λ and R_L will be established now. It is convenient to introduce a non-dimensionalization based on Λ for the description of streaks, for which the following non-dimensional wavenumbers are defined

$$k_1 = k_1^*\Lambda, \quad k_3 = k_3^*\Lambda = \mathcal{O}(1). \tag{4.7}$$

For the receptivity problem, the distance from the neutral position to the leading edge, L, is more convenient instead, leading to the introduction of β_v

$$\beta_v \equiv k_3^* L = R_L^{3/8}C^{-3/8}\tau_w^{-3/2}\hat{\beta}_v. \tag{4.8}$$

It follows from the second equation in (4.7) and (4.8) that

$$\Lambda/L = R_L^{-3/8}C^{3/8}\tau_w^{3/2}(k_3/\hat{\beta}_v). \tag{4.9}$$

Using (4.9), the relation between R_Λ and R_L can be established

$$R_\Lambda = R_L^{5/8} C^{3/8} \tau_w^{3/2} (k_3/\hat{\beta}_v). \tag{4.10}$$

In terms of the rescaled quantities, the resonance conditions for the difference interaction are expressed as

$$\hat{\alpha}_s = \hat{\alpha}_{TS}, \quad \hat{\beta}_s - \hat{\beta}_v = \hat{\beta}_{TS}, \quad \hat{\omega}_s = \hat{\omega}_{TS}. \tag{4.11}$$

In view of (4.6), we introduce the time, streamwise and spanwise variables

$$\bar{x} = R_L^{3/8} C^{-3/8} \tau_w^{-3/2} x, \quad \bar{z} = R_L^{3/8} C^{-3/8} \tau_w^{-3/2} z, \quad \bar{t} = R_L^{2/8} C^{-1/4} \tau_w^{-1} t \tag{4.12}$$

The impingement of the sound wave is also described by the triple-deck theory, which allows us to calculate the reflection coefficient and the signature induced in the boundary layer.

The dominant interaction between the sound and vortical waves takes place in the main and lower decks; in particular, the unsteady fluctuation driven by the acoustic pressure acquires $\mathcal{O}(\varepsilon_s R_L^{1/8})$. As was first pointed out by Wu (1999) for the vortical–sound interaction, the forced response evolves into a T–S mode on approaching the neutral point, x_0, where the resonance conditions in (4.11) are met. In order to describe this change of the character, it is necessary to include the non-parallel-flow effect, which becomes important in an $\mathcal{O}(\bar{\varepsilon})$ neighbourhood of x_0, where $\bar{\varepsilon} = R_L^{-3/16} C^{3/16} \tau_w^{3/4}$ (Ruban, 1983, Hall and Smith, 1984). The evolution of the forced response to an eigenmode is described by the variable (Wu, 1999)

$$x_1 = (x - x_0)/\bar{\varepsilon}, \tag{4.13}$$

and the amplitude of the T-S wave will be a function of x_1. We may set $x_0 = 1$ by taking L to be the disturbance from neutral point to the leading edge. The wall shear stress of the base flow, $\lambda = \lambda_0 x^{-1/2}$, is therefore to be expanded about $x_0 = 1$ as

$$\lambda = \lambda_0 + \bar{\varepsilon} \lambda_1 x_1 \quad \text{with} \quad \lambda_1 = -\lambda_0/2. \tag{4.14}$$

4.2.4 Vortical wave

The convecting gust propagates with the free stream, and so in general its solution can be represented as a superposition of Fourier modes. For simplicity, we consider only one Fourier component in the gust so that the solution of the velocity

fluctuations can be sought of the form (Leib et al., 1999, Ricco and Wu, 2007)

$$\mathbf{u_v} = \hat{\mathbf{u}}_\mathbf{v}(\bar{y})e^{\{i(k_1(\bar{x}-\bar{t})+k_3\bar{z})\}} + \text{c.c.}, \tag{4.15}$$

where

$$\left.\begin{aligned} \hat{u}_v &= \hat{u}_\infty e^{ik_2\bar{y}} + \tfrac{ik_1}{\gamma}\hat{v}_\infty e^{-\gamma\bar{y}} \\ \hat{v}_v &= \hat{v}_\infty(e^{ik_2\bar{y}} - e^{-\gamma\bar{y}}) \\ \hat{w}_v &= \hat{w}_\infty e^{ik_2\bar{y}} + \tfrac{ik_3}{\gamma}\hat{v}_\infty e^{-\gamma\bar{y}} \end{aligned}\right\} \tag{4.16}$$

where $\gamma = \sqrt{k_1^2 + k_3^2}$, and $\hat{\mathbf{u}}_\infty \equiv (\hat{u}_\infty, \hat{v}_\infty, \hat{w}_\infty)$ satisfy

$$k_1\hat{u}_\infty + k_2\hat{v}_\infty + k_3\hat{w}_\infty = 0 \tag{4.17}$$

by continuity equation and τ_v and ρ_v have similar form, while p_v is an order of magnitude ($\mathcal{O}(\varepsilon_v^2)$) smaller. The solution for the entropy mode in the gust is given by

$$\hat{\tau}_v = \hat{\tau}_\infty e^{ik_2\bar{y}}, \quad \hat{\rho}_v = -\hat{\tau}_\infty e^{ik_2\bar{y}}. \tag{4.18}$$

At the surface of the plate we will have

$$\hat{u}_v(0) = \hat{u}_\infty + \frac{ik_1}{\gamma}\hat{v}_\infty, \quad \hat{v}_v(0) = 0, \quad \hat{w}_v(0) = \hat{w}_\infty + \frac{ik_3}{\gamma}\hat{v}_\infty, \quad \hat{\tau}_v(0) = \hat{\tau}_\infty, \quad \hat{\rho}_v(0) = -\hat{\tau}_\infty. \tag{4.19}$$

Now, using (4.9) and (4.10) we obtain the order of magnitude of the streamwise wavenumber k_1 as

$$k_1 = k_1^*\Lambda = \frac{2\pi}{L}\Lambda \sim \frac{\Lambda}{L} \sim R_\Lambda^{-3/5} \ll 1. \tag{4.20}$$

For convenience, we define

$$k_1 = R_\Lambda^{-3/5}\bar{k}_1, \quad \text{with} \quad \bar{k}_1 = \mathcal{O}(1). \tag{4.21}$$

For a single Fourier component of the disturbance, the solution in the main part of the boundary layer can be expressed as

$$\varepsilon_v\{\tilde{u}_0(\tilde{x},\eta), (2R_\Lambda^{-8/5}\tilde{x})^{1/2}\tilde{v}_0(\tilde{x},\eta), \tilde{w}_0(\tilde{x},\eta), \tilde{\tau}_0(\tilde{x},\eta)\} \times e^{i(k_3\bar{z} - R_\Lambda^{-3/5}\bar{k}_1\bar{t})} + \text{c.c.}, \tag{4.22}$$

where $k_1 x = \bar{k}_1\tilde{x}$, or $\tilde{x} = R_\Lambda^{-3/5}x$ by using (4.20), and $\tilde{x}$ is the streamwise variable. According to Goldstein et al. (1987) and Gulyaev et al. (1989), the solution can be expressed as a sum of a 'two-dimensional' part and a three-dimensional part,

namely

$$\{\tilde{u}_0, \tilde{v}_0, \tilde{\tau}_0\} = \left(\hat{u}^\infty + \frac{i\bar{k}_1}{\sqrt{\bar{k}_1^2 + \left(k_3 R_\Lambda^{3/5}\right)^2}} \hat{v}^\infty \right) \left\{ \tilde{u}^0, \tilde{v}^0, \tilde{\tau}^0 \right\} + ik_3 R_\Lambda^{3/5} \left(\hat{w}^\infty + \frac{ik_3 R_\Lambda^{3/5}}{\sqrt{\bar{k}_1^2 + \left(k_3 R_\Lambda^{3/5}\right)^2}} \hat{v}^\infty \right) \{\tilde{u}, \tilde{v}, \tilde{\tau}\}, \tag{4.23}$$

$$\tilde{w}_0 = \left(\hat{w}^\infty + \frac{ik_3 R_\Lambda^{3/5}}{\sqrt{\bar{k}_1^2 + \left(k_3 R_\Lambda^{3/5}\right)^2}} \hat{v}^\infty \right) \tilde{w}. \tag{4.24}$$

Expressions (4.23) and (4.24) are essentially the same as those in Ricco and Wu (2007), accounting for the newly introduced (4.21). The 'two-dimensional' part $\{\tilde{u}^0, \tilde{v}^0, 0, \tilde{\tau}^0\}$ is driven directly by the streamwise slip velocity. This part of the signature is smaller than the three-dimensional part by a factor $R_\Lambda^{-3/5}/k_3 \ll 1$, and therefore will not be considered any further. The three-dimensional part $\{\tilde{u}, \tilde{v}, \tilde{w}, \tilde{\tau}\}$ satisfies the LUBL equations which read (Ricco and Wu, 2007)

$$\frac{\partial \tilde{u}}{\partial \tilde{x}} + \frac{\eta_c}{2\tilde{x}} \left(\frac{T'}{T}\tilde{u} - \frac{\partial \tilde{u}}{\partial \eta} \right) - \frac{T'}{T}\tilde{v} + \frac{1}{T}\frac{\partial \tilde{v}}{\partial \eta} + \tilde{w} + \left(\frac{i\bar{k}_1}{T} - \frac{FT'}{2\tilde{x}T^2} \right) \tilde{\tau} - \frac{F'}{T}\frac{\partial \tilde{\tau}}{\partial \tilde{x}} + \frac{F}{2\tilde{x}T}\frac{\partial \tilde{\tau}}{\partial \eta} = 0 \tag{4.25}$$

$$- \left(i\bar{k}_1 + \frac{\eta_c F''}{2\tilde{x}} \right) \tilde{u} + F'\frac{\partial \tilde{u}}{\partial \tilde{x}} - \frac{1}{2\tilde{x}} \left(F + \frac{\mu' T'}{T} - \frac{\mu T'}{T^2} \right) \frac{\partial \tilde{u}}{\partial \eta} - \frac{\mu}{2\tilde{x}T}\frac{\partial^2 \tilde{u}}{\partial \eta^2} + \frac{F''}{T}\tilde{v} + \left(\frac{FF'' - \mu'' T' F'' - \mu' F'''}{2\tilde{x}T} + \frac{\mu' F'' T'}{2\tilde{x}T^2} \right) \tilde{\tau} - \frac{\mu' F''}{2\tilde{x}T}\frac{\partial \tilde{\tau}}{\partial \eta^2} = 0, \tag{4.26}$$

$$- i\bar{k}_1 \tilde{w} + F'\frac{\partial \tilde{w}}{\partial \tilde{x}} - \frac{1}{2\tilde{x}} \left(F + \frac{\mu' T'}{T} - \frac{\mu T'}{T^2} \right) \frac{\partial \tilde{w}}{\partial \eta} - \frac{\mu}{2\tilde{x}T}\frac{\partial^2 \tilde{w}}{\partial \eta^2} = 0, \tag{4.27}$$

$$- \frac{\eta_c T'}{2\tilde{x}}\tilde{u} - \frac{M^2(\gamma-1)\mu F''}{\tilde{x}T}\frac{\partial \tilde{u}}{\partial \eta} + \frac{T'}{T}\tilde{v} - \left[i\bar{k}_1 - \frac{FT'}{2\tilde{x}T} + \frac{1}{2Pr\tilde{x}} \left(\frac{\mu' T'}{T} \right)' + \frac{M^2(\gamma-1)\mu' F''^2}{2\tilde{x}T} \right] \tilde{\tau} + F'\frac{\partial \tilde{\tau}}{\partial \tilde{x}} \left(F + \frac{2\mu' T'}{PrT} - \frac{\mu T'}{PrT^2} \right) \frac{\partial \tilde{\tau}}{\partial \eta} - \frac{\mu}{2Pr\tilde{x}T}\frac{\partial^2 \tilde{\tau}}{\partial \eta^2} = 0, \tag{4.28}$$

where $T' = dT/d\eta$, but $\mu' = d\mu/dT$. The equations (4.25)-(4.28) satisfy the following boundary conditions (isothermal or adiabatic)

$$\tilde{u} = \tilde{v} = \tilde{w} = 0, \quad \tilde{\tau} = 0 \text{ or } \tilde{\tau}' = 0 \quad \text{at} \quad \eta = 0, \quad \tilde{\tau} \to 0 \quad \text{as} \quad \eta \to \infty. \tag{4.29}$$

Matching with the inviscid free-stream solution implies that

$$\tilde{u} \to 0, \quad \tilde{w} \to e^{i\bar{k}_1\tilde{x}}, \quad \tilde{\tau} \to 0 \quad \text{as} \quad \eta \to \infty. \tag{4.30}$$

In order to solve the parabolic system (4.25)-(4.28) by a marching procedure, upstream velocity and temperature profiles must be specified. These can be derived by considering the limit $\bar{k}_1\tilde{x} \ll 1$, for which the solution expands as (Ricco and Wu, 2007)

$$\{\tilde{u}, \tilde{v}, \tilde{w}, \tilde{\tau}\} = \{\tilde{x}U_I, V_I, W_I, \tilde{x}T_I\} + i\bar{k}_1\tilde{x}\,\{\tilde{x}U_{II}, V_{II}, W_{II}, \tilde{x}T_{II}\}\,. \tag{4.31}$$

The equations for the leading-order term $\{U_I, V_I, W_I, T_I\}$ in (4.31) are (Ricco and Wu, 2007)

$$\left(\frac{\eta_c T'}{2T} + 1\right) U_I - \frac{\eta_c}{2}U_I' - \frac{T'}{T^2}V_I + \frac{1}{T}V_I' + W_I - \left(\frac{F'}{T} + \frac{FT'}{2T^2}\right) T_I + \frac{F}{2T}T_I' = 0, \tag{4.32}$$

$$\begin{aligned} &\left(F' - \frac{\eta_c F''}{2}\right) U_I - \frac{1}{2}\left(F + \frac{\mu' T'}{T} - \frac{\mu T'}{T^2}\right) U_I' - \frac{\mu}{2T}U_I'' + \frac{F''}{T}V_I \\ &+ \left(\frac{FF'' - \mu'' T' F'' - \mu' F'''}{2T} + \frac{\mu' F'' T'}{2T^2}\right) T_I - \frac{\mu' F''}{2T}T_I' = 0, \end{aligned} \tag{4.33}$$

$$\left(F + \frac{\mu' T'}{T} - \frac{\mu T'}{T^2}\right) W_I' + \frac{\mu}{T}W_I'' = 0, \tag{4.34}$$

$$\begin{aligned} &-\frac{\eta_c T'}{2}U_I - \frac{M^2(\gamma-1)\mu F''}{T}U_I' + \frac{T'}{T}V_I + \left(\frac{FT'}{2T} - \frac{\mu'' T'^2 + \mu' T''}{2PrT} + \frac{\mu' T'^2}{2PrT^2}\right. \\ &\left. - \frac{M^2(\gamma-1)\mu' F''^2}{2T} + F'\right) T_I - \frac{1}{2}\left(F + \frac{2\mu' T'}{PrT} - \frac{\mu T'}{PrT^2}\right) T_I' - \frac{\mu}{2PrT}T_I'' = 0. \end{aligned} \tag{4.35}$$

The equations for the second-order term $\{U_{II}, V_{II}, W_{II}, T_{II}\}$ in (4.31) are (Ricco and Wu, 2007)

$$\begin{aligned} &\left(\frac{\eta_c T'}{2T} + 2\right) U_{II} - \frac{\eta_c}{2}U_{II}' - \frac{T'}{T^2}V_{II} + \frac{1}{T}V_{II}' + W_{II} - \left(\frac{2F'}{T} + \frac{FT'}{2T^2}\right) T_{II} \\ &+ \frac{F}{2T}T_{II}' = -\frac{T_I}{T}, \end{aligned} \tag{4.36}$$

$$\begin{aligned} &\left(2F' - \frac{\eta_c F''}{2}\right) U_{II} - \frac{1}{2}\left(F + \frac{\mu' T'}{T} - \frac{\mu T'}{T^2}\right) U_{II}' - \frac{\mu}{2T}U_{II}'' + \frac{F''}{T}V_{II} \\ &+ \left(\frac{FF'' - \mu'' T' F'' - \mu' F'''}{2T} + \frac{\mu' F'' T'}{2T^2}\right) T_{II} - \frac{\mu' F''}{2T}T_{II}' = U_I, \end{aligned} \tag{4.37}$$

$$F'W_{II} - \frac{1}{2}\left(F + \frac{\mu' T'}{T} - \frac{\mu T'}{T^2}\right) W'_{II} - \frac{\mu}{2T} W''_{II} = W_I, \tag{4.38}$$

$$\begin{aligned} &- \frac{\eta_c T'}{2} U_{II} - \frac{M^2(\gamma-1)\mu F''}{T} U'_{II} + \frac{T'}{T} V_{II} + \left(\frac{FT'}{2T} - \frac{\mu'' T'^2 + \mu' T''}{2PrT}\right. \\ &\left. + \frac{\mu' T'^2}{2PrT^2} - \frac{M^2(\gamma-1)\mu' F''^2}{2T} + 2F'\right) T_{II} - \frac{1}{2}\left(F + \frac{2\mu' T'}{PrT} - \frac{\mu T'}{PrT^2}\right) T'_{II} \\ &- \frac{\mu}{2PrT} T''_{II} = T_I. \end{aligned} \tag{4.39}$$

4.2.5 Upper deck

The transverse extent of the upper deck is $\mathcal{O}(R_L^{-3/8} L)$ and thus a wall-normal variable $\bar{y} = R_L^{-1/8} C^{-3/8} \tau_w^{-3/2} y$ is introduced. The mean flow is $(U, V, W, P, R, T) = (1, 0, 0, \frac{1}{\gamma M^2}, 1, 1)$, and the expansion for the perturbation takes the form

$$\tilde{\mathbf{u}} = \varepsilon_s \mathbf{u_s} + \varepsilon_v \mathbf{u_v} + \varepsilon_s \varepsilon_v \bar{\varepsilon}^{-1} R_L^{3/8} (\mathbf{u}_{TS} E_{TS} + \text{c.c.}) + \varepsilon_s \varepsilon_v R_L^{3/8} \mathbf{u_2} + \cdots, \tag{4.40}$$

$$\tilde{p} = \varepsilon_s p_s + \varepsilon_v^2 p_v + \varepsilon_s \varepsilon_v \bar{\varepsilon}^{-1} R_L^{3/8} (p_{TS} E_{TS} + \text{c.c.}) + \varepsilon_s \varepsilon_v R_L^{3/8} p_2 + \cdots, \tag{4.41}$$

$$\tilde{\rho} = \varepsilon_s \rho_s + \varepsilon_v \rho_v + \varepsilon_s \varepsilon_v \bar{\varepsilon}^{-1} R_L^{3/8} (\rho_{TS} E_{TS} + \text{c.c.}) + \varepsilon_s \varepsilon_v R_L^{3/8} \rho_2 + \cdots, \tag{4.42}$$

$$\tilde{\tau} = \varepsilon_s \tau_s + \varepsilon_v \tau_v + \varepsilon_s \varepsilon_v \bar{\varepsilon}^{-1} R_L^{3/8} (\tau_{TS} E_{TS} + \text{c.c.}) + \varepsilon_s \varepsilon_v R_L^{3/8} \tau_2 + \cdots, \tag{4.43}$$

where

$$E_{TS} = \exp\left\{ i(\hat{\alpha}_{TS} \bar{x} + \hat{\beta}_{TS} \bar{z} - \hat{\omega}_{TS} \bar{t}) \right\}.$$

The $\mathcal{O}(\varepsilon_s)$ terms represent the impinging and reflected sound waves and the $\mathcal{O}(\varepsilon_v)$ terms stand for the vortical wave. The $\mathcal{O}(\varepsilon_s \varepsilon_v R_L^{3/8})$ terms represent the upper-deck signature of the perturbation forced by the sound-vortical interaction in the lower and main decks; these terms are greater than $\mathcal{O}(\varepsilon_s \varepsilon_v)$ terms which would be generated by the sound-vortical interaction in the upper deck. Due to the resonant nature of the forcing, the T-S mode excited has a magnitude larger by a factor $\bar{\varepsilon}^{-1} = \mathcal{O}(R_L^{3/16})$.

Leading order and T-S wave

Substitution of (4.40) – (4.43) along with the base flow and (4.12) into the equations for the perturbation yields, at $\mathcal{O}(\varepsilon_s)$ and $\mathcal{O}(\varepsilon_s \varepsilon_v \bar{\varepsilon}^{-1} R_L^{3/8})$, the linearized equations for the acoustic signature (2.35)-(2.36) and the T-S wave (2.43), respectively.

Response in the upper deck

The interaction in the upper deck is too weak to compete with those in the main and lower decks, therefore the solution remains the same as in Chapter 2. At $\mathcal{O}(\varepsilon_s\varepsilon_v R_L^{3/8})$, the equations are

$$\frac{\partial \rho_2}{\partial \bar{x}} + \nabla \cdot \mathbf{u_2} = -\left(\frac{\partial \rho_{TS}}{\partial x_1} + \frac{\partial u_{TS}}{\partial x_1}\right) E_{TS}, \tag{4.44}$$

$$\frac{\partial \mathbf{u_2}}{\partial \bar{x}} = -\nabla p_2 + \left(\frac{\partial \mathbf{u}_{TS}}{\partial x_1} - \frac{\partial p_{TS}}{\partial x_1}\mathbf{i}\right) E_{TS}, \tag{4.45}$$

$$\frac{\partial \tau_2}{\partial \bar{x}} = -\frac{\partial \tau_{TS}}{\partial x_1} E_{TS} + (\gamma-1)M^2 \frac{\partial p_2}{\partial \bar{x}} + (\gamma-1)M^2 \frac{\partial p_{TS}}{\partial x_1} E_{TS}, \tag{4.46}$$

$$\gamma M^2 p_2 = \tau_2 + \rho_2. \tag{4.47}$$

Elimination of $\mathbf{u}_2$, τ_2 and ρ_2 among (4.44) − (4.47), gives the equation for the pressure p_2,

$$M^2 \frac{\partial^2 p_2}{\partial \bar{x}^2} - \nabla^2 p_2 = 2i(1-M^2)\hat{\alpha}_{TS} A'(x_1) \hat{p}_{TS} e^{-\hat{\gamma}_{TS}\bar{y}} E_{TS}. \tag{4.48}$$

The solution for p_2 takes the form $p_2 = (\hat{P}_2(\bar{y})E_{TS} + \text{c.c.})$, where

$$\hat{P}_2 = \left\{\hat{p}_2 + \frac{i\hat{\alpha}_{TS}}{\hat{\gamma}_{TS}}(1-M^2)A'\bar{y}\right\} e^{-\hat{\gamma}_{TS}\bar{y}}. \tag{4.49}$$

with $\hat{p}_2$ being an arbitrary function of x_1. The vertical velocity v_2 can readily be obtained from the vertical momentum equation in (4.45) after substituting p_2, but it suffices to note that as $\bar{y} \to 0$,

$$p_2 \to \hat{p}_2 E_{TS}, \tag{4.50}$$

$$v_2 \to \left(-\frac{(1-M^2)}{\hat{\gamma}_{TS}} A' \hat{p}_{TS} + \frac{\hat{\gamma}_{TS}}{i\hat{\alpha}_{TS}} \hat{p}_2 + \frac{\hat{\gamma}_{TS}}{\hat{\alpha}_{TS}^2} A' \hat{p}_{TS}\right) E_{TS}. \tag{4.51}$$

4.2.6 Main deck

The transverse variable is now $\tilde{y} = C^{-1/2}\tau_w^{-1} y = \mathcal{O}(1)$ and the expansion for the perturbation takes the form

$$\tilde{u} = C^{1/8}\tau_w^{1/2}\left[\varepsilon_s R_L^{1/8}\hat{u}_s E_s + \varepsilon_s\varepsilon_v\bar{\varepsilon}^{-1} R_L^{4/8}\tilde{u}_{TS} + \varepsilon_s\varepsilon_v R_L^{4/8}\hat{u}_2 E_{TS} + \cdots\right], \tag{4.52}$$

$$\tilde{v} = C^{1/4}\left[\varepsilon_s \hat{v}_s E_s + \varepsilon_s\varepsilon_v\bar{\varepsilon}^{-1} R_L^{3/8}\tilde{v}_{TS} + \varepsilon_s\varepsilon_v R_L^{3/8}\hat{v}_2 E_{TS} + \cdots\right], \tag{4.53}$$

$$\tilde{w} = C^{1/4}\tau_w\left[\varepsilon_s \hat{w}_s E_s + \varepsilon_s\varepsilon_v\bar{\varepsilon}^{-1} R_L^{3/8}\tilde{w}_{TS} + \varepsilon_s\varepsilon_v R_L^{3/8}\hat{w}_2 E_{TS} + \cdots\right], \tag{4.54}$$

$$\tilde{p} = C^{1/4}\left[\varepsilon_s \hat{p}_s E_s + \varepsilon_s\varepsilon_v\bar{\varepsilon}^{-1} R_L^{3/8}\tilde{p}_{TS} + \varepsilon_s\varepsilon_v R_L^{3/8}\hat{p}_2 E_{TS} + \cdots\right], \tag{4.55}$$

$$\tilde{\rho} = C^{1/8}\tau_w^{1/2}\left[\varepsilon_s R_L^{1/8}\hat{R}_s E_s + \varepsilon_s\varepsilon_v\bar{\varepsilon}^{-1} R_L^{4/8}\tilde{R}_{TS} + \varepsilon_s\varepsilon_v R_L^{4/8}\hat{R}_2 E_{TS} + \cdots\right], \tag{4.56}$$

$$\tilde{\tau} = C^{1/8}\tau_w^{1/2}\left[\varepsilon_s R_L^{1/8}\hat{\tau}_s E_s + \varepsilon_s\varepsilon_v\bar{\varepsilon}^{-1} R_L^{4/8}\tilde{\tau}_{TS} + \varepsilon_s\varepsilon_v R_L^{4/8}\hat{\tau}_2 E_{TS} + \cdots\right]. \tag{4.57}$$

Leading order - acoustic wave

Inserting $(4.52)-(4.57)$ into the disturbance equations, we obtain at leading order $\mathcal{O}(\varepsilon_s R_L^{1/8})$ the equations (2.59) (chapter 2).

Leading order - vortical wave

The expansion for the perturbation takes the form

$$\tilde{u} = \varepsilon_v R_L^{3/8}\hat{u}_v E_v, \tag{4.58}$$

$$\tilde{v} = \varepsilon_v R_L^{-1/8}\hat{v}_v E_v, \tag{4.59}$$

$$\tilde{w} = \varepsilon_v \hat{w}_v E_v, \tag{4.60}$$

$$\tilde{\rho} = \varepsilon_v R_L^{3/8}\hat{R}_v E_v, \tag{4.61}$$

$$\tilde{\tau} = \varepsilon_v R_L^{3/8}\hat{\tau}_v E_v. \tag{4.62}$$

where

$$E_v = e^{i(k_3 z - R_\Lambda^{-3/5}\bar{k}_1 t)}. \tag{4.63}$$

The relation between $(\tilde{u}_v, \tilde{v}_v, \tilde{w}_v, \tilde{\rho}_v, \tilde{\tau}_v)$ in (4.22)-(4.24) and $(\hat{u}_v, \hat{v}_v, \hat{w}_v, \hat{\rho}_v, \hat{\tau}_v)$ in (4.58)-(4.62) is given by

$$\begin{aligned}
&\varepsilon_v i k_3 R_\Lambda^{3/5}\left(\hat{w}^\infty + \frac{i k_3 R_\Lambda^{3/5}}{\sqrt{\bar{k}_1^2 + \left(k_3 R_\Lambda^{3/5}\right)^2}}\hat{v}^\infty\right)\Big\{\tilde{u}_v(\tilde{x}_n,\eta), (2R_\Lambda^{-8/5}\tilde{x}_n)^{1/2}\tilde{v}_v(\tilde{x}_n,\eta),\\
&\tilde{w}_v(\tilde{x}_n,\eta)/(i k_3 R_\Lambda^{3/5}), \tilde{\rho}_v(\tilde{x}_n,\eta), \tilde{\tau}_v(\tilde{x}_n,\eta)\Big\} e^{i(\bar{k}_1\tilde{x}_n + k_3 z - R_\Lambda^{-3/5}\bar{k}_1 t)}\\
&= \varepsilon_v\left\{R_L^{3/8}\hat{u}_v, R_L^{-1/8}\hat{v}_v, \hat{w}_v, R_L^{3/8}\hat{\rho}_v, R_L^{3/8}\hat{\tau}_v\right\} E_v,
\end{aligned} \tag{4.64}$$

where the relation between R_L and R_Λ is given by (4.10) and the solution has been calculated at the neutral position $\tilde{x}_n$. Only $\hat{u}_v(\tilde{x}_n,\eta)$ and $\hat{\tau}_v(\tilde{x}_n,\eta)$ will be needed

$$\{\hat{u}_v,\hat{\tau}_v\}=C^{9/40}\tau_w^{9/10}(k_3/\hat{\beta}_v)^{3/5}ik_3\left(\hat{w}^\infty+\frac{ik_3R_\Lambda^{3/5}}{\sqrt{\bar{k}_1^2+\left(k_3R_\Lambda^{3/5}\right)^2}}\hat{v}^\infty\right)e^{i\bar{k}_1\tilde{x}_n}\left\{\tilde{u}_v,\tilde{\tau}_v\right\}(\tilde{x}_n,\eta). \tag{4.65}$$

T-S wave

The streamwise and normal velocities of the T-S wave are given by (2.62) in chapter 2.

Response in the main deck

At $\mathcal{O}(\varepsilon_s\varepsilon_v R_L^{4/8})$, the equations read

$$\left.\begin{aligned}
&i\hat{\alpha}_{TS}U\hat{R}_2+i\hat{\alpha}_{TS}R\hat{u}_2+R'\hat{v}_2+R\tfrac{\partial\hat{v}_2}{\partial\tilde{y}}=N_c,\\
&i\hat{\alpha}_{TS}U\hat{u}_2+U'\hat{v}_2=N_1,\\
&i\hat{\alpha}_{TS}RU\hat{w}_2=-i\hat{\beta}_{TS}\tau_w\hat{p}_2+N_3,\\
&\hat{p}_{2,\tilde{y}}=0,\\
&i\hat{\alpha}_{TS}U\hat{\tau}_2+T'\hat{v}_2=N_\tau,\\
&T\hat{R}_2+R\hat{\tau}_2=-N_s,
\end{aligned}\right\} \tag{4.66}$$

where the nonlinear term N_c of equations (4.66) is

$$N_c=-i\hat{\alpha}_s(\hat{\rho}_s\hat{u}_v+\hat{\rho}_v\hat{u}_s)-(\hat{\rho}_v\hat{v}_s)_{\tilde{y}}=-(i\hat{\alpha}_s\hat{\rho}_s\hat{u}_v+\hat{\rho}_{v,\tilde{y}}\hat{v}_s)-\hat{\rho}_v(i\hat{\alpha}_s\hat{u}_s+\hat{v}_{s,\tilde{y}}), \tag{4.67}$$

and the last term is the continuity equation and therefore 0, so

$$N_c=-(i\hat{\alpha}_s\hat{\rho}_s\hat{u}_v+\hat{\rho}_{v,\tilde{y}}\hat{v}_s). \tag{4.68}$$

Note that the streak signature takes its local value at the neutral point, which implies that $\hat{\alpha}_{TS}=\hat{\alpha}_s$, and so $\partial_x=i\hat{\alpha}_s$. The term N_1 is

$$N_1=-i\hat{\alpha}_s\hat{u}_s\hat{u}_v-\hat{v}_s\hat{u}_{v,\tilde{y}}, \tag{4.69}$$

and, by using the sound wave solution at leading order (2.60), we obtain

$$N_1 = -i\hat{\alpha}_s \hat{A}_s (U'\hat{u}_v - U\hat{u}_{v,\tilde{y}}). \tag{4.70}$$

The spanwise momentum equation, in which the nonlinear term is $\mathcal{O}(\varepsilon_s \varepsilon_v R^{6/8})$, smaller than that in the streamwise momentum equation. The term N_3 is

$$N_3 = -i\hat{\alpha}_s \hat{w}_s \hat{u}_v + i\hat{\beta}_s \hat{\rho}_v \hat{p}_s / R^2. \tag{4.71}$$

The term N_τ is

$$N_\tau = -(i\hat{\alpha}_s \hat{u}_v \hat{\tau}_s + \hat{v}_s \hat{\tau}_{v,\tilde{y}}), \tag{4.72}$$

where $\hat{\tau}_v = -\hat{\rho}_v / R^2$. The term N_s is

$$N_s = \hat{\rho}_s \hat{\tau}_v + \hat{\rho}_v \hat{\tau}_s. \tag{4.73}$$

In summary, the (dominant) nonlinear terms in the RHS of equations (4.66) are

$$\left.\begin{aligned} N_c &= -(i\hat{\alpha}_s \hat{\rho}_s \hat{u}_v + \hat{\rho}_{v,\tilde{y}} \hat{v}_s), \\ N_1 &= -i\hat{\alpha}_s \hat{A}_s (U'\hat{u}_v - U\hat{u}_{v,\tilde{y}}), \\ N_3 &= -i\hat{\alpha}_s \hat{w}_s \hat{u}_v + i\hat{\beta}_s \hat{\rho}_v \hat{p}_s / R^2, \\ N_\tau &= -(i\hat{\alpha}_s \hat{u}_v \hat{\tau}_s + \hat{v}_s \hat{\tau}_{v,\tilde{y}}), \\ N_s &= \hat{\rho}_s \hat{\tau}_v + \hat{\rho}_v \hat{\tau}_s. \end{aligned}\right\} \tag{4.74}$$

In order to solve the equations (4.66) with (4.74) we take the energy equation, written in terms of the temperature $\hat{\tau}_2$,

$$i\hat{\alpha}_{TS} U \hat{\tau}_2 + T' \hat{v}_2 = N_\tau, \tag{4.75}$$

and the state equation

$$T\hat{R}_2 + R\hat{\tau}_2 = -N_s, \tag{4.76}$$

which we substitute back in (4.75) to give

$$i\hat{\alpha}_{TS} U(-N_s - T\hat{R}_2) + RT'\hat{v}_2 = RN_\tau, \tag{4.77}$$

which can be combined with the continuity equation in (4.66) to further give

$$i\hat{\alpha}_{TS} \hat{u}_2 + \hat{v}_{2,\tilde{y}} = TN_c + (i\alpha_{TS} U N_s + RN_\tau). \tag{4.78}$$

Elimination of $\hat{u}_2$ between (4.78) and the x-momentum equation leads to an equation for $\hat{v}_2$

$$U\hat{v}_{2,\tilde{y}} - U'\hat{v}_2 = U\left[TN_c + (i\hat{\alpha}_{TS}UN_s + RN_\tau)\right] - N_1 \equiv TF_D, \tag{4.79}$$

where F_D is defined by

$$F_D = \frac{U\left[TN_c + (i\hat{\alpha}_{TS}UN_s + RN_\tau)\right] - N_1}{T}. \tag{4.80}$$

The solution for $\hat{v}_2$ is

$$\hat{v}_2 = -i\hat{\alpha}_{TS}UB_2 + U\int_0^{\tilde{y}} \frac{TF_D}{U^2}d\tilde{y}, \tag{4.81}$$

and the corresponding solution for $\hat{u}_2$ is found from (4.78)

$$i\hat{\alpha}_{TS}\hat{u}_2 = i\hat{\alpha}_{TS}U'B_2 - U'\int_0^{\tilde{y}} \frac{TF_D}{U^2}d\tilde{y} + N_1/U. \tag{4.82}$$

In order to match (4.81)-(4.82) with the lower- and upper-deck solutions, it is necessary to consider the isothermal and adiabatic cases. For the former we have, as $\tilde{y} \to 0$,

$$(\tilde{u},\tilde{v},\tilde{w},\tilde{\rho})_v \to \varepsilon_v\left[R_L^{2/8}\hat{u}_v'(0)Y, R_L^{-3/8}\hat{v}_v''(0)Y^2/2, R_L^{-1/8}\hat{w}_v'(0)Y, R_L^{2/8}\hat{\rho}_v'(0)Y\right]E_v + \text{c.c.}, \tag{4.83}$$

so the nonlinear terms have the following order of magnitude

$$N_c = \mathcal{O}(\tilde{y}), \quad N_1 = \mathcal{O}(\tilde{y}^2), \quad N_3 = \mathcal{O}(1), \quad N_\tau = \mathcal{O}(\tilde{y}), \quad N_s = \mathcal{O}(\tilde{y}^2), \tag{4.84}$$

and

$$F_D = \mathcal{O}(\tilde{y}^2). \tag{4.85}$$

For the adiabatic case, we have

$$N_c = \mathcal{O}(\tilde{y}), \quad N_1 = \mathcal{O}(\tilde{y}^2), \quad N_3 = \mathcal{O}(1), \quad N_\tau = \mathcal{O}(\tilde{y}), \quad N_s = \mathcal{O}(1). \tag{4.86}$$

In either case, the integral in (4.81) and (4.82) is regular at $\tilde{y} = 0$. In the limit $\tilde{y} \to \infty$, all the nonlinear terms decay exponentially because $\hat{u}_v$ and $\hat{\tau}_v$ do. The outer limit ($\tilde{y} \to \infty$) of the main-deck solution is

$$\hat{v}_2 \to -i\hat{\alpha}_{TS}\hat{A}_2 + \int_0^{\infty} \frac{TF_D}{U^2}d\tilde{y}, \tag{4.87}$$

which will be used to match with the upper deck. The particular solution tends to zero as $\tilde{y} \to 0$, therefore the matching with the lower deck leads to

$$\hat{u}_2 \to \lambda_0 \hat{A}_2. \tag{4.88}$$

Noting that $\tilde{p}_{TS} = \hat{P}_{TS} E_{TS}$, and matching the upper-deck solutions (2.44) and (4.51) with the leading-order and second terms of the main-deck solution (2.65) respectively, we have,

$$\hat{\gamma}_{TS} \hat{P}_{TS} = \hat{\alpha}_{TS}^2 B_1, \tag{4.89}$$

$$\hat{\alpha}_{TS}^2 B_2 - 2i\hat{\alpha}_{TS} A'(x_1) B_1 + i\hat{\alpha}_{TS} \int_0^\infty \frac{TF_D}{U^2} d\tilde{y} = \hat{\gamma}_{TS} \hat{P}_2 - i\frac{\hat{\alpha}_{TS}}{\hat{\gamma}_{TS}} (1 - M^2) A'(x_1) \hat{P}_{TS}. \tag{4.90}$$

4.2.7 Lower deck

The wall-normal variable is $Y = R_L^{1/8} C^{-5/8} \tau_w^{-3/2} y$. The base flow is approximated as

$$U_B(Y) = R_L^{-1/8} C^{1/8} \tau_w^{1/2} (\lambda_0 + \bar{\varepsilon} \lambda_1 x_1) Y + \cdots . \tag{4.91}$$

The expansion takes the form

$$\tilde{u} = C^{1/8} \tau_w^{1/2} \left[\varepsilon_s R_L^{1/8} \hat{U}_s E_s + \varepsilon_s \varepsilon_v R_L^{4/8} (\bar{\varepsilon}^{-1} A(x_1) \hat{U}_{TS} + \hat{U}_2) E_{TS} + \cdots \right], \tag{4.92}$$

$$\tilde{v} = C^{3/8} \tau_w^{1/2} \left[\varepsilon_s R_L^{-1/8} \hat{V}_s E_s + \varepsilon_s \varepsilon_v R_L^{2/8} (\bar{\varepsilon}^{-1} A(x_1) \hat{V}_{TS} + \hat{V}_2) E_{TS} + \cdots \right], \tag{4.93}$$

$$\tilde{w} = C^{1/8} \tau_w^{1/2} \left[\varepsilon_s R_L^{1/8} \hat{W}_s E_s + \varepsilon_s \varepsilon_v R_L^{4/8} (\bar{\varepsilon}^{-1} A(x_1) \hat{W}_{TS} + \hat{W}_2) E_{TS} + \cdots \right], \tag{4.94}$$

$$\tilde{p} = C^{1/4} \left[\varepsilon_s \hat{P}_s E_s + \varepsilon_s \varepsilon_v R_L^{3/8} (\bar{\varepsilon}^{-1} A(x_1) \hat{P}_{TS} + \hat{P}_2) E_{TS} + \cdots \right], \tag{4.95}$$

The temperature and density disturbances are not considered since it is well known that in the lower deck they do not enter the continuity and momentum equations at leading order. The solution for each term in the expansion (4.92)-(4.95) is now considered.

Signature of sound wave

The equations of the acoustic signature in the lower deck are given by (2.73), in chapter 2.

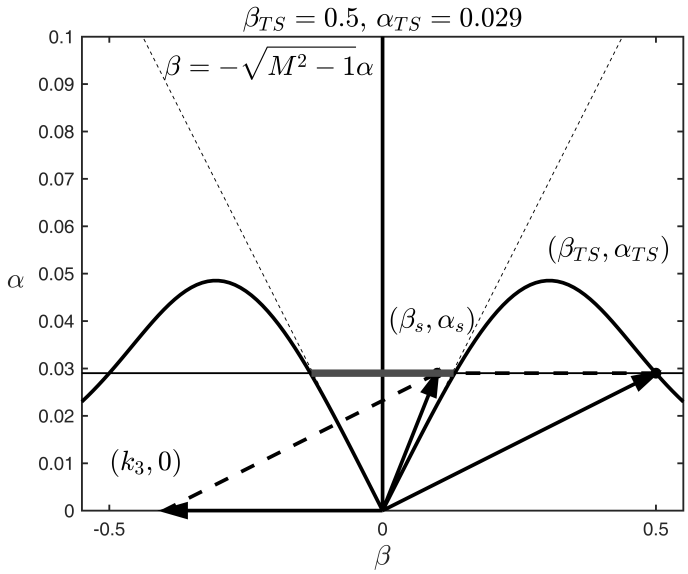


Figure 4.1: An illustration showing the selection of the acoustic and vortical waves which satisfy the resonance conditions (4.11) for a given T-S wave at $M = 4.5$. The shaded region in the centre (horizontal segment) represents the parameter space for the acoustic wave.

Signature of vortical wave

The expansion for the vortical wave takes the form

$$\tilde{u} = \varepsilon_v R_L^{2/8} \hat{U}_v E_v, \tag{4.96}$$

$$\tilde{v} = \varepsilon_v R_L^{-3/8} \hat{V}_v E_v, \tag{4.97}$$

$$\tilde{w} = \varepsilon_v R_L^{-1/8} \hat{W}_v E_v. \tag{4.98}$$

Now, in the lower deck, the signature of the streak can be simply calculated as the Taylor expansion of the solution in the main deck as follows

$$\left\{\hat{U}_v, \hat{V}_v, \hat{W}_v, \hat{\tau}_v\right\} = \left\{\hat{u}_v'(0)Y, \hat{v}_v''(0)Y^2/2, \hat{w}_v'(0)Y, \hat{\tau}_v'(0)Y\right\} E_v, \tag{4.99}$$

where

$$E_v = e^{i(k_3 z - R_\Lambda^{-3/5}\bar{k}_1 t)}. \tag{4.100}$$

T-S waves

The T-S wave satisfies the equations (2.73) (chapter 2), provided that $\hat{\alpha}_s$, $\hat{\beta}_s$ and $\hat{\omega}_s$ are replaced by $\hat{\alpha}_{TS}$, $\hat{\beta}_{TS}$ and $\hat{\omega}_{TS}$, respectively. A T-S mode can be excited by different combinations of a slow sound wave and a streak. A procedure for the

choice of the two is illustrated in figure 4.1 and described below.

1. Choice of the T-S mode to be excited ($\hat{\alpha}_{TS}$, $\hat{\beta}_{TS}$, $\hat{\omega}_{TS}$).

2. Choice of vortical wave ($\bar{k}_1$, $\hat{\beta}_v$). When $k_1 \neq 0$, the time variation would slightly affect the resonance condition (4.11). To account for this, we introduce ω_v and $\hat{\omega}_v$ via

$$\omega_v = k_1 \equiv k_1^* L = R_L^{2/8} C^{-1/4} \tau_w^{-1} \hat{\omega}_v, \tag{4.101}$$

in the same manner as $\hat{\omega}_s$ so that the resonance condition now reads

$$\hat{\omega}_s - \hat{\omega}_v = \hat{\omega}_{TS}, \tag{4.102}$$

where $\bar{k}_1$ and $\hat{\omega}_v$ are given by

$$\bar{k}_1 = R_\Lambda^{3/5} k_1^\Lambda = R_L^{2/8} C^{7/20} \tau_w^{7/5} (k_3/\hat{\beta}_v)^{8/5} \hat{\omega}_v, \quad \text{or} \quad \hat{\omega}_v = R_L^{-2/8} C^{-7/20} \tau_w^{-7/5} (k_3/\hat{\beta}_v)^{-8/5} \bar{k}_1. \tag{4.103}$$

Since $\hat{\omega}_v = \mathcal{O}(R_L^{-2/8}) \ll \mathcal{O}(1)$, the resonance condition on frequency can be approximated at leading order by

$$\omega_s \approx \omega_{TS}. \tag{4.104}$$

This approximation is acceptable only when $\hat{\omega}_v \ll \hat{\omega}_{TS}$, otherwise the exact condition (4.102) needs to be used.

3. Then the sound wave ($\hat{\alpha}_s$, $\hat{\beta}_s$, $\hat{\omega}_s$) is given by the resonance conditions. Its frequency and streamwise wavenumber are imposed by the T-S wave, but its spanwise wavenumber must satisfy $\mid \hat{\beta}_s \mid < \sqrt{M^2 - 1}\hat{\alpha}_s$, which is the shaded region in figure 4.1.

Forced response

At next order, the equations in the lower deck read

$$\left.\begin{aligned} &i\hat{\alpha}_{TS}\hat{U}_2 + \hat{V}_{2,Y} + i\hat{\beta}_{TS}\hat{W}_2 = -A'(x_1)\hat{u}_{TS} + \tau_w \hat{N}_c, \\ &i(\hat{\alpha}_{TS}\lambda_0 Y - \hat{\omega}_{TS})\hat{U}_2 + \lambda_0 \hat{V}_2 = -i\hat{\alpha}_{TS}\hat{P}_2 + \hat{U}_{2,YY} - \lambda_1 x_1 \hat{v}_{TS} \\ &\qquad\qquad -\Lambda(x_1) Y \hat{u}_{TS} - A'(x_1)\hat{p}_{TS} + \hat{N}_1, \\ &i(\hat{\alpha}_{TS}\lambda_0 Y - \hat{\omega}_{TS})\hat{W}_2 = -i\hat{\beta}_{TS}\hat{P}_2 + \hat{W}_{2,YY} - \Lambda(x_1) Y \hat{w}_{TS} + \hat{N}_3, \end{aligned}\right\} \tag{4.105}$$

where Λ is defined by

$$\Lambda(x_1) = \lambda_0 A'(x_1) + i\hat{\alpha}_{TS}\lambda_1 x_1 A, \tag{4.106}$$

and the inhomogeneous terms $\hat{N}_1$ and $\hat{N}_3$ (which differ depending on the case considered - isothermal or adiabatic) are given by

$$\left.\begin{aligned} \hat{N}_c^{iso} &= 0, \\ \hat{N}_1^{iso} &= -C^{1/8}\tau_w^{1/2}(i\hat{\alpha}_s\hat{U}_s\hat{U}_v + i\hat{\beta}_v\hat{W}_s\hat{U}_v + \hat{V}_s\hat{U}_{vY}), \\ \hat{N}_3^{iso} &= -C^{1/8}\tau_w^{1/2}i\hat{\alpha}_s\hat{W}_s\hat{U}_v, \end{aligned}\right\} \tag{4.107}$$

$$\left.\begin{aligned} \hat{N}_c^{adi} &= -(i\hat{\alpha}_s\hat{\rho}_v(0)\hat{U}_s(Y) + \hat{\rho}_v(0)\hat{V}_{s,Y} + i\hat{\beta}_{TS}\hat{\rho}_v(0)\hat{W}_s) = -i\hat{\beta}_v\hat{\rho}_v(0)\hat{W}_s, \\ \hat{N}_1^{adi} &= -i\hat{\alpha}_s\hat{\tau}_v(0)\hat{p}_s - C^{1/8}\tau_w^{1/2}(i\hat{\alpha}_s\hat{U}_s\hat{U}_v + i\hat{\beta}_v\hat{W}_s\hat{U}_v + \hat{V}_s\hat{U}_{vY}), \\ \hat{N}_3^{adi} &= -i\hat{\beta}_s\hat{\tau}_v(0)\hat{p}_s - C^{1/8}\tau_w^{1/2}i\hat{\alpha}_s\hat{W}_s\hat{U}_v. \end{aligned}\right\} \tag{4.108}$$

The nonlinear term in the continuity equation for the isothermal case is $\mathcal{O}(\varepsilon_s\varepsilon_v R_L^{6/8})$ much smaller than $\mathcal{O}(\varepsilon_s\varepsilon_v R_L^{7/8})$ as required to balance the linear term. Note that $\hat{N}_c \to 0$ as $Y \to \infty$, and $\hat{N}_c = 0$ at $Y = 0$. For the particular case of a two-dimensional sound wave, $\hat{N}_c \equiv 0$.

After rearranging (4.105) as we did before with (2.73), an inhomogeneous Airy equation for $\hat{V}_{2,YY}$ can be obtained,

$$\left\{\frac{\partial^2}{\partial Y^2} - i(\hat{\alpha}_{TS}\lambda_0 Y - \hat{\omega}_{TS})\right\}\hat{V}_{2,YY} = \Lambda Y\hat{V}_{TS,YY} + i(\hat{\alpha}_{TS}\hat{N}_1 + \hat{\beta}_{TS}\hat{N}_3)_Y \\ - \tau_w(i(\hat{\alpha}_{TS}\lambda_0 Y - \hat{\omega}_{TS})\hat{N}_c - \hat{N}_{c,YY})_Y, \tag{4.109}$$

where the extra terms in $\hat{N}_1^{adi}$ and $\hat{N}_3^{adi}$ disappear (the acoustic pressure is a constant therefore its derivative is zero) in $i(\hat{\alpha}_{TS}\hat{N}_1 + \hat{\beta}_{TS}\hat{N}_3)_Y$ and the vortical-wave (4.99) and sound-wave (2.85)-(2.87) solutions in the lower deck have been substituted in (4.108),

$$i(\hat{\alpha}_{TS}\hat{N}_1 + \hat{\beta}_{TS}\hat{N}_3)_Y = C^{1/8}\tau_w^{1/2}\left[2\hat{\alpha}_s\hat{\beta}_v\hat{u}_v'(0)(\hat{W}_s + Y\hat{W}_{s,Y}) + i\hat{\alpha}_s\hat{u}_v'(0)Y\hat{V}_{s,YY}\right], \tag{4.110}$$

where the resonance conditions for the sum mode have been used. By substituting $\hat{W}_s$, $\hat{W}_{s,Y}$ and $\hat{V}_{s,YY}$ (2.85)-(2.86) into (4.110), we obtain

$$i(\hat{\alpha}_{TS}\hat{N}_1 + \hat{\beta}_{TS}\hat{N}_3)_Y = C^{1/8}\tau_w^{1/2}\hat{\alpha}_s\hat{u}_v'(0)\left[2\hat{\beta}_v A(d_0 Ai(\eta) - Gi(\eta)\right. \\ \left. + (\tilde{\eta} - \tilde{\eta}_0)(d_0 Ai'(\eta) - Gi'(\eta))) + iq_s(\tilde{\eta} - \tilde{\eta}_0)Ai(\eta), \right. \tag{4.111}$$

where A is a constant given by (2.86). Note that as $Y \to \infty$, $\hat{W}_s = \mathcal{O}(Y^{-1} + Y^{-4})$ and by substituting in (4.108) and (4.110), it leads to $\hat{N}_{c,Y} = \mathcal{O}(Y^{-2})$, $\hat{N}_{c,Y} = \mathcal{O}(Y^{-2})$, $(Y\hat{N}_c)_Y = \mathcal{O}(Y^{-4})$ and $(\hat{\alpha}_{TS}\hat{N}_1 + \hat{\beta}_{TS}\hat{N}_3)_Y = \mathcal{O}(Y^{-4})$. The total forcing in (4.109) decays like Y^{-2}.

The term arising from $\hat{N}_c^{adi}$ can be further simplified

$$\begin{aligned}
&-\tau_w \left[i(\hat{\alpha}_{TS}\lambda_0 Y - \hat{\omega}_{TS})\hat{N}_c - \hat{N}_{c,YY} \right]_Y = -\tau_w \left[i\hat{\alpha}_{TS}\lambda_0 \hat{N}_c + i(\hat{\alpha}_{TS}\lambda_0 Y - \hat{\omega}_{TS})\hat{N}_{c,Y} - \hat{N}_{c,YYY} \right] \\
&= -\tau_w \left[\hat{\alpha}_{TS}\lambda_0 \hat{\beta}_v \hat{\rho}_v(0)\hat{W}_s + \hat{\beta}_v\hat{\rho}_v(0)(\hat{\alpha}_{TS}\lambda_0 Y - \hat{\omega}_{TS})\hat{W}_{s,Y} + i\hat{\beta}_v\hat{\rho}_v(0)\hat{W}_{s,YYY} \right] \\
&= i\tau_w \hat{\beta}_v \hat{\rho}_v(0) \left[i\hat{\alpha}_{TS}\lambda_0 \hat{W}_s + (i\hat{\alpha}_{TS}\lambda_0)^{2/3}\tilde{\eta}\hat{W}_{s,Y} - \hat{W}_{s,YYY} \right].
\end{aligned} \tag{4.112}$$

Now, the expressions for $\hat{W}_s$ and its derivatives are given by

$$\hat{W}_s = A(d_0 Ai(\eta) - Gi(\eta)), \quad \text{where} \quad A = \frac{i\hat{\beta}_s \pi \hat{P}_1}{(i\hat{\alpha}_s\lambda_0)^{2/3}}, \tag{4.113}$$

$$\hat{W}_{s,Y} = (i\hat{\alpha}_s\lambda_0)^{1/3} A(d_0 Ai'(\eta) - Gi'(\eta)), \tag{4.114}$$

$$\hat{W}_{s,YYY} = (i\hat{\alpha}_s\lambda_0) A(d_0 Ai(\eta) - Gi(\eta)) + \eta(d_0 Ai'(\eta) - Gi'(\eta)), \tag{4.115}$$

Therefore, by substituting (4.113)-(4.115) into $-\tau_w \left[i(\hat{\alpha}_{TS}\lambda_0 Y - \hat{\omega}_{TS})\hat{N}_c - \hat{N}_{c,YY} \right]_Y$,

$$\begin{aligned}
&i\tau_w \hat{\beta}_v \hat{\rho}_v(0)(i\hat{\alpha}_{TS}\lambda_0) A \left[(d_0 Ai(\eta) - Gi(\eta)) + \tilde{\eta}(d_0 Ai'(\eta) - Gi'(\eta)) \right. \\
&\left. -(d_0 Ai(\eta) - Gi(\eta)) - \eta(d_0 Ai'(\eta) - Gi'(\eta)) \right] \\
&= i\tau_w \hat{\beta}_v \hat{\rho}_v(0)(i\hat{\alpha}_{TS}\lambda_0) A \left[\tilde{\eta}(d_0 Ai'(\eta) - Gi'(\eta)) - \eta(d_0 Ai'(\eta) - Gi'(\eta)) \right].
\end{aligned} \tag{4.116}$$

For the particular case in which $\tilde{\eta} = \eta$ (same variable for sound and T-S waves, or in other words, approximate resonance condition on frequency or steady streak), this term is 0. The forcing in (4.109) can be expressed as a combination of Ai, Gi, their derivatives and ηAi, ηAi$'$, ηGi$'$. It is useful to note the set of relations

$$\begin{aligned}
&\mathcal{L}Ai = 0, \qquad \mathcal{L}Ai' = Ai, \quad \mathcal{L}Ai'' = 2Ai', \quad \cdots, \quad \mathcal{L}Ai^{(n)} = nAi^{(n-1)}; \\
&\mathcal{L}Gi = 1/\pi, \quad \mathcal{L}Gi' = Gi, \quad \mathcal{L}Gi'' = 2Gi', \quad \cdots, \quad \mathcal{L}Gi^{(n)} = nGi^{(n-1)},
\end{aligned} \tag{4.117}$$

which follow from repeatedly differentiating the first respective equations, where $\mathcal{L} = d^2/d\eta^2 - \eta$ is the Airy operator. Using (4.117), ηAi, ηAi$'$ and ηGi$'$ in the forcing term can also be expressed in terms of Ai, Gi and their derivatives. This approximation ($\tilde{\eta} = \eta$) will be used to derive 'Formulation II'. The following 'Formulation I' corresponds to the original formulation used in Hernández and Wu (2019) with the extra terms derived here for the adiabatic case.

Formulation I

The solution can be expressed as (cf. Wu, 2001a)

$$\hat{V}_{2,Y} = \frac{1}{3}(i\hat{\alpha}_{TS}\lambda_0)^{-1}\Lambda(x_1)\left\{(\tilde{\eta}-3\tilde{\eta}_0)Ai(\tilde{\eta})+2\tilde{\eta}_0 Ai(\tilde{\eta}_0)\right\} + \int_{\tilde{\eta}_0}^{\tilde{\eta}} \tilde{M}(\eta',\tilde{\eta}_0)d\eta' + q_2\int_{\tilde{\eta}_0}^{\tilde{\eta}} Ai(\eta')d\eta', \quad (4.118)$$

where q_2 is a function of x_1, and $\tilde{M}$ is given by

$$\tilde{M}(\tilde{\eta},\tilde{\eta}_0) = \pi\left\{Bi(\tilde{\eta})\int_{\infty}^{\tilde{\eta}} Ai(\eta')H(Y')d\eta' - Ai(\tilde{\eta})\int_{\tilde{\eta}_0}^{\tilde{\eta}} Bi(\eta')H(Y')d\eta'\right\}, \quad (4.119)$$

with Bi being the Airy function and $H = H_1 + H_2$ given by

$$H_1 = (\hat{\alpha}_{TS}\lambda_0)^{-1}\left[\hat{\alpha}_{TS}N_1+\hat{\beta}_{TS}N_3\right]_Y, \quad H_2 = -\tau_w(i\hat{\alpha}_{TS}\lambda_0)^{-1}\left[i(\hat{\alpha}_{TS}\lambda_0 Y-\hat{\omega}_{TS})\hat{N}_c - \hat{N}_{c,YY}\right]_Y. \quad (4.120)$$

At this order, the matching condition with the main-deck solution (2.64) reads

$$\hat{V}_{2,Y} \to -i\hat{\alpha}_{TS}\lambda_0 B_2 - (i\hat{\alpha}_{TS}\lambda_1 x_1 A + \lambda_0 A'(x_1))B_1 \quad \text{as} \quad Y\to\infty, \quad (4.121)$$

and thus

$$-i\hat{\alpha}_{TS}\lambda_0 B_2 - (i\hat{\alpha}_{TS}\lambda_1 x_1 A + \lambda_0 A'(x_1))B_1 = \frac{2}{3}(i\hat{\alpha}_{TS}\lambda_0)^{-1}\Lambda\tilde{\eta}_0 Ai(\tilde{\eta}_0) + \int_{\tilde{\eta}_0}^{\infty}\tilde{M}(\eta',\tilde{\eta}_0)d\eta' + q_2\int_{\tilde{\eta}_0}^{\infty} Ai(\eta')d\eta'. \quad (4.122)$$

The no-slip condition can be calculated from the continuity equation differentiated with respect to Y twice, combined with the x- and z-momentum equations (4.105), at $Y = 0$,

$$\hat{V}_{2,YYY} = (\hat{\alpha}_{TS}^2+\hat{\beta}_{TS}^2)\hat{P}_2 - 2i\hat{\alpha}_{TS}A'(x_1)\hat{P}_{TS} + F_B \quad \text{at} \quad Y=0, \quad (4.123)$$

leading to (using (4.118) and taking derivative with respect to Y twice)

$$\frac{2}{3}(i\hat{\alpha}_{TS}\lambda_0)^{-1/3}\Lambda\left\{Ai'(\tilde{\eta}_0)-\tilde{\eta}_0 Ai''(\tilde{\eta}_0)\right\}+(i\hat{\alpha}_{TS}\lambda_0)^{2/3}\left\{\pi Bi'(\tilde{\eta}_0)\int_{\infty}^{\tilde{\eta}_0} Ai(\eta')H(Y')d\eta'\right\} + (i\hat{\alpha}_{TS}\lambda_0)^{2/3}q_2 Ai'(\tilde{\eta}_0) = (\hat{\alpha}_{TS}^2+\hat{\beta}_{TS}^2)\hat{P}_2 - 2i\hat{\alpha}_{TS}A'(x_1)\hat{P}_{TS} + F_B, \quad (4.124)$$

where F_B is only present in the adiabatic case and is given by

$$F_B = \tau_w \hat{N}_{c,YY}(0) + (i\hat{\alpha}_{TS}\hat{N}_1(0) + i\hat{\beta}_{TS}\hat{N}_3(0)) = -i\tau_w\hat{\beta}_v\hat{\rho}_v(0)\hat{W}_{s,YY}(0) + \hat{\tau}_v(0)(\hat{\alpha}_s^2 + \hat{\beta}_{TS}\hat{\beta}_s)\hat{p}_s. \tag{4.125}$$

With B_1 and $\hat{P}_{TS}$ being determined from (2.91) and (2.92), the relations (4.122), (4.90) and (4.124) form a system of 3 equations for 4 unknowns: q_2, P_2, B_2 and $A(x_1)$. The elimination of P_2 and B_2 yields

$$aA' + b(i\hat{\alpha}_{TS}\lambda_1 x_1/\lambda_0)A + (\hat{\alpha}_{TS}^2 + \hat{\beta}_{TS}^2)^{-1}\Delta(\lambda_0)q_2 = \mathcal{F}, \tag{4.126}$$

where

$$\begin{aligned}
a =& \frac{2}{3}\tilde{\eta}_0 Ai(\tilde{\eta}_0) + \left(\frac{\hat{\beta}_{TS}^2}{\hat{\gamma}_{TS}^2} + \frac{2\hat{\alpha}_{TS}^2}{\hat{\alpha}_{TS}^2 + \hat{\beta}_{TS}^2}\right)\int_{\tilde{\eta}_0}^{\infty} Ai(\eta')d\eta' \\
&+ \frac{2}{3}\frac{\hat{\gamma}_{TS}(i\hat{\alpha}_{TS}\lambda_0)^{5/3}}{\hat{\alpha}_{TS}^2(\hat{\alpha}_{TS}^2 + \hat{\beta}_{TS}^2)}\left\{Ai'(\tilde{\eta}_0) - \tilde{\eta}_0 Ai''(\tilde{\eta}_0)\right\}, \\
b =& \frac{2}{3}\tilde{\eta}_0 Ai(\tilde{\eta}_0) - \int_{\tilde{\eta}_0}^{\infty} Ai(\eta')d\eta' + \frac{2}{3}\frac{\hat{\gamma}_{TS}(i\hat{\alpha}_{TS}\lambda_0)^{5/3}}{\hat{\alpha}_{TS}^2(\hat{\alpha}_{TS}^2 + \hat{\beta}_{TS}^2)}\left\{Ai'(\tilde{\eta}_0) - \tilde{\eta}_0 Ai''(\tilde{\eta}_0)\right\}, \\
\mathcal{F} =& \chi\int_{\infty}^{\tilde{\eta}_0} Ai(\eta')H(Y')d\eta' - i\hat{\alpha}_{TS}\int_{\tilde{\eta}_0}^{\infty}\tilde{M}(\eta',\tilde{\eta}_0)d\eta' - \frac{\lambda_0\hat{\gamma}_{TS}}{\hat{\alpha}_{TS}^2 + \hat{\beta}_{TS}^2}F_B \\
&- (i\hat{\alpha}_{TS}\lambda_0)\int_0^{\infty}\frac{TF_D}{U^2}d\tilde{y}', \\
\chi =& \pi\lambda_0\hat{\gamma}_{TS}(i\hat{\alpha}_{TS}\lambda_0)^{2/3}Bi'(\tilde{\eta}_0)/(\hat{\alpha}_{TS}^2 + \hat{\beta}_{TS}^2).
\end{aligned}$$

Since $\Delta(\lambda_0) = 0$, we arrive at the evolution equation for $A(x_1)$,

$$A'(x_1) = \sigma x_1 A + N, \tag{4.127}$$

where

$$\sigma = -i\hat{\alpha}_{TS}\lambda_1 b/(\lambda_0 a), \quad N = \mathcal{F}/a. \tag{4.128}$$

Formulation II

The solution for $\hat{V}_{2,YY}$ can be written in terms of Ai, Gi$'$ and their derivatives by using the relations tabled in (4.117), since the approximation $\tilde{\eta} = \eta$ has been made. Note that $\hat{V}_{2,YY}$ contains Gi$'$ and higher-order derivatives but no Gi itself and hence $\hat{V}_{2,Y}$ involves only single integrals. Let the last two terms of the right-hand side of (4.109) be denoted by $\tilde{H}$. It can be expressed as

$$\tilde{H} = \sum_{n=0}\left[\tilde{a}_n Ai^{(n)} + \tilde{g}_n Gi^{(n)}\right], \tag{4.129}$$

where the coefficients $\tilde{a}_n$, $\tilde{g}_n$ are given by

$$\begin{aligned}&\tilde{a}_0 = -iq_s\eta_0\tilde{f}, \quad \tilde{g}_0 = 0, \quad \tilde{a}_1 = -2\hat{\beta}_v A\eta_0 d_0\tilde{f}, \quad \tilde{g}_1 = 2\hat{\beta}_v A\eta_0\tilde{f},\\ &\tilde{a}_2 = iq_s\tilde{f}, \quad \tilde{g}_2 = 0, \quad \tilde{a}_3 = 2\hat{\beta}_v A d_0\tilde{f}, \quad \tilde{g}_3 = -2\hat{\beta}_v A\tilde{f},\end{aligned} \tag{4.130}$$

where $\tilde{f} = C^{1/8}\tau_w^{1/2}\hat{\alpha}_s\hat{u}_v'(0)$. The solution for $\hat{V}_{2,YY}$ can be written as

$$\begin{aligned}\hat{V}_{2,YY} = \frac{1}{3}(i\hat{\alpha}_{TS}\lambda_0)^{-2/3}\Lambda(x_1)\left\{Ai(\tilde{\eta}) + (\tilde{\eta} - 3\tilde{\eta}_0)Ai'(\tilde{\eta})\right\}\\ + (i\hat{\alpha}_{TS}\lambda_0)^{-2/3}S_v'(\tilde{\eta}) + (i\hat{\alpha}_{TS}\lambda_0)^{1/3}q_2 Ai(\tilde{\eta}),\end{aligned} \tag{4.131}$$

where S_v is a combination of Ai, Gi and their derivatives, namely,

$$S_v = \sum_{n=0}\frac{1}{(n+1)}\left[\tilde{a}_n Ai^{(n)} + \tilde{g}_n Gi^{(n)}\right] \tag{4.132}$$

Integrating, we obtain

$$\begin{aligned}\hat{V}_{2,Y} = \frac{1}{3}(i\hat{\alpha}_{TS}\lambda_0)^{-1}\Lambda(x_1)\left\{(\tilde{\eta} - 3\tilde{\eta}_0)Ai(\tilde{\eta}) + 2\tilde{\eta}_0 Ai(\tilde{\eta}_0)\right\}\\ + (i\hat{\alpha}_{TS}\lambda_0)^{-1}\left[S_v(\tilde{\eta}) - S_v(\tilde{\eta}_0)\right] + q_2\int_{\tilde{\eta}_0}^{\tilde{\eta}} Ai(\eta')d\eta'.\end{aligned} \tag{4.133}$$

The relation between the two formulations is then given by

$$\int_{\tilde{\eta}_0}^{\tilde{\eta}}\tilde{M}(\eta',\tilde{\eta}_0)d\eta' = (i\hat{\alpha}_{TS}\lambda_0)^{-1}\left[S_v(\tilde{\eta}) - S_v(\tilde{\eta}_0)\right]. \tag{4.134}$$

At this order, the matching condition with the main-deck solution (2.64) reads

$$\hat{V}_{2,Y} \to -i\hat{\alpha}_{TS}\lambda_0 B_2 - (i\hat{\alpha}_{TS}\lambda_1 x_1 A + \lambda_0 A'(x_1))B_1 \quad \text{as} \quad Y \to \infty, \tag{4.135}$$

and thus

$$\begin{aligned}-i\hat{\alpha}_{TS}\lambda_0 B_2 - (i\hat{\alpha}_{TS}\lambda_1 x_1 A + \lambda_0 A'(x_1))B_1 = \frac{2}{3}(i\hat{\alpha}_{TS}\lambda_0)^{-1}\Lambda\tilde{\eta}_0 Ai(\tilde{\eta}_0)\\ + (i\hat{\alpha}_{TS}\lambda_0)^{-1}\left[S_v(\infty) - S_v(\tilde{\eta}_0)\right] + q_2\int_{\tilde{\eta}_0}^{\infty} Ai(\eta')d\eta',\end{aligned} \tag{4.136}$$

where $S_v(\infty) = 0$. The no-slip condition can be calculated from the continuity equation derivated with respect to Y twice, combined with the x- and z-momentum equations (4.105), particularized at $Y = 0$,

$$\hat{V}_{2,YYY} = (\hat{\alpha}_{TS}^2 + \hat{\beta}_{TS}^2)\hat{P}_2 - 2i\hat{\alpha}_{TS}A'(x_1)\hat{P}_{TS} + F_B \quad \text{at} \quad Y = 0, \tag{4.137}$$

leading to (using (4.133) and taking derivative with respect to Y twice)

$$\frac{2}{3}(i\hat{\alpha}_{TS}\lambda_0)^{-1/3}\Lambda\left\{Ai'(\tilde{\eta}_0)-\tilde{\eta}_0 Ai''(\tilde{\eta}_0)\right\}+(i\hat{\alpha}_{TS}\lambda_0)^{-1/3}S_v{}''(\tilde{\eta}_0)$$
$$+(i\hat{\alpha}_{TS}\lambda_0)^{2/3}q_2 Ai'(\tilde{\eta}_0)=(\hat{\alpha}_{TS}^2+\hat{\beta}_{TS}^2)\hat{P}_2-2i\hat{\alpha}_{TS}A'(x_1)\hat{P}_{TS}+F_B, \quad (4.138)$$

where F_B is only present in the adiabatic case and is given by

$$F_B=\tau_w\hat{N}_{c,YY}(0)+(i\hat{\alpha}_{TS}\hat{N}_1(0)+i\hat{\beta}_{TS}\hat{N}_3(0))=-i\tau_w\hat{\beta}_v\hat{\rho}_v(0)\hat{W}_{s,YY}(0)+\hat{\tau}_v(0)(\hat{\alpha}_s^2+\hat{\beta}_{TS}\hat{\beta}_s)\hat{p}_s. \quad (4.139)$$

With B_1 and $\hat{P}_{TS}$ being determined from (2.91) and (2.92), the relations (4.136), (4.137) and (4.138) form a system of 3 equations for 4 unknowns: q_2, P_2, B_2 and $A(x_1)$. The elimination of P_2 and B_2 yields

$$aA'+b(i\hat{\alpha}_{TS}\lambda_1 x_1/\lambda_0)A+(\hat{\alpha}_{TS}^2+\hat{\beta}_{TS}^2)^{-1}\Delta(\lambda_0)q_2=\mathcal{F}, \quad (4.140)$$

where

$$\begin{aligned}
a=&\frac{2}{3}\tilde{\eta}_0 Ai(\tilde{\eta}_0)+\left(\frac{\hat{\beta}_{TS}^2}{\hat{\gamma}_{TS}^2}+\frac{2\hat{\alpha}_{TS}^2}{\hat{\alpha}_{TS}^2+\hat{\beta}_{TS}^2}\right)\int_{\tilde{\eta}_0}^{\infty}Ai(\eta')d\eta'\\
&+\frac{2}{3}\frac{\hat{\gamma}_{TS}(i\hat{\alpha}_{TS}\lambda_0)^{5/3}}{\hat{\alpha}_{TS}^2(\hat{\alpha}_{TS}^2+\hat{\beta}_{TS}^2)}\left\{Ai'(\tilde{\eta}_0)-\tilde{\eta}_0 Ai''(\tilde{\eta}_0)\right\},\\
b=&\frac{2}{3}\tilde{\eta}_0 Ai(\tilde{\eta}_0)-\int_{\tilde{\eta}_0}^{\infty}Ai(\eta')d\eta'+\frac{2}{3}\frac{\hat{\gamma}_{TS}(i\hat{\alpha}_{TS}\lambda_0)^{5/3}}{\hat{\alpha}_{TS}^2(\hat{\alpha}_{TS}^2+\hat{\beta}_{TS}^2)}\left\{Ai'(\tilde{\eta}_0)-\tilde{\eta}_0 Ai''(\tilde{\eta}_0)\right\},\\
\mathcal{F}=&\tilde{\chi}S_v''(\tilde{\eta}_0)+\lambda_0^{-1}\left[S_v(\tilde{\eta}_0)\right]-\frac{\lambda_0\hat{\gamma}_{TS}}{\hat{\alpha}_{TS}^2+\hat{\beta}_{TS}^2}F_B-(i\hat{\alpha}_{TS}\lambda_0)\int_0^{\infty}\frac{TF_D}{U^2}d\tilde{y}',\\
\tilde{\chi}=&\lambda_0\hat{\gamma}_{TS}(i\hat{\alpha}_{TS}\lambda_0)^{-1/3}/(\hat{\alpha}_{TS}^2+\hat{\beta}_{TS}^2).
\end{aligned}$$

Since $\Delta(\lambda_0)=0$, we arrive at the evolution equation for $A(x_1)$,

$$A'(x_1)=\sigma x_1 A+N, \quad (4.141)$$

where

$$\sigma=-i\hat{\alpha}_{TS}\lambda_1 b/(\lambda_0 a), \quad N=\mathcal{F}/a. \quad (4.142)$$

4.3 Receptivity: evolution from the forced response to eigenmode

4.3.1 Matching between T-S wave solution and upstream forced response

The matching between the T-S wave and the upstream forced response is carried out in the same way as section 2.3.1 in chapter 2.

4.3.2 Coupling coefficients

A convenient representation of the magnitude of the T-S wave is the maximum value of its streamwise velocity, which can be directly measured in experiments, e.g. King and Breuer (2002). Solving the spanwise momentum equation, we obtain the spanwise velocity

$$\hat{W}_{TS} = \frac{i\hat{\beta}_{TS} Ai'(\tilde{\eta}_0)}{\hat{\alpha}_{TS}^2 + \hat{\beta}_{TS}^2} L(\tilde{\eta}), \tag{4.143}$$

where $L(\tilde{\eta})$ is the solution to the equation $L'' - \tilde{\eta}L = 1$ satisfying the boundary conditions $L(\tilde{\eta}_0) = 0$ and $L(\infty) = 0$. From the continuity equation, (2.89) and (4.92), it follows that the streamwise velocity at the neutral point is given by

$$u_{TS} = \varepsilon_s \varepsilon_v \bar{\varepsilon}^{-1} R_L^{4/8} C^{1/8} \tau_w^{1/2} \hat{\alpha}_{TS}^{-1} A_\infty U_m, \tag{4.144}$$

where

$$U_m = \max_{\tilde{\eta}} \left| \int_{\tilde{\eta}_0}^{\tilde{\eta}} Ai(\eta')d\eta' - \frac{\beta_N^2}{\alpha_N^2 + \beta_N^2} Ai'(\tilde{\eta}_0) L(\tilde{\eta}) \right|. \tag{4.145}$$

The coupling coefficient for the sound-vortical interaction can be defined as

$$C_V \equiv u_{TS}/\varepsilon_s = \varepsilon_v R_L^{11/16} C^{-1/16} \tau_w^{-1/4} \hat{\alpha}_{TS}^{-1} A_\infty U_m \equiv \varepsilon_v R_L^{11/16} \Lambda_{SV}. \tag{4.146}$$

Clearly, Λ_{SV} is the rescaled coupling coefficient, and depends on the parameters such as $\hat{\omega}_s$, $\hat{c}_s$, etc. C_V is $\mathcal{O}(R_L^{3/8})$ higher than the sound-vortical interaction mechanism proposed in Wu (1999) and $\mathcal{O}(R_L^{1/8})$ higher than the slow sound-sound interaction mechanism in Chapter 2.

4.4 Parametric study and discussion

The acoustic wave and the streak velocity profiles need to be computed at the neutral position. Using MATLAB, we will now evaluate the coupling coefficient Λ_{SV} for typical values of the relevant parameters.

4.4.1 Neutral position

The velocity profiles of the sound wave and the streak need to be calculated at the neutral position, which is determined by the frequency of the T-S (Mack) mode, ω_{TS}, whose triple-deck scaling is (4.11)

$$\omega_{TS} = R_L^{2/8} C^{-1/4} \tau_w^{-1} \hat{\omega}_{TS}, \quad \hat{\omega}_{TS} = \lambda_0^{3/2} \omega_N, \tag{4.147}$$

from which we have

$$R_L = C \tau_w^4 \lambda_0^{-6} (\omega_{TS}/\hat{\omega}_N)^4. \tag{4.148}$$

In order to find the value of $\tilde{x} \equiv R_\Lambda^{-3/5} x^*/\Lambda$ at the neutral position, we need to make use of the precise relations between Λ and L (4.9), and between R_Λ and R_L (4.10). If we take $L = x^*$, the corresponding $\tilde{x}$ is given by

$$\tilde{x}_n \equiv R_\Lambda^{-3/5} x^*/\Lambda = R_\Lambda^{-3/5} L/\Lambda = C^{-3/5} \tau_w^{-12/5} (k_3/\hat{\beta}_v)^{-8/5}, \tag{4.149}$$

where we have used (4.9) and (4.10).

4.4.2 Streak signature

The present streak solution (4.23) and that in Ricco and Wu (2007) are essentially equivalent, being the rescaling of the dependent and independent variables the only difference. The scaled streamwise variable in Ricco and Wu (2007) is $\bar{x} = k_1 x$, and the scaled velocity and temperature variables are $\bar{u}$ and $\bar{\tau}$, respectively. The disadvantage of this formulation is that it becomes problematic when the disturbances are steady, $k_1 = 0$ (k_1 is in the denominator in 3.7 Ricco and Wu, 2007). In the present formulation, the streamwise variable is $\tilde{x} = R_\Lambda^{-3/5} x$ and the relation between the velocity variables in the two cases is

$$(\bar{u}, \bar{\tau}) = (k_1 R_\Lambda^{3/5})(\tilde{u}, \tilde{\tau}), \tag{4.150}$$

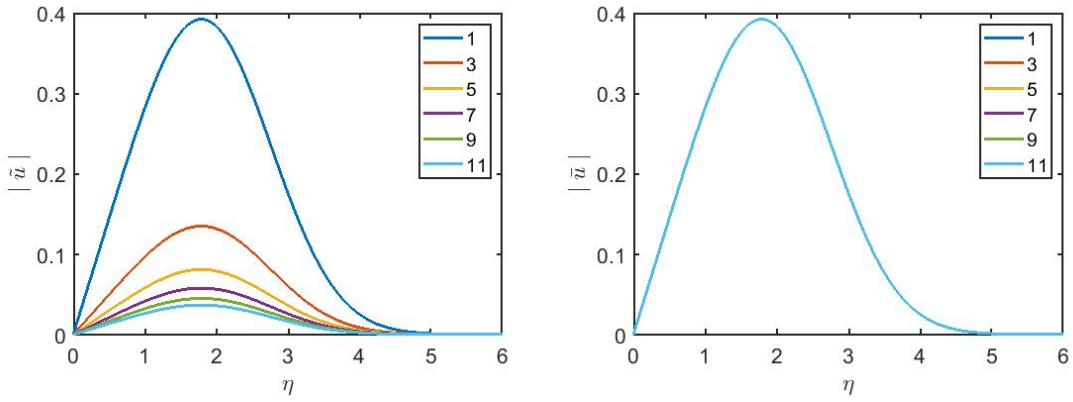


Figure 4.2: Streamwise velocity profiles of streaks (main deck) at the position ($\tilde{x} = 1$) for $M = 4.5$ and various $\bar{k}_1$. The collapse of curves is plotted on the right, each calculated at $\tilde{x} = 1/\bar{k}_1$ (this is equivalent to plotting $\bar{u}$ at $\bar{x} = 1$) for various $\bar{k}_1$.

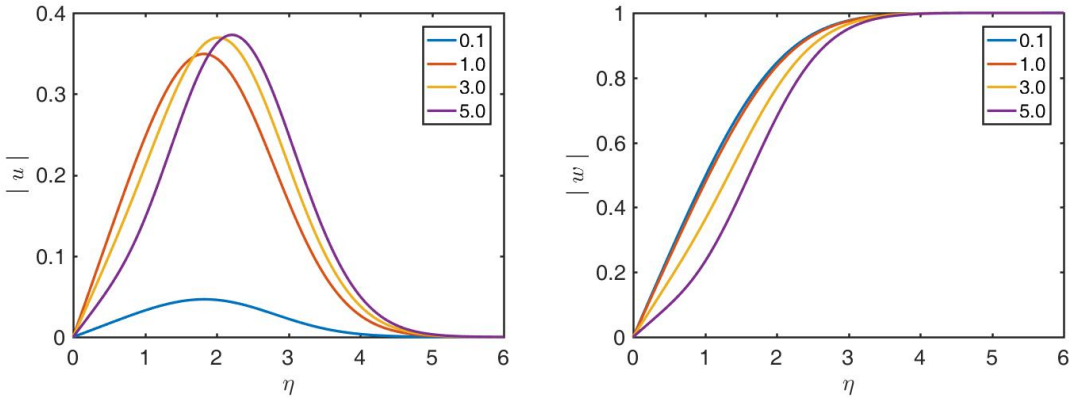


Figure 4.3: Velocity profiles of streaks $\bar{u}$ (left) and $\bar{w}$ (right) for $M = 3$, for validation against the solution of Ricco and Wu (2007), for $\bar{k}_1 = 1$. The numbers in the figure indicate the values of $\bar{x}$.

where we defined a parameter connecting the two cases $\bar{k}_1 = k_1 R_\Lambda^{3/5}$ (when $\bar{k}_1 = 1$, both versions are identical). Therefore, if for example the solution in the present formulation is obtained (tilde variables) at $\tilde{x} = 1/\bar{k}_1$ and rescaled according to (4.150), then the resulting solution should collapse onto a single curve for different $\bar{k}_1$, and this is equivalent to the solution at $\bar{x} = 1$ (bar variables) in Ricco and Wu (2007). This validation is shown in figure (4.2).

Now, the numerical method used to calculate the streak signature (appendix B) will be validated against the results obtained in Ricco and Wu (2007). Their velocity profiles at $M = 3$ for different streamwise locations $\bar{x}$ (figure 2 in Ricco and Wu, 2007) are in agreement with the present work, figure (4.3).

The streamwise velocity profiles of streaks are plotted at the neutral position for

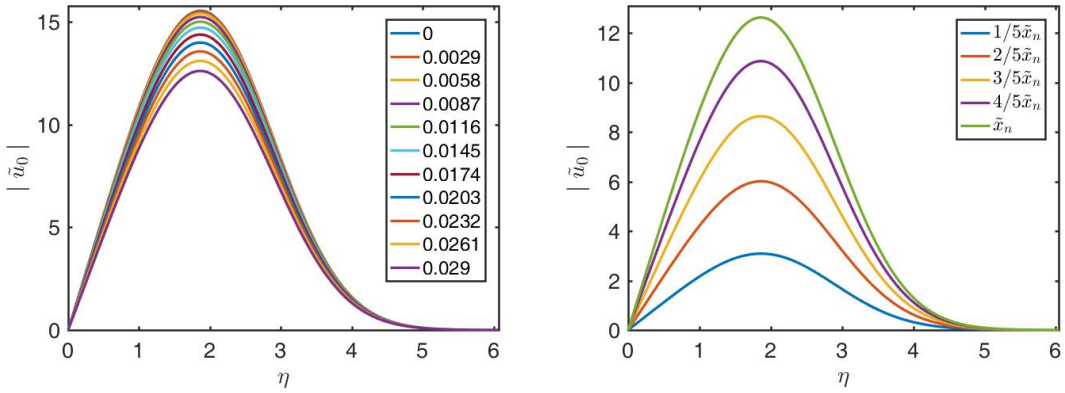


Figure 4.4: Streamwise velocity profiles of streaks ($\tilde{u}_0$) for various $\hat{\omega}_v$ (left) at the neutral position for $M = 1.2$. Profiles at various $\tilde{x}$ at $\hat{\omega}_v = \hat{\omega}_{TS}/10 = 0.029$ (right). The spanwise wavenumber has been chosen to be $\hat{\beta}_v = 0.2$.

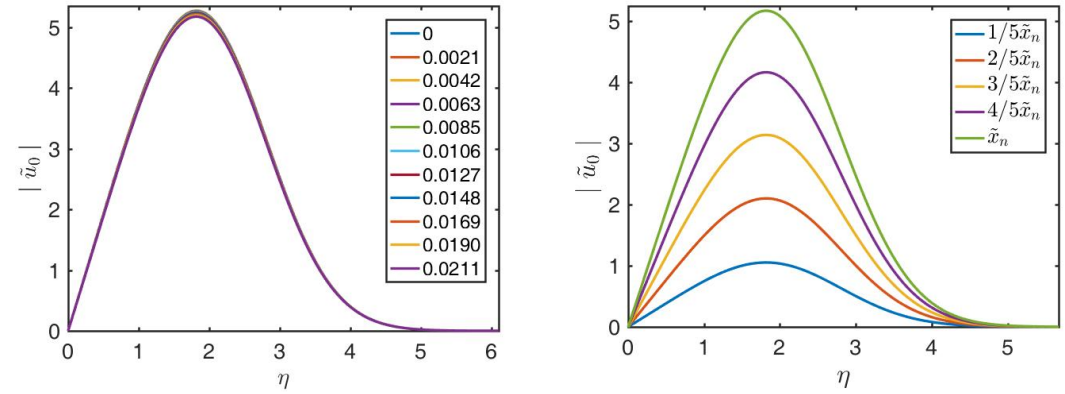


Figure 4.5: Streamwise velocity profiles of streaks ($\tilde{u}_0$) for various $\hat{\omega}_v$ (left) at the neutral position for $M = 3$. Profiles at various $\tilde{x}$ at $\hat{\omega}_v = \hat{\omega}_{TS}/10 = 0.0211$ (right). The spanwise wavenumber has been chosen to be $\hat{\beta}_v = 0.2$.

various $\hat{\omega}_v$ and $\hat{\beta}_v = 0.2$ and for different supersonic Mach numbers in figures 4.4-4.6 (on the left). We observe that the effect of increasing $\hat{\omega}_v$ is the reduction of the streamwise velocity of the streak, and this weakens at higher Mach numbers. Moreover, the streamwise velocity of streaks decreases in magnitude at higher Mach numbers. Additionally, several velocity profiles have been plotted in figures 4.4-4.6 (on the right) at various locations $\tilde{x}$ up to the neutral position for $\hat{\omega}_v = \hat{\omega}_{TS}/10$ and for different Mach numbers. It can be observed that the maximum of velocity is attained at the neutral position for all the cases considered.

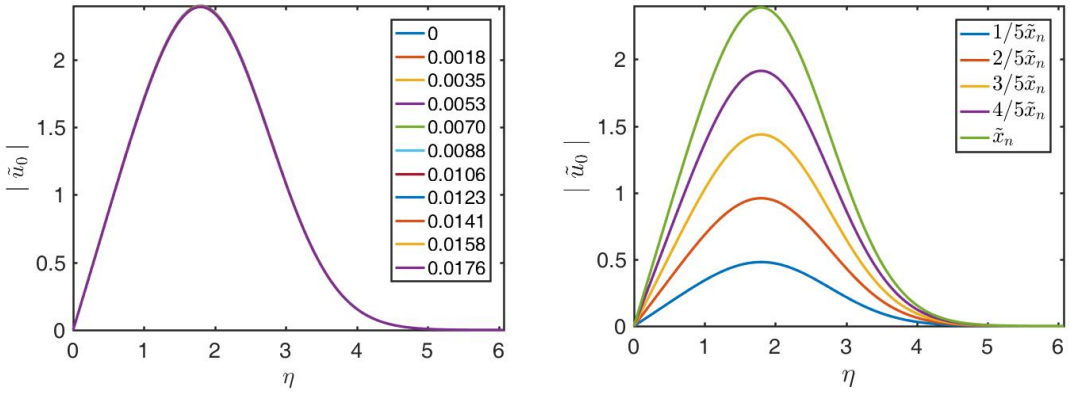


Figure 4.6: Streamwise velocity profiles of streaks ($\tilde{u}_0$) for various $\hat{\omega}_v$ (left) at the neutral position for $M = 4.5$. Profiles at various $\tilde{x}$ at $\hat{\omega}_v = \hat{\omega}_{TS}/10 = 0.0176$ (right). The spanwise wavenumber has been chosen to be $\hat{\beta}_v = 0.2$.

4.4.3 Coupling coefficient for sound-vortical interaction

The coupling coefficient is computed here for different conditions, using formulation I (which requires the evaluation of double integrals). Formulation II is simpler and does only require the evaluation of Airy functions and their derivatives, but the evaluations of formulation I only require a few seconds on a standard laptop, therefore the difference in computational time is not appreciable in practice. The sum mode has been chosen for the parametric study, the calculations for the difference mode are similar.

Figure 4.7 shows contour plots of the coupling coefficient Λ_{SV} as a function of $\hat{\omega}_v$ and $\hat{\beta}_v$ for $M = 1.2$, $M = 3$, $M = 4.5$ and $M = 6$. In the first case, the peak is achieved for an almost-steady streak (whose frequency is about $\hat{\omega}_v \approx \hat{\omega}_{TS}/70$). In the $M = 3$, $M = 4.5$ and $M = 6$ cases, the streak's frequency does not appear to largely vary the coupling coefficient for a given $\hat{\beta}_v$. The coupling coefficient appears to be the largest for large values of $\hat{\beta}_v$.

In figure 4.8, the coupling coefficient has been plotted against $\hat{\beta}_v$ for the steady streak case and various Mach numbers. It is interesting to observe that the minima are attained for two-dimensional sound waves ($\hat{\beta}_v = \hat{\beta}_{TS}$) in the $M = 3$, $M = 4.5$ and $M = 6$ cases. This is in agreement with the conclusions in chapter 2, where oblique ($\hat{\beta}_v \neq 0$) acoustic waves result in the highest receptivity. The coupling coefficient is found to be around $\mathcal{O}(1)$.

Figure 4.9 shows the coupling coefficient against $\hat{\omega}_v \in [0, \hat{\omega}_{TS}/10]$ for a streak with $\hat{\beta}_v = \hat{\beta}_{TS}$ and for a two-dimensional acoustic wave ($\hat{\beta}_s = 0$). The magnitude

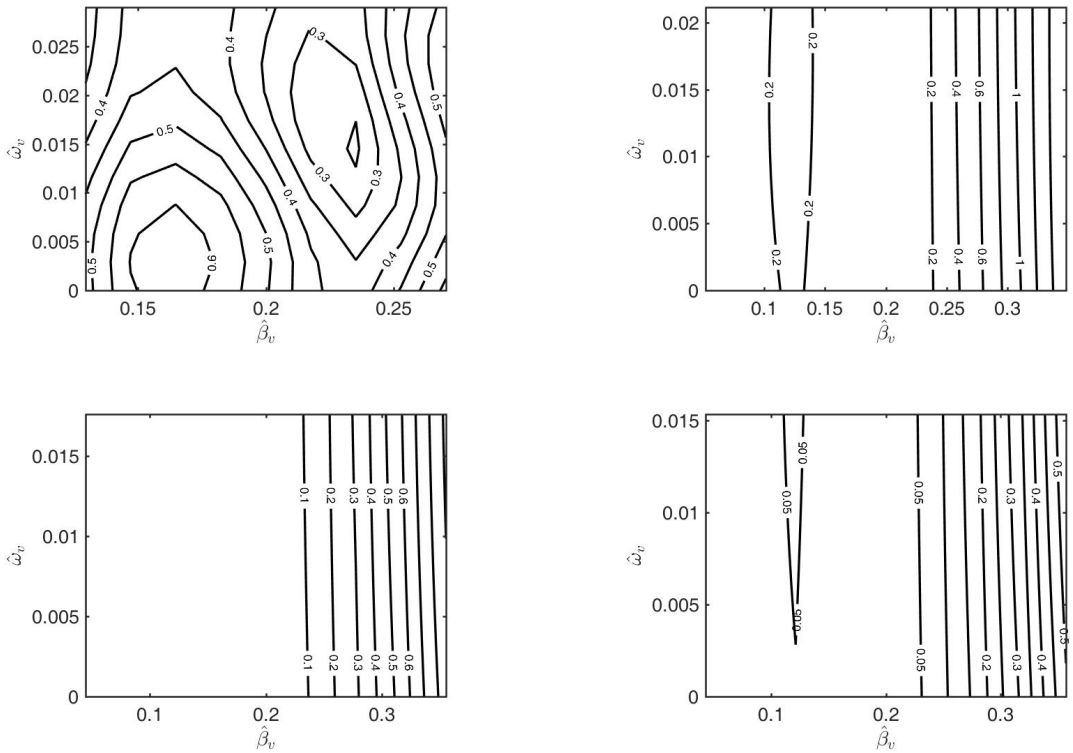


Figure 4.7: Contour plot Λ_{SV} as a function of $\hat{\beta}_v$ and $\hat{\omega}_v \in [0, \hat{\omega}_{TS}/10]$ (sum-mode interaction) at Reynolds number 10^6 for Mach numbers $M = 1.2$ (top left), $M = 3$ (top right), $M = 4.5$ (bottom left), and $M = 6$ (bottom right). The neutral T-S mode excited has $\hat{\beta}_{TS} = 0.2$.

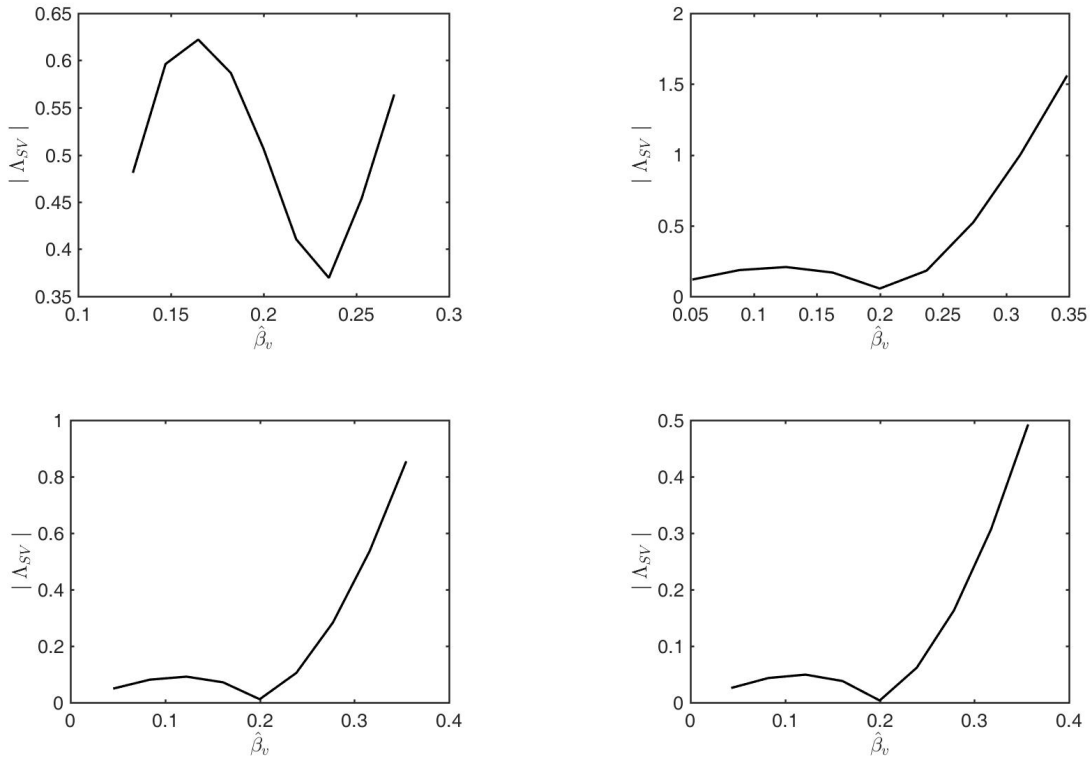


Figure 4.8: Value of Λ_{SV} as a function of $\hat{\beta}_v$ (sum-mode interaction) at Reynolds number 10^6 for Mach numbers $M = 1.2$ (top left), $M = 3$ (top right), $M = 4.5$ (bottom left), and $M = 6$ (bottom right). Results for steady streak ($\bar{k}_1 = 0$). The neutral T-S mode excited has $\hat{\beta}_{TS} = 0.2$.

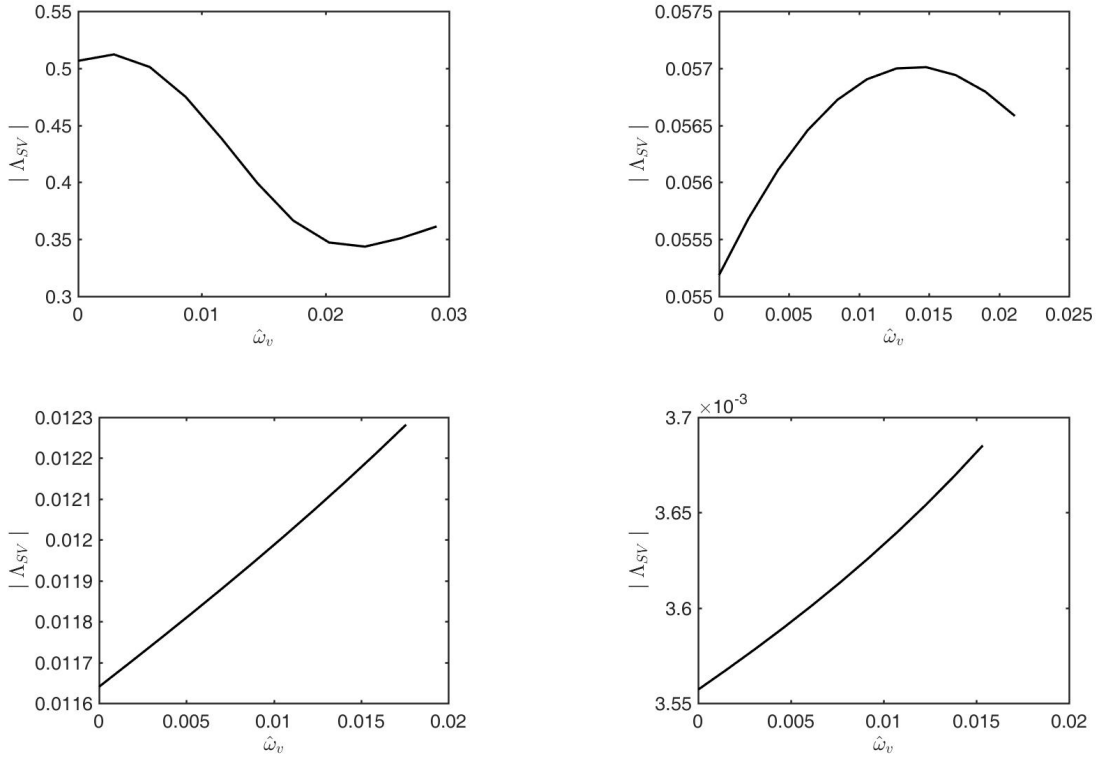


Figure 4.9: Value of Λ_{SV} as a function of $\hat{\omega}_v \in [0, \hat{\omega}_{TS}/10]$ (sum-mode interaction) at Reynolds number 10^6 for Mach numbers $M = 1.2$ (top left), $M = 3$ (top right), $M = 4.5$ (bottom left), and $M = 6$ (bottom right). The chosen spanwise wavenumbers are $\hat{\beta}_v = \hat{\beta}_{TS}$ and $\hat{\beta}_s = 0$. The neutral T-S mode excited has $\hat{\beta}_{TS} = 0.2$.

decays as the Mach number increases. For the chosen $\hat{\beta}_v$ and $\hat{\beta}_s$, the maximum value of the coupling coefficient is attained near $\hat{\omega}_v \approx 0$ in the $M = 1.2$ case and at $\hat{\omega}_v = 0.015$ in the $M = 3$. For $M = 4.5$ and $M = 6$, the coupling coefficient increases as $\hat{\omega}_v$ does.

We now choose to excite a different T-S wave: $\hat{\beta}_{TS} = 0.5$. Figure 4.10 shows contour plots of the coupling coefficient Λ_{SV} featuring larger values than those obtained earlier for $\hat{\beta}_{TS} = 0.2$: in this case, $\Lambda_{SV} \sim \mathcal{O}(1-10)$. A weak dependence with $\hat{\omega}_v$ for a given $\hat{\beta}_v$ is also observed.

In figure 4.11, the coupling coefficient has been plotted against $\hat{\beta}_v$ for the steady streak case and different Mach numbers, for a T-S wave which has $\hat{\beta}_{TS} = 0.5$. The minima are attained at $\hat{\beta}_v = \hat{\beta}_{TS}$ (two-dimensional acoustic waves) for all Mach numbers considered. The magnitude of the coupling coefficient is $\mathcal{O}(10)$, in contrast to the results for $\hat{\beta}_{TS} = 0.2$, which are $\mathcal{O}(1)$, in figure 4.8.

Table 4.1 contains a number of cases calculated, for both exact and approximate resonance conditions and various Mach numbers. Given the results in this sec-

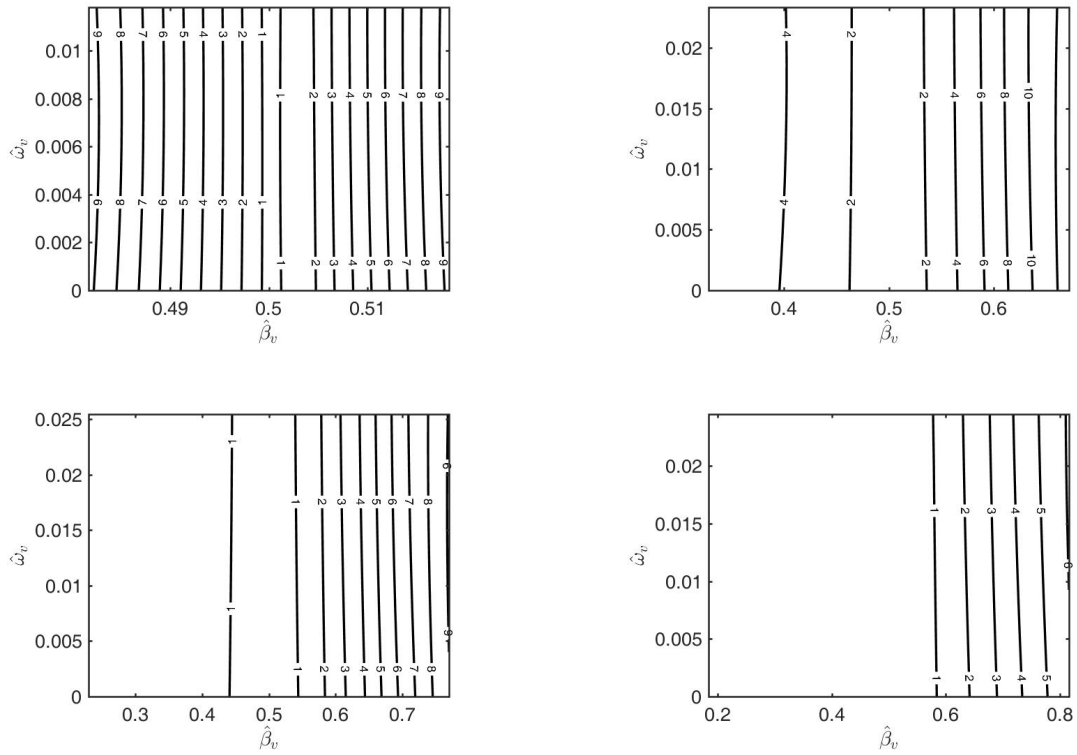


Figure 4.10: Contour plot of Λ_{SV} as a function of $\hat{\beta}_v$ and $\hat{\omega}_v \in [0, \hat{\omega}_{TS}/10]$ (sum-mode interaction) at Reynolds number 10^6 for Mach numbers $M = 1.2$ (top left), $M = 3$ (top right), $M = 4.5$ (bottom left), and $M = 6$ (bottom right). The neutral T-S mode excited has $\hat{\beta}_{TS} = 0.5$.

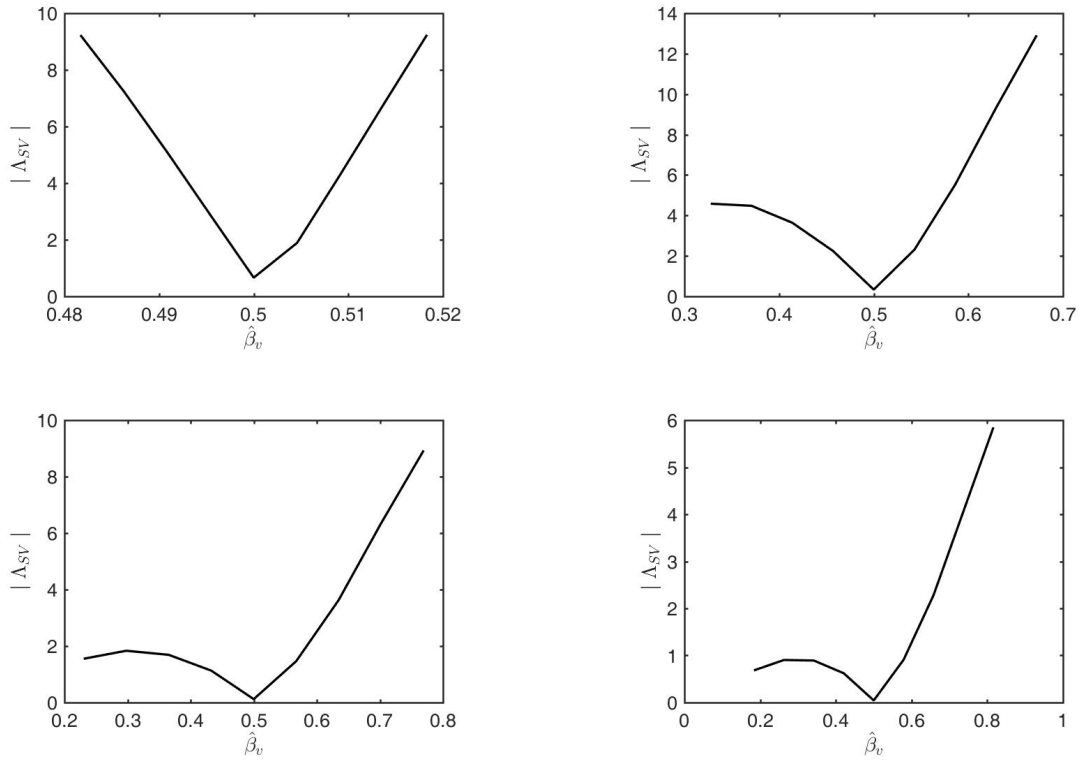


Figure 4.11: Value of Λ_{SV} as a function of $\hat{\beta}_v$ (sum-mode interaction) at Reynolds number 10^6 for Mach numbers $M = 1.2$ (top left), $M = 3$ (top right), $M = 4.5$ (bottom left), and $M = 6$ (bottom right). Results for a steady streak ($\bar{k}_1 = 0$). The neutral T-S mode excited has $\hat{\beta}_{TS} = 0.5$.

M	R_L	$\tilde{x}_n$	$\hat{\beta}_{TS}$	$\hat{\alpha}_{TS}$	$\hat{\omega}_{TS}$	$\hat{\beta}_v$	$\hat{\omega}_v$	Λ_{SV}	$\bar{k}_1$	c_{TS}	c_1	EXACT
1.2	10^6	0.0415	0.2	0.1328	0.29	0.2	0.0017	0.478	1	0.44	0.44	YES
1.2	10^6	0.0415	0.2	0.1328	0.29	0.2	0.017	0.356	10	0.44	0.42	YES
1.2	10^6	0.0183	0.2	0.1328	0.29	0.12	0	0.212	0	0.44	0.44	YES
1.2	10^6	0.0183	0.2	0.1328	0.29	0.12	0.0007	0.213	1	0.44	0.44	YES
1.2	10^6	0.0183	0.2	0.1328	0.29	0.12	0.0075	0.212	10	0.44	0.43	YES
4.5	10^6	0.0016	0.2	0.044	0.176	0.2	0	0.011	0	1.59	1.59	YES
4.5	10^6	0.0016	0.2	0.044	0.176	0.2	0.0002	0.011	1	1.59	1.59	YES
4.5	10^6	0.0016	0.2	0.044	0.176	0.2	0.0025	0.011	10	1.59	1.57	YES
4.5	10^6	0.0016	0.2	0.044	0.176	0.2	0	0.011	10	1.59	1.59	NO
4.5	10^6	0.0005	0.2	0.044	0.176	0.1	0	0.084	0	1.59	1.59	YES
4.5	10^6	0.0005	0.2	0.044	0.176	0.1	0.00008	0.084	1	1.59	1.59	YES
4.5	10^6	0.0005	0.2	0.044	0.176	0.1	0.0008	0.084	10	1.59	1.58	YES

Table 4.1: Typical values of Λ_{SV} (sum-mode interaction) at Reynolds number 10^6 for two different Mach numbers ($M = 1.2$ and $M = 4.5$). "EXACT" means that the exact resonance condition (4.102) has been employed in contrast to the approximate condition (4.104). The parameters chosen for the evaluation of the profiles and coupling coefficients are $Pr = 0.7$, $\omega = 0.76$, $k_3 = 1$, $\hat{v}_\infty = 1$ and $\hat{w}_\infty = 1$. The boundary condition at the surface of the plate is adiabatic for the base flow.

tion, a more extensive study of the parameter space is needed in order to explore the appearance of larger values of Λ_{SV}. In particular, the study of the effect of isothermal/adiabatic boundary condition at the wall or the viscosity law used (as investigated previously in chapter 2 for the S-S and S-R mechanisms) is left for future work.

4.5 Summary and conclusions

In this work, a new and extremely efficient receptivity mechanism for the generation of T-S waves which involves an incident sound wave with its frequency and wavelength on the triple-deck scale and free-stream vortical disturbances with spanwise wavelength on the triple-deck scale too but long streamwise wavelength comparable with L, was investigated theoretically in the limit of asymptotically large Reynolds numbers. As shown by Hernández and Wu (2019) and by Liu et al. (2020), such a sound wave has the special feature that its streamwise velocity and temperature/density fluctuations in the boundary layer acquire an amplitude of $\mathcal{O}(\varepsilon_s R^{1/8})$, much stronger than the $\mathcal{O}(\varepsilon_s)$ fluctuation in the free-stream. The long-wavelength vortical disturbances with $\mathcal{O}(\varepsilon_v)$ intensity in the free-stream induce in the boundary layer much larger $\mathcal{O}(\varepsilon_v R^{3/8})$ streamwise velocity and temperature/density, which manifest as streaks. With the appropriate choice of the spanwise wavelength on the triple deck scale, the acoustic signature and streaks

interact in the main boundary layer as well as in the lower deck, to generate a forcing that is in resonance with a neutral first Mack mode. The latter is thus excited near the lower branch of the neutral curve, and subsequently undergoes exponential amplification. At a high Reynolds number, the triple-deck formalism was adopted to describe the scale conversion process and make quantitative predictions of impingement and reflection of the acoustic wave and the streak's spanwise length scale. An expression for the coupling coefficient to sound-vortical interaction was derived, and a parametric study as a function of the oncoming perturbations was carried out for four representative Mach numbers and two T-S modes. The receptivity of this mechanism was found to be greater than those in Hernández and Wu (2019) and Wu (1999) by a factor of $\mathcal{O}(R^{1/8})$ and $\mathcal{O}(R^{3/8})$, respectively.

5

Summary and future work

5.1 Summary and conclusions

In this thesis we have considered three problems concerning the instability and receptivity of supersonic boundary layers using high-Reynolds-number asymptotic techniques: the mathematical description of the connection between the upper and lower branches of the neutral curve, and the receptivity to sound-sound, sound-roughness and sound-streak interactions.

In chapter 2, we investigated two new receptivity mechanism to impinging acoustic waves, whose phase velocity ($\mathcal{O}(R^{-1/8}U_\infty)$) is much slower than the free-stream velocity U_∞, where R is the Reynolds number based on L, the distance to the leading edge, and U_∞. The sound-sound, or sound-roughness, interactions generate a forcing in resonance with a neutral T-S wave. The triple-deck formalism was adopted to describe impingement and reflection of the acoustic waves, and ensuing receptivity, allowing the coupling coefficient to be calculated. The two receptivity processes were found to be much more effective compared with those involving usual sound waves, with the coupling coefficient being greater by a factor of $\mathcal{O}(R^{1/4})$ and $\mathcal{O}(R^{1/8})$ in the S-S (sound-sound) and S-R (sound-roughness) interactions, respectively. A parametric study was conducted for representative T-S waves, to assess the influence of the streamwise and spanwise wavenumbers, and the phase speed of the sound wave.

In chapter 3, the possible connection of the inviscid and viscous branches of insta-

bility modes in supersonic boundary layers was investigated theoretically, following the previous study of Goldstein and Ricco (2018). The upper and lower branches of the neutral curve are connected, as indicated by finite-Reynolds-number calculations. A new intermediate regime, identified in a previous preliminary study (Yang, 2017), was discussed further in the chapter. This regime is described by triple-deck theory, although its scaling is not standard. The instability was studied and the dispersion relation was calculated for different Mach numbers. It was shown that this regime had been missed by the previous work of Goldstein and Ricco (2018).

In chapter 4, a new mechanism for the generation of T-S waves was investigated, which involved an incident sound wave with its frequency and wavelength on the triple-deck scale and free-stream vortical disturbances with spanwise wavelength on the triple-deck scale too but long streamwise wavelength. The long-wavelength vortical disturbances with $\mathcal{O}(\varepsilon_v)$ intensity in the free-stream induce in the boundary layer much larger $\mathcal{O}(\varepsilon_v R^{3/8})$ streamwise velocity in response to them, which manifests as streaks. With the appropriate choice of the spanwise wavelength on the triple deck scale, the acoustic signature and streaks interact in the main boundary layer as well as in the lower deck, to generate a forcing in resonance with a neutral T-S wave. The receptivity of this mechanism was found to be greater than those in Hernández and Wu (2019) and Wu (1999) by a factor of $\mathcal{O}(R^{1/8})$ and $\mathcal{O}(R^{3/8})$, respectively.

5.2 Future work

There a few possible extensions regarding the work in chapter 2. The first extension is to study the receptivity to the sound-sound interaction of more general form, i.e. sound waves with phase speeds $c = \mathcal{O}(1)$, with only their length scale on the triple-deck scale, but with higher frequencies. In this case, the interactions in the upper and main decks are important and cannot be neglected. This future investigation is interesting for two reasons: first, sound waves (noise) have a broad spectrum, even if the receptivity mechanism is not as effective as that considered in the supersonic regime. Second, the mechanisms studied in chapter 2 (Hernández and Wu, 2019) and chapter 4 cease to operate in the subsonic regime, therefore the sound-sound interaction on non triple deck ($c = \mathcal{O}(1)$) becomes important.

A second possible extension is to study the transonic limit of the mechanisms described in chapters 2 and 4, sound-sound, sound-roughness and sound-vortical

interactions. They still remain effective in the transonic regime, but the mathematical description (scaling and upper-deck dynamics) need to be modified.

A natural third extension is to verify these mechanisms numerically. This has been done in the work of Liu et al. (2020) for the case of localised wall roughness. Moreover, receptivity experiments could be conducted, guided by theoretical results.

The work in chapter 3 could be extended to include the effect of leading-edge shock waves (important in the hypersonic regime) in Fedorov's theory. Lastly, the numerical calculations carried out by Goldstein and Ricco (2018) could be extended to investigate the receptivity of the $r = 1/3$ regime, which was not studied in that work.

References

P. Andersson, L. Brandt, A. Bottaro, and D. S. Henningson. On the breakdown of boundary layer streaks. *J. Fluid Mech.*, 428:29–60, 2001.

D. Arnal and J. C. Juillen. Contribution expérimental à l'étude de la receptivité d'une couche limite laminaire, à la turbulence de l'ecoulement general. *CERT RT 1/5018 AYD - ONERA*, 1978.

A. A. Bakchinov, G. R. Grek, B. G. B. Klingmann, and V. V. Kozlov. Transition experiments in a boundary layer with embedded streamwise vortices. *Phys. Fluids*, 7(4):820–832, 1995.

P. Balakumar. Transition in a supersonic boundary layer due to roughness and acoustic disturbances. *AIAA Paper*, 2003. 2003–3589.

P. Balakumar. Transition in a supersonic boundary layer due to acoustic disturbances. *AIAA Paper*, 2005. 2005–0096.

N. D. Blackaby, S. J. Cowley, and P. Hall. On the instability of hypersonic flow past a flat plate. *J. Fluid Mech.*, 247:369–416, 1993.

R. J. Bodonyi, W. J. C. Welch, P. W. Duck, and M. Tadjfar. A numerical study of the interaction between unsteady free-stream disturbances and localized variations in surface geometry. *J. Fluid Mech.*, 209:285–308, 1989.

L. Brandt, P. Schlatter, and D. Henningson. Transition in boundary layers subject to free-stream turbulence. *J. Fluid Mech.*, 517:167–198, 2004.

T. Cebeci. *Convective Heat Transfer*. Springer, 2002.

M. Choudhari. Boundary-layer receptivity due to distributed surface imperfections of a deterministic or random nature. *Theor. Comput. Fluid Dyn.*, 4 (3):101, 1993.

M. Choudhari and C. L. Streett. A finite Reynolds-number approach for the prediction of boundary-layer receptivity in localized regions. *Phys. Fluids A*, 4 (11):2495–2514, 1992.

C. Cossu and L. Brandt. Stabilization of Tollmien–Schlichting waves by finite amplitude optimal streaks in the blasius boundary layer. *Phys. Fluids*, 14(8): L57–L60, 2002.

S. J. Cowley and X. Wu. Asymptotic approaches to transition modeling. *Progress in Transition Modelling, AGARD Rep.*, 793, 1994.

S. J. Cowley and X. Wu. Asymptotic approaches to transition modelling. *AGARD Rep.*, 793:1–38, 1999.

J. D. Crouch. Localized receptivity of boundary layers. *Phys. Fluids*, 4:1408–1414, 1992.

J. D. Crouch. Distributed excitation of Tollmien–Schlichting waves by vortical free-stream disturbances. *Phys. Fluids*, 6:217–223, 1994.

N. De Tullio and A. I. Ruban. A numerical evaluation of the asymptotic theory of receptivity for subsonic compressible boundary layers. *J. Fluid Mech.*, 771: 520–546, 2015.

A. J. Dietz. Local boundary-layer receptivity to a convected free-stream disturbance. *J. Fluid Mech.*, 378:291–317, 1999.

M. Dong, Y. Liu, and X. Wu. Receptivity of inviscid modes in supersonic boundary layers due to scattering of free-stream sound by localised wall roughness. *J. Fluid Mech.*, 896:A23, 2020.

H.L. Dryden. Air flow in the boundary layer near a plate. *NACA Rep.*, 562, 1936.

H.L. Dryden. Transition from laminar to turbulent flow at subsonic and supersonic speeds. *Conference on High-Speed Aeronautics, 41, Polytechnic of Brooklyn, New York*, 1955.

P. W. Duck, A. I. Ruban, and C. N. Zhikharev. The generation of Tollmien-Schlichting waves by free stream turbulence. *J. Fluid Mech.*, 312:341–371, 1996.

H. F. Fasel. Numerical investigation of the interaction of the Klebanoff-mode with a Tollmien–Schlichting wave. *J. Fluid Mech.*, 450:1–33, 2002.

A. V. Fedorov. Receptivity of a high-speed boundary layer to acoustic disturbances. *J. Fluid Mech.*, 491:101–129, 2003a.

A. V. Fedorov. Receptivity of hypersonic boundary layer to acoustic disturbances scattered by surface roughness. *AIAA Paper*, 2003b. 2003-3731.

A. V. Fedorov. Transition and stability of high-speed boundary layers. *Ann. Rev. Fluid Mech.*, 43(1):79–95, 2011.

A. V. Fedorov. Receptivity of a supersonic boundary layer to solid particulates. *J. Fluid Mech.*, 737:105–131, 2013.

A. V. Fedorov and A. P. Khokhlov. Excitation of unstable modes in a supersonic boundary layer by acoustic waves. *Fluid Dyn.*, 26 (4):531–537, 1991.

A. V. Fedorov and A. P. Khokhlov. Prehistory of instability in a hypersonic boundary layer. *Theor. Comput. Fluid Dyn*, 14 (6):359–375, 2001.

J. Fransson, L. Brandt, A. Talamelli, and C. Cossu. Experimental study of the stabilization of Tollmien-Schlichting waves by finite amplitude streaks. *Phys. Fluids*, 17:054110, 2005a.

J. Fransson, M. Matsubara, and P. H. Alfredsson. Transition induced by free-stream turbulence. *J. Fluid Mech.*, 527:1–25, 2005b.

J. Gao, J. Luo, and X. Wu. Receptivity of hypersonic boundary layer due to fast-slow acoustics interaction. *Acta Mech. Sin.*, 31(6):899–909, 2015.

M. E. Goldstein. The evolution of Tollmien-Schlichting waves near a leading edge. *J. Fluid Mech.*, 127:59–81, 1983.

M. E. Goldstein. Scattering of acoustic waves into Tollmien-Schlichting waves by small streamwise variations in surface geometry. *J. Fluid Mech.*, 154:509–529, 1985.

M. E. Goldstein and L. S. Hultgren. Boundary-layer receptivity to long-wave free-stream disturbances. *Ann. Rev. Fluid Mech.*, 21(1):137–166, 1989.

M. E. Goldstein and P. Ricco. Non-localized boundary layer instabilities resulting from leading edge receptivity at moderate supersonic Mach numbers. *J. Fluid Mech.*, 838:435–477, 2018.

M. E. Goldstein, S. J. Leib, and S. J. Cowley. Generation of Tollmien–Schlichting waves on interactive marginally separated flows. *J. Fluid Mech.*, 181:485–517, 1987.

P. Graziosi and G. Brown. Experiments on stability and transition at Mach 3. *J. Fluid Mech.*, 472:83–124, 2002.

A. Gulyaev, V. Kozlov, V. Kuzenetsov, B. Mineev, and A. Sekundov. Interaction of a laminar boundary layer with external turbulence. *Izv. Akad. Nauk. SSSR Mekh. Zhid. i Gaza*, 6:700–710, 1989.

P. Hall and F. T. Smith. On the effects of nonparallelism, three-dimensionality, and mode interaction in nonlinear boundary-layer stability. *Studies in Appl. Math.*, 70(2):91–120, 1984. ISSN 1467-9590.

W. Heisenberg. Über Stabilität und Turbulenz von Flüssigkeitsströmen. *Ann. der Phys.*, 74:577–627, 1924.

C. G. Hernández and X. Wu. Receptivity of supersonic boundary layers over smooth and wavy surfaces to impinging slow acoustic waves. *J. Fluid Mech.*, 872:849–888, 2019.

R. Jacobs and P. Durbin. Simulation of bypass transition. *J. Fluid Mech.*, 428: 185–212, 2001.

I. Kachanov and O. Tararykin. An experimental study of the stability of a relaxing boundary layer. *Akademiia Nauk SSSR Sibirskoe Otdelenie Izvestiia Seriia Tekhnicheskie Nauki*, 10 1987.

K. Kachanov, V. V. Kozlov, and V. Y. Levchenko. Origin of Tollmien–Schlichting waves in boundary layer under the influence of external disturbances. *Fluid Dyn.*, 13:704–711, 1979.

Y S Kachanov. Physical mechanisms of laminar-boundary-layer transition. *Ann. Rev. Fluid Mech.*, 26(1):411–482, 1994.

N. Kemp. *The laminar three-dimensional boundary layer and a study of the flow past a side edge*. MAcs thesis, Cornell University, 1951.

J. Kendall. Experimental study of disturbances produced in a pre-transitional boundary layer. *AIAA Paper*, pages 85–1695, 1985.

J. Kendall. Boundary layer receptivity to free stream turbulence. *AIAA Paper*, pages 90–1504, 1990.

J. Kendall. Studies on laminar boundary layer receptivity to free-stream turbulence near a leading edge. in. *Boundary Layer Stability and Transition to Turbulence*, 114:23–30, 1991.

J. Kendall. Experiments on boundary-layer receptivity to freestream turbulence. *AIAA Paper*, pages 98–0530, 1998.

J. M. Kendall. Wind tunnel experiments relating to supersonic and hypersonic boundary-layer transition. *AIAA Paper*, 1975. 74-133.

J. M. Kendall. Experimental study of laminar boundary layer receptivity to a traveling pressure field. *AIAA Paper*, 1987. 87-1257.

R. A. King and K. S. Breuer. Oblique transition in a laminar Blasius boundary layer. *J. Fluid Mech.*, 453:177–200, 2002.

P. Klebanoff. Effect of free-stream turbulence on a laminar boundary layer. *Bull. Am. Phys. Soc*, 16, 1971.

L. S. G. Kovasznay. Turbulence in supersonic flow. *J. Aero. Sci.*, 20:657–682, 1953.

S. H. Lam and N. Rott. Eigen-functions of linearized unsteady boundary layer equations. *J. Fluid Eng.*, 115:597:311–349, 1993.

J. Laufer. Aerodynamic noise in supersonic wind tunnels. *J. Aero. Sci.*, 28:685–692, 1961.

S. J. Leib, D. W. Wundrow, and M. E. Goldstein. Effect of free-stream turbulence and other vortical disturbances on a laminar boundary layer. *J. Fluid Mech.*, 380:169–203, 1999.

C. C. Lin. On the stability of two-dimensional parallel flows. I. General theory. *Quart. Appl. Math.*, 3(2):117–142, 1945.

C. C. Lin. On the stability of two-dimensional parallel flows. III. Stability in a viscous fluid. *Quart. Appl. Math.*, 3(4):277–301, 1946.

C. C. Lin. On the instability of laminar flow and transition to turbulence. In *Grenzschichtforschung/Boundary Layer Research*, pages 144–57. Berlin: Springer–Verlag, 1957.

Y. Liu, M. Dong, and X. Wu. Generation of first mack modes in supersonic boundary layers by slow acoustic waves interacting with streamwise isolated wall roughness. *J. Fluid Mech.*, 888:A10, 2020.

Y. Ma and X. Zhong. Receptivity of a supersonic boundary layer over a flat plate. Part 2. Receptivity to free-stream sound. *J. Fluid Mech.*, 488:79–121, 2003.

Y. Ma and X. Zhong. Receptivity of a supersonic boundary layer over a flat plate. Part 3. Effects of different types of free-stream disturbances. *J. Fluid Mech.*, 532:63–109, 2005.

L. M. Mack. Linear stability theory and the problem of supersonic boundary-layer transition. *AIAA J.*, 13(3):278–289, 1975.

L. M. Mack. Boundary-layer linear stability theory. *AGARD Rep., Spec. Course Stab. Transit. Laminar Flows*, 709, 1984.

E. Marensi. *Nonlinear unsteady disturbances generated by the interaction of free-stream vorticity with a laminar boundary layer.* PhD thesis, University of Sheffield, 2016.

A. A. Maslov, A. N. Shiplyuk, A. A. Sidorenko, and D. Arnal. Leading-edge receptivity of a hypersonic boundary layer on a flat plate. *J. Fluid Mech.*, 426: 73–94, 2001.

M. Matsubara and P. H. Alfredsson. Disturbance growth in boundary layers subjected to free-stream turbulence. *J. Fluid Mech.*, 430:149–168, 2001.

G. Mengaldo, M. Kravtsova, A. I. Ruban, and S. J. Sherwin. Triple-deck and direct numerical simulation analyses of high-speed subsonic flows past a roughness element. *J. Fluid Mech.*, 774:311–323, 2015.

A. F. Messiter. Boundary-layer flow near the trailing edge of a flat plate. *SIAM J. Appl. Maths*, 18(1):241–257, 1970.

M. Morkovin. Bypass transition to turbulence and research desiderata. *Transition in Turbines NASA CP*, 2386:161–204, 1984.

M. V. Morkovin. Critical evaluation of transition from laminar to turbulent shear layers with emphasis on hypersonically travelling bodies. *Tech. Rep. AFFDL-TR*, pages 68–149, 1969.

M. V. Morkovin, E. Reshotko, and T. Herbert. Transition in open flow systems-a reassessment. *Bull. Am. Phys. Soc.*, 39:1882, 1994.

A. H. Nayfeh and O. N. Ashour. Acoustic receptivity of a boundary layer to Tollmien–Schlichting waves resulting from a finite-height hump at finite reynolds numbers. *Phys. Fluids*, 6(11):3705–3716, 1994.

V. Y. Neiland. Theory of laminar boundary layer separation in supersonic flow. *Fluid Dyn.*, 4(4):33–35, 1969.

W. McF Orr. The stability or instability of the steady motions of a perfect liquid and of a viscous liquid. *Proc. R. Irish Acad. A*, 27:1–138, 1907.

S. R. Pate. Supersonic boundary-layer transition: effects of roughness and free-stream disturbances. *AIAA J.*, 9:797–803, 1971.

F. Qin and X. Wu. Response and receptivity of the hypersonic boundary layer past a wedge to free-stream acoustic, vortical and entropy disturbances. *J. Fluid Mech.*, 797:874–915, 2016.

Lord Rayleigh. On the stability, or instability, of certain fluid motions. *Proc. Lond. Math. Soc.*, 1(1):57–72, 1879.

E. Reshotko. Boundary layer stability and transition. *Ann. Rev. Fluid Mech.*, 8: 311–349, 1976.

O. Reynolds. On the dynamical theory of incompressible viscous fluids and the determination of the criterion. *Phil. Trans. R. Soc. Lond.*, (186):123–164, 1895.

P. Ricco and X. Wu. Response of a compressible laminar boundary layer to free-stream vortical disturbances. *J. Fluid Mech.*, 587:97–138, 2007.

P Ricco, J Luo, and X Wu. Evolution and instability of unsteady nonlinear streaks generated by free-stream vortical disturbances. *J. Fluid Mech.*, 677:1–38, 2011.

A. I. Ruban. Nonlinear equation for the amplitude of Tollmien-Schlichting waves in the boundary layer. *Izv. Akad. Nauk. SSSR Mekh. Zhid. Gaza*, 6:60–67, 1983.

A. I. Ruban. On Tollmien-Schlichting wave generation by sound. *Izv. Akad. Nauk. SSSR Mekh. Zhid. Gaza*, 5:44 (English Translation: Fluid Dyn. 19, 709–716 (1985)), 1984.

A. I. Ruban, T. Bernots, and M. A. Kravtsova. Linear and nonlinear receptivity of the boundary layer in transonic flows. *J. Fluid Mech.*, 786:154–189, 2016.

W. S. Saric and E. B. White. Influence of high-amplitude noise on boundary-layer transition to turbulence. *AIAA Paper*, 1998. 98-2645.

W. S. Saric, H. L. Reed, and E. J. Kerschen. Boundary-layer receptivity to freestream disturbances. *Ann. Rev. Fluid Mech.*, 34(1):291–319, 2002.

H. Schlichting. Zur entstechung der turbulenz bei der plattenströmung. *Math. Phys. Klasse. Nachr. Ges. Wiss. Göttingen*, pages 181–208, 1933.

S. P. Schneider. Effects of high-speed tunnel noise on laminar-turbulent transition. *J. Spacecr. Rockets*, 38 (3):323–333, 2001.

G. Schubauer and H. Skramstad. Laminar boundary-layer oscillations and transition on a flat plate. *NACA TN*, 909, 1947.

N. V. Semionov and A. D. Kosinov. An experimental study of receptivity of supersonic boundary layer on a blunted plate. *Intl. J. Mech.*, 2 (3):87–95, 2008.

A. Sescu, S. Yassir, and M. Visbal. *Compressible boundary layer receptivity to free-stream disturbances and step excrescences.* In: 46th AIAA Fluid Dynamics Conference., 2016.

P. J. Shapiro. The influence of sound upon laminar boundary layer instability. Technical report, MIT Acoustics and Vibration Laboratory, 1977.

F. T. Smith. Instability of flow through pipes of general cross-section. Part 1. *Mathematika*, 26(2):187–210, 1979a.

F. T. Smith. On the non-parallel flow stability of the Blasius boundary layer. *Proc. R. Soc. Lond. A*, 366(1724):91–109, 1979b. ISSN 00804630.

F. T. Smith. On the first-mode instability in subsonic, supersonic or hypersonic boundary layers. *J. Fluid Mech.*, 198:127–153, 1989.

F. T. Smith and S. N. Brown. The inviscid instability of a Blasius boundary layer at large values of the mach number. *J. Fluid Mech.*, 219:499–518, 1990.

F. T. Smith, R. I. Sykes, and P. W. M. Brighton. A two-dimensional boundary layer encountering a three-dimensional hump. *J. Fluid Mech.*, 83(1):163–176, 1977.

A. Sommerfeld. Ein Beitrag zur hydrodynamischen Erklarung der turbulenten Flussigkeisbewegung. *Atti Congr. Int. Math. 4th*, 1908.

K. Stewartson. *The Theory of Laminar Boundary Layers in Compressible Fluids.* Oxford Mathematical Monographs, 1964.

K. Stewartson and P. G. Williams. Self-induced separation. 312(1509):181–206, 1969.

R. I. Sykes. Stratification effects in boundary layer flow over hills. *Proc. R. Soc. Lond. A*, 361(1705):225–243, 1978.

G. Taylor. Some recent developments in the study of turbulence. *Fifth Intl Congr. for Appl. Mech.*, pages 294–310, 1939.

E. D. Terent'ev. The linear problem of a vibrator in a subsonic boundary layer. *Prikl. Math. Mech.*, 45:1049–1055, 1981.

W. Tollmien. Uber die entstehung der turbulenz l. mitteilung. in math. phys. kl. *Nachr. Ges. Wiss. Göttingen*, pages 21–44, 1929.

K. Westin, A. Boiko, B. Klingmann, V. Kozlov, and P. Alfredsson. Experiments in a boundary layer subjected to free stream turbulence. part 1. boundary layer structure and receptivity. *J. Fluid Mech.*, 281:193–218, 1994.

X. Wu. Generation of Tollmien-Schlichting waves by convecting gusts interacting with sound. *J. Fluid Mech.*, 397:285–316, 1999.

X. Wu. Receptivity of boundary layers with distributed roughness to vortical and acoustic disturbances: a second-order asymptotic theory and comparison with experiments. *J. Fluid Mech.*, 431:91–133, 2001a.

X. Wu. On local boundary-layer receptivity to vortical disturbances in the free stream. *J. Fluid Mech.*, 449:373–393, 2001b.

X. Wu. Nonlinear theories for shear flow instabilities: Physical insights and practical implications. *Ann. Rev. Fluid Mech.*, 51(1):451–485, 2019.

X. Wu and M. Choudhari. Linear and nonlinear instabilities of a blasius boundary layer perturbed by streamwise vortices. Part 2. Intermittent instability induced by long-wavelength klebanoff modes. *J. Fluid Mech.*, 483:249–286, 2003.

X. Wu and M. Dong. A local scattering theory for the effects of isolated roughness on boundary-layer instability and transition: transmission coefficient as an eigenvalue. *J. Fluid Mech.*, 794:68–108, 2016a.

X. Wu and M. Dong. Entrainment of short-wavelength free-stream vortical disturbances in compressible and incompressible boundary layers. *J. Fluid Mech.*, 797:683–728, 2016b.

X. Wu and L. W. Hogg. Acoustic radiation of Tollmien–Schlichting waves as they undergo rapid distortion. *J. Fluid Mech.*, 550:307–347, 2006.

X. Wu and J. Zhang. Instability of a stratified boundary layer and its coupling with internal gravity waves. Part 2. coupling with internal gravity waves via topography. *J. Fluid Mech.*, 595:409–433, 2008.

X. Wu, D. Zhao, and J. Luo. Excitation of steady and unsteady görtler vortices by free-stream vortical disturbances. *J. Fluid Mech.*, 682:66–100, 2011.

W. Würz, S. Herr, A. Wörner, U. Rist, S. Wagner, and Y. S. Kachanov. Three-dimensional acoustic-roughness receptivity of a boundary layer on an airfoil: experiment and direct numerical simulations. *J. Fluid Mech.*, 478:135–163, 2003.

D. Xu, Y. Zhang, and X. Wu. Nonlinear evolution and secondary instability of steady and unsteady görtler vortices induced by free-stream vortical disturbances. *J. Fluid Mech.*, 829:681–730, 2017.

D. Xu, J. Liu, and X. Wu. Görtler vortices and streaks in boundary layer subject to pressure gradient: excitation by free stream vortical disturbances, nonlinear evolution and secondary instability. *J. Fluid Mech.*, 900:A15, 2020.

Y. Yang. *Instability and receptivity of supersonic boundary layer*. MSc thesis, Imperial College London, 2017.

T. Zaki and P. Durbin. Mode interaction and the bypass route to transition. *J. Fluid Mech.*, 531:85–111, 2005.

V. N. Zhigulev and A. V. Fedorov. Boundary-layer receptivity to acoustic disturbances. *J. Appl. Mech. And Tech. Phys*, 28(1):28–34, 1987.

X. Zhong and X. Wang. Direct numerical simulation on the receptivity, instability, and transition of hypersonic boundary layers. *Ann. Rev. Fluid Mech.*, 44(1): 527–561, 2012.

A

Mean-flow distortion equations in the lower deck

The linearized equations hold when $h \ll 1$, namely,

$$\left.\begin{aligned} &i\hat{\alpha}_w \hat{U}_M + \hat{V}_{M,Y} + i\hat{\beta}_w \hat{W}_M = 0, \\ &i\hat{\alpha}_w \lambda_0 Y \hat{U}_M + \lambda_0 \hat{V}_M = -i\hat{\alpha}_w \hat{P}_M + \hat{U}_{M,YY}, \\ &i\hat{\alpha}_w \lambda_0 Y \hat{W}_M = -i\hat{\beta}_w \hat{P}_M + \hat{W}_{M,YY}. \end{aligned}\right\} \tag{A.1}$$

After linearizing the no-slip boundary condition at $Y = hF_w + \text{c.c.}$ for $h \ll 1$, we obtain

$$\hat{U}_M = -\lambda_0 \hat{F}_w, \quad \hat{V}_M = \hat{W}_M = 0 \quad \text{at} \quad Y = 0. \tag{A.2}$$

The matching condition with the main-deck solution (2.140) reads

$$\hat{U}_M \to \lambda_0 \hat{A}_M, \quad \hat{W}_M \to 0 \quad \text{as} \quad Y \to \infty. \tag{A.3}$$

Eliminating $\hat{P}_M$ from (A.1), we arrive at

$$\left\{ \frac{\partial^2}{\partial Y^2} - i\hat{\alpha}_w \lambda_0 Y \right\} \hat{V}_{M,YY} = 0. \tag{A.4}$$

After the change of variable

$$\eta = (i\hat{\alpha}_w \lambda_0)^{1/3} Y, \tag{A.5}$$

we can write (A.4) into the Airy equation for $\hat{V}_{M,YY}$, and its solution is found as

$$\hat{V}_{M,Y} = i\hat{\alpha}_w\lambda_0\hat{F}_w + q_w\int_0^\eta Ai(\eta)d\eta, \tag{A.6}$$

where q_w is constant. The matching condition (A.3) implies that $\hat{V}_{M,Y} \to -i\hat{\alpha}_w\lambda_0\hat{A}_M$, which gives

$$i\hat{\alpha}_w\lambda_0\hat{A}_M + q_w\int_0^\infty Ai(\eta)d\eta + i\hat{\alpha}_w\lambda_0\hat{F}_w = 0. \tag{A.7}$$

After combining the x- and z-momentum equations in $(A.1)$ and applying boundary conditions (A.2) again, another relation follows,

$$(\hat{\alpha}_w^2 + \hat{\beta}_w^2)\hat{P}_M = (i\hat{\alpha}_w\lambda_0)^{2/3}q_w Ai'(0). \tag{A.8}$$

The pressure is transmitted from the upper deck down to the lower deck, and the matching condition (2.42), applied to the mean-flow distortion, gives

$$i\sqrt{(M^2-1)\hat{\alpha}_w^2 - \hat{\beta}_w^2}\hat{P}_M = \hat{\alpha}_w^2\hat{A}_M, \tag{A.9}$$

if the branch $e^{-i\sqrt{(M^2-1)\hat{\alpha}_w^2-\hat{\beta}_w^2}\bar{y}}$ is chosen. On the other hand, if $(M^2-1)\hat{\alpha}_w^2 < \hat{\beta}_w^2$, the matching condition changes to

$$\sqrt{\hat{\beta}_w^2 - (M^2-1)\hat{\alpha}_w^2}\hat{P}_M = \hat{\alpha}_w^2\hat{A}_M. \tag{A.10}$$

From $(A.7)$, $(A.8)$ and $(A.9)$ or (A.10), it follows that

$$\hat{P}_M = -3(i\hat{\alpha}_w\lambda_0)^{5/3}\hat{\alpha}_w^2 Ai'(0)\hat{F}_w/\mathcal{D}, \tag{A.11}$$

where $\mathcal{D}$ is defined as

$$\mathcal{D}_I(\hat{\alpha}_w,\hat{\beta}_w) = \hat{\alpha}_w^2(\hat{\alpha}_w^2+\hat{\beta}_w^2) + 3i(i\hat{\alpha}_w\lambda_0)^{5/3}Ai'(0)\sqrt{(M^2-1)\hat{\alpha}_w^2-\hat{\beta}_w^2}, \tag{A.12}$$

or

$$\mathcal{D}_{II}(\hat{\alpha}_w,\hat{\beta}_w) = \hat{\alpha}_w^2(\hat{\alpha}_w^2+\hat{\beta}_w^2) + 3(i\hat{\alpha}_w\lambda_0)^{5/3}Ai'(0)\sqrt{\hat{\beta}_w^2-(M^2-1)\hat{\alpha}_w^2}, \tag{A.13}$$

depending on the branch considered. The solution for the velocities can be ob-

tained from (A.1) as (Smith et al., 1977, Sykes, 1978, Wu and Zhang, 2008)

$$\hat{V}_M = (i\hat{\alpha}_w\lambda_0)^{2/3}\hat{F}_w\left[\eta - \frac{3\hat{\alpha}_w^2(\hat{\alpha}_w^2+\hat{\beta}_w^2)}{\mathcal{D}}\left(\eta\int_0^\eta Ai(\eta')d\eta' - Ai'(\eta) + Ai'(0)\right)\right], \tag{A.14}$$

$$\hat{W}_M = -i\pi\hat{\beta}_w(i\hat{\alpha}_w\lambda_0)^{-2/3}\hat{P}_M\left(Gi(\eta) - \frac{Bi(0)}{3Ai(0)}Ai(\eta)\right), \tag{A.15}$$

$$\hat{U}_M = -\lambda_0\hat{F}_w + \frac{3\lambda_0\hat{\alpha}_w^2(\hat{\alpha}_w^2+\hat{\beta}_w^2)\hat{F}_w}{\mathcal{D}}\int_0^\eta Ai(\eta')d\eta' - \frac{\hat{\beta}_w}{\hat{\alpha}_w}A\left(Gi(\eta) - \frac{Bi(0)}{3Ai(0)}Ai(\eta)\right). \tag{A.16}$$

B

Numerical solution and validation of numerical method

The system of equations (4.25)–(4.28) with the boundary conditions (4.29) and (4.30) is solved by a second-order Keller-box finite difference scheme (Cebeci, 2002) which is central in η and forward in $\tilde{x}$. The derivatives of the velocity components are approximated by

$$\left.\frac{\partial u}{\partial \tilde{x}}\right|_{i+\frac{1}{2},j} \approx \frac{u_{i+1,j} - u_{i,j}}{\Delta \tilde{x}}, \tag{B.1}$$

$$\left.\frac{\partial u}{\partial \eta}\right|_{i+\frac{1}{2},j} = \frac{1}{2}\left[\left.\frac{\partial u}{\partial \eta}\right|_{i,j} + \left.\frac{\partial u}{\partial \eta}\right|_{i+1,j}\right] \approx \frac{1}{2}\left[\frac{u_{i,j+1} - u_{i,j-1}}{2\Delta\eta} + \frac{u_{i+1,j+1} - u_{i+1,j-1}}{2\Delta\eta}\right], \tag{B.2}$$

$$\left.\frac{\partial^2 u}{\partial \eta^2}\right|_{i+\frac{1}{2},j} = \frac{1}{2}\left[\left.\frac{\partial^2 u}{\partial \eta^2}\right|_{i,j} + \left.\frac{\partial^2 u}{\partial \eta^2}\right|_{i+1,j}\right] \approx \frac{1}{2}\left[\frac{u_{i,j+1} - 2u_{i,j} + u_{i,j-1}}{(\Delta\eta)^2} + \frac{u_{i+1,j+1} - 2u_{i+1,j} + u_{i+1,j-1}}{(\Delta\eta)^2}\right]. \tag{B.3}$$

The stencil used in the numerical scheme is represented in figure B.1. The values of the quantities of interest at the $i+1$ step (in the $\tilde{x}$ direction) are computed using their values at the previous i step. Starting from the two-term approximation for the initial profiles (4.31), the solution is marched in the downstream direction.

Since the equations and the boundary conditions are linear, the system can be

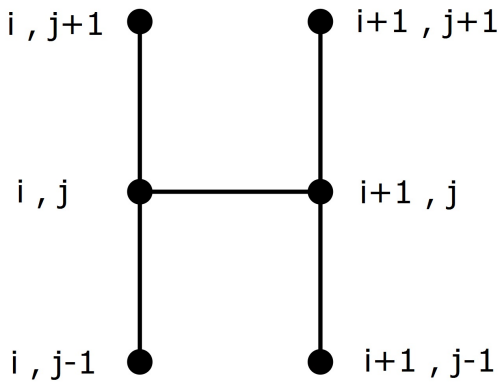


Figure B.1: Stencil used in the numerical scheme for the computation of the LUBL equations.

written in the following matrix-vector form

$$\mathbf{A} \cdot \mathbf{X} = \mathbf{R}, \tag{B.4}$$

$$\mathbf{A} = \begin{bmatrix} A_0 & C_0 & & & & \\ B_1 & A_1 & C_1 & & & \\ & \cdots & \cdots & \cdots & & \\ & & B_j & A_j & C_j & \\ & & & B_{J-1} & A_{J-1} & C_{J-1} \\ & & & & B_J & A_J \end{bmatrix}, \mathbf{X} = \begin{bmatrix} X_0 \\ X_1 \\ \vdots \\ X_j \\ \vdots \\ X_J \end{bmatrix}, \mathbf{R} = \begin{bmatrix} R_0 \\ R_1 \\ \vdots \\ R_j \\ \vdots \\ R_J \end{bmatrix}.$$

where $\mathbf{A}_j$, $\mathbf{B}_j$ $(1 \leq j \leq J)$, $\mathbf{C}_j$ $(1 \leq j \leq J-1)$ are 4×4 matrices, where the j index refers to the location along the η direction and J is the number of mesh points along the same direction. These matrices are obtained by the finite-difference discretization outlined in (B.1)-(B.3). A standard block-elimination algorithm, consisting of two sweeps, has been employed to solve the above system. In the forward sweep, the matrices $\mathbf{G}_j$, $\mathbf{D}_j$ and the vector $\mathbf{W}_j$ are computed as follows

$$\mathbf{D}_0 = \mathbf{A}_0.$$

For $1 \leq j \leq J$,

$$\mathbf{G}_j \cdot \mathbf{D}_{j-1} = \mathbf{B}_j,$$

$$\mathbf{D}_j = \mathbf{A}_j - \mathbf{G}_j \cdot \mathbf{C}_{j-1},$$

$$\mathbf{W}_0 = \mathbf{R}_0.$$

For $1 \leq j \leq J$,

$$\mathbf{W}_j = \mathbf{R}_j - \mathbf{G}_j \cdot \mathbf{W}_{j-1}.$$

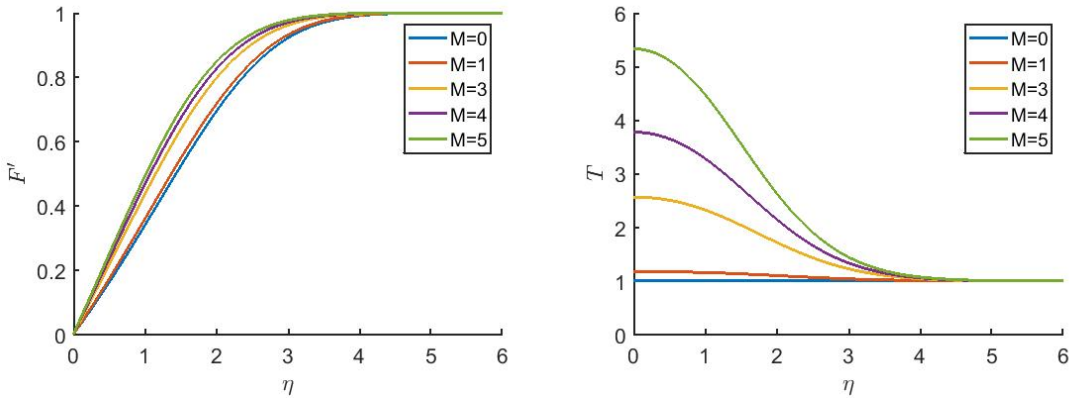


Figure B.2: Profiles of the streamwise velocity $U_B = F'$ and temperature T of a compressible Blasius boundary layer, calculated numerically solving the compressible boundary layer equations for various Mach numbers.

In the backward sweep, the vector $\mathbf{X}$ is computed as follows

$$\mathbf{D}_J \cdot \mathbf{X}_J = \mathbf{W}_J,$$

$$\mathbf{D}_j \cdot \mathbf{X}_j = \mathbf{W}_j - \mathbf{C}_j \cdot \mathbf{X}_{j+1},$$

for $j = J-1, J-2, \ldots, 0$.

For a compressible boundary layer, the velocity and temperature fluctuations are coupled. As a result, external disturbances of the hydrodynamic kind (i.e. the convected gust) trigger thermal disturbance $\tilde{\tau}$ inside the boundary layer.

The compressible boundary layer equations have been solved using the numerical method described in this appendix, for various Mach numbers, in figure B.2. The solution to equations (I) and (II) (section 4.2.4, and Ricco and Wu, 2007) has also been plotted in figures B.3 and B.4, respectively.

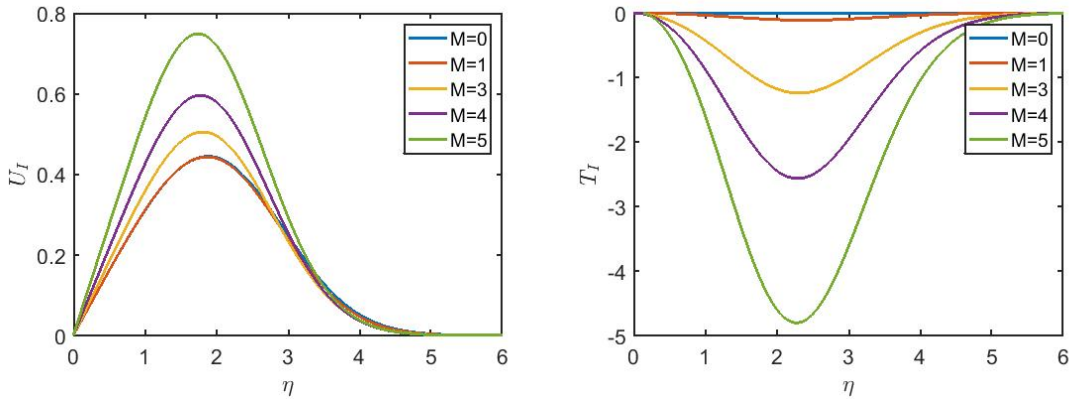


Figure B.3: Numerical solution of equations (I), (4.32)-(4.35). Velocity (left) and temperature (right) profiles for various Mach numbers.

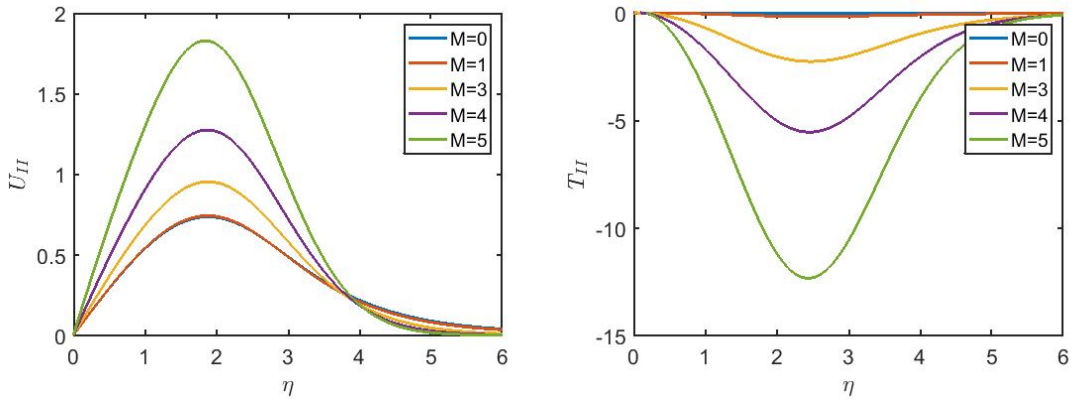


Figure B.4: Numerical solution of equations (II), (4.36)-(4.39). Velocity (left) and temperature (right) profiles for various Mach numbers.